The Paleobiology, Paleoecology, and Evolution of Thescelosauridae (Ornithischia) from Alberta, Canada

By

Michael Naylor Hudgins

A thesis submitted in partial fulfillment of the requirements for the degree of

Master of Science

in

Systematics and Evolution

Department of Biological Sciences

University of Alberta

Abstract

Thescelosauridae is a basal neornithischian dinosaur clade that flourished in the Cretaceous from the Aptian to the Maastrichtian. This diverse but poorly studied group of small-bodied herbivores is divided taxonomically into Orodrominae and Thescelosaurinae, and existed in Asia and North and South America. The limited extent to which thescelosaurids have been studied is due to their generalized, plesiomorphic ornithischian anatomy and their comparatively sparse fossil record, which reflects at least in part their susceptibility to post-mortem damage. Here, I describe new thescelosaurid material from the Late Cretaceous of Alberta and establish dental differences between thescelosaurids and pachycephalosaurids, another small-bodied, ornithischian group. A new partial thescelosaurid skeleton (UALVP 56885) from the Horseshoe Canyon Formation can be referred to the unusual thescelosaurine *Parksosaurus warreni* based on diagnostic features present in the pelvic girdle. The referral of UALVP 56885 to *P. warreni* allows recognition of new postcranial autapomorphies for the taxon. New thescelosaurid remains from the Dinosaur Park and Wapiti Formations can be identified as those of indeterminate orodromines and indeterminate thescelosaurines, respectively. Qualitative and quantitative analyses of *in situ* pachycephalosaurid and thescelosaurid teeth reveal differences between the two clades, in crown and denticle morphology, root and crown cross-sections, crown ornamentation, and wear facet patterns. Taken together, the results presented here provide fresh evidence for temporal separation between orodromines and thescelosaurines in Alberta, implying a complex pattern of thescelosaurid evolution, and suggest that the dental differences between pachycephalosaurids and thescelosaurids should facilitate identification of isolated teeth in microfossil sites and museum settings. More reliable tooth identification will in turn prove useful

in testing hypotheses on the biogeography, macroevolution, paleoecology, and temporal distribution of Pachycephalosauridae and Thescelosauridae using the microfossil record.

Preface

This thesis is an original work by Michael Naylor Hudgins. Corwin Sullivan was the supervisor for this thesis and was involved with the concept formation and manuscript edits for all the chapters.

Chapter 5 ("Qualitative and Quantitative Assessment of Dental Differences between *Stegoceras validum* (Ornithischia: Pachycephalosauridae) and *Thescelosaurus neglectus* (Ornithischia: Thescelosauridae), with Implications for Paleoecology and Isolated Tooth Identification) was submitted on March 22, 2021 and is under review at Cretaceous Research. Michael Naylor Hudgins originally produced the manuscript and its contents. Co-authors (Drs. Philip J. Currie and Corwin Sullivan) provided valuable discussion and edits that improved the quality of the manuscript. The content of Chapter 5 was only altered to reflect the format for this thesis document.

Hudgins, M. N., Currie, P. J., and Sullivan, C. 2021. Qualitative and Quantitative Assessment of Dental Differences between *Stegoceras validum* (Ornithischia: Pachycephalosauridae) and *Thescelosaurus neglectus* (Ornithischia: Thescelosauridae), with Implications for Paleoecology and Isolated Tooth Identification. Submitted to *Cretaceous Research* on March 22, 2021.

Dedication

"…Science is more than a body of knowledge. It is a way of thinking; a way of skeptically interrogating the universe with a fine understanding of human fallibility."

-Carl Sagan

To my family, friends, and all of my ancestors who came before me.

Acknowledgements

First, I would like to thank the COVID-19 pandemic for changing my plans and research activities in fantastic ways and making research streamlined and straightforward!

I would like to sincerely thank my supervisor, Dr. Corwin Sullivan. Thank you for giving me the opportunity to pursue a childhood dream, the constant help and support over the last couple of years, and the stimulating intellectual rigor. I would like to thank Dr. Philip J. Currie for his assistance and feedback throughout my degree; letters of recommendation; and the countless edits to manuscripts for publications and abstracts for conferences. I would like to thank the multiple mentors from various institutions that guided me in becoming a better scientist: Peter Berquist (TNCC), Dr. Michael Caldwell (UALVP), Dr. Eva Koppelhus (UALVP), Dr. Linda Hinnov (GMU), Dr. Aaron LeBlanc (KCL), Dr. Lindsey Leighton (UALVP), Lynsey LeMay (TNCC), Bruce Penrose (TNCC), Dr. Audrey Reid (UALVP), Dr. Michael J. Ryan (CU) and Dr. Mark Uhen (GMU).

For academic discussion and support, I would like to thank Clive Coy (UALVP), Meghan Dueck (UALVP), Aaron Dyers (UALVP), Dr. Greg Funston (UofE), Howard Gibbons (UALVP), Samantha Hamilton (UALVP), Yubo Ma (UALVP), Annie McIntosh (UALVP), Nathaniel Morley (UALVP), Ilaria Paparella (UALVP), Mark Powers (UALVP), Matthew Rhodes (UALVP), Catie Strong (UALVP), Dr. Oksana Vernyogora (UALVP), Rebekah Vice (UALVP), Nicholas Visalden (GMU), Yan-Yin Wang (UALVP), Taia Wyenberg-Henzler (UALVP). Thank you to the Boreal Alberta Dinosaur Project members: Dr. Phil Bell (UNE), Dr. Nicolás E. Campione (UNE), Dr. Federico Fanti (UB), Dr. Matthew J. Vavrek, and Derek Larson. For access to specimens, I thank Amanda Millhouse (USNM) and Dr. Lindsey Zanno

(NCSM). A special thank you to Dr. Caleb Brown (TMP) and Dr. Feng-Lu Han (CUG) for providing a huge inventory of thescelosaurid images that were crucial in completing this thesis. Thank you to the Grande Prairie Regional College, Natural Sciences and Engineering Research Council of Canada Discovery Grant (RGPIN-2017-06246), an endowment associated with the Philip J. Currie Professorship at the University of Alberta, and the Dinosaur Research Institute Student Grant for supporting this research.

Finally, I would like to thank Michael Todd Hudgins, Inessa Spruill, Chris Spruill, Deanna Naylor, Isa Hill, Charles “Donnie” Naylor, Mr. Julius, Ms. Brown, Eric Sappington, Uncle Bruddie, Grandma Janet, Grandpa Sammie, and Kristen Chiama for love and support, and to Charlene Naylor-Hudgins who was the catalyst that started this adventure. Last but not least, a bereaved thank you to Mary and Donald Naylor for motivation and helping me find this calling in life.

Table of Contents

List of Tables

List of Figures

Institutional Abbreviations

AMNH, American Museum of Natural History, New York City, New York, USA.

BMNH, British Museum of Natural History, London, United Kingdom.

CMN, Canadian Museum of Nature, Ottawa, Ontario, Canada.

CU, Carleton University, Ottawa, Ontario, Canada.

CUG, China University of Geosciences, Wuhan, People's Republic of China.

GMU, George Mason University, Fairfax, Virginia, USA.

IGM, Institute of Geology, Ulanbaatar, Mongolia.

IMNH, Idaho Museum of Natural History, Pocatello, Idaho, USA.

INREC, Royal Belgian Institute of Natural Sciences, Brussels, Belgium.

IVPP, Institute of Vertebrate Paleontology and Paleoanthropology, Beijing, People's Republic of China.

JLUM, Jilin University Geological Museum, Changchun, People's Republic of China

KCL, King's College London, London, United Kingdom.

KDRC, Korea Dinosaur Research Center, Gwangju, Republic of Korea.

LACM, Natural History Museum of Los Angeles County, Los Angeles, California, USA.

MCF-PVPH, Museo Carmen Funes, Paleontologia de Vertebrados Plaza Huincul, Neuquen, Argentina.

MCZ, Museum of Comparative Zoology, Cambridge, Massachusetts, USA.

MOR, Museum of the Rockies, Bozeman, Montana, USA.

MPM, Museo Padre Molina, Santa Cruz, Argentina.

MUCPv, Museo Universidad Nacional del Comahue, Neuquen, Argentina.

NCSM, North Carolina Museum of Natural Sciences, Raleigh, North Carolina, USA.

ROM, Royal Ontario Museum, Toronto, Ontario, Canada.

RSM, Royal Saskatchewan Museum, Regina, Saskatchewan, Canada.

TMP, Royal Tyrrell Museum of Palaeontology, Drumheller, Alberta, Canada.

TNCC, Thomas Nelson Community College, Hampton, Virginia, USA.

UALVP, University of Alberta Laboratory of Vertebrate Palaeontology, Edmonton, Alberta, Canada.

UB, University of Bologna, Bologna, Italy.

UNE, University of New England, Armidale, New South Wales, Australia.

UNPSJB-Pv, Universidad Nacional de la Patagonia, San Juan Bosco, Argentina.

UofE, University of Edinburgh, Edinburgh, United Kingdom.

USNM, Smithsonian Natural History Museum, Washington, D.C., USA.

ZDM, Zigong Dinosaur Museum, Dashanpu, People's Republic of China.

Chapter 1. Introduction

Neornithischians were a major component of dinosaur dominated ecosystems, and include taxa more closely related to *Parasaurolophus* than to *Ankylosaurus* or *Stegosaurus* (Cooper, 1985). Within Neornithischia, Thescelosauridae is a poorly studied clade of small, cursorial, herbivorous bipeds that flourished from the Aptian to the Maastrichtian and were likely more abundant in Late Cretaceous dinosaur communities than their larger bodied relatives (Brown et al., 2013a, b). Historically, thescelosaurids were placed taxonomically in the now-defunct "Hypsilophodontidae" (Scheetz, 1999). Thescelosaurids have a comparatively sparse fossil record due to the vulnerability of their gracile skeletons due to postmortem damage (Brown et al., 2013a; O'Gorman and Hone, 2012). Divided taxonomically into Orodrominae and Thescelosaurinae, Thescelosauridae is a diverse but poorly studied group of small-bodied herbivores that existed in Asia, and in North and South America (Fig. 1.1). The evolutionary relationships amongst thescelosaurids are contentious, as is their position within Ornithischia, but they are considered to be basal (non-cerapodan) neornithischians, and to represent the sister group to cerapodans (Brown et al., 2013b; Boyd, 2015; Dieudonné et al., 2020; Herne et al., 2019; Madzia et al., 2018; Rozadilla et al., 2016).

Within the past decade, advances in thescelosaurid research have produced new insights into their paleobiology, paleoecology, biogeography, evolution, taxonomy, and systematics (Barrett and Han, 2009; Barta and Norell, 2021; Boyd et al., 2009; Han et al., 2012; Han et al., 2020; Krumenacker, 2017; Makovicky et al., 2011; Norell and Barta, 2016; Wyenberg-Henzler, 2020). However, thescelosaurids are severely understudied, and a number of intriguing and fundamental questions still need addressing (e.g., autapomorphy identification, basic anatomical

description, diversity, evolution, and growth and development). The lack of interest may be due to the oversimplified perception that they display a generalized, plesiomorphic ornithischian anatomy, and to their relatively sparse fossil record. However, the thescelosaurid fossil record is nevertheless significant, as it captures an important part of the otherwise underrepresented biodiversity of small-bodied Late Cretaceous ornithischians and, in particular, a non-cerapodan lineage that retained basal traits well into the Late Cretaceous.

1.1. Current Study

This thesis contains a review of the literature on Thescelosauridae (Chapter 2), descriptions of new partial skeleton from the Horseshoe Canyon Formation (Chapter 3), descriptions of new unassociated material from the Dinosaur Park and Wapiti Formations (Chapter 4), and qualitative and quantitative teeth differentiation between pachycephalosaurids and thescelosaurids (Chapter 5). The material described and analyzed within these chapters has broad implications for understanding thescelosaurid paleobiology, paleoecology, and evolution.

Chapter 2 serves as an extensive literature review of Thescelosauridae which introduces previous studies of the group, surveys unresolved problems pertaining to thescelosaurids, and proposes future avenues of research for investigation. Chapter 3 provides an osteological description and tests whether the new material (UALVP 56885) from the Horseshoe Canyon Formation represents a new specimen of *Parksosaurus warreni*, and establishes previously unrecognized postcranial autapomorphies for this species based on both the new specimen and the holotype (ROM 804). Investigation of the postcranial autapomorphies of *P. warreni* sheds light on the need for future research on postcranial differences among, and identification of autapomorphies in basal neornithischians, in general. Such studies will facilitate testing of

systematic hypotheses regarding the taxa in question. Chapter 4 provides an osteological description and tests whether the new material from the Dinosaur Park and Wapiti Formations indeed represent new thescelosaurid taxa, and examines the implications of the new material for understanding patterns of thescelosaurid evolution in Alberta during the Campanian. Chapter 5 tests whether there are dental differences between pachycephalosaurids and thescelosaurids, through qualitative descriptions and quantitative morphometric analysis of *in situ* tooth series preserved in the pachycephalosaurid *Stegoceras validum* and the thescelosaurid *Thescelosaurus neglectus*. The analyses within Chapter 5 will facilitate accurate identification of isolated teeth in microfossil sites and museum settings, and will have implications for understanding the paleoecology of both pachycephalosaurids and thescelosaurids.

1.2. Tables and Figures

A.

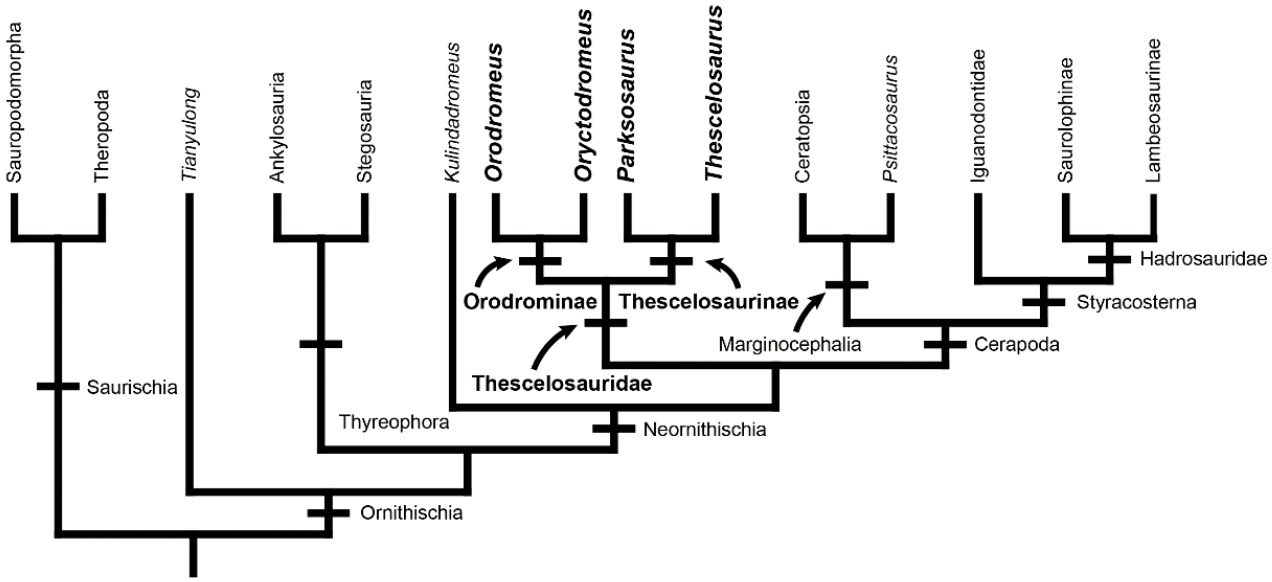

(B.) Thescelosauridae
Boyd, 2015
MPT: 36
TL: 868
CI: 0.37
RI: 0.65

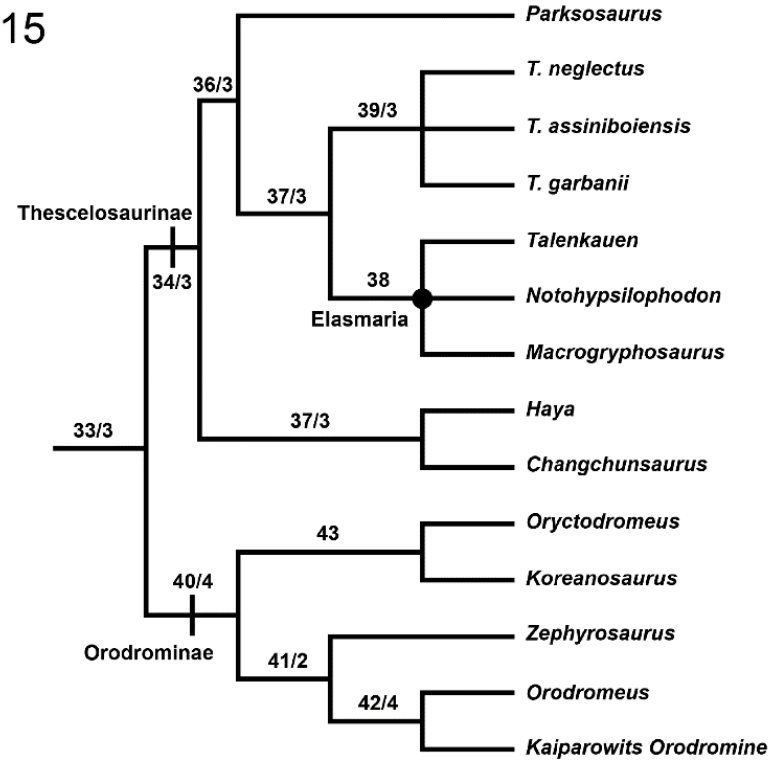

Figure 1.1. Phylogenetic overview of Thescelosauridae within Ornithischia.

(A) Phylogeny of Ornithischia and the placement of Thescelosauridae within this clade. (B) Evolutionary relationships of taxa within Thescelosauridae from Boyd (2015). Values to the left of "/" are bootstrap values and to the right are Bremer support >1. Abbreviations: MPT, most parsimonious tree; TL, tree length; CI, consistency index; RI, retention index.

Chapter 2. From Neglected to Appreciated: A Review of the Literature on the Paleobiology and Evolution of Thescelosauridae

2.1. Introduction

Within the clade Neornithischia, Thescelosauridae were small cursorial herbivorous bipeds that flourished from the Aptian to the Maastrichtian. Their fossil record is fragmentary due to the vulnerability of their gracile skeletons to post-mortem destruction (Brown et al., 2013a, b; O'Gorman and Hone, 2012), and is interrupted by large ghost lineages (Boyd, 2015). The evolutionary relationships of taxa within Thescelosauridae are contentious, as is their overall position within Ornithischia. However, they are considered to be basal neornithischians (non-cerapodans), sister to cerapodans (all descendants of the most recent common ancestor of *Parasaurolophus* and *Triceratops*), in contrast to earlier suggestions that they belonged within Ornithopoda (all taxa more closely related to *Parasaurolophus* than to *Triceratops*) (Brown et al., 2013b; Boyd, 2015; Dieudonné et al., 2020; Madzia et al., 2018; Sereno, 1986 and 1999). Thescelosauridae can be divided taxonomically into Orodrominae and Thescelosaurinae, with thescelosaurines having longer skulls and larger, more robust bodies than orodromines (Fig. 2.1 and 2.2). Thescelosaurines have a wide distribution throughout Argentina, western North America, northeast China, and Mongolia, and are confined to the Aptian - Maastrichtian (126-66 Ma) (Ogg and Hinnov, 2012). The oldest known thescelosaurine occurs in the Quantou Formation (*Changchunsaurus*) and the youngest (*Thescelosaurus*) occurs in various Maastrichtian age formations of Canada and the United States (Brown et al., 2011; Fisher et al., 2000; Gilmore, 1913; Morris, 1976; Zan et al., 2005). Orodromine taxa are confined to the Aptian - Campanian (125-76 Ma) of North America and Asia, with the oldest (*Zephyrosaurus*)

occurring in the Cloverly Formation of Montana and the youngest (*Albertadromeus*) occurring in the Oldman Formation of Alberta (Brown et al., 2013b; Ogg and Hinnov, 2012; Sues, 1980).

Despite the clade's poor fossil record, recent advances in thescelosaurid research have produced new insights into their, biogeography, evolution, paleobiology, systematics, and taxonomy. Furthermore, the record does capture an important part of the otherwise underrepresented fossil biodiversity of small-bodied Late Cretaceous ornithischians and represents a non-cerapodan lineage that retained basal neornithischian traits well into the Late Cretaceous. This chapter briefly reviews and discusses individual thescelosaurid taxa and the research on their biogeography, evolution, and paleobiology. Future research should focus on establishing and identifying homologies and autapomorphies among thescelosaurids; describing new fossil material; testing hypotheses about their paleobiology, paleoecology, and evolution; critically reassessing their morphological characters and establishing robust phylogenies; and using osteohistology to investigate their ontogeny, and to establish growth curves.

2.2. Materials and Methods

The broad overview of thescelosaurids presented in this chapter is based on information gathered by scouring the published literature. Specimens discussed in this chapter were examined either firsthand or through digital imagery. This chapter avoids making taxonomic revisions. "Small-bodied" is a relative size definition used in this chapter and is based on femoral length. The use of "small-bodied" should be interpreted as a comparative scale when discussing thescelosaurid body sizes relative to Ornithischia as a whole. Ankylosaurids (380-770 mm femoral length), Ceratopsidae (567-1030 mm femoral length), and Hadrosauridae (565-1650 mm

femoral length) are large-bodied whereas Thescelosauridae are small bodied (128-428 mm femoral length). See Appendix A for raw femoral lengths of Late Cretaceous ornithischians.

2.3. Phylogenetic Definitions

The evolutionary relationships among thescelosaurids and their position within Ornithischia are extremely problematic. In general, the evolutionary relationships of basal ornithischians are in need of additional research. Multiple researchers have developed data sets in order to investigate various parts of the basal neornithischian (non-cerapodan) tree using parsimony-based analyses, and have obtained disparate topologies (Boyd et al., 2009; Boyd, 2015; Brown et al., 2013b; Butler et al., 2008; Dieudonné et al., 2016, 2020; Herne et al., 2019; Madzia et al., 2018; Rozadilla et al., 2016). Several of these workers did not recover Thescelosauridae as a monophyletic group (Butler et al., 2008; Dieudonné et al., 2016 and 2020; Herne et al., 2019; Rozadilla et al., 2016). Thescelosaurid phylogenies, and basal neornithischian phylogenies in general, are often in conflict because their fossil record is fragmentary with low sample sizes (Brown et al., 2013a, b; Butler et al., 2008; Irmis et al., 2007; O'Gorman and Hone, 2012; Scheetz, 1999; Spencer, 2007; White et al., 1998), causing misinterpretations of their anatomy and evolution from a lack of comparable material with other taxa (Boyd et al., 2009; Galton, 1995; Irmis et al., 2007; Morris, 1976; Zheng et al., 2012). Their poor fossil record is due at least in part to a taphonomic bias against the preservation of small-bodied animals in favor of larger body sizes in dinosaur dominated communities (Brown et al., 2013a, b; O'Gorman and Hone, 2012). This leads to phylogenies with large ghost lineages for small-bodied animals (Boyd, 2015). Furthermore, there is a lack of detailed anatomical comparisons of basal neornithischians that would establish cranial and postcranial autapomorphies and homologies

(Brown et al., 2011; Brown et al., 2013a; Parks, 1926; Morris, 1976; Sues, 1980; Zheng et al., 2012), causing researchers to focus on developing characters for one area of the ornithischian tree without considering how other parts of the tree might be affected (Boyd, 2015; Dieudonné et al., 2016 and 2020).

Previous research on the phylogenetics of basal ornithischians has been unduly limited in scope, in that studies have tended to include too few taxa and concentrate on particular geographic areas (Butler et al., 2008; Scheetz, 1999; Spencer, 2007). Spencer (2007) focused on relatively complete ornithischians and disregarded informative fragmentary taxa. Scheetz (1999) largely sampled basal ornithischians from North America, geographically biasing the analysis. Concentrating on basal ornithischians, Butler et al. (2008) attempted to address the relationships of ornithischians from around the world, but achieved only limited phylogenetic resolution.

Despite the quagmire of understanding thescelosaurid relationships, this thesis for simplicity follows three phylogenetic analyses that have recovered Thescelosauridae as a monophyletic group. These analyses were originally conducted to resolve different parts of the neornithischian tree. Brown et al.'s (2013b) character matrix was modified from Boyd et al. (2009) and was developed to resolve the taxonomy of, and determine relationships amongst Late Cretaceous small-bodied non-cerapodan ornithischians of North America. The phylogeny of Boyd (2015) was derived from various published matrices (Butler et al., 2008; Scheetz, 1999; Weishampel and Heinrich, 1992; Weishampel et al., 2003) and was developed to determine the interrelationships of basal neornithischians. Madzia et al.'s (2018) character matrix was modified from Boyd (2015) and was developed to assess the phylogenetic position of *Burianosaurus* amongst non-ankylopollexian ornithopods.

These three analyses recovered Thescelosauridae as a monophyletic group, divided taxonomically into the subclades Orodrominae and Thescelosaurinae. In one analysis (Boyd, 2015), Elasmaria was recovered as a small monophyletic clade (*Macrogryphosaurus*, *Notohypsilophodon*, and *Talenkauen*) nested within Thescelosaurinae, a finding tentatively accepted here.

The Boyd (2015), Brown et al. (2013b), and Madzia et al. (2018) analyses largely agree with respect to the relationships of Thescelosauridae amongst Ornithischia and the relationships of thescelosaurids within their clades (Fig. 2.3). However, the analyses disagree regarding the position of some taxa within Orodrominae and Thescelosaurinae, and regarding whether Elasmaria is inside or outside Thescelosauridae. Boyd (2015) found that *Jeholosaurus* forms a clade with *Yueosaurus* that is sister to *Othnielosaurus*, whereas Brown et al. (2013b) recovered *Jeholosaurus* within Thescelosaurinae, in a polytomy with other Asian thescelosaurines (Fig. 2.3). Brown et al. (2013b) did not include *Koreanosaurus* within the original analysis (Fig. 2.3). A major difference is that Madzia et al. (2018) recover the Asian thescelosaurids (*Changchunsaurus* and *Haya*) as basal orodromines, whereas Boyd (2015) and Brown et al. (2013b) found them to be basal thescelosaurines (Fig. 2.3). Boyd (2015) recovered the endemic South American clade Elasmaria within Thescelosaurinae as sister to the genus *Thescelosaurus* (Boyd, 2015; Calvo et al., 2007). Elasmarians where not included in the Brown et al.'s (2013b) analysis, however, this group has occupied different parts of the ornithischian tree (Dieudonné et al., 2016 and 2020; Herne et al., 2019; Madzia et al., 2018; Rozadilla et al., 2016). Madzia et al. (2018) does not recover this clade within Thescelosauridae, but rather in a basal position within Ornithopoda, as sister to Iguanodontia. However, *Notohypsilophodon*, which has been recovered

as an elasmarian in previous analyses, was recovered in a large polytomy with other North American thescelosaurines (Boyd, 2015; Madzia et al., 2018) (Fig. 2.3). Brown et al. (2013b) recovered *Jeholosaurus* in a polytomy with *Changchunsaurus*, *Haya*, and *Thescelosaurus* within Thescelosaurinae. However, in this thesis I do not consider *Jeholosaurus* to be a thescelosaurid, as this taxon has been placed outside Thescelosauridae and within a separate, monophyletic Jeholosauridae based on multiple analyses (Boyd, 2015; Dieudonné et al., 2020; Madzia et al., 2018).

Thescelosauridae (Sternberg, 1937) is a stem-based clade including all neornithischians more closely related to *Parksosaurus* (Parks, 1926) than to *Hypsilophodon* (Huxley, 1869), *Dryosaurus* (Marsh, 1878), or *Parasaurolophus* (Parks, 1922). Initially erected by (Sternberg, 1937) to differentiate *Thescelosaurus* from *Hypsilophodon*, Thescelosauridae was given a new phylogenetic definition by Brown et al. (2013b), but still fulfilled its original function of highlighting the diversity within small-bodied non-cerapodan ornithischians. Synapomorphies assigned to Thescelosauridae, and the subclades within, vary between analyses, but anatomical features that designate Thescelosauridae occur within the skull and hindlimb (Boyd, 2015; Brown et al., 2013b).

Nested within Thescelosaurinae, Elasmaria (Calvo et al., 2007) is a node-based clade including *Talenkauen* (Novas et al., 2004), *Macrogryphosaurus* (Calvo et al., 2007) and their most recent common ancestor and all descendants. Calvo et al. (2007) originally diagnosed Elasmaria by two unambiguous synapomorphies where epipophysis are present on cervical vertebra three and thin mineralized plates are present on the lateral thoracic ribcage. The mineralized plates were interpreted as uncinate processes that aided in thoracic movements of the

thorax (Calvo et al., 2004; Novas et al., 2004), but their presence does not diagnose Elasmaria as they are widely distributed in other basal neornithischians such as *Hypsilophodon*, *Othnielosaurus*, *Parksosaurus*, and *Thescelosaurus*. The diagnosable characters for Elasmaria cannot be assessed in *Notohypsilophodon* and it is unclear if these two characters unite all Elasmaria (Boyd, 2015). Elasmarian synapomorphies occur within the vertebral series, pelvic girdle, and forelimb (Boyd, 2015). However, Elasmaria was not recovered as an inclusive clade in other analyses (Dieudonné et al., 2016 and 2020; Herne et al., 2019; Madzia et al., 2018; Rozadilla et al., 2016). For simplicity, this paper considers Elasmaria as clade nested within Thescelosaurinae. However, improved phylogenetic analyses ultimately may not recover them within Thescelosauridae.

Orodrominae (Brown et al., 2013b) is a stem-based clade including all neornithischians more closely related to *Orodromeus* (Horner and Weishampel, 1988) than to *Thescelosaurus* (Gilmore, 1913) or *Parasaurolophus* (Parks, 1922). This clade was established to differentiate taxa more closely related to *Orodromeus* from those more closely related to *Thescelosaurus* (Thescelosaurinae). Orodrominae synapomorphies occur in the skull, vertebral series, pelvic girdle, and fore- and hindlimb (Boyd, 2015; Brown et al., 2013b).

Thescelosaurinae (Sternberg, 1940) is a stem-based clade including all neornithischians more closely related to *Thescelosaurus* (Gilmore, 1913) than to *Orodromeus* (Horner and Weishampel, 1988) or *Parasaurolophus* (Parks, 1922). Thescelosaurinae (Sternberg, 1940) was originally erected to differentiate *Thescelosaurus* from *Dysalotosaurus*, *Hypsilophodon*, and *Parksosaurus*. *Thescelosaurus* and *Parksosaurus* were recognized as sister taxa (Boyd et al., 2009) and were later united as a stem-based clade (Brown and Druckenmiller, 2011). Boyd

(2015) recovered Thescelosaurinae within Thescelosauridae and Elasmaria as sister to the genus *Thescelosaurus*, to the exclusion of all other thescelosaurids (Fig. 2.3). Thescelosaurinae synapomorphies occur in the skull, dorsal ribs, pelvic girdle, and hindlimb (Boyd, 2015; Brown et al., 2013a).

2.4. Thescelosauridae Taxa

2.4.1. *Albertadromeus syntarsus*

Albertadromeus is a small-bodied thescelosaurid represented by one fragmentary postcranial skeleton from the Oldman Formation (Campanian) of southern Alberta consisting of dorsal and caudal vertebrae, ossified tendons, tibia, fibulae, metatarsals, and unguals (Brown et al., 2013b; Ogg and Hinnov, 2012). Despite the fragmentary nature of the holotype, two autapomorphies were present: reduction of the distal end of the fibula to a thin sheet of bone fused to the anterior surface of the tibia, and lateral condyle of the proximal tibia is strongly bilobed with a prominent, dorsally projecting cnemial crest. The fusion of the distal fibula to the tibia has been interpreted as an adaptation for cursoriality, and has not been documented in other thescelosaurids and cerapodans, although it also occurs in heterodontosaurids (Brown et al., 2013b). However, this purported correlation between fibular morphology and cursorial behavior has not been tested empirically. The phylogenetic position of *Albertadromeus* is difficult to determine because the only available specimen is so fragmentary, but Brown et al. (2013b) and Madzia et al. (2018) recovered *Albertadromeus* within Orodrominae.

2.4.2. *Changchunsaurus parvus*

Changchunsaurus is from Jilin Province of the People's Republic of China and was collected from Quantou Formation (Aptian-Cenomanian). The holotype of *Changchunsaurus* is a partially preserved skeleton consisting of the cervical and dorsal vertebral series, some dorsal ribs and a partial skull (Butler et al., 2011; Jin et al., 2010; Ogg and Hinnov, 2012; Zan et al., 2005) (Fig 2.4, 2.5). *Changchunsaurus*, a small-bodied thescelosaurid, is characterized by three autapomorphies: an elongate and narrow foramen on the midline of the premaxillary palate, medial to crowns three and four; a thickened and slightly rugose dorsolateral surface of the dentary adjacent to the first three dentary teeth; and a groove extending anteromedially along the lateral surface of the distal half of the dentary and onto the medial surface of the coronoid process. Potentially the oldest thescelosaurine, *Changchunsaurus* was originally described by Zan et al. (2005), who summarized the taxon's anatomy but did not identify autapomorphies. Jin et al. (2010) and Butler et al. (2011) redescribed the cranial and postcranial material and identified autapomorphies in the skull. Phylogenetic analyses that have included *Changchunsaurus* typically place it as part of a radiation within Thescelosaurinae of small-bodied Asian taxa (Boyd, 2015; Brown et al., 2013b) or within the orodromine clade (Madzia et al., 2018). The Asian clade has typically been found to include *Haya* and *Jeholosaurus* (Brown et al., 2013b), but some analyses have found *Changchunsaurus* to group only with *Haya* (Boyd, 2015; Madzia et al., 2018).

2.4.3. *Haya griva*

Haya griva is a thescelosaurid that is known from a handful of individuals from the Javkhlant Formation (Santonian(?):86.3-83.6 Ma) of Dorngobi Province, Mongolia (Barta and

Norell, 2021; Norell and Barta, 2016; Makovicky et al., 2011; Ogg and Hinnov, 2012) (Fig. 2.4, 2.5). The skeleton is completely known from this taxon because multiple individuals have been combined, and different stages of growth are represented by individual partial skeletons (Barta and Norell, 2021; Norell and Barta, 2016; Makovicky et al., 2011). *Haya* represents a small-bodied thescelosaurid with the largest specimen having a femoral length of 148 mm (Barta and Norell, 2021). Makovicky et al. (2011) could not establish autapomorphies in *Haya* due to the complex distribution of characters and unresolved phylogenies in basal neornithischians. However, Makovicky et al. (2011) did provide five potential autapomorphies including: five homodont, bulbous, unserrated premaxillary teeth; an absent rugosity on the ramphothecal pad of the premaxilla; triangular accessory maxillary fenestrae; a bifid posterior ramus on the jugal that contacts the quadratojugal; a quadratojugal foramen; a midline depression running along the internasal suture; and a bifid ventral ramus on the predentary. Barta and Norell (2021) added an additional skull autapomorphy where the anterior process of the jugal is bifid. However, several of these autapomorphies are common throughout Thescelosauridae (e.g., premaxillary tooth morphology and presence of a quadratojugal foramen). The phylogenetic resolution of *Haya* is contentious, which overall reflects the phylogeny of basal neornithischians (Barta and Norell, 2021; Boyd, 2015; Han et al., 2018; Madzia et al., 2018) as this taxon can either be an orodromine or a thescelosaurine.

2.4.4. Kaiparowits Orodromine

This taxon is known only from the Kaiparowits Formation (Campanian: 83.6-72.1 Ma) of Utah. The fragmentary skeletal remains consist of cranial and postcranial elements from multiple individuals and the specimens were identified as an immature individual. Autapomorphies that

distinguish the Kaiparowits Orodrominae from other orodromines include: a postorbital with a ventral ramus that inserts into the anterolateral margin of the jugal dorsal ramus; an ovoid foramen on the ventral margin of the sternal process of the coracoid; and two rather than three phalanges on manual digit IV (Boyd, 2012). Boyd (2015) recovered the Kaiparowits Orodrominae within Orodrominae, as sister to *Orodromeus*.

2.4.5. *Koreanosaurus boseongensis*

Consisting of five cervical vertebrae, seven dorsal vertebrae, seventeen dorsal ribs, nearly complete right and left scapulae, coracoids, sternal plates, the proximal part of the left humerus and an incomplete right humerus, and the proximal parts of the left ulna and radius, to the holotype of *Koreanosaurus* is a small-bodied orodromine from the Seonso Conglomerate (Santonian(?)-Campanian: 86.3-72.1 Ma) of the Republic of Korea (Boyd, 2015; Huh et al., 2010; Ogg and Hinnov, 2012). *Koreanosaurus* is diagnosed by the following characters: elongate anterior cervicals; a highly keeled posterior border of proximal ulna; femoral head and shaft form an obtuse angle; and anteroposteriorly elongate femoral head. Other characters initially identified as putative autapomorphies of *Koreanosaurus* include a blade-like keel present on the ventral surface of each cervical centrum; sharp ventral keel on each of the centra of the first seven dorsals; a fused scapulocoracoid plate; and a low tibia/femur length ratio where the tibia is unusually short relative to the femur. However, at least some of these putative autapomorphies are ontogenetically variable and/or common throughout Orodrominae or even Thescelosauridae. Common throughout Orodrominae are the sharp ventral keels on the cervical and dorsal centra (Scheetz, 1999; Varricchio et al., 2007). Fusion of the scapulocoracoid plates is present in *Orodromeus* and *Oryctodromeus* and is an ontogenetic feature that diagnoses skeletal maturity

(Krumenacker, 2017). The hindlimb ratio in *Koreanosaurus* is similar to *Thescelosaurus* (Gilmore, 1915; Galton, 1974b; Galton, 1995). *Koreanosaurus* and *Oryctodromeus* are sister taxa with similar morphologies, which suggests that *Koreanosaurus* had a fossorial lifestyle (Boyd, 2015; Huh et al., 2010; Varricchio et al., 2007). Further evidence that *Koreanosaurus* was fossorial includes the shortness of both the femur and the tibia, relative to the forelimb. Such proportions also indicate that *Koreanosaurus* was quadrupedal (Huh et al., 2011). In addition, the femoral head forms an angle of 135° with the shaft, which would have enabled *Koreanosaurus* to abduct the hindlimbs through a large angle as in burrowing mammals (Huh et al., 2011).

2.4.6. *Macrogryphosaurus gondwanicus*

Macrogryphosaurus is a large-bodied elasmarian from the Coniacian Portezuelo Formation of Argentina (Calvo et al., 2007; Ogg and Hinnov, 2012). This taxon is based on a partially articulated specimen consisting of the cervical, dorsal, sacral, and caudal vertebral series, thoracic ribs, ilia, pubes, and sternal plates. *Macrogryphosaurus* is distinguished from other thescelosaurids by the following autapomorphies: three processes extend from the anterior border of each sternal plate; sternal ribs are flattened, twisted, and distally expanded; and the last dorsal vertebra has a well-developed hyposphene (Calvo et al., 2007). The mineralized sternal plates were originally interpreted as an autapomorphy; however, this feature is common in other thescelosaurids and basal neornithischians, and is present in *Hypsilophodon*, *Othnielosaurus*, *Parksosaurus*, *Talenkauen*, and *Thescelosaurus* (Boyd et al., 2011; Fisher et a., 2000; Huxley, 1870; Marsh, 1877; Novas and Cambiaso, 2004; Parks, 1926). Calvo et al. (2007) originally recovered *Macrogryphosaurus* as a basal euiguanodontian (Ankylopollexia, Dryosauridae, *Gasparinisaura*, and all their most recent common ancestors and all descendants) that formed a

new clade, Elasmaria, with *Talenkauen* (Boyd, 2015). Boyd (2015) recovered *Macrogryphosaurus* as sister to the genus *Thescelosaurus* within Thescelosaurinae.

2.4.7. *Notohypsilophodon comodorensis*

Notohypsilophodon is a South American taxon from the Bajo Barreal Formation of Argentina. Cenomanian (100.5-93.9 Ma) in age, the holotype of *Notohypsilophodon* is a partial skeleton consisting of cervical, dorsal, sacral, and caudal sacral series, thoracic ribs, pectoral girdles, fore- and hindlimbs, ankle material, and pes (Martinez, 1998; Ogg and Hinnov, 2012). Autapomorphies diagnosing *Notohypsilophodon* are an anteromedial bulge on the proximal extremity of the tibia, a pronounced posterodistal projection on the calcaneum, a strongly posteriorly directed sacral neural spine, and a reduced sternal process on the coracoid (Ibiricu et al., 2014; Martinez, 1998). Boyd (2015) recovered *Notohypsilophodon* in Elasmaria. However, the only known specimen of *Notohypsilophodon* is too incomplete for the presence of the synapomorphies that diagnosis Elasmaria to be assessed (Boyd, 2015).

2.4.8. *Orodromeus makelai*

Orodromeus makelai is an orodromine that is represented by numerous individuals and has been recovered from the Two Medicine Formation Egg Mountain site in the Willow Creek Anticline of Montana (Horner and Weishampel, 1988; Scheetz, 1999) (Fig. 2.4). The complete skeleton of this taxon is known from the multiple individuals at various stages of development. This small-bodied Late Campanian (83.6-72.1 Ma) taxon is distinguished from other thescelosaurids based on the palpebral being anchored to the postorbital; a lateral boss is present on the jugal; the maxillary and dentary teeth are broadly triangular in lateral view; a rounded

apical ridge subequally divides the anterior and posterior regions of the crown; the anterior and posterior edges of the crown each bear five to six uniformly sized denticles; and the radiale, intermedium, ulnare, and one distal carpal form an unfused wrist. *Orodromeus* was the first reported orodromine from North America. It was initially described by Horner and Weishampel (1988), although detailed comparative work was later done in an unpublished thesis by Scheetz (1999). Based on the phylogeny of Boyd's (2015), *Orodromeus* is a thescelosaurid orodromine that is sister to *Zephyrosaurus*.

2.4.9. *Oryctodromeus cubicularis*

The entire skeleton of *Oryctodromeus* is known, based on numerous individuals at various stages of growth. *Oryctodromeus* is recovered from the Vaughn Member of the Blackleaf Formation in Montana and the Wayan Formation of Idaho. The two formations are Albian-Cenomanian (113-93.9 Ma) in age (Ogg and Hinnov, 2012). *Oryctodromeus* was initially described by Varricchio et al. (2007), and additional material was described in Krumenacker's (2017) unpublished dissertation. Autapomorphic features of *Oryctodromeus* are long paraoccipital processes; basioccipital with a steeply sided ventral box that is anterior to the occipital condyle; seven sacral vertebrae, a large scapula with a sharply angled and narrow acromion process with a scapular spine and a distinct posterior bend to the scapular blade; an ilium with short preacetabular process and long postacetabular process; a brevis shelf that slopes mediolaterally; and a long prepubic process with a transversely broad proximal portion possessing an elongate ventral fossa. Referred specimens potentially provide additional diagnosable characters for *Oryctodromeus* such as vertebral count, and the dimensions, morphologies of the coracoid, ulna, femur, and ankle (Krumenacker, 2017). The cervical

vertebrate are elongate, dorsal vertebrae are tall; sacral vertebrae are short dorsoventrally and have articular faces that are transversely expanded with W or U-shaped cross sections; elongate caudal vertebrae; a coracoid with an elongate ovoid fossa below the glenoid cavity; a robust olecranon process; a femoral head with the neck projecting from the femoral shaft at 38°; a laterally flattened greater trochanter; a modest to weak anterior intercondylar groove on the distal end of the femur; and an ascending process of the astragalus that bifurcates. *Oryctodromeus* has a relatively extensive geographical range compared to other orodromines (Krumenacker, 2017; Varricchio et al., 2007). Varricchio et al. (2007) reported that *Oryctodromeus* had a fossorial lifestyle based on forelimb features, despite having forelimb and hindlimb proportions suggestive of cursoriality (Carrano, 1999). Boyd (2015) recovered *Oryctodromeus* within the Orodrominae clade, sister to *Koreanosaurus*.

2.4.10. *Parksosaurus warreni*

Parks (1926) described a partial thescelosaurid skeleton from Alberta under the name *Thescelosaurus warreni*, a putative new species of *Thescelosaurus*. He referred it to the now defunct taxonomic group "Hypsilophodontidae". Sternberg (1937) subsequently reassigned ROM 804 to the new genus *Parksosaurus* as *Parksosaurus warreni* based on morphological comparisons with *Thescelosaurus neglectus* (USNM 7757). Clarifying the differences between *Parksosaurus* and *Thescelosaurus*, additional research identified that *Parksosaurus* lacked skull autapomorphies and characteristic hindlimb proportions of *T. neglectus* (Boyd et al., 2009; Galton, 1973, 1974; Sternberg, 1940). *Parksosaurus* is considered to be a thescelosaurine, and is from the early Maastrichtian Horseshoe Canyon Formation of southern Alberta, Canada (Brown and Druckenmiller, 2011; Boyd, 2015; Ogg and Hinnov, 2012; Parks, 1926) (Fig. 2.4).

Parksosaurus was smaller than the any of the known *Thescelosaurus* species, but is larger than the majority of other thescelosaurid taxa, with a maximum femoral length of 270 mm (Brown, 2009). The cranial autapomorphies of *Parksosaurus* include: a deep posterior process of the premaxilla; extensive sutural contact between maxilla and nasal; a small, oval antorbital fenestra; a transversely wide squamosal; and each cheek tooth has one well-enameled surface bearing numerous low, round ridges (Galton, 1995). *Parksosaurus* does not have any of the autapomorphic features present in *Thescelosaurus*, however, the presence of some of these features cannot be assessed because the relevant parts of the skeleton are not preserved in the holotype.

2.4.11. *Talenkauen santacrucensis*

Collected form the Maastrichtian age Pari Aike Formation of Argentina, *Talenkauen* is a partially articulated skeleton that includes the premaxilla, maxilla, dentary; cervical, dorsal, and sacral vertebrae; ribs, pectoral and pelvic girdles, and fore and hindlimbs. At ~4 meters in length, *Talenkauen* is first large-bodied non-iguanodontian ornithischian recovered from South America (Novas and Cambiaso, 2004). Autapomorphies of *Talenkauen* consist of a well-developed epipophysis on cervical three; the lacrimal and premaxilla do not contact each other; and the dentaries are convergent anteriorly. *Talenkauen* possesses intercostal plates in its thoracic rib region, as in *Macrogryphosaurus, Parksosaurus* and *Thescelosaurus* (Fisher et al., 2000; Parks, 1926). The intercostal plates in *Macrogryphosaurus*, *Parksosaurus*, *Talenkauen*, and *Thescelosaurus* may have had a function in aiding respiration (see subsequent section on respiration). Boyd (2015) recovered *Talenkauen* in Elasmaria.

2.4.12. *Thescelosaurus*

Thescelosaurus is known from a handful of specimens that have been classified into three separate species. It is the largest-bodied thescelosaurid taxon. Occurring during the Maastrichtian (72.1-66 Ma) of North America, the largest *Thescelosaurus* femur is 534 mm (Brown, 2009; Ogg and Hinnov, 2012) (Fig. 2.4). *Thescelosaurus* specimens can be found in Canada and the United States in the Frenchman Formation of Saskatchewan, the Scollard Formation of Alberta, the Hell Creek Formation of Montana and South Dakota, and the Lance Formation of Wyoming. *Thescelosaurus* was the first thescelosaurid to be described by Charles Gilmore (1913). He initially placed it in the Camptosauridae but after further osteological description in 1915, he placed it in the now defunct 'Hypsilophodontidae' based on similarities with *Hypsilophodon* (Scheetz, 1999). *Thescelosaurus* autapomorphies include: frontals that are mediolaterally wider than anteroposteriorly long at the midorbital margin; a prominent horizontal ridge the on maxilla covered by a series of coarse, rounded, obliquely inclined ridges posterodorsally; a depression on the posterior half of ventral edge of the jugal covered by anterolaterally obliquely inclined ridges; and a foramen on the dorsal surface of the prefrontal that is dorsomedial to sutural surface for palpebral that opens into the orbit. Two additional characters are likely to be unique in *Thescelosaurus* but cannot be evaluated in the sister taxon *Parksosaurus*. These unique characters include the dorsal edge of the opisthotic is idented by a deep 'Y-shaped' excavation in dorsal view; and the palpebral is flattened dorsoventrally and rugose along the medial and distal margins (Boyd et al., 2009). Furthermore, two additional characters are considered to be local apomorphies for *Thescelosaurus*, but converge with other neornithischians or cannot be evaluated in other thescelosaurids. These local apomorphies include the angle between the

ventral margin of the braincase and the posterodorsal hypoglossal foramen, where a line is drawn through the center of the trigeminal foramen and is less than fifteen degrees; and the femur is longer than the tibia (Boyd et al., 2009; Galton, 1974b, 1995). The systematic position of *Thescelosaurus* has been revisited numerous times (Boyd et al., 2009; Galton, 1974b, 1995). Historically, the genus has been thought to be closely related to *Camptosaurus* (Gilmore, 1913) and *Hypsilophodon* (Gilmore, 1915), and has been placed either within its own group Thescelosaurinae (Sternberg, 1937) or the Iguanodontidae (Galton, 1974b). Recent phylogenetic analyses place all species of *Thescelosaurus* outside Cerapoda in their own distinct clade (Thescelosauridae, Thescelosaurinae) with other closely related Asian, North American, and potentially South American relatives (Boyd, 2015; Brown et al., 2013b; Madzia et al., 2018).

2.4.12.1. *Thescelosaurus neglectus*

Recovered from the Lance and Hell Creek Formation, *Thescelosaurus neglectus* is known from four specimens and is Maastrichtian (72.1-66 Ma) in age (Fig. 2.4). The holotype (USNM 7577) was recovered from the Lance Formation and is a nearly complete postcranial skeleton, although the skull and cervical vertebrae are not preserved (Gilmore, 1915). The paratype (USNM 7758) comprises fragmentary cranial and postcranial remains (Boyd et al., 2009). Referred specimens include NCSM 15728 and TLAM.BA.2014.027.0001. NCSM 15728 postcranial skeleton is partially complete, whereas the skull is complete and was collected from the Hell Creek Formation. It was initially reported but not described by Fisher et al. (2000). An extensive description of the skull (NCSM 15728) and other *T. neglectus* skull material (TLAM.BA.2014.027.0001) was published by Boyd (2014). However, a description of the postcranial skeleton still needs to be done. *T. neglectus* is distinguished from other

Thescelosaurus species by a couple of characters such as: the exclusion or inclusion of the calcaneum in the midtarsal joint; the shapes of the squamosals; and a foramen present on the supraoccipitals (Brown et al., 2011; Boyd et al., 2009; Morris, 1976).

2.4.12.2. *Thescelosaurus garbanii*

Thescelosaurus garbanii (LACM 33542) is represented only by a fragmentary postcranial skeleton consisting of cervical and dorsal vertebrae, the distal end of the femur, tibia, fibula, tarsus, and the left pes. It was recovered from the Hell Creek Formation of Montana (Maastrichtian: 72.1-66 Ma) (Morris, 1976; Ogg and Hinnov, 2012). *T. garbanii* is linearly one third larger than *Thescelosaurus neglectus*, and was diagnosed by an autapomorphic exclusion of the calcaneum from the midtarsal joint by the laterally expanded astragalus. Galton (1995) referred the specimen to "*Bugenasaura*". However, there are no elements of the skeleton that can be directly compared between the only known specimens of "*Bugenasaura*" and *T. garbanii*. Boyd et al. (2009) separated "*Bugenasaura*" from *T. garbanii* and referred *Bugenasaura* to *Thescelosaurus* sp. Exclusion of the calcaneum from the midtarsal joint is unique to *T. garbanii* as other comparable *Thescelosaurus* specimens (CMN 8537, MOR 979, RSM P.1225.1, and USNM 7757) lack this feature.

2.4.12.3. *Thescelosaurus assiniboiensis*

Thescelosaurus assiniboiensis is known from one specimen from the Frenchman Formation (Maastrichtian: 72.1-66 Ma) of Saskatchewan. It is based on a partial skeleton consisting of a partial skull, dorsal, sacral, and caudal vertebrae, dorsal ribs, pelvic girdle, and hindlimbs (Brown et al., 2011; Ogg and Hinnov, 2012). Two autapomorphies diagnosis this

species: the presence of convex posterior and dorsal margins of the squamosal; and a distinct foramen present on the supraoccipital passing through the roof of the myelencephalon to the dorsal surface. *T. assiniboiensis* is distinct from *Thescelosaurus garbanii* as the calcaneum participates in the midtarsal joint. Brown et al. (2011) noted that *T. assiniboiensis* may represent a skeletally immature individual due to its relatively small size, and discerned that the autapomorphies were not due to ontogenetic variation as the autapomorphies of *T. assiniboiensis* are not present in juvenile specimens of *T. neglectus*.

2.4.13. *Zephyrosaurus schaffi*

Zephyrosaurus schaffi is a small taxon based on one fragmentary specimen from the Himes Member of the Cloverly Formation, Montana (Sues, 1980) (Fig. 2.4). Aptian-Albian (126.3-100.5 Ma) in age, *Zephyrosaurus* is a partially preserved skeleton with only braincase, premaxillary, maxillary, dentary, cervical and dorsal vertebrae, and ribs. *Zephyrosaurus* is diagnosed by a diastema separating the premaxillary teeth from the maxillary teeth, a small anterolateral boss on the maxilla, narrow frontals, the expanded central portion of the postorbital, a short and massive supraorbital, and a quadrate with the dorsal head set off from the pterygoid flange. *Zephyrosaurus* is an understudied orodromine, although specimens of a potential *Zephyrosaurus* at the Noble Oklahoma Museum of Natural History in Oklahoma awaits description (Kutter, 2004). Several diagnosable features present in *Zephyrosaurus* are also present in other ornithischians such as the diastema between the premaxillary and maxillary teeth (present in *Heterodontosaurus*, *Stegoceras*, and *Thescelosaurus*) and narrow frontals (present in other Orodrominae) (Boyd, 2014; Brown et al., 2013b; Galton and Sues, 1983; Krumenacker,

2017; Norman et al., 2011). The phylogenetic analysis of Boyd (2015) recovers *Zephyrosaurus* within the clade Orodrominae.

2.5. Fossil Record

2.5.1. Biogeography and Distribution

Thescelosauridae have been found in sedimentary deposits extending from the middle Lower Cretaceous to the K/Pg Boundary (Fig. 2.6 and Table 2.1), and in North and South America, and Asia. Thescelosaurids have been primarily found in Cretaceous formations that were continental fluvial deposits laid down in floodplains or river channels that were seasonally variable (e.g., Hell Creek Formation, Horseshoe Canyon Formation, and Quantou Formation) (Bamforth et al., 2014; Brown et al., 2011; Brown et al., 2013a; Calvo et al., 2007; Currie and Koppelhus, 2005; Eberth et al., 2013; Freimuth and Varricchio, 2019; Gilmore, 1915; Ibiricu et al., 2014; Krumenacker, 2017; Krumenacker et al., 2019; Lyson and Longrich, 2011; Makovicky et al., 2011; Martinez, 1998; McIver, 2002; Morris, 1976; Novas and Cambiaso, 2004; Parks, 1926; Scheetz, 1999; Sternberg, 1940; Sues, 1980; Wang et al., 2009; Xu et al., 2009; Zan et al., 2005 and 2006).

The thescelosaurid fossil record exhibits a North American bias, as most taxa come from Upper Cretaceous (Aptian-Maastrichtian) strata of North America that yield members of the thescelosaurine and orodromine clades (Fig. 2.6 and Table 2.1). The earliest North American taxon is *Zephyrosaurus*, an orodromine, from the Himes Member in the Cloverly Formation (Aptian) of Montana (Sues, 1980). Thescelosaurids are present in North America right up to the K/Pg extinction and the three youngest thescelosaurids, all species of *Thescelosaurus*, coexisted

with such classic latest Cretaceous (68-66 Ma) dinosaurs as *Edmontosaurus annectens*, *Triceratops prorsus*, and *Tyrannosaurus rex* (Brown et al., 2011; Eberth et al., 2013; Fisher et al., 2000; Gilmore, 1913; Morris, 1976; Ogg and Hinnov, 2012). Thescelosaurid fossil material is not commonly found in bonebeds, except for the Frenchman Formation 'Convenience Store' locality in Saskatchewan (*Thescelosaurus* sp.), the Wapiti Formation Dinosaur-Chelonian Bonebed in Alberta (indeterminate thescelosaurines), and in microsites from the Scollard (*Thescelosaurus neglectus*) and Prince Creek Formations (an indeterminate thescelosaurine) of Canada and Alaska, respectively (Brown, 2009; Brown and Druckenmiller, 2011; Eberth et al., 2013). In the Campanian and Maastrichtian of southern Alberta, orodromines typically occur in the Belly River Group (Albian-Campanian) and thescelosaurines in the younger Edmonton Group (Maastrichtian) (Brown et al., 2013b; Hudgins et al., 2020a). These two stratigraphic groups are separated by shale deposits of the Bearpaw Formation, laid down during a Campanian transgression of the Western Interior Seaway. The transition from older orodromines to younger thescelosaurines is obscured by the Campanian transgression of the Western Interior Seaway.

Although rare, all South American thescelosaurids were collected from Argentina, belong to the thescelosaurine clade Elasmaria, and occur from the late Early Cretaceous to the Maastrichtian (Calvo et al., 2007; Ibiricu et al., 2014; Novas et al., 2004) (Fig. 2.6). The oldest South American thescelosaurid is *Notohypsilophodon*, and the youngest is *Talenkauen* (Ibiricu et al., 2014; Novas et al., 2004). The Bajo Barreal Formation has been dated to the Cenomanian based on Ar-Ar dating of volcanic tuff and ignimbrites and palynology studies (Martinez and Novas, 2006). Support for the age of the Pari Aike Formation is based on the biostratigraphy of foraminifera and dinoflagellates (Novas et al., 2004)

Asian thescelosaurids occur in China, Mongolia, and the Republic of Korea, range in age from Early to Late Cretaceous (Aptian-Campanian), and include relatively basal members of thescelosaurines and orodromines (Fig. 2.6). Asian thescelosaurid material has been found from various stratigraphic ages throughout the Cretaceous, including the Javkhlant Formation (Santonian) of Mongolia (Barta and Norell, 2021; Makovicky et al., 2011; Norell and Barta, 2016); the Seonso Conglomerate (Santonian-Campanian) of the Republic of Korea (Huh et al., 2011); and the Quantou Formation in the Songliao Basin (Aptian-Cenomanian) of the People's Republic of China (Butler et al., 2011; Jin et al., 2010). The oldest confirmed Asian thescelosaurid is *Changchunsaurus* from the Quantou Formation, and the youngest is *Koreanosaurus* from the Seonso Conglomerate. The Quantou Formation is estimated to be Aptian – Albian in age (Butler et al., 2011; Jin et al., 2010; Zan et al., 2006). The imprecise and long geologic time range of the Quantou Formation is based on the biostratigraphy of fossil invertebrates, plants, and microfossils, and widely ranging radiometrically dated basaltic intrusions (Zan et al., 2006). Based on isotopic dating, the age of the Seonso Conglomerate is thought to be Santonian to early Campanian (Huh et al., 2011). Well-preserved specimens of multiple individuals from *Haya* have been described and were collected from the Santonian aged Javkhlant Formation (Barta and Norell, 2021; Makovicky et al., 2011; Norell and Barta, 2016).

2.5.2. Evolution and Dispersal

Thescelosaurid evolution is poorly understood due to a preservational bias against small-bodied vertebrates in fossil assemblages (Brown et al., 2013b; O'Gorman and Hone, 2012; White et al., 1998), outdated anatomical descriptions (Gilmore, 1913; Gilmore, 1915; Parks, 1926), and an incomplete understanding of phylogenetic relationships amongst basal neornithischians in

general (Boyd et al., 2009; Boyd, 2015; Brown et al., 2013a; Butler et al., 2008; Dieudonné et al., 2016 and 2020; Herne et al., 2019; Madzia et al., 2018; Rozadilla et al., 2016). Within the past decade, several substantial discoveries and published descriptions of basal neornithischians (Barta and Norell, 2021; Boyd, 2014; Brown et al., 2011; Brown et al., 2013a; Butler et al., 2011; Huh et al., 2011; Jin et al., 2010; Krumenacker, 2017; Makovicky et al., 2011; Zheng et al., 2012) have substantially advanced scientific understanding of the evolution of thescelosaurids (Boyd, 2015), greatly extending and building upon the results obtained in previous research (Butler et al., 2008; Scheetz, 1999; Spencer, 2007).

Boyd (2015) produced the most recent analysis of thescelosaurid evolution and dispersal patterns, using parsimony and likelihood with equal branch lengths and time calibrated branch lengths set to the missing fossil record.

Boyd (2015) hypothesized that Thescelosauridae originated in North America, with at least two dispersals to Asia and South America. However, Thescelosauridae have a long ghost lineage that extends for 40 Ma, from the Bathonian to the Aptian. The phylogenetic position and geologic age of *Callovosaurus* (the oldest known cerapodan) causes the large ghost lineage between Thescelosauridae and Cerapoda (Boyd, 2015). A basal split between Orodrominae and Thescelosaurinae occurred during the Aptian in North America (Boyd, 2015). Asian thescelosaurines (*Changchunsaurus* and *Haya*) lived during the Aptian. Orodrominae appeared approximately in the early Late Cretaceous with the presence of *Koreanosaurus*. Interestingly, no thescelosaurines are known to occur in North America before the Maastrichtian (Boyd, 2015; Brown et al., 2013a; Hudgins et al., 2020a). Based on Boyd (2015), the biogeographic history of thescelosaurines was complex as the clade potentially originated in North America, dispersed

into Asia (where it is represented by *Changchunsaurus*, and *Haya*), and then dispersed into North America again. Potentially two waves of thescelosaurine dispersal occurred from South America into North America where the first wave gave rise to *Parksosaurus* and the second to *Thescelosaurus* (Boyd, 2015). Orodromine dispersal appears more straightforward with their clade originating and diversifying during the Aptian of North America with *Koreanosaurus* diverging from *Oryctodromeus* and dispersing into Asia during or preceding the Cenomanian. The dispersal hypothesis of thescelosaurids may explain the dominance of Orodrominae taxa prior to the Maastrichtian in North America and the sudden appearance of thescelosaurines in North America during this time (Boyd, 2015). Given the rapidly evolving picture of thescelosaurid interrelationships, the evolution and dispersal of this group, based on Boyd (2015), likely does not reflect the true pattern of their evolution and dispersal and should be questioned until a more robust and well-supported phylogeny is analyzed.

2.6. Paleobiology

2.6.1. Ecology and Diet

The dearth of thescelosaurid fossil material and the tendency of researchers to neglect this group has made it difficult to understand their paleoecology. Thescelosaurid fossil material is primarily found in continental fluvial deposits comprised of sandstone laid down in river channels. However, there are some instances of material recovered from siltstone, mudstone, and limestone deposits that are interpreted as having formed either in river channels or on floodplains (Bamforth et al., 2014; Brown et al., 2011; Brown et al., 2013a; Calvo et al., 2007; Currie and Koppelhus, 2005; Eberth et al., 2013; Freimuth and Varricchio, 2019; Gilmore, 1915; Ibiricu et al., 2014; Krumenacker, 2017; Krumenacker et al., 2019; Lyson and Longrich, 2011; Makovicky

et al., 2011; Martinez, 1998; McIver, 2002; Morris, 1976; Novas and Cambiaso, 2004; Parks, 1926; Scheetz, 1999; Sternberg, 1940; Sues, 1980; Wang et al., 2009; Xu et al., 2009; Zan et al., 2005 and 2006). The dinosaur dominated environment of some thescelosaurids has been interpreted as subtropical forested floodplains of meandering rivers, which supported a large diversity of angiosperms and gymnosperms in a habitat with ample precipitation and substantial seasonal variability (Currie and Koppelhus, 2005; Eberth et al., 2013; Norman et al., 2004).

Lyson and Longrich (2011) noticed that *Thescelosaurus* fossils commonly occur in sandstone deposits and suggested that members of this genus preferred environments near river channels. However, this study had low statistical power, and the observed pattern may have merely reflected a preservational bias (Behrensmeyer et al., 1979; Brown et al., 2013a; Brown et al., 2013b; Lyson and Longrich, 2011). Additionally, other workers have obtained conflicting results with respect to the habitat preference of *Thescelosaurus* (Carpenter and Young, 2002). Nonetheless, the consistent pattern of other thescelosaurids tending to occur in sandstone deposits suggests that, in general, thescelosaurids may have potentially preferred to live near river channels. Given this, further taphonomic studies need to be conducted to determine the habitat preference of thescelosaurids.

Thescelosaurids have relatively gracile bodies by dinosaurian standards (Fig. 2.7), and were typically bipedal and cursorial (Gilmore, 1913; Horner and Weishampel, 1988; Maidment and Barrett, 2011b; Norman et al., 2004). The morphology of the femur suggests a parasagittal stance that could produce quick and sustained bursts of speed (Galton, 1969; Persons and Currie, 2020). In the majority of thescelosaurids, except *Thescelosaurus*, the tibia is long in proportion to the femur, suggesting a cursorial lifestyle (Carrano, 1999). Thescelosaurid tibia/femur length

ratios typically range from 1.09-1.41, although those of *Thescelosaurus* specimens range from 0.84-0.96. Interestingly, *Koreanosaurus* has a low tibia/femur length ratio of 1.04 which may potentially support its fossorial lifestyle (Huh et al., 2011). *Albertadromeus* displays derived features of the tibia and fibula that may indicate that this taxon was particularly cursorial, but this interpretation awaits rigorous testing (Brown et al., 2013b).

Although their body plans and hindlimb proportions appear to be adapted for a cursorial lifestyle, numerous authors have interpreted some thescelosaurids as possessing fossorial behaviors, particularly within Orodrominae (Fearon and Varricchio, 2015, 2016; Huh et al., 2011; Krumenacker, 2017; Varricchio et al., 2007). Varricchio et al. (2007) described *Oryctodromeus* from the remains of an adult and two juveniles, which were found in a burrow-like, sediment filled chamber and show anatomical similarities to extant fossorial organisms (Fearon and Varricchio, 2015, 2016; Varricchio et al., 2007). Furthermore, the association of the adult specimen with juvenile individuals provides evidence of parental care in this thescelosaurid. Burrows have been used as dens for rearing young among extant digging cursors (e.g., *Hyaena hyaena* and *Proteles cristatus*) (Varricchio et al., 2007). The burrow consisted of a sinuous descending tunnel with a terminal chamber. This structure is similar to extant fossorial vertebrate burrows (Varricchio et al., 2007). Orodromines, in general, may have been specialized for fossoriality in possessing an expanded acromion with a sharp scapular spine, and a posteroventral expanded margin of the scapular blade. These features have been reported to be present in *Koreanosaurus*, *Orodromeus*, *Oryctodromeus*, and *Zephyrosaurus* (Fearon and Varricchio, 2006; Huh et al., 2011; Scheetz, 1999; Sues, 1980; Varricchio et al., 2007). Except for *Oryctodromeus*, specimens of these taxa have never been in association with burrow-like

structures. Thescelosaurines lack the adaptations present in orodromines for fossoriality, and this behavior may have been exclusive to orodromines. Within this group, however, fossorial behavior may have been an important adaptation for rearing young and finding sanctuary from large terrestrial predators between bouts of foraging in the Cretaceous landscape (Huh et al., 2011; Varricchio et al., 2011).

Unusually among thescelosaurids, *Koreanosaurus* was likely quadrupedal based on the proportionally short femur (196.5 mm) and tibia (204 mm), a tibia/femur ratio of 1.07, and the robustness and size of the humerus (215 mm) (Huh et al., 2011). This divergence from the bipedal posture thought to have been characteristic of other thescelosaurids is likely the result of a fossorial lifestyle, *Koreanosaurus* shares apparent fossorial adaptations with *Oryctodromeus*. However, fossorial adaptations did not lead to quadrupedality in other orodromines (e.g., *Orodromeus* and *Oryctodromeus*). Whether *Koreanosaurus* was more fossorial than *Oryctodromeus* awaits testing (Fearon and Varricchio, 2016; Huh et al., 2011; Varricchio et al., 2007). The quadrupedal stance is not unusual for extant fossorial behaviors (Fearon and Varricchio, 2015, 2016).

Thescelosaurids are thought to have been herbivorous, based on their bulbous premaxillary, leaf-like maxillary, and triangular dentary teeth (Norman et al., 2004; Norman, 2012; Weishampel, 1984) (Fig. 2.8). Herbivorous characteristics commonly seen in thescelosaurids include close packed, thickly enameled, and interlocking and imbricating maxillary and dentary teeth, and wear facet and tooth wear patterns. These are supported by skull morphometrics and biomechanical proxies, which are consistent with other herbivorous ornithischians. A ridge on the maxilla above the tooth row that has been interpreted as marking

the presence of a fleshy cheek (Barrett, 2014; Barrett and Han, 2009; Boyd, 2014; Button and Zanno, 2020; Jin et al., 2010; Mallon and Anderson, 2013; Scheetz, 1999; Sues, 1980; Virag and Ősi, 2017; Wyenberg-Henzler, 2020).

Based on femoral dimensions and trigonometry, thescelosaurids have a range of body lengths, body masses, and feeding heights (Campione et al., 2014; Persons and Currie, 2020; Wyenberg-Henzler, 2020). Based on feeding height calculations, thescelosaurids likely foraged on low vegetation, and various taxa were capable of reaching different heights (Wyenberg-Henzler, 2020). *Thescelosaurus neglectus*, the largest thescelosaurid, is estimated to have had a maximum feeding height of 2 meters (Wyenberg-Henzler, 2020). The rostrum is narrow in thescelosaurids, and the anterior end of the premaxilla is edentulous and presumably bore a keratinous rhamphotheca. The narrow rostrum would suggest that thescelosaurids were browsers, and the edentulous, keratinous rhamphotheca would likely crop food materials (Hofmann, 1973; Norman et al., 2004; Solounias et al., 1988).

Tooth development, microstructure, and histology have been much less studied in thescelosaurids than in derived ornithischians (e.g., ceratopsids and hadrosaurids) (Bramble et al., 2017; Erickson et al., 2012; Hwang, 2005 and 2011; LeBlanc et al., 2016). Given this shortcomings, understanding of dental evolution in derived ornithischians is limited by the absence of the context that extensive information from thescelosaurids and other basal forms would provide (Fong et al., 2016). Chen et al. (2018) investigated the histology, development, and qualitative microstructure of the teeth of *Changchunsaurus*, which may approximate the ancestral condition in basal cerapodans. The teeth are anchored in their sockets by a gomphosis-type attachment, and replacement teeth develop on the lingual sides of the functional teeth. The

developing replacement tooth spends most of its development on the lingual side, and root resorption occurs early in the tooth replacement cycle (Chen et al., 2018; LeBlanc et al., 2017). Replacement teeth that are fully developed do not invade the functional tooth pulp cavity, unlike in hadrosaurids and theropods. By the time the functional tooth is about to be shed, the replacement tooth is nearly erupted, and ready to migrate buccally into position when shedding occurs. These shed teeth were rapidly replaced, to maintain a uniform shearing surface for the mastication of plants. *Changchunsaurus* has fully enameled teeth, as opposed to teeth that are enameled only on one side as in derived ornithischians, and represents the most basal ornithischian in which wavy enamel is known to occur. Prior to the work of Chen et al. (2018), wavy enamel was thought to exist only in derived ornithopods (e.g., hadrosaurids, *Camptosaurus*, and *Dryosaurus*) (Hwang, 2011). The presence of this enamel type in a neornithischian outside Ornithopoda suggests that it may in fact have originated much earlier in ornithischian evolution. However, it is unknown if wavy enamel appeared independently in *Changchunsaurus* and in derived ornithopods, or represents an ornithischian symplesiomorphy that would imply a loss of this enamel type in marginocephalians. Many of the developmental, histological, and microstructural traits seen in *Changchunsaurus* teeth may prove to be widespread among thescelosaurids, but some diversity in tooth structure does not exist within the group, as *Thescelosaurus* does not have wavy enamel (Chen et al., 2018; Hwang, 2011).

2.6.2. Ontogeny

Ontogenetic studies of extinct vertebrate animals typically involve histological sampling of their long bones, a method which has been used successfully to infer patterns of growth and development in multiple clades of extinct taxa (Enlow & Brown, 1957; Padian et al., 2001).

Ontogeny, growth rates, and osteohistology have been extensively studied in several dinosaur clades (Brusatte et al., 2010; Chinsamy, 1995; Cooper et al., 2008; Curry, 1999; Erickson, 2005; Han et al., 2020; Horner et al., 1999, 2000, and 2009; Horner and Lamm, 2011; Ősi et al., 2012; Padian et al., 2001; Reid, 1985; Werning, 2012), but only a few such studies (Barta and Norell, 2021; Chinsamy et al., 1998; Horner et al., 2009; Krumenacker, 2017; Scheetz, 1999) have been conducted on thescelosaurids owing to the rarity and the often fragmentary nature of the available fossils. Typically, members of this group exhibit slower growth rates than derived ornithischians (Barta and Norell, 2021; Horner et al., 2009; Krumenacker, 2017; Han et al., 2020).

The first osteohistological study of any thescelosaurid examined the long bones of *Orodromeus* (Horner et al., 2009). These bones were described as exhibiting moderate vascularity, although adults had nearly avascular tissue in the outermost cortex, and both juveniles (3-4 years of age) and adults (4-6 years of age) had lines of arrested growth (LAGs). The cortical bone was fibrolamellar, similar to other ornithischians (Horner et al., 2009). *Orodromeus* was characterized by determinate growth, and by a moderate growth rate, relative to larger-bodied dinosaurs. *Orodromeus* probably grew more rapidly than crocodilians, but not as rapidly as avians. Horner et al. (2009) inferred that growth was rapid in the immediate post-hatching period, slowed throughout the juvenile stage, and nearly ceased when adult size was reached (Horner et al., 2009). Overall, *Orodromeus* had the pattern of growth generally present in dinosaurs, but it was a slower growth compared to that of a derived ornithischian (Horner et al., 2000 and 2009; Werning, 2012).

Krumenacker (2017) established the characteristics associated with different growth stages in *Oryctodromeus* by examining the osteohistology and morphology of juvenile, subadult, and adult skeletons (Fig 2.9). The bones sectioned in this analysis were the femur and tibia. Juveniles are characterized by moderately vascularized fibrolamellar primary bone, an absence of zonal parallel-fibered bone in the outer cortex, and an absence of lines of arrested growth (LAGs). The scapulae are not fused to the coracoids, and the neurocentral sutures are visible from the anterior cervical to the proximal caudal vertebrae (Krumenacker, 2017). LAGs are present in sub-adults and suggest a minimum ages of three to four years, assuming that the LAGs were deposited annually. Subadults are also characterized osteohistologically by moderate secondary bone growth and by reworking of the inner cortex, in which secondary osteons and erosion rooms occur (Erickson et al., 2009; Lee and Werning, 2007). Fibrolamellar bone is present in the inner cortex and parallel fibered bone in the outer cortex, and Krumenacker (2017) interpreted the change in bone type as evidence of sexual maturity. Sub-adult skeletal characteristics include fusion of the neurocentral sutures in the anterior caudals through mid-caudals, and variable fusion in the anterior vertebrae and scapulocoracoids (Krumenacker, 2017). Adults exhibit dense avascular bone in the outermost cortex, and almost complete fusion of the vertebral neurocentral sutures and the scapulocoracoids (Krumenacker, 2017). *Oryctodromeus* appears to have been histologically similar to *Orodromeus* (Horner et al., 2009). Growth rates slowed as sexual maturity approached, a change indicated by decreased spacing between LAGs and deposition of zonal parallel fibred bone tissue.

Barta and Norell (2021) described the femoral osteohistology of *Haya* and attempted to establish a growth curve from an ontogenetic series of this taxon, despite low sample size (Fig

2.9). The sampled element of the smallest individual (IGM 100/2020) consisted primarily of woven-fibered bone, but parallel-fibered bone sporadically dominated throughout the section. Osteonal lamellar bone was not-well developed in appearance and was confined to the insides of the large longitudinal vascular canals. Radial vasculature occurred near the lateral side of the bone, and reticular vasculature near the posterior side. Osteocyte density was variable throughout the section, and no LAGs were preserved. Based on the observed osteohistological features, the smallest individual was interpreted as a perinate or hatchling. Juveniles (IGM 100/2015 and 100/3672) possessed woven-fibered bone in the inner cortex, and parallel-fibered bone in the outer cortex. However, fungal alteration obscures much of the bone microstructure and vasculature patterns in IGM 100/3672. Juveniles consisted of longitudinal and anastomosing vasculature that lack secondary osteons. Two LAGs were present in IGM 100/2015, which was interpreted to have died in its third year of life, whereas IGM 100/3672 had four annuli that consisted of narrow bands of parallel-fibered bone. The section from the subadult (IGM 100/1324) primarily consisted of parallel-fibered bone, interspersed with narrower bands of woven-fibered bone. Similar to the juvenile, longitudinal and anastomosing vasculature was present throughout. Primary osteons were present at the periosteum, with some lamellar bone surrounding them, and osteocyte density is high in the larger specimen (IGM 100/1324). Four LAGs are present, but there is no external fundamental system (EFS). An EFS is a long bone microstructure that is present in the outermost cortex, which is characterized by closely packed layers of subperiosteal lamellar bone that is avascular and acellular and indicates a cessation of growth (Padian and Lamm, 2013; Woodward et al., 2011). Of the histologically sampled *Haya* specimens, none represent a skeletally mature individual, given that any EFS is lacking,

vascularity and LAG spacing do not decrease periosteally, and the growth rate of the sampled specimens in fact appears to have been accelerating at the time of death. Retrocalculation of the LAGs involving all the specimens suggested that the largest specimen was six years old at death. Growth curves of the specimens revealed that none had reached a growth plateau, every specimen being skeletally immature. Skeletal immaturity at the time of death appears to be common not only in sampled thescelosaurids, but among basal neornithischians in general. This pattern lacks a clear explanation, but may represent a consequence of preservational bias, a random signal, or the result of a particular growth strategy (e.g., r-strategist) (Erickson et al., 2009; Woodward et al., 2015).

2.6.3. Myology and Locomotion

Numerous ornithischian researchers have attempted to reconstruct ornithischian appendicular musculature, with an emphasis on cerapodans (Dollo, 1888; Romer, 1927). Notable studies have been conducted on *Camptosaurus* (Carpenter and Wilson, 2008), the hadrosaurid *Maiasaura* (Dilkes, 2000), *Hypsilophodon* (Galton, 1969), and ceratopsians (Johnson and Ostrom, 1995; Russell, 1935). Maidment and Barrett (2011b) reconstructed basal ornithischian myology, and Romer (1927) reconstructed *Thescelosaurus neglectus* pelvic musculature. These two studies provide the only myological reconstructions currently available for non-cerapodan ornithischians.

Maidment and Barrett (2011b) and Romer (1927) concluded that basal ornithischians and *Thescelosaurus* were bipeds. Thescelosaurids possess the synapomorphic ornithischian pelvic condition where the pubis is retroverted and is parallel with the ischium, a feature convergently shared with extant avians. The thescelosaurid iliac blade is transversely thin, and possesses an

anteriorly directed preacetabular process (Gilmore, 1915; Maidment and Barrett, 2011b). The ornithischian pelvic condition is highly derived relative to the typical basal archosaurian condition. However, the pelvic myology in different archosaur clades is highly conservative despite differences in pelvic morphology (Maidment and Barrett, 2011b). The elongate preacetabular process on the ilium of *Thescelosaurus* is interpreted as the attachment site for the puboischiofemoralis, which has shifted from its primitive position on the dorsal vertebrae. This suggests that the lateral movement of the puboischiofemoralis internus muscle in ornithischians occurred in tandem with the retroversion of the pubis (Gilmore, 1915; Maidment and Barrett, 2011b; Romer, 1927).

To test whether *Oryctodromeus* possessed fossorial behaviors, Fearon and Varricchio (2016) reconstructed its forelimb myology and identified osteological features, including the positions of some muscle attachment sites, which were potentially related to burrowing. Shoulder and forelimb muscles that tend to be particularly prominent in extant burrowing mammals include the deltoideus scapularis, latissimus dorsi, teres major, and triceps longus. However, some of these muscle groups have no certain homologues in *Oryctodromeus*, and it is difficult to determine if the reconstructed muscles sufficiently support fossorial behaviors. Muscle reconstructions were based on muscle dissections of extant crocodilians and avians and were used for the extant phylogenetic bracketing method (Witmer, 1995). The posterior scapular blade expands ventrally, which suggests an increased attachment area for the deltoideus scapularis and the teres major, assuming that these muscle groups are homologous in mammals and dinosaurs. These muscle groups are based in mammalian myology and have no osteological correlates in *Oryctodromeus*, making it difficult to assess the musculature of this taxon. Although it should be

possible to determine fossorial adaptations of *Oryctodromeus* based on a combination of mechanical principles and analogies to fossorial mammals, even if homologies are difficult to determine.

Thescelosaurids are relatively gracile compared to other dinosaurs (Fig. 2.7), and are thought to have been typically bipedal and cursorial (Gilmore, 1913; Horner and Weishampel, 1988; Maidment and Barrett, 2011b; Norman et al., 2004). The parasagittal stance and especially the morphology of the thescelosaurid femur suggests that they could produce quick and sustained bursts of speed (Galton, 1969; Persons and Currie, 2020). Osteological features that may suggest thescelosaurids were bipedal include the absence of hoof-like unguals, tibia longer than femur, fourth trochanter pendent and proximally positioned, high pes/hindlimb length ratio, and transversely thin ilium (Maidment and Barrett, 2012; Persons and Currie, 2020). However, some of these purported correlates of bipedality may be related to body size and/or be linked to aspects of stance and locomotion other than bipedality (Maidment and Barrett, 2012). For example, smaller neornithischians consistently have a pendent fourth trochanter located proximally on the femoral shaft, which facilitates rapid retraction of the femur (Persons and Currie, 2020). The pendent fourth trochanter may be a plesiomorphic feature in Ornithischia. However, in derived large-bodied quadrupedal ornithischians, the fourth trochanter is non-pendent and distally positioned on the femoral shaft. This difference in fourth trochanter morphology reflects a functional shift in larger quadrupedal ornithischians, in which the caudofemoralis musculature was able to powerfully retract the femur (Persons and Currie, 2020). The presence of the proximal pendent fourth trochanter indicates adaptations for sustained swift running as opposed to the rapid acceleration or propulsion of a heavy body. Fearon and Varricchio (2015) suggested

that ornithischian locomotion modes can be correlated with morphological trends in the forelimb. Quadrupeds have strap-like scapulae, and humeri with long, laterally deflected deltopectoral crests. Bipeds have scapulae with pronounced acromion processes and expanded posterior scapular blades, and shorter humeri with anteriorly directed deltopectoral crests. Furthermore, a few thescelosaurids lack at least some of the possible correlates of bipedality mentioned previously for *Koreanosaurus* (hindlimb and forelimb of equal proportions) and *Thescelosaurus* (tibia is shorter than the femur) (Galton, 1974b; Huh et al., 2011).

2.6.4. Integument and Soft Tissue

There is an extensive literature on feathers preserved in some theropods (Chen et al., 1998, Ji and Ji, 1996; Qiang et al., 1998; Witmer, 2009) and their close relationship with extant Aves (Godefroit et al., 2013; Hu et al., 2009; Xu et al., 2001). There is literature on the soft-tissue integumentary features preserved in ornithischians (e.g., hadrosaurids) that have been analyzed through multiple geochemical and biochemical methods (Barbi et al., 2019; Bell et al., 2014; Evans and Reisz, 2007; Fabbri et al., 2020). However, feathers have not been observed in iguanodontians and hadrosaurids, with the possible exceptions of heterodontosaurids, basal ceratopsians, and one basal neornithischian (Godefroit et al., 2014, 2020; Vinther et al., 2016; Zheng et al., 2009). Given this, the preservation of soft-tissue integument structures (skin or feathers) have yet to be observed in thescelosaurids and it is uncertain what they had. Bristle-like structures have been observed in the ceratopsian *Psittacosaurus* and the heterodontosaurid *Tianyulong* (Vinther et al., 2016; Zheng et al., 2009). However, these taxa are distantly related to thescelosaurids and may not furnish accurate indications of thescelosaurid integuments (Witmer, 1995) (Fig. 2.10). *Kulindadromeus*, a basal neornithischian (sister to Jeholosauridae and

Hexinlusaurus) that is relatively close to Thescelosauridae, has feather-like structures that have been interpreted as avian-like (Godefroit et al., 2014; Madzia et al., 2018). Whether these monofilaments present in *Kulindadromeus*, *Psittacosaurus*, and *Tianyulong* are homologous to feathers or evolved independently is still unclear (Godefroit et al., 2014; Vinther et al., 2016; Zheng et al., 2009). Given the relatively close relationship and similar body plan of *Kulindadromeus* to thescelosaurids, relative to *Psittacosaurus* and *Tianyulong*, possibly suggest thescelosaurid integument resembled that of *Kulindadromeus* (Godefroit et al., 2014; Witmer, 1995). However, thescelosaurids could also potentially have had a novel integument quite distinct from *Kulindadromeus*, *Psittacosaurus*, and *Tianyulong*.

Fisher et al. (2000) described a ferruginous concretion within its chest region of a partially articulated Thescelosaurus (NCSM 15278) from the Hell Creek Formation of South Dakota. It was interpreted it as a petrified heart based on computed tomography that supposedly included one aorta but no foramen of Panizza (Fig. 2.11). Fisher et al. (2000) suggested that ornithischians had a cardiovascular system that was intermediate between Aves and crocodilians. Given this, Fisher et al. (2000) inferred an intermediate or high metabolic rate in ornithischians. However, Rowe et al. (2001) and Cleland et al. (2011) used high resolution computed tomography and geochemical analyses to conclude that the heart was of geologic origin, composed of quartz and plagioclase cemented together by goethite. An iron concretion with similar geochemical composition is present around the femur of the specimen, further supporting the geologic origin of the ‘heart’ (Fig. 2.11). There were no chemical signals that were biological in origin (Cleland et al., 2011).

2.6.5. Respiration

The bony plate-like structures on the posterior margins of the anterior dorsal ribs (intercostal plates) in some thescelosaurids (*Macrogryphosaurus*, *Parksosaurus*, *Talenkauen*, and *Thescelosaurus*), as well as other ornithischians (e.g., *Hypsilophodon* and *Othnielosaurus*), are thought to have either functioned as dermal armor or aided in respiration (Boyd et al., 2011; Butler and Galton, 2008; Hulke, 1874). In the articulated *Thescelosaurus* specimen NCSM 15728, the anterior portion of the intercostal plate sits on top of the lateral margin of the second dorsal rib. Then the posterior margin of the intercostal plate overlaps the following rib and the anterior portion of the subsequent intercostal plate (Fig. 2.12). The association of intercostal plates with the dorsal ribs continues posteriorly until the seventh rib where the seventh intercostal plate touches the anterior margin of the eighth dorsal rib. Intercostal plates become gradually smaller posteriorly, however, the seventh one is substantially smaller compared to the sixth. These intercostal plates were proposed as a synapomorphy for elasmarians (Calvo et al., 2007), but this is unlikely as they also occur in other ornithischians such as *Hypsilophodon*, *Othnielosaurus*, *Parksosaurus*, *Talenkauen*, and *Thescelosaurus* (Boyd et al., 2011; Butler and Galton, 2008; Fisher et a., 2000; Galton, 1974a; Huxley, 1869 and 1870; Marsh, 1877; Novas et al., 2004; Parks, 1926). The initial interpretation that the intercostal plates served mainly as dermal armor (Hulke, 1874) was dismissed – on the grounds that they would have been too thin to be effective in this capacity – by numerous workers who instead suggested they were analogous with the uncinate processes observed in extant Aves (Butler and Galton, 2008; Novas et al., 2004). Uncinate processes play a key role in lung ventilation by facilitating movements in the ribcage and sternum during breathing (Codd et al., 2005, 2008; Boyd et al., 2011; Butler and

Galton, 2008; Novas et al., 2004). Boyd et al. (2011) investigated the mineralization, homology, and potential function of intercostal plates in *Thescelosaurus* (NCSM 15278) through a histological analysis. The results of Boyd et al.'s (2011) analysis showed that the intercostal plates of *Thescelosaurus* had a different pattern of osteogenesis than avian uncinate processes but are similar to Sharpey's fibers. In *Thescelosaurus*, Sharpey's fibers are present on the lateral and, to a lesser degree, medial margins of the intercostal plates. The presence of Sharpey's fibers on the lateral surface of the intercostal plates. This suggests that tendons were inserted along their surfaces and therefore the plates were not passively embedded in the surrounding tissue as is the case with osteoderms. Boyd et al. (2011) concluded that intercostal plates and uncinate processes are not homologs, but nevertheless were functionally analogous in that both assisted in breathing. It is unclear whether the intercostal plates within thescelosaurids had a role similar to that of uncinate processes, or served some other, unknown function. The problem is further exacerbated because there are no extant analogs to thescelosaurids with similar intercostal plates. They are similar in shape to the broad cartilaginous uncinate processes of crocodilians, which appear to help anchor the intercostal musculature involved in respiration. Until there is a better understanding of intercostal plate, ribcage, and sternum musculature in thescelosaurids, it is difficult to test these hypotheses.

A unidirectional respiratory system is characterized by a rigid lung that possesses pulmonary air sacs with diverticula that invade the postcranial skeleton (O'Connor, 2004, 2006). Aves, crocodilians, and other extant reptiles possess this unique respiratory system. The unidirectional respiratory system was once thought to be unique among avians, but appears to have originated earlier and may be the plesiomorphic condition in Archosauria and possibly

Reptilia (Butler et al., 2012; Cieri et al., 2014; Gower, 2001; Sanders and Farmer, 2012; Schachner et al., 2013 and 2014). However, the evolution of respiration within Archosauria is complicated (Benson et al., 2012; Brocklehurst et al., 2018 and 2020; Butler et al., 2012; O'Connor, 2004 and 2006; Hudgins et al., 2020b; Lambertz et al., 2018; Schachner et al., 2009, 2011, and 2013). Given this, the respiration style amongst Saurischia has been interpreted to be unidirectional (Britt, 1993 and 1997) and it is parsimonious to assume that ornithischians had a similar ventilation. The respiration style within Ornithischia has remained elusive because their skeletons lack the correlates of unidirectional respiration that saurischians possess. However, some workers have proposed a link between the retroversion of the pubis and the morphology of the anterior pubic process to their respiratory style (Carrier and Farmer, 2000; Macaluso and Tschopp, 2018). Radermacher et al. (2021) proposed an ornithischian respiration model called the 'pelvic bellows' where the anterior pubic process served as the origin for a muscle analogous with the diaphragmaticus in extant crocodilians. Radermacher et al. (2021) called this novel muscle the puboperitoneal and suggested it served as the main ventilatory apparatus. If this respiration model is correct, then thescelosaurids would have had this unique respiration style as well. This model is a step towards a fuller understanding of ventilation in ornithischians, but should be tested using explicit modeling.

2.7. Tables and Figures

Table 2.1. Taxa of Thescelosauridae.

Abbreviations: Alb, Albian; Apt, Aptian; BBFm, Bajo Barreal Formation; BLFm, Blackleaf Formation; CFm, Cloverly Formation; Camp, Campanian; Ceno, Cenomanian; Coni, Coniacian; FFm, Frenchman Formation; HCF, Horseshoe Canyon Formation; HCFm, Hell Creek Formation; JFm, Javkhlant Formation; LFm, Lance Formation; Maas, Maastrichtian; PAFm, Pari Aike Formation; PFm, Portezuelo Formation; OFm, Oldman Formation; QFm, Quantou Formation; Sant, Santonian; SCg, Seonso Conglomerate; TMFm, Two Medicine Formation; WFm, Wayan Formation.

Taxa	Specimen	Formation	Age	Reference
Elasmaria				
Macrogryphosaurus	MUCPv-321	PFm	Coni	Calvo et al., 2007
Notohypsilophodon	UNPSJB-Pv 942	BBFm	Ceno	Martinez, 1998
Talenkauen	MPM-10001	PAFm	Maas	Novas et al., 2004
Orodrominae				
Albertadromeus	TMP 2009.037.0044	OFm	Camp	Brown et al., 2013b
Orodromeus	Various MOR specimens	TMFm	Camp	Horner and Weishampel, 1988
Oryctodromeus	Various MOR and IMNH specimens	BLFm and WFm	Alb-Ceno	Varricchio et al., 2007
Koreanosaurus	KDRC-BB2 and BB3	SCg	Sant- Camp	Huh et al., 2011
Zephyrosaurus	MCZ 4392 and 8799	CFm	Apt-Alb	Sues, 1980
Thescelosaurinae				
Changchunsaurus	Various JLUM specimens	QFm	Apt-Ceno	Zan et al., 2005
Haya	Various IGM specimens	JFm	Sant	Makovicky et al., 2011
Parksosaurus	ROM 804	HCF	Maas	Park, 1926
T. assiniboiensis	RSM P 1225.1	FFm	Maas	Brown et al., 2011
T. garbanii	LACM 33542	HCFm	Maas	Morris, 1976
T. neglectus	USNM 7757 and NCSM 15278	LFm and HCFm	Maas	Gilmore, 1913

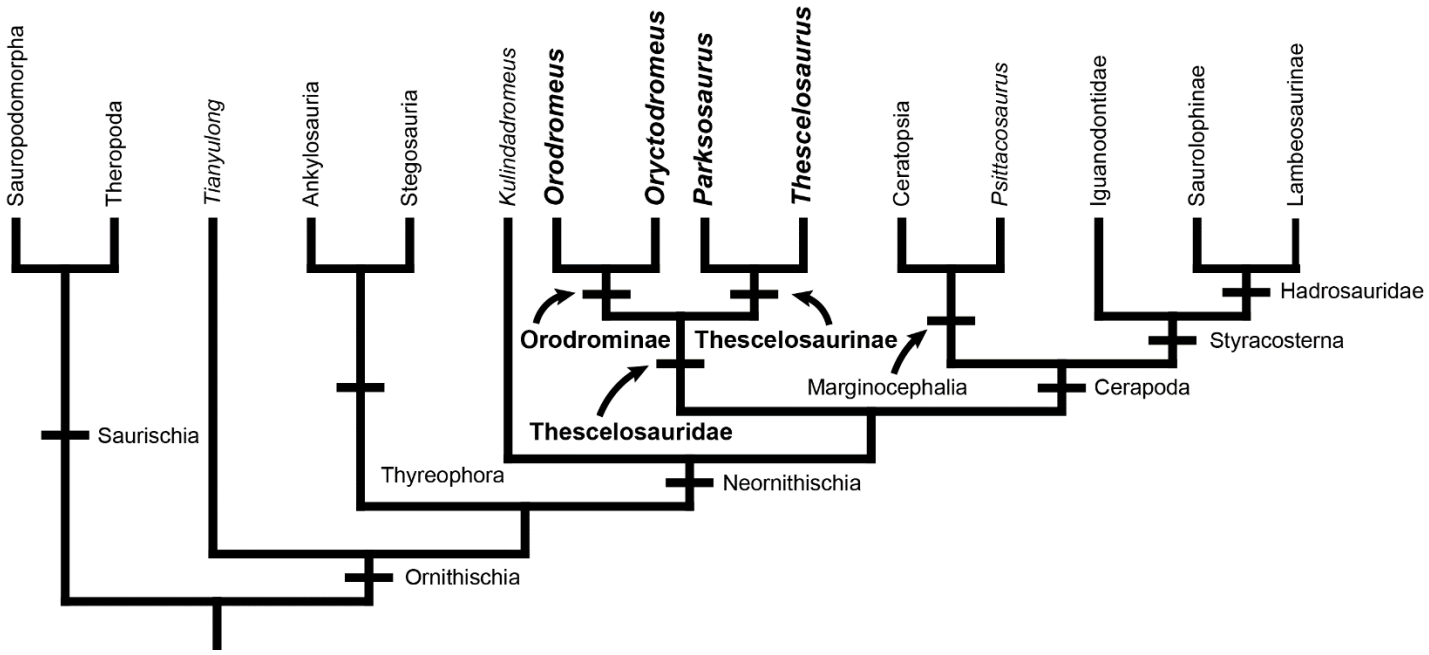

Figure 2.1. Phylogenetic position of Thescelosauridae within Ornithischia.

Thescelosaurid taxa in bold.

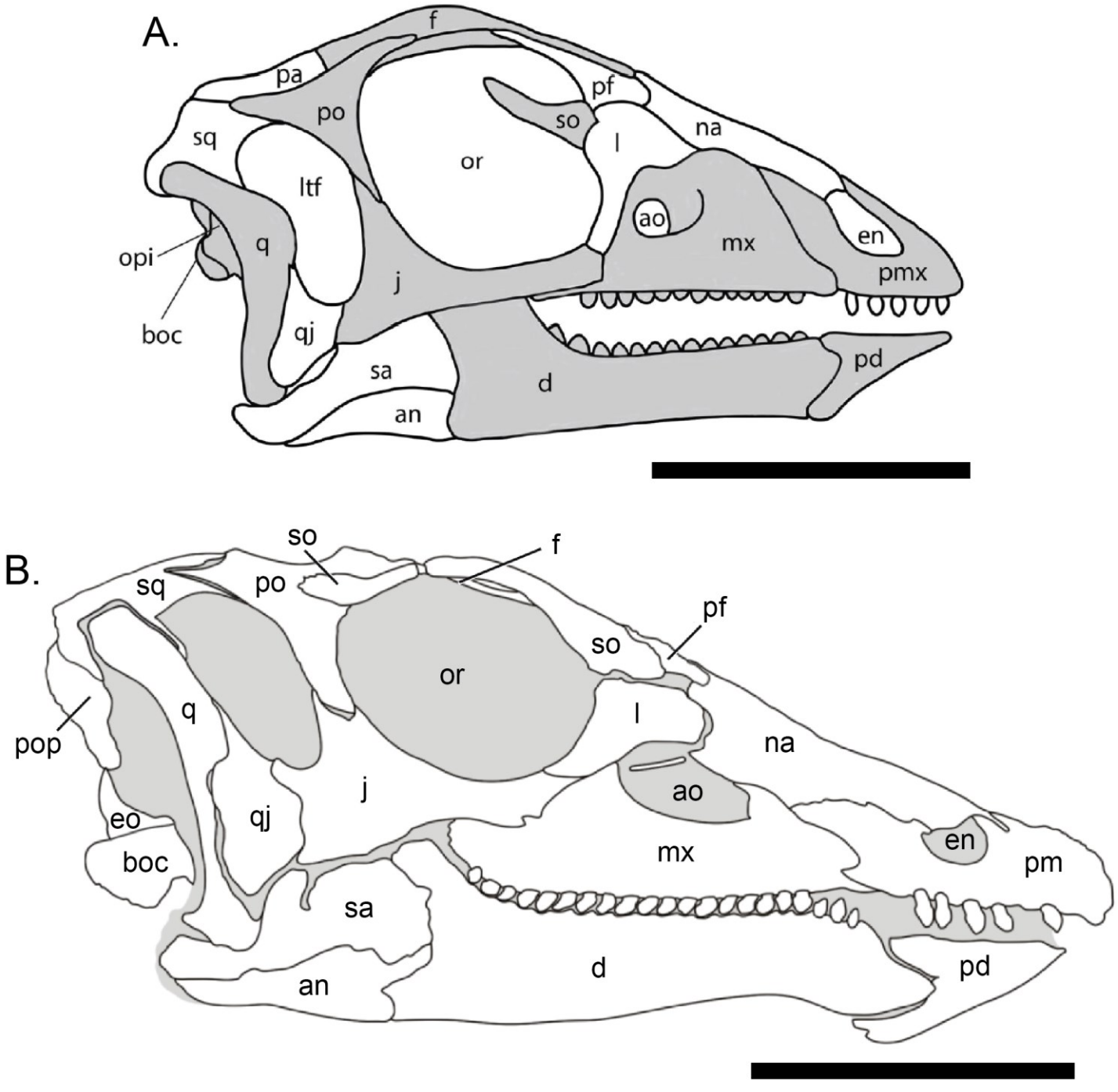
A.
f
pa
po
pf
so
na
sq
l
or
ltf
ao
en
opi
q
mx
pmx
j
boc
qj
sa
d
pd
an
B.
so
f
sq
po
pf
so
or
q
l
pop
na
j
ao
eo
qj
en
mx
pm
boc
sa
d
pd
an

Figure 2.2. Skulls of Representatives of Orodrominae and Thescelosaurinae.

Reconstructed skull of *Oryctodromeus* (A) and a specimen drawing of *Thescelosaurus* in right lateral view (B). Preserved elements in *Oryctodromeus* are shaded grey (A). Figure modified from Boyd (2014) and Krumenacker (2017). Abbreviations: an, angular; ao, antorbital fenestra; boc, basioccipital; d, dentary; en, external naris; f, frontal; j, jugal; l, lachrymal; ltf, lateral temporal fenestra; mx, maxilla; na, nasal; opi, opisthotic; or, orbit; pa, parietal; pd, predentary; pf, prefrontal; pmx, pm, premaxilla; po, postorbital; pop, paroccipital process; q, quadrate; qj, quadratojugal; sa, surangular; so, supraorbital; sq, squamosal. Skull reconstructions were modified from Krumenacker (2017) and Boyd (2014). Scale bar for 7 cm for *Oryctodromeus* (A) and 10 cm for *Thescelosaurus* (B).

(A.) Brown et al., 2013
MPT: 3
TL: 401
CI: 0.47
RI: 0.66

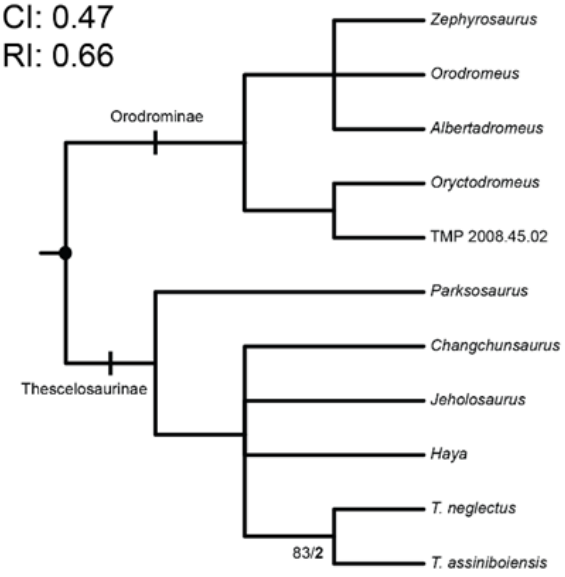

(B.) Boyd, 2015
MPT: 36
TL: 868
CI: 0.37
RI: 0.65

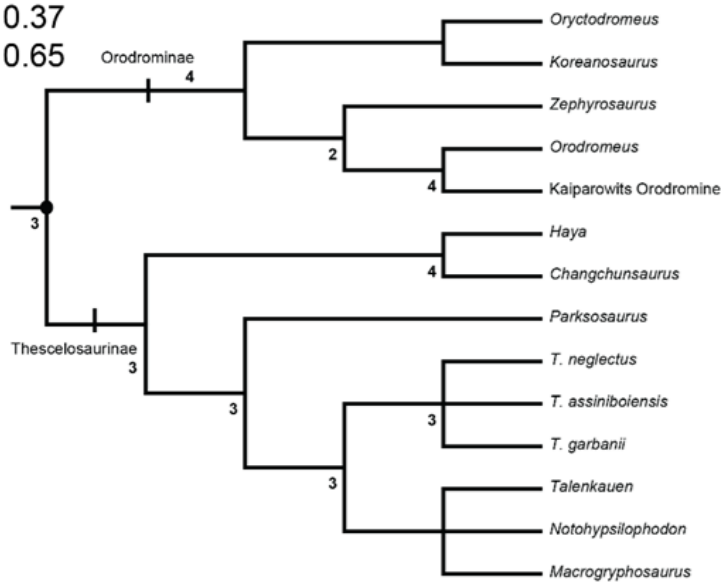

(C.) Madzia et al., 2018
MPT: 13,547
TL: 905
CI: unreported
RI: unreported

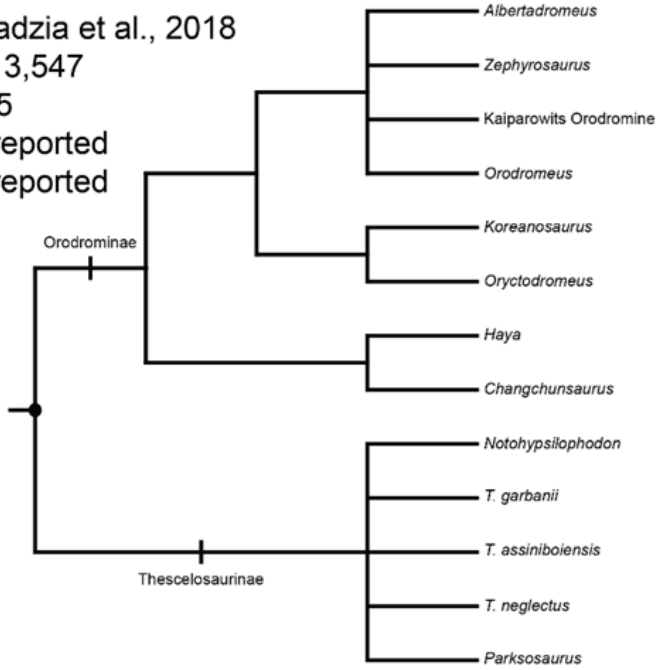

Figure 2.3. Results of three analyses of thescelosaurid phylogeny.

Brown et al. (2013b) (A), Boyd, (2015) (B), Madzia et al. (2018) (C). Bold numbers are Bremer support values >1, whereas numbers in plain text are bootstrap support values >50%. Abbreviations: MPT, most parsimonious tree; TL, tree length; CI, consistency index; RI, retention index.

A.

B.

C.

D.

E.

F.

Figure 2.4. Thescelosauridae skulls.

(A) Skull of *Thescelosaurus* (NCSM 15278); (B) skull of *Orodromeus* (MOR 436); (C) skull of *Parksosaurus* (ROM 804); (D) skull of *Haya* (IGM 100/2017); (E) skull of *Changchunsaurus* (JLUM L0403-j-Zn2) (Jin et al., 2010); and (G) skull fragments of *Zephyrosaurus* (MCZ 4392). Scale bar = 5 cm.

A.

10 cm

B.

5 cm

C.

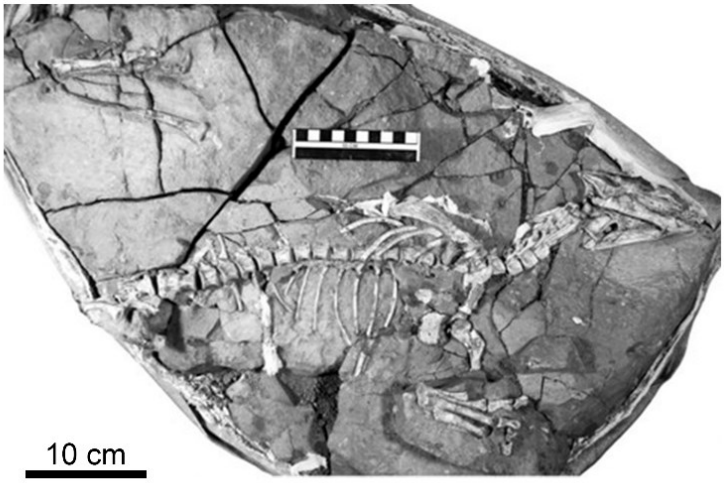

10 cm

Figure 2.5. Postcrania of Thescelosauridae.

(A) A partially articulated *Haya* (IGM 100/2015); a taxon occasionally recovered in Thescelosauridae, *Jeholosaurus*, partial articulated postcrania (IVPP 15719); and partial articulated skeleton of *Changchunsaurus* (JLUM L0403-j-Zn2) (Jin et al., 2010).

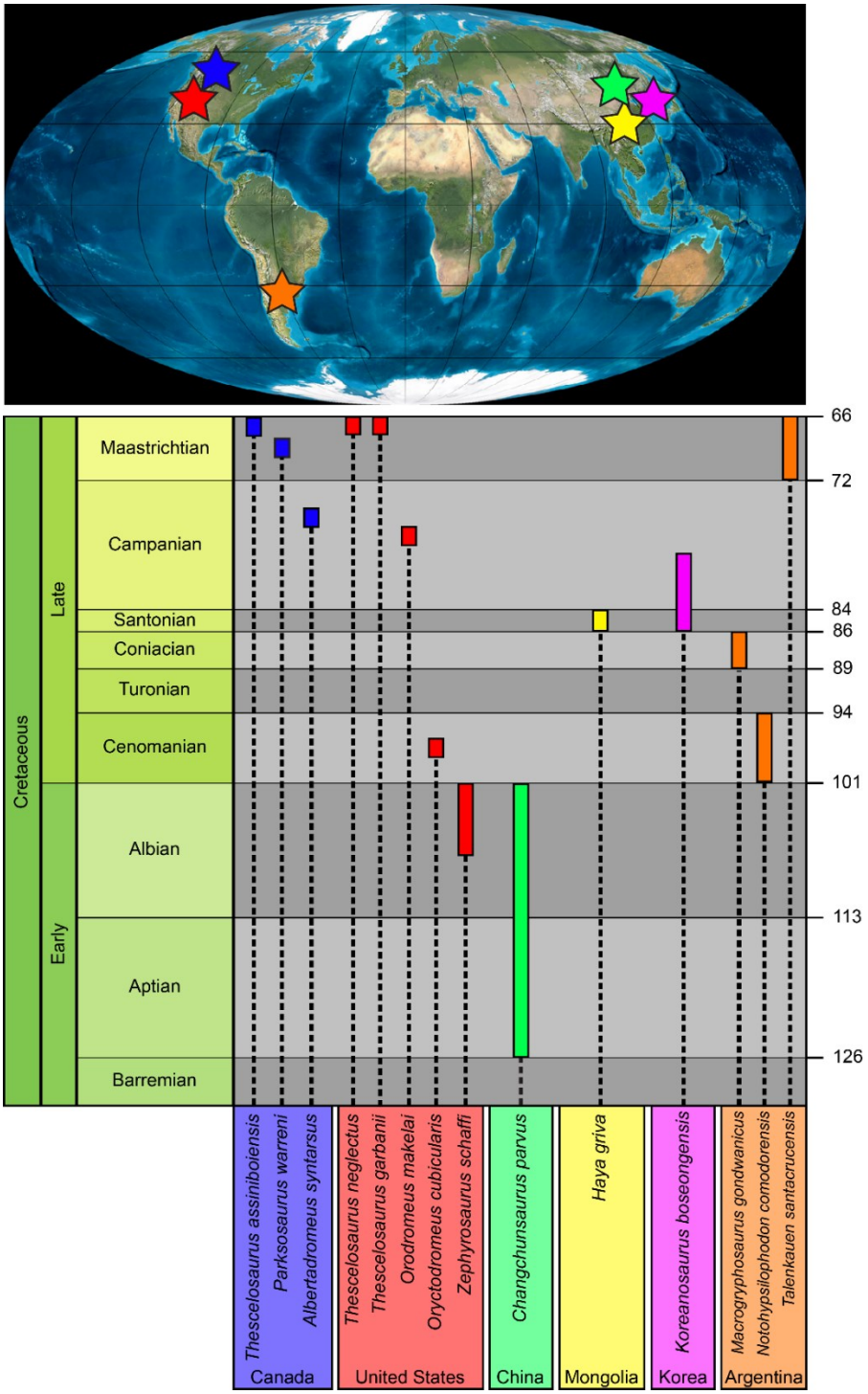
Cretaceous
Late
Early
Maastrichtian
Campanian
Santonian
Coniacian
Turonian
Cenomanian
Albian
Aptian
Barremian
66
72
84
86
89
94
101
113
126
Thescelosaurus assiniboiensis
Parksosaurus warreni
Albertadromeus syntarsus
Thescelosaurus neglectus
Thescelosaurus garbanii
Orodromeus makelai
Oryctodromeus cubicularis
Zephyrosaurus schaffi
Changchunsaurus parvus
Haya griva
Koreanosaurus boseongensis
Macrogryphosaurus gondwanicus
Notohypsilophodon comodorensis
Talenkauen santacrucensis
Canada
United States
China
Mongolia
Korea
Argentina

Figure 2.6. Spatiotemporal distribution of thescelosaurids.

Taxon stratigraphic ranges represent geologic age error.

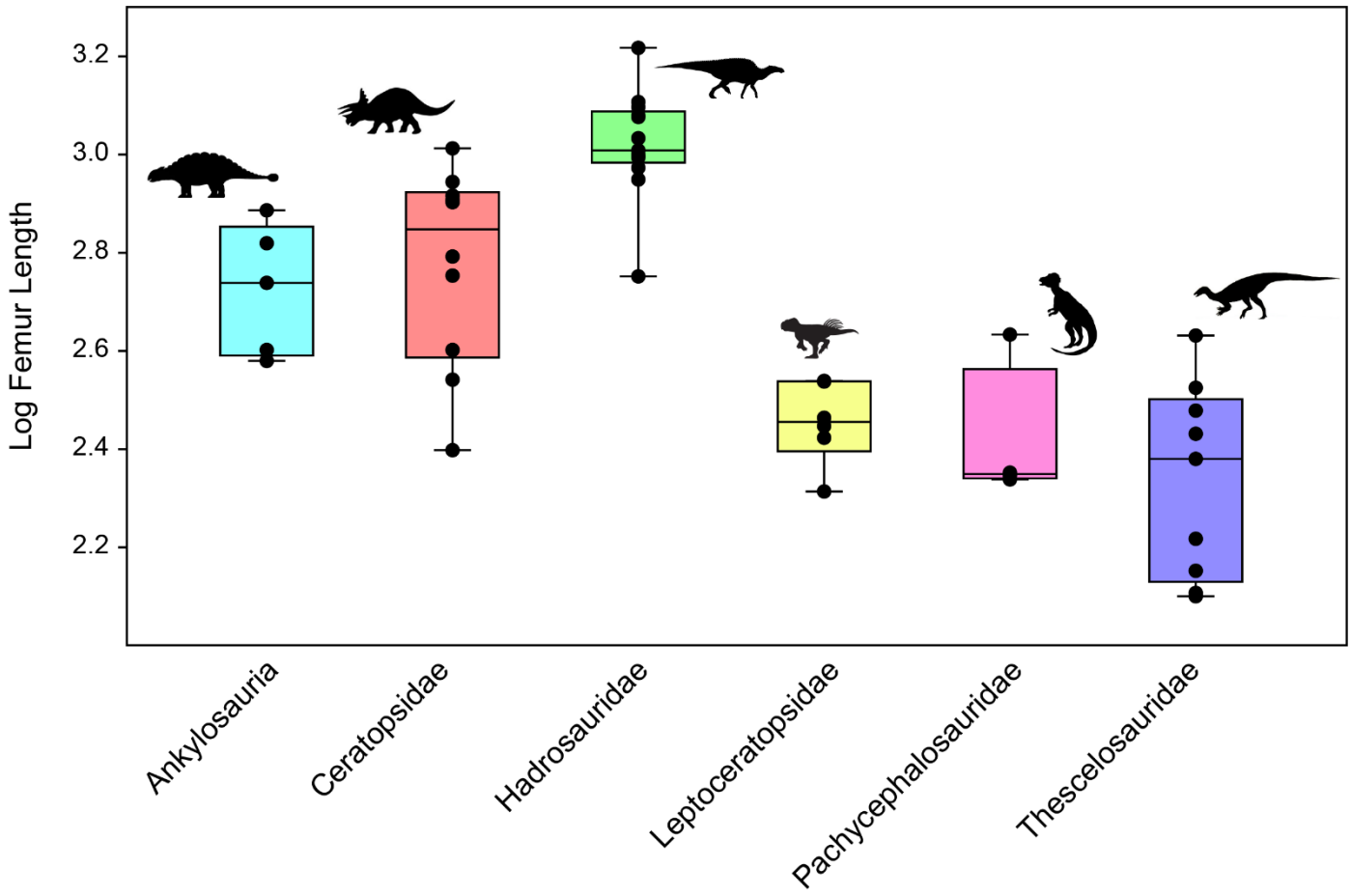

Figure 2.7. Box and whisker plot of logarithmically transformed femoral length (a proxy for body size) in different groups of late Cretaceous ornithischians.

See appendix A for data used in this figure.

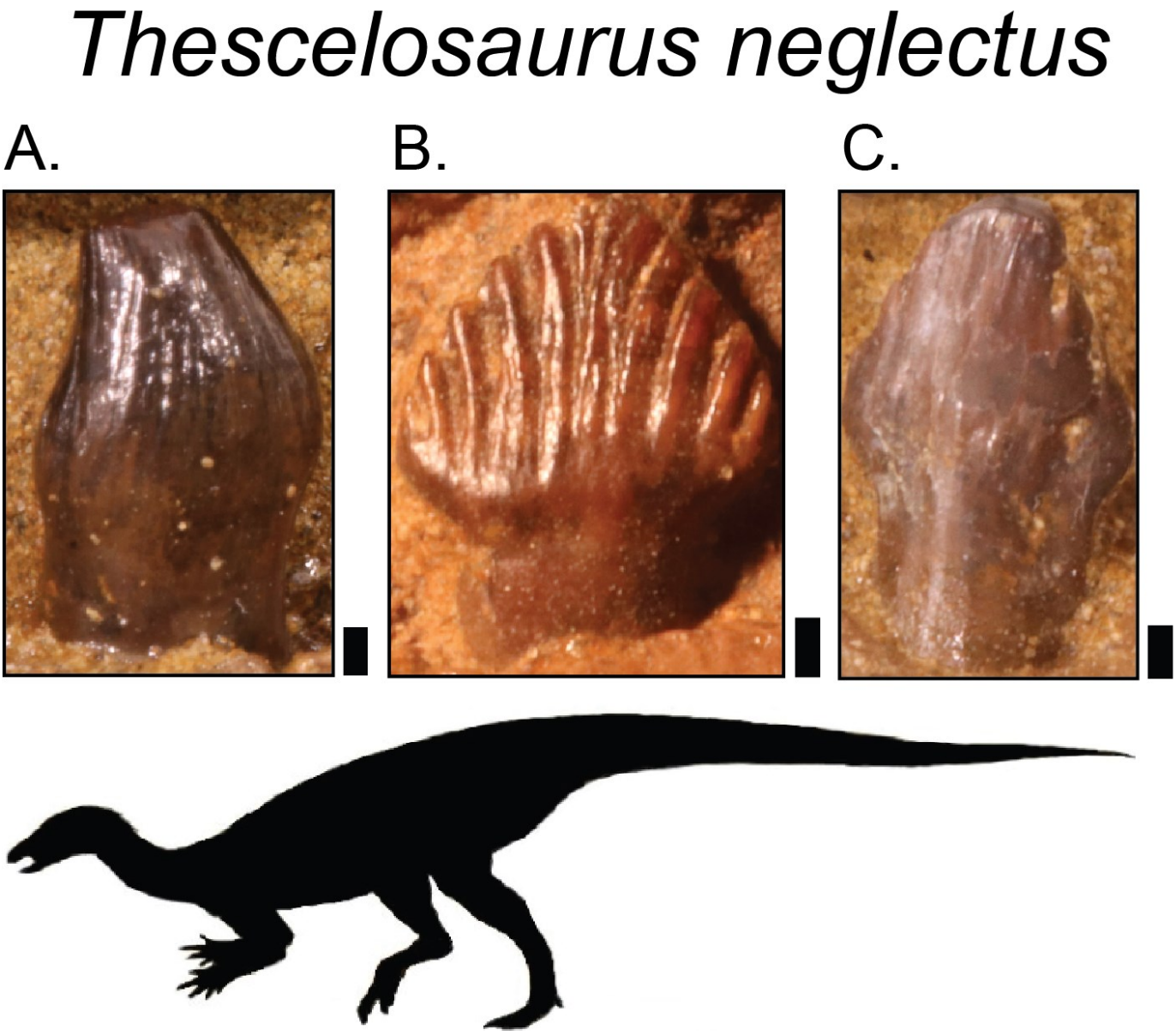

Figure 2.8. ***Thescelosaurus neglectus*** **(NCSM 15728) dentition in lateral view.**

The generalized pattern of thescelosaurid heterodonty. (A) Premaxillary, (B) maxillary, and (C) dentary teeth. Scale bar = 1 mm.

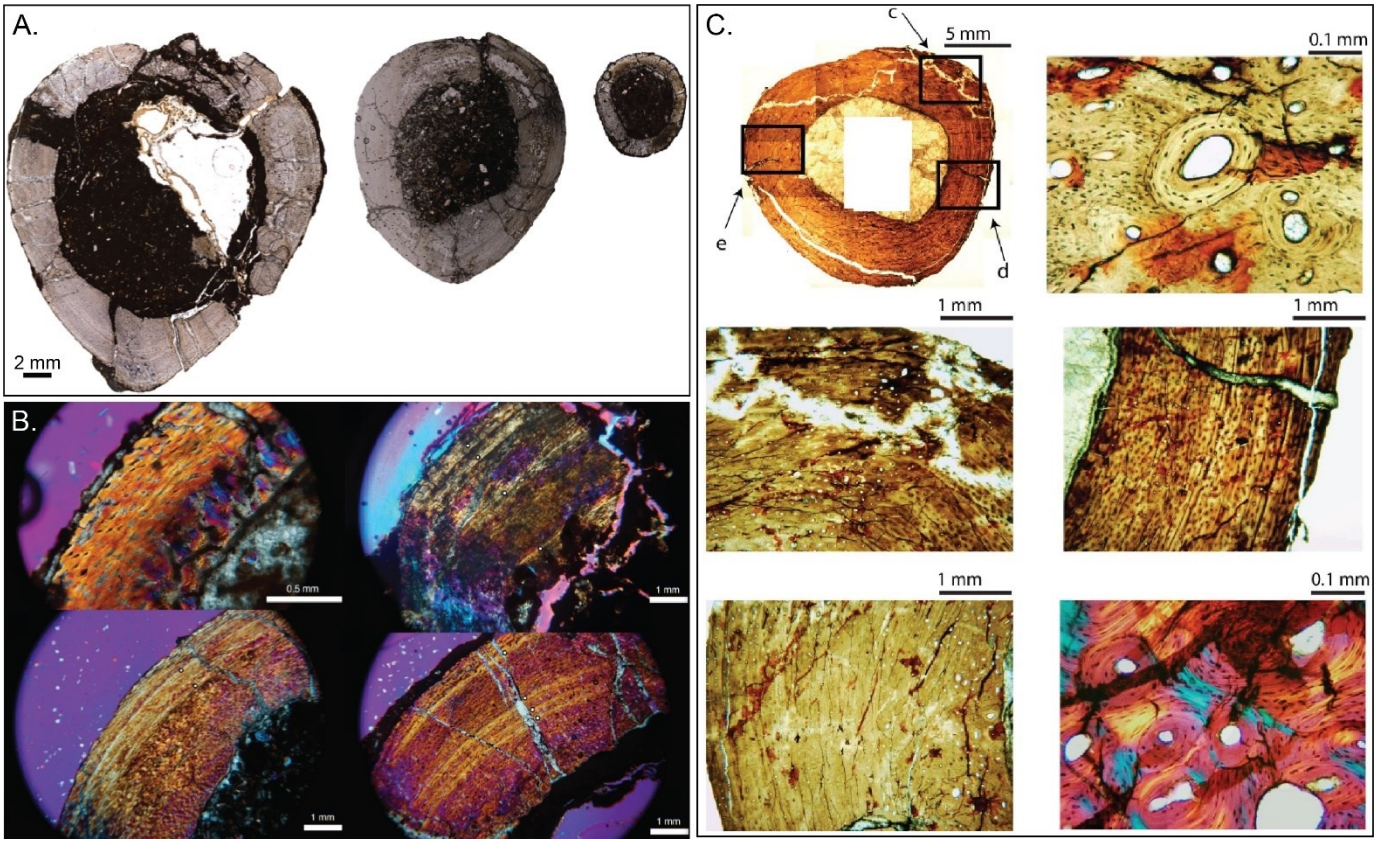

Figure 2.9. Examples of osteohistological sections of thescelosaurid long bones.

(A) Femoral transverse thin sections, under plane-polarized light, of *Haya* (IGM 100/2020, 100/2015, 100/1324) (Barta and Norell, 2021). (B) Femoral transverse thin sections, under crossed-polarized light, of *Haya* (IGM 100/2020, 100/2015, 100/3672) (Barta and Norell, 2021). (C) Femoral transverse thin sections under plane- and crossed-polarized light of *Oryctodromeus* (IMNH 44920) (Krumenacker, 2017).

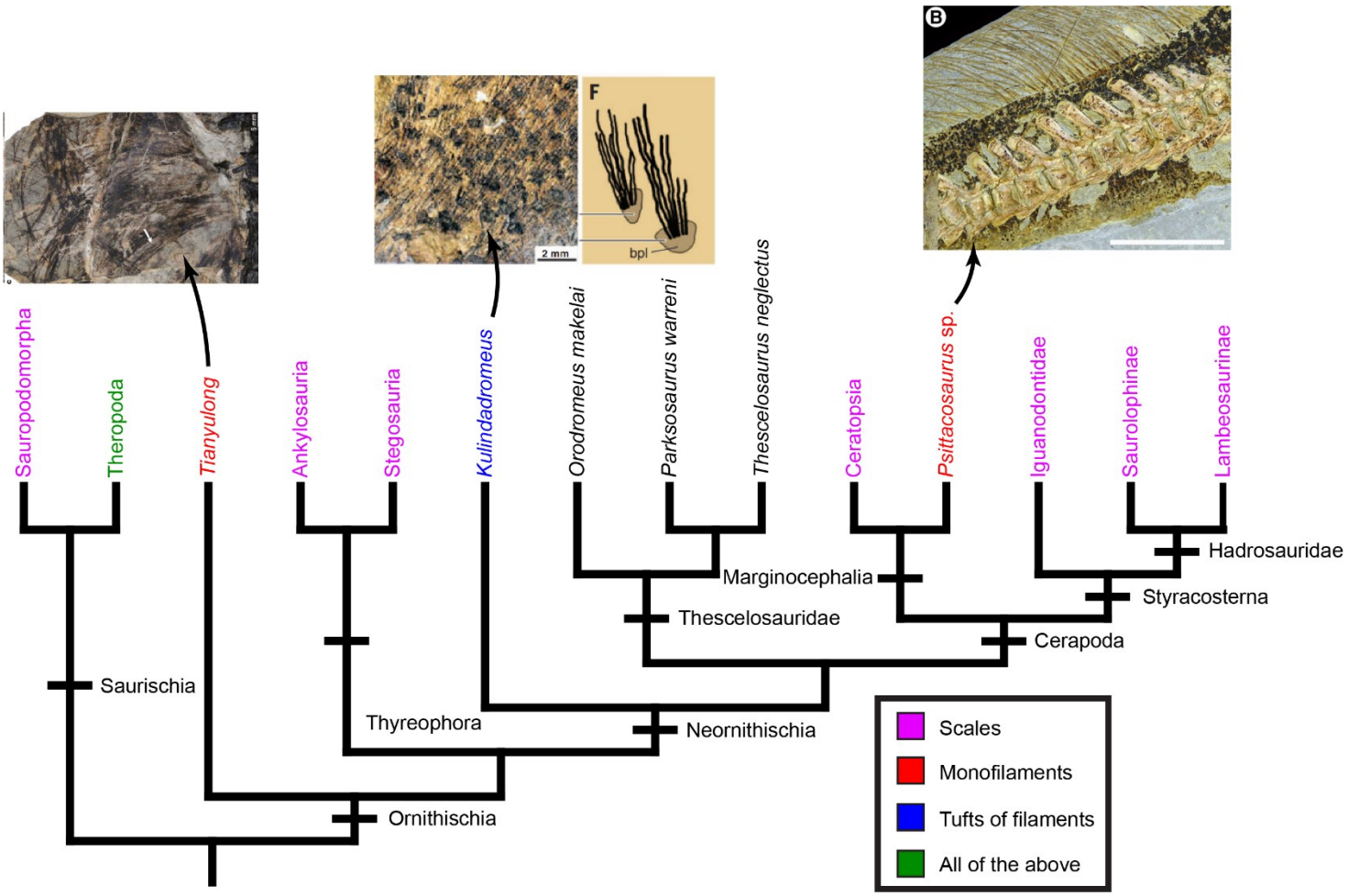

Figure 2.10. Documented distribution of soft-tissue integumentary structures across Dinosauria.

Colored taxa represent the type of soft-tissue integumentary structure. Thescelosauridae is black as their fossils do not preserve integumentary structures. Specimen images are from Godefroit et al. (2014), Vinther et al. (2016), and Zheng et al. (2009).

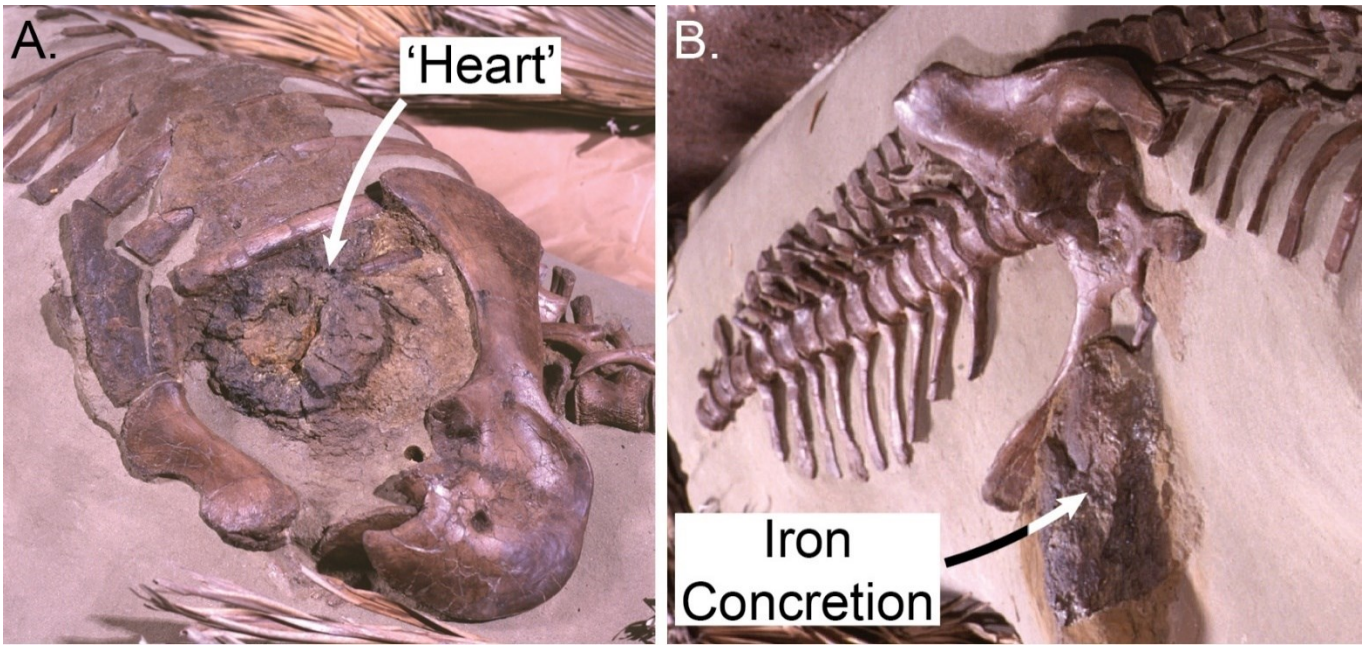

Figure 2.11. The supposed 'heart' (iron concretion) of *Thescelosaurus neglectus* (NCSM 15728).

'Heart' of *Thescelosaurus* (A). Iron concretion located around the femoral and pelvic region of the same specimen (B).

Figure 2.12. Lateral views of the rib cage, showing intercostal plates (arrows) in thescelosaurids.

(A) *Thescelosaurus* (NCSM 15728), (B) *Parksosaurus* (ROM 804), and (C) *Talenkauen* (MPM 10001) (Novas et al., 2004).

Chapter 3. A New Specimen of *Parksosaurus warreni* (Dinosauria: Ornithischia) from the Upper Cretaceous Horseshoe Canyon Formation of Alberta, Canada, and the Distinctive Pelvic Morphology of this Taxon

3.1. Introduction

Thescelosauridae is a clade of small, cursorial herbivorous, bipedal neornithischian dinosaurs that flourished from the Aptian to the Maastrichtian. Thescelosaurids are relatively poorly understood, partly because their poor fossil record has led to controversy regarding their taxonomy (Boyd et al., 2009) and phylogenetic interrelationships (Brown et al., 2013b; Boyd, 2015; Dieudonné et al., 2020; Herne et al., 2019; Madzia et al., 2018; Rozadilla et al., 2016). Few thescelosaurids are represented by large sample sizes, and morphological comparisons amongst taxa are often limited by the fragmentary nature of the available material. Typically, thescelosaurids suffer from having only one specimen per species representing their taxon (Brown et al., 2013b; Brown et al., 2011; Morris, 1976; Parks, 1926; Sues, 1980), and autapomorphies are commonly identified in the skulls (Barrett and Han, 2009; Boyd et al., 2009; Brown et al., 2011; Galton, 1995; Jin et al., 2010; Makovicky et al., 2011; Scheetz, 1999; Sues, 1980; Varricchio et al., 2007) with few known from the postcrania (Brown et al., 2013b; Huh et al., 2010; Morris, 1976; Scheetz, 1999; Varricchio et al., 2007). However, recent descriptions of new thescelosaurid fossils representing both novel and established taxa have led to progress in understanding the phylogenetic relationships and basic paleobiology of members of the clade (Barrett and Han, 2009; Barta and Norell, 2021; Boyd et al., 2009; Han et al., 2012; Han et al., 2020; Krumenacker, 2017; Makovicky et al., 2011; Norell and Barta, 2016).

Among the thescelosaurid taxa historically known from only a single specimen is *Parksosaurus warreni*, represented by a partial skeleton (ROM 804) from the Tolman Member of the Horseshoe Canyon Formation in Alberta, Canada (Boyd et al., 2009; Eberth et al., 2013; Parks, 1926). Parks (1926) initially assigned ROM 804 to the genus *Thescelosaurus*, as the holotype of the newly erected species *Thescelosaurus warreni.* He considered *Thescelosaurus* to belong to the now defunct taxonomic group "Hypsilophodontidae". *Thescelosaurus* and its purported close relatives (*Hypsilophodon*, *Orodromeus*, *Parksosaurus*, and *Yandusaurus*) were typically placed in this wastebasket group for small, bipedal ornithischians during the 20th century (Thulborn, 1971), but the dissolution of Hypsilophodontidae is supported by phylogenetic analyses (Butler et al., 2008; Scheetz, 1999). The re-diagnosis of ROM 804 occurred when Sternberg (1937) reassigned *T. warreni* to the genus *P. warreni* based on a comparison of morphological characters with *Thescelosaurus neglectus* (USNM 7757). Additional research identified that *P. warreni* lacked the skull autapomorphies, and had different hindlimb proportions to those of *T. neglectus* (Boyd et al., 2009; Galton, 1973; Galton, 1974b; Sternberg, 1940). *P. warreni* is a thescelosaurine thescelosaurid that occurred in the lower Maastrichtian Horseshoe Canyon Formation of southern Alberta, Canada (Brown and Druckenmiller, 2011; Boyd, 2015; Parks, 1926). As with many other thescelosaurids, *P. warreni* lacks genus and species level diagnosable postcranial characters despite comparable material with *Haya*, *Orodromeus*, *Oryctodromeus*, and *Thescelosaurus*.

A second, previously undescribed specimen of *Parksosaurus warreni* (UALVP 56885) was recovered by Tim Schowalter in 1972. It is a small, highly incomplete, partially articulated skeleton from the Morrin or Tolman member of the Horseshoe Canyon Formation. The specimen

was originally identified as a Hypsilophodontidae(?) on its specimen label and can be identified as a new specimen of *Parksosaurus warreni* based on distinctive, seemingly autapomorphic features present in the ilia and ischia. It represents the only new *Parksosaurus* material ever to have come to light since the holotype was first reported.

This study investigates the seemingly unusual features of the ilium and ischium to determine whether they represent plausible autapomorphies of *Parksosaurus warreni*. It also describes UALVP 56885, and tests its phylogenetic position within Ornithischia. The purpose of the phylogenetic analyses was to confirm that the *Parksosaurus* holotype (ROM 804) and UALVP 56885 would be posited as sister taxa when treated as separate operational taxonomic units. Having UALVP 56885 as a separate operational taxonomic unit was performed to verify that the specimen's observed morphologies were consistent with that of the holotype (ROM 804). The *Parksosaurus* holotype (ROM 804) is also compared with other basal neornithischians, thescelosaurids, and cerapodans to establish new postcranial autapomorphies. UALVP 56885 was compared with *Parksosaurus*, other thescelosaurids, and multiple ornithischian groups. Phylogenetic analyses of UALVP 56885 were conducted using previous published character matrices to understand its evolutionary position within Thescelosauridae.

3.1.1. Geologic Context

In southern Alberta, the Horseshoe Canyon Formation was deposited between 74.9 and 66.8 Ma and is a clastic wedge in the Western Canada Sedimentary Basin. This formation represents coastal plain strata consisting of coal beds, sandstone, siltstone, and mudstone (Eberth and Braman, 2012; Eberth and Kamo, 2019; Heller et al., 1988; Ogg and Hinnov, 2012) (Fig. 3.1). The accumulation and sediment supply of the Horseshoe Canyon Formation was facilitated

by tectonically controlled subsidence during the Late Cretaceous (Eberth and Braman, 2012; Heller et al., 1988).

The holotype (ROM 804) of *Parksosaurus warreni* was collected from the Tolman Member of the Horseshoe Canyon Formation, but the exact horizon and locality are unfortunately unknown (Parks, 1926). *Parksosaurus* lies within the *Hypacrosaurus altispinus* - *Saurolophus osborni* biozone of the Horseshoe Canyon Formation. This biozone is characterized by the presence of *Edmontonia*, *Hypacrosaurus*, *Montanoceratops*, *Parksosaurus*, *Saurolophus*, and *Spaerotholus*, and encompasses all of the Morrin and Tolman members (~68.4-71.0 Ma). The paleoenvironment associated with this biozone has been interpreted as a cool, seasonally wet, and well-drained coastal plain (Eberth et al., 2013; Larson et al., 2010).

UALVP 56885 was recovered from a terrestrial unit laterally equivalent to the Drumheller Marine Tongue between the Tolman Crossing and Morrin Bridge, but closer to the latter (pers. comm. Tim Schowalter, 2020) (Fig. 3.2). The rock surrounding the specimen is a fine to very fine angular litharenite that is brown to tannish brown in color, with flecks of black scattered throughout. The litharenite was composed of quartz, feldspar, lithics, and small iron concretions. Based on the stratigraphy from Eberth and Braman (2012), the specimen likely came from the Morrin or Tolman member of the Horseshoe Canyon Formation (Fig. 3.1). The two stratigraphic members have the same lithology, and are thought to have been deposited under similar paleoclimatic conditions (Eberth et al., 2013; Eberth and Braman, 2012). Although its exact stratigraphic placement is uncertain, UALVP 56885 is clearly from a level within the *Hypacrosaurus altispinus* - *Saurolophus osborni* biozone (Eberth et al., 2013).

3.2. Materials and Methods

3.2.1. Anatomical Comparisons

Parksosaurus warreni ROM 804 is a partial skull and skeleton of a small-bodied thescelosaurine thescelosaurid from the Tolman Member of the Horseshoe Canyon Formation. UALVP 56885 is an associated partial sacral vertebral series with articulated right and left ilia, disarticulated right and left ischia, and partially articulated caudal vertebral series. The specimen is described and compared to other Cretaceous ornithischians with the aid of digital calipers, measuring tape, and the line tool in the software ImageJ (Table 3.1 and 3.2). ImageJ allows for accurate measurements of specimens that are too fragile or small to be measured directly, or which are not physically available (Schneider et al., 2012).

3.2.2. Phylogenetic Analysis

Treating UALVP 56885 as separating operational taxonomic unit to posit a sister relationship with *Parksosaurus* (ROM 804) and to verify the observed morphologies, three phylogenetic analyses, using the character matrices of Brown et al. (2013b), Boyd (2015), and Madzia et al. (2018), were performed to assess the relationships of UALVP 56885 amongst thescelosaurids. Dieudonné et al.'s (2020) character matrix was excluded from the analysis because it was rampant with scoring errors. The three included data sets were initially developed to analyze patterns of relationships in various parts of the neornithischian tree.

Brown et al.'s (2013b) character matrix was modified from Boyd et al. (2009) and was developed to resolve the relationships amongst thescelosaurids. The operational taxonomic units of this matrix included non-thescelosaurids in the analysis (e.g., *Dryosaurus*, *Iguanodon*, and

Scutellosaurus). The version analyzed here of the matrix from Brown et al. (2013b) contained 29 operational taxonomic units and 137 characters. *Herrerasaurus* was set as the outgroup taxon. The character matrix from Boyd (2015) was modified from various published matrices (Butler et al., 2008; Scheetz, 1999; Weishampel and Heinrich, 1992; Weishampel et al., 2003), and was developed to explore the relationships among basal neornithischians. Boyd's (2015) operational taxonomic units included non-thescelosaurid clades in the analysis (e.g., Thyreophora, Marginocephalia, and Ornithopoda). Analysis of the final matrix contained 66 operational taxonomic units and 255 characters with *Marasuchus* set as the outgroup taxon. Madzia et al.'s (2018) character matrix was modified from Boyd (2015) and was developed to assess the phylogenetic position of *Burianosaurus* amongst non-ankylopollexian ornithopods. Madzia et al'. (2018) operational taxonomic units included non-thescelosaurid clades in the analysis (e.g., Thyreophora, Marginocephalia, and Ornithopoda). The final matrix contained 75 operational taxonomic units and 255 characters with *Marasuchus* as the outgroup taxon. Although the matrices vary in characters and taxa, they essentially represent different versions of each other and should give an increasing phylogenetic resolution for UALVP 56885. The character matrices make it possible to test the phylogenetic position of UALVP 56885, determine whether Thescelosauridae and its main constituent clades are recovered when the new material is included in each analysis, compare phylogenetic statistical results, and test whether the specimen emerges as the sister taxon of ROM 804 when the two are treated as separate operational taxonomic units.

The three character matrices were compiled in Mesquite v.3.6 (Maddison and Maddison, 2009) then exported as TNT files and were separately analyzed in Tree analysis using New

Technology (TNT) phylogenetic software (Goloboff et al., 2008). Characters were run as unordered and the traditional search option was used. Traditional search was run using Wagner trees and the tree bisection reconnection swapping algorithm utilizing 1,000 replicates and saving 100 trees per replication. Branches were collapsed if their minimum length equaled to zero. Most parsimonious trees were held in memory and subjected to a second run of the tree bisection reconnection swapping algorithm to optimize the total number of most parsimonious trees. A standard bootstrap analysis of 1,000 replicates and Bremer support values using tree bisection reconnection from existing trees. A strict consensus tree was recovered from the analyses and a majority rule tree using the 50% cut off method was used to resolve any polytomies in the results.

3.3. Systematic Paleontology

DINOSAURIA Owen, 1842

ORNITHISCHIA Seeley, 1887

NEORNITHISCHIA Cooper, 1985 (sensu Butler et al., 2008)

THESCELOSAURIDAE Sternberg, 1937

Phylogenetic Definition- The most recent common ancestor of *Thescelosaurus neglectus* Gilmore, 1913 and *Orodromeus makelai* Horner and Weishampel, 1988, and all of its descendants.

Comments- Initially erected by Sternberg (1937), Thescelosauridae is used to differentiate *Thescelosaurus* and *Hypsilophodon*. Recent research advancements in non-cerapodan phylogenetics has revealed a monophyletic Thescelosauridae (Boyd et al., 2009;

Boyd, 2015; Brown et al., 2013b; Madzia et al., 2018). The stem-based clade Thescelosauridae was described by Buchholz (2002) and included *Parksosaurus*, but not *Dryosaurus*, *Hypsilophodon*, or *Iguanodon*. Brown et al. (2013b) used the phylogenetic definition of Thescelosauridae to recognize its monophyly by preserving its original intention to differentiate *Thescelosaurus* and closely related taxa from *Hypsilophodon* and to reflect the increasing diversity of small-bodied non-cerapodans in the Late Cretaceous. Boyd (2015) recovered Thescelosauridae (=Parksosauridae) in the analysis with the original fourteen taxa and the clades within, similar to Brown et al. (2013b). However, the evolutionary relationships of basal neornithischian are strongly debated with different studies resulting in disparate phylogenetic topologies (Dieudonné et al., 2020; Herne et al., 2019; Madzia et al., 2018; Rozadilla et al., 2016).

THESCELOSAURINAE Sternberg, 1940

Phylogenetic Definition- A stem-based clade including all neornithischians more closely related to *Thescelosaurus neglectus* Gilmore (1913) than to *Orodromeus makelai* Horner and Weishampel (1988) or *Parasaurolophus walkeri* Parks (1922).

Comments- Thescelosaurinae was originally proposed by Sternberg (1940) to differentiate *Thescelosaurus* from *Dysalotosaurus*, *Hypsilophodon*, and *Parksosaurus*. Brown and Druckenmiller (2011) defined Thescelosaurinae as a stem-based clade. Boyd (2015), Brown et al. (2013b), Madzia et al. (2018) recovered Thescelosaurinae as a subclade in Thescelosauridae. Evolutionary relationships of basal neornithischians are strongly debated with different studies resulting in disparate phylogenetic topologies where thescelosaurine taxa shift

in and out of Thescelosauridae (Boyd, 2015; Brown et al., 2013b; Dieudonné et al., 2020; Herne et al., 2019; Madzia et al., 2018; Rozadilla et al., 2016).

PARKSOSAURUS Sternberg, 1937

Type Species- Parksosaurus warreni (Parks, 1926)

Distribution- Horseshoe Canyon Formation, Alberta (Maastrichtian; 72.1 - 66.0 Ma) (Ogg and Hinnov, 2012).

Diagnosis- As for type and only known species.

PARKSOSAURUS WARRENI Parks, 1926

Thescelosaurus warreni Parks, 1926

Parksosaurus warreni Sternberg, 1937

Holotype- ROM 804: partial skull and postcranial skeleton.

Locality- One half mile from the Red Deer River, on the east side, immediately south of the road to Rumsey ferry.

Horizon- Exact horizon is unknown, but the specimen was collected in the Tolman Member of the Horseshoe Canyon Formation, Alberta (Maastrichtian; 72.1 - 66.0 Ma) (Ogg and Hinnov, 2012). Parks (1926) noted that the specimen was collected 300 meters above the water level of the Red Deer River.

Referred Specimen- UALVP 56885 is an incomplete skeleton including a sacrum preserved together with the paired ilia and ischia, and part of the tail. The ilia, sacrals, and sacral ribs were in articulation, as were portions of the caudal vertebral series. The specimen includes

four left and five right sacral ribs, four sacral vertebrae, the partial ilia and ischia, nine caudal vertebrae, and a number of ossified tendons.

Horizon- A terrestrial layer that is laterally equivalent to the Drumheller Marine Tongue of the Horseshoe Canyon Formation in southern Alberta (Pers. Comm. Tim Schowalter, 2020). Based on the lithology of the sediments surrounding the specimen and the stratigraphy (Eberth and Braman, 2012), the specimen was likely recovered from either the Morrin or Tolman member of the Horseshoe Canyon Formation.

Locality- The specimen was recovered along the Red Deer River between the Tolman Crossing and Morrin Bridge, but closer to the latter (Pers. Comm. Tim Schowalter).

Diagnosis- Galton (1995) gave the following diagnosis: a deep posterior process of the premaxilla; an extensive sutural contact between the maxilla and nasal; a small, oval antorbital fenestra; a transversely wide squamosal; and well-enameled teeth with numerous low, rounded ridges. New postcranial autapomorphies of *Parksosaurus warreni* identified in this study include: the distal part of the ischium paddle-shaped, medioventrally expanded, and dorsoventrally thin; dorsal margin of ischial shaft is concave; mound-like obturator process situated at the proximal end of the paddle-shaped portion of the ischium; brevis fossa is a narrow, oval facet that extends anteroposteriorly along the ventral margin of the postacetabular process; and the obturator process is placed 60% down the ischial shaft (Fig. 3.3).

Comments- Parks (1926) initially described the holotype (ROM 804) as *Thescelosaurus warreni*, but this specimen was reassigned to *Parksosaurus warreni* by Sternberg (1937). An extensive redescription of ROM 804 will not be given here, as the specimen is currently

undergoing further preparation and will be redescribed elsewhere (Boyd et al., 2009). This study aims to identify additional postcranial autapomorphies for *Parksosaurus*. The ilium and ischium of UALVP 56885 display unusual, evidently autapomorphic features also present in the *Parksosaurus warreni* holotype (ROM 804). However, UALVP 56885 does not preserve any cranial elements, so the presence or absence of the skull autapomorphies seen in ROM 804 cannot be assessed.

3.4. Description of UALVP 56885

3.4.1. Sacral Vertebrae

Four articulated sacral vertebrae are preserved, and retain the centra and neural arches together with the sacral ribs (Fig. 3.4). Anterior sacral ribs are fused to the medial side of the ilium, but the most posterior one has visible sutures with the vertebrae and the medial walls of the ilia. It is unknown how many sacral vertebrae and sacral ribs were present, but based on *Parksosaurus* ROM 804, UALVP 56885 likely preserves four out of the six vertebrae, and is missing the most anterior and posterior ones. The anteriormost and posteriormost sacral ribs and vertebrae are damaged and/or missing. The sacral ribs and centra are similar to those of *Parksosaurus* ROM 804, despite slight differences in the morphology of the posterior centrum that are apparent in ventral view (Parks, 1926). The first three sacral ribs contact the centra intervertebrally, but the most posterior rib contacts only the posteriormost centrum. The shift from intervertebral sacral rib contacts to a single sacral rib attaching to a single vertebra occurs in *Changchunsaurus*, *Orodromeus*, *Parksosaurus*, and *Thescelosaurus* (Brown et al., 2011b; Butler et al., 2011; Galton 1974; Gilmore, 1915; Parks, 1926; Scheetz, 1999). Anteroposteriorly broader than tall, the anterior sacral rib appears hourglass-shaped in dorsal and ventral views,

and bears midline ridges on dorsal and ventral surfaces (Table 3.1, 3.2). The most anterior sacral centra are anteroposteriorly longer than transversely wide. However, more posterior sacral centra progressively become transversely wider than anteroposteriorly long. The most posterior sacral centrum is transversely wider than dorsoventrally tall. Its sacral rib is somewhat robust at the medial end and gradually becomes conical at the lateral end. It bears a midline ridge like its more anteriorly positioned counterparts. The most anterior sacral rib has the widest transverse contact with the vertebra but the most posterior one has a larger surface area contact with the vertebra compared to the others, which are round. All four centra preserve neural spines that are dorsoventrally taller than anteroposteriorly long, but are increasingly damaged posteriorly. The average neural spine angle is 66.5º and the spines appear to be fused together at their bases, although their dorsal portions are separate. The most posterior vertebra preserves the postzygapophyses and the most anterior vertebra does not preserve the prezygapophyses. The first three sacral centra are ankylosed, although the most posterior vertebra does not appear to be fused to the others. The missing most posterior centrum may have been unfused as well. The missing first sacral centrum was likely fused to the most anterior preserved one. In morphology and pattern of fusion, the sacral ribs broadly resemble those of *Hypsilophodon*, *Parksosaurus* ROM 804, and *Thescelosaurus* (Brown et al., 2011; Galton, 1974a and b; Parks, 1926).

3.4.2. Caudal Vertebrae

Nine caudal vertebrae from the partial tail that varies in quality of preservation (Fig. 3.5). This partial tail does not form a continuous series but some are in articulation with one another, and the vertebrae are from different parts of the tail. The positions of the vertebrae within the

caudal series were determined by morphological comparisons to the caudals of *Parksosaurus* ROM 804 and other thescelosaurids.

The caudal vertebrae are similar in morphology and size to the most anterior caudal vertebrae of thescelosaurids (Gilmore, 1915; Han et al., 2012; Huh et al., 2010; Krumenacker, 2017; Makovicky et al., 2011; Parks, 1926; Scheetz, 1999) (Fig. 3.5a, b, c). Three anterior caudal vertebrae are preserved and six posterior ones are preserved. The most anterior caudal vertebra preserved is interpreted as being at least the seventh in the series due to the presence of chevron facets, tall neural spines, and transverse processes (Gilmore, 1915; Han et al., 2012; Huh et al., 2010; Krumenacker, 2017; Makovicky et al., 2011; Parks, 1926; Scheetz, 1999). These features tend to disappear around the 12th vertebra in *Parksosaurus* ROM 804 and the 10th in *Thescelosaurus* (Gilmore, 1915; Parks, 1926). An anteriorly positioned centrum is the most complete and is amphicoelous. It measures 23.1 mm, 24.3 mm, and 18.1 mm in anteroposterior length, transverse width, and dorsoventral height, respectively (Table 3.1). The lateral sides of all the centra are pinched in below the separate sutures of the transverse processes and neural arch (Fig. 3.5). The centrum is pinched inward around the midpoint of its length but expands laterally both anteriorly and posteriorly, producing an hourglass-shaped outline in ventral view. The articular facet for the chevron is present as in other thescelosaurids and forms an oval-shape on the most anterior and most posterior ventral margins of the centrum (Gilmore, 1915; Han et al., 2012; Huh et al., 2010; Krumenacker, 2017; Makovicky et al., 2011; Parks, 1926; Scheetz, 1999). Transverse processes are present on the most anterior caudal vertebra, but their lateral ends are damaged. The transverse processes and neural arches are not fused to the centra, but are attached by sutures (Fig. 3.5). The transverse processes each have a dorsoventrally thin, oval

cross-section, and their lateral ends curve ventrally. In dorsal view, the transverse processes curve either the posterior or the anterior direction. As the direction of the bending may differ between the two transverse processes of the same centrum, at least some of the caudals have undergone plastic distortion. The average anteroposterior length, transverse width, and dorsoventral height of the transverse processes are 12.05 mm, 14.9 mm, and 6.6 mm, respectively (Table 3.1).

The most anterior neural spine is the best preserved in the series, and is laterally compressed, dorsoventrally tall, and inclined posteriorly. The anteroposterior length, transverse width, dorsoventral height, and posterior inclination are 14.8 mm, 3.8 mm, 20.3 mm and 62.4°, respectively (Table 3.1). The dorsal end of the neural spine has a squared-off appearance in lateral view, with rounded anterior and posterior corners. The pre- and postzygapophyses are strongly inclined mediodorsally and lateroventrally, respectively, and lack anteroposterior grooves on the pre- and postzygapophyses that are seen in pachycephalosaurids (Galton and Sues, 1983).

The posteriorly positioned caudal vertebrae are badly damaged, in that the neural spines, pre- and postzygapophyses, centra, transverse processes, and chevrons are missing. Some of these damaged caudal vertebrae are obscured by ossified tendons (Fig. 3.5). The most anterior of the posterior positioned caudal vertebrae is interpreted as being no farther anteriorly than the 29th in the series (mid-series) based on morphological comparisons to other ornithischians (Gilmore, 1915; Han et al., 2012; Huh et al., 2010; Krumenacker, 2017; Makovicky et al., 2011; Parks, 1926; Scheetz, 1999). The maximum number of caudal vertebrae in a series varies between thescelosaurids where *Thescelosaurus* had approximately 50 caudal vertebrae and *Parksosaurus*

ROM 804 had 42. UALVP 56885 likely had a caudal vertebra count closer to *Parksosaurus* ROM 804 based on similar morphology with the holotype. The features that are characteristic of mid-caudals include small chevrons, lack of transverse processes, and ossified tendons that extend parallel with the vertebral column (Fig. 3.5d). Three chevrons are present, but are badly damaged. The chevrons articulate intervertebrally and each has a ~45° posteroventral inclination, relative to the damaged centra. The proximal chevron head contacts the posterior ventral margin of the anteriorly positioned centrum. Due to the inclination of the chevron, the posterior dorsal margin of the chevron shaft contacts the anterior ventral margin of the posteriorly positioned centrum (Fig. 3.5).

3.4.3. Ossified Tendons

Trellis structured ossified tendons are present on multiple caudal vertebrae of UALVP 56885 (Fig. 3.5d, e). Ossified tendons extend anteroposteriorly along the series of the caudal vertebrae. The tendons are anteroposteriorly elongate, and subparallel to one another in orientation. Ossified tendons are present in many neornithischians (Galton, 1974a; Gilmore, 1915; Han et al., 2012; Krumenacker, 2017; Parks, 1926; Scheetz, 1999; Varricchio et al., 2007).

3.4.4. Ilium

The posterior portions of the left and right ilia are both preserved. Each includes the dorsal portion of the acetabulum, damaged ischial peduncle, and postacetabular process, although the right ilium is more complete (Fig. 3.4, 3.6, 3.7). Refer to Tables 3.1 and 3.2 for measurements of the ilium in UALVP 56885 and other thescelosaurids. The width of the ilium (including both ilia and articulated sacrals) is transversely wider than the ilia's postacetabular

dorsoventral height, above the ischial peduncle. In lateral view, the postacetabular process is morphologically similar to those of *Parksosaurus* ROM 804 and *Jeholosaurus* (Han et al., 2012; Parks, 1926) (Fig. 3.4, 3.6, 3.7). In dorsal view, the postacetabular process is transversely thin but is convex on its lateral sides, rather than concave as in *Haya*, *Parksosaurus* ROM 804, *Jeholosaurus*, *Orodromeus*, and *Thescelosaurus* (Gilmore, 1915; Han et al., 2012; Makovicky et al., 2011; Parks, 1926; Scheetz, 1999). The concavity of the lateral postacetabular surface may not reflect the condition during life, as the area could have been crushed diagenetically.

The ilia's lateral margin is vertically oriented and transversely thin, although the portion dorsal to the ischial peduncle is thicker than the rest of the bone. The postacetabular process is rounded at its posterior end as in *Parksosaurus* and *Jeholosaurus*. However, in UALVP 56885 the height of the ilium gradually decreases posteriorly and the posterior part of the dorsal margin is relatively straight, rather than convex as in ROM 804 (Fig. 3.4, 3.6, 3.7). The most dorsal portion of the lateral surface of the iliac blade bears dorsoventral striations that can be interpreted as marking the origin of the iliotibialis (Maidment and Barrett, 2011b; Maidment et al., 2014). Maidment and Barrett (2011b) reconstructed the pelvic myology of *Hypsilophodon*, *Lesthosaurus*, and *Scelidosaurus*, whereas Maidment et al. (2014) reconstructed that of *Edmontosaurus*. The lateral surface of the postacetabular process is slightly concave, similar to *Thescelosaurus* and *Haya*, rather than flat as in *Parksosaurus* (Fisher et al., 2000; Gilmore, 1915; Makovicky et al., 2011; Parks, 1926). The iliofibularis would have attached to the postacetabular process at the center of its posterior margin and acted as the primary extensor for the hindlimb (Maidment et al., 2011b; Maidment et al., 2014). A concavity is present on the iliac blade above

the acetabulum, and can be interpreted as the origination area of the iliofemoralis (Maidment and Barrett, 2011b; Maidment et al., 2014).

The ischial peduncle is transversely wider than anteroposteriorly long, and projects laterally outward. The ischial peduncle is similar in morphology and position to those of *Haya* and *Parksosaurus* (Makovicky et al., 2011; Parks, 1926) (Fig. 3.7). Posterior to the ischial peduncle, the brevis shelf's orientation is strikingly similar to that of *Parksosaurus* ROM 804 and is distinct from other thescelosaurids. However, the brevis shelf of *Parksosaurus* ROM 804 is a more prominent feature (Fig. 3.7 and Table 3.2). UALVP 56885, the shelf is medioventrally orientated. The brevis shelf orientation in *Parksosaurus* ROM 804 is difficult to discern based on images of the specimen. However, a conservative interpretation of its orientation would either be ventral or medioventral (Fig. 3.7). In other thescelosaurids, the brevis shelf orientation is likewise either medioventral (*Haya*, *Oryctodromeus*, and *Thescelosaurus*) or ventral (*Orodromeus*) (Fig. 3.7 and Table 3.3) (Gilmore, 1915; Han et al., 2012; Krumenacker, 2017; Makovicky et al., 2011, Parks, 1926; Scheetz, 1999). The brevis fossa in UALVP 56885 forms a small, narrow oval facet that extends anteroposteriorly along the ventral margin of the postacetabular process. The brevis fossa acts as the origination point for the caudofemoralis brevis (Maidment and Barrett, 2011b; Maidment et al., 2014). The brevis fossa morphology and orientation in UALVP 56885 is similar to *Parksosaurus* ROM 804, although it is larger in the latter (Fig. 3.7). The brevis fossa morphology and orientation vary in thescelosaurids. In both specimens, the brevis fossa orientation extends in the posteroventral direction along the postacetabular process's ventral margin (*Haya*, *Oryctodromeus*, and *Thescelosaurus*) or it extends ventrally along the ventral margin of the postacetabular process (*Orodromeus*) (Fig. 3.7)

(Gilmore, 1915; Makovicky et al., 2011; Krumenacker, 2017; Scheetz, 1999). The brevis fossa in thescelosaurids may be an elongated broad feature (*Haya*), a broad sub-rectangular feature (*Thescelosaurus*), a narrow rectangular feature (*Oryctodromeus*), or a broad triangular feature (*Orodromeus*) (Gilmore, 1915; Makovicky et al., 2011; Krumenacker, 2017; Scheetz, 1999). For example, outside of Thescelosauridae, the brevis fossa of *Jeholosaurus* is a narrow oval feature that extends anteroposteriorly along the ventral margin of the postacetabular process but has a slight tilt in the posteroventral direction, and the brevis shelf is ventrally oriented. The differences in brevis fossa and shelf morphology, size, orientation, and positions in thescelosaurids maybe ontogenetically dependent (see discussion).

3.4.5. Ischium

Both ischia are preserved, but the left element is more complete than the right. Each ischium preserves the shaft, obturator process, and paddle-shaped distal expansion (Fig. 3.6, 3.8). The left ischium also preserves a damaged portion of the iliac peduncle and the base of the pubic peduncle. Overall, the ischia are morphologically similar to those of *Parksosaurus* ROM 804 in possessing a distinct paddle-shaped distal expansion, a mound-like obturator process, and a dorsal concavity of the ischial mid-shaft. In contrast, other thescelosaurids have rod-like distal shafts of the ischia, tab-shaped obturator processes, and straight dorsal margins of the mid-shaft regions (Gilmore, 1915; Han et al., 2012; Krumenacker, 2017; Makovicky et al., 2011, Parks, 1926; Scheetz, 1999) (Fig. 3.6, 3.8).

The margin between the iliac and pubic peduncles, which forms the posteroventral margin of the acetabulum, is concave and is rimmed by a laterally protruding ridge. Posteroventral to this ridge is a depression situated between the articular heads. The iliac

peduncle expands broadly (Fig. 3.6). Distal to the iliac and pubic peduncles, the ischium contracts to form a slender shaft that is rectangular in cross-section and dorsally concave where the dorsoventral height exceeds its transverse width. In medial view, the ischial shaft possesses an anteroposteriorly directed ridge that is deflected ventrally. The ridge terminates prior to the mediolateral expansion of the distal part of the ischium. In medial view, the ischial mid-shaft has a flat facet starting in its proximal region and terminating prior to the obturator process. This flat facet may have contacted the other ischium in life. The distal portion of the shaft twists about its longitudinal axis and broadly expands mediolaterally into a sub-rectangular, paddle-shaped plate that is dorsoventrally thin. This distal expansion would have contacted the corresponding part of the opposite ischium to form a single laterally broad sheet of bone. The obturator process is a mound-like medial prominence at the level of the proximal end of the paddle-shaped portion of the ischium. The obturator process is present in most neornithischians, but varies in form. This structure is a roughened tuberosity in UALVP 56885, similar to that of *Parksosaurus* (Fig. 3.6, 3.8 and Table 3.2) but differing from the tab-shaped obturator processes observed in other thescelosaurids (Gilmore, 1915; Han et al., 2012; Krumenacker, 2017; Makovicky et al., 2011, Norman et al., 2004; Parks, 1926; Scheetz, 1999) (Table 3.3). A flat facet is present and is teardrop-shaped in ventral view, prior to the obturator process. This facet originates as a point at the distal portion of the ischial shaft and terminates as a rounded margin that abuts the obturator process.

3.5. Phylogenetic Analysis

3.5.1. Brown et al., 2013b

Addition of UALVP 56885 to the data matrix of Brown et al. (2013b) resulted in six most parsimonious trees, with a tree length of 431 steps, a consistency index of 0.43, and a retention index of 0.61. Bootstrap values (>50) and Bremer support (>1) are shown at the nodes and stems of the strict consensus tree (Fig. 3.9). The resulting topology diverges from that obtained in the original analysis, and inclusion of UALVP 56885 has resulted in decreased phylogenetic resolution and lower levels of node support. Thescelosauridae was not recovered, but a polytomy was recovered involving Orodrominae (*Albertadromeus*, *Orodromeus*, *Oryctodromeus*, and *Zephyrosaurus*), Ornithopoda, Thescelosaurinae (*Changchunsaurus*, *Haya*, *Jeholosaurus*, and *Thescelosaurus*), *Hypsilophodon* and *Parksosaurus* ROM 804 (Fig. 3.9). It should be of note that both *Parksosaurus* specimens (ROM 804 and UALVP 56885) were the only thescelosaurids that were not placed in Thescelosaurinae or Orodrominae in the analysis. These results are in contrast with Brown et al. (2013b) original analysis where Thescelosauridae was not recovered, instead a large polytomy between Orodrominae, Ornithopoda, Thescelosaurinae, *Hypsilophodon* and *Parksosaurus* ROM 804 was recovered. UALVP 56885 was recovered in the polytomy. One character, namely the presence of an obturator process placed 60% of the way down the ischial shaft (character 102), was posited as autapomorphic for UALVP 56885. A 50% majority rule consensus of the most parsimonious trees placed UALVP 56885 in the same position as did the strict consensus.

Orodrominae and Thescelosaurinae were recovered, but were not united as a monophyletic Thescelosauridae in the strict consensus. Orodrominae is supported in the analysis

by the following synapomorphies: quadrate ventral condyles are tilted (character 7; convergent in Thescelosaurinae); the posterior process of posterolateral recess of the premaxilla is present (character 29; convergent in *Haya*); the foramen magnum is 20-30% as wide as the occipital condyle (character 71); the pubis is supported by a sacral centrum (character 84; convergent in *Haya* and *Rhabdodon*); the tail lacks ossified hypaxial tendons (character 86; convergent in *Haya* and *Jeholosaurus*); the scapular spine is sharp and pronounced (character 89); the acetabulum is dorsoventrally low and anteroposteriorly long (character 98); and the fibular shaft is D-shaped in cross-section (character 115).

Thescelosaurinae is supported in the analysis by the following synapomorphies: quadrate ventral condyles slope dorsolaterally (character 7; convergent in Orodrominae); the jugal wing of the quadrate terminates ventrally at or near the level of the ventral condyles of the quadrate (character, 9); the margin of the orbit is striated and rugose (character 18); a jugal horn is present (character 44); the dentaries are straight in dorsal view (character 61); the predentary possesses a bifurcated posteroventral process (character 64); the first caudal rib is not the longest (character 87); the width of the coracoid is less than 60% of its length (character 90); and the palpebral is dorsoventrally flat, with rugose medial and distal edges (character 125).

3.5.2. Boyd, 2015

Addition of UALVP 56885 to the Boyd (2015) data matrix resulted in 36 most parsimonious trees, with a tree length of 881 steps, a consistency index of 0.36, and a retention index of 0.64 (Table 3.4). Bootstrap values (>50) and Bremer support (>1) are shown at the nodes and stems of the strict consensus tree (Fig. 3.10). UALVP 56885 and ROM 804 had identical character coding in this matrix. The topology of the resulting consensus tree is identical

to that of Boyd (2015) and all major ornithischian clades are recovered (e.g., Marginocephalia, Neornithischia, Ornithopoda, and Thyreophora). However, Bootstrap and Bremer support for the resulting clades are reduced when UALVP 56885 is included. Thescelosauridae (=Parksosauridae) and subclades within (Elasmaria, Orodrominae, and Thescelosaurinae) are recovered in this analysis. The clade Orodrominae consists of *Koreanosaurus*, *Orodromeus*, *Oryctodromeus*, *Zephyrosaurus*, and the Kaiparowits Orodromine. The clade Thescelosaurinae is comprised of *Changchunsaurus*, *Haya, Parksosaurus*, and *Thescelosaurus*. The South American clade, Elasmaria, was recovered and contains *Macrogryphosaurus*, *Notohypsilophodon*, and *Talenkauen* and was nested within Thescelosaurinae, sister to *Thescelosaurus*. In the strict consensus tree, UALVP 56885 was recovered in the thescelosaurine Thescelosauridae clade and is sister to *Parksosaurus* (Fig. 3.10). No autapomorphies were recovered for UALVP 56885 in this analysis. However, a synapomorphy was recovered between UALVP 56885 and *Parksosaurus*: the dorsal margin of the ischial shaft is posterodorsally concave at its mid-length in lateral view (character 201).

Thescelosauridae is supported in this analysis by an everted oral margin of the premaxillae on the lateral surface (character 5; convergent in *Agilisaurus* and reversed in *Zephyrosaurus*); the presence of a concavity on the posterior end of the premaxilla is the receipt of the anterolateral boss of the maxilla (character 14); the angle between the base and the long axis of the braincase is less than 35 degrees (character 98; convergent with *Hypsilophodon*); the pubis is supported by at least one sacral centrum (character 193; convergent with *Rhabdodon*); the lateral surface of the greater trochanter is flattened (character 213; convergent with the

Zalmoxes clade); and the lateral distal tarsal is 'square' (character 242); the premaxillae is fused (character 255; reversed in *Haya* and *Orodromeus*).

Elasmaria is recovered as an inclusive clade within Thescelosauridae and is supported by epipophyses present on the anterior three cervicals (character 145); the deltopectoral crest is reduced (character 168); the prepubic process if mediolaterally flattened (character 197); and the ischial shaft is ovoid to subcylindrical (character 205; convergent in *Zephyrosaurus*).

The clade Orodrominae is supported in this analysis by possessing a foramen magnum that occupies 20-30% of the dorsal margin of the occipital condyle (character 108; convergent with *Othnielosaurus*); ridges are absent on the dentary teeth but denticles are present (character 114; convergent in *Changchunsaurus* and *Wannanosaurus*); the sacrum is composed of seven or more fused vertebra centra (character 148; convergent with the *Zalmoxes* clade); the scapular spine is sharp and pronounced (character 158); and the fibular shaft is 'D-shaped' in transverse section throughout its length (character 233).

Thescelosaurinae is supported by possessing two or more supraorbitals (character 23; convergent in *Agilisaurus* and *Wannanosaurus*); the supraorbital extends across at least 71% of the maximum anteroposterior length of the orbit (character 25; convergent in *Agilisaurus*); the quadrate notch is present (character 51); a ridge or process on the lateral surface of surangular has dorsally directed finger-like process present (character 86); and the angle between the femoral head and femoral shaft is less than or equal to 100 degrees (character 210).

3.5.3. Madzia et al., 2018

Addition of UALVP 56885 into Madzia et al. (2018) character matrix resulted in 16830 most parsimonious trees, with a tree length of 924 steps, a consistency index of 0.34, and a retention index of 0.63. Bootstrap values (>50) and Bremer support (>1) are shown at the nodes and stems of the strict consensus tree (Fig. 3.11 and Table 3.4). UALVP 56885 and ROM 804 had identical character coding in this matrix. The resulting consensus tree does not change the topology found within the original analysis and all major ornithischian clades were recovered (e.g., Marginocephalia, Neornithischia, Ornithopoda, and Thyreophora). Bootstrap and Bremer support for clades were not reported in the original analysis and cannot be compared with the results of this study. Overall, Bootstrap and Bremer support in this analysis is weak where clade support is only strong for Dinosauria, Ornithischia, and Ankylopollexia (Fig. 3.11). Thescelosauridae and its two major subclades, Orodrominae and Thescelosaurinae, are recovered. Thescelosaurinae results in a polytomy consisting of *Notohypsilophodon*, *Parksosaurus*, *Thescelosaurus assiniboiensis*, *Thescelosaurus garbanii*, and *Thescelosaurus neglectus*, whereas Orodrominae consists of *Albertadromeus*, *Changchunsaurus*, *Haya*, the kaiparowits orodromine, *Koreanosaurus*, *Orodromeus*, *Oryctodromeus*, and *Zephyrosaurus* (Fig. 3.11). UALVP 56885 is recovered within the Thescelosaurinae polytomy with no autapomorphies (Fig. 3.11). A 50% majority rule consensus of the most parsimonious trees placed UALVP 56885 in the same position as did the strict consensus.

Thescelosauridae is supported by the presence of a concavity on the posterior end of the premaxilla that acts as to receive of the anterolateral boss of the maxilla (character 14); the orbital edge of the postorbital possesses an anteriorly directed process into the orbit (character

59; convergent in *Lesthosaurus* and *Manidens* and reversed in *Changchunsaurus*); the frontals are flattened dorsally (character 65; reversed in *Orodromeus*); the angle between the neck of the femoral head and the femoral shaft is less than or equal to 100 degrees (character 210; reversed in *Haya* and *Notohypsilophodon*); the lateral surface of the greater trochanter is flattened (character 213); a square lateral distal tarsal (character 242; convergent in *Valdosaurus* and reversed in the Kaiparowits orodromine); and fused premaxillae (character 255; reversed in *Orodromeus*).

Orodrominae is supported by possessing a length of the mandible posterior to the coronoid process that is 36% or greater of the total length of the mandible (character 83); four to five teeth in each premaxilla (character 112; convergent in *Agilisaurus*); absence of partial ossification of the sternal segments of the anterior dorsal ribs (character 157); low olecranon process (character 169; convergent in *Anabiseta*, *Lesthosaurus*, and *Rhabdodon*); a postacetabular process of the ilium that is more than 40% of the total length of the ilium (character 188); and a pubis that is supported by at least one sacral centrum (character 193).

Thescelosaurinae is supported by possessing a groove on the base of the posterior side of the pterygoid wing of the quadrate (character 55); having a frontal that occupies less than 25% of the orbital margin (character 63; convergent in *Muttaburrasaurus* and *Wannanosaurus*); a supraoccipital that contributes less than 5% of the margin of the foramen magnum (character 102); a postemporal foramen that is positioned at the boundary between the parietals and the paraoccipital process (character 103); a dorsally open groove around the postemporal foramen (character 104); anterior cervical centra are equal or greater than 1.5 times longer than tall (character 144); an obturator process that is 60% along the ischial shaft (character 204;

convergent with *Hypsilophodon*); a bowed femoral shaft in anterior view (character 209; convergent with *Dryosaurus*, *Dysalotosaurus*, *Eousdryosaurus*, and *Jeholosaurus*); a fourth trochanter is at or below the midshaft of the femur (character 221); lack of an anterior intercondylar groove on the distal end of the femur (character 222; convergent in *Orodromeus* and *Tianyulong*); and one lateral proximal condyle on the tibia (character 228).

3.6. Discussion

Although fragmentary, UAVLP 56885 can be diagnosed as a new specimen of *Parksosaurus warreni* based on postcranial autapomorphies that are shared with the holotype (ROM 804). Those elements that can be compared between the two specimens, and particularly the ilium and ischium, are closely similar (Fig. 3.4-3.8). Three separate character matrices were analyzed with UALVP 56885 added in as an OTU separate from the *Parksosaurus* holotype, and in each case the two specimens had identical character scoring and were recovered either as sister taxa or within a polytomy that also included other taxa (Fig. 3.9-11). The following discussion considers newly identified postcranial autapomorphies in *Parksosaurus*, morphological comparisons, stratigraphic position, and musculature involving UALVP 56885, as well as the results of its phylogenetic analyses, and the evidence for referring UALVP 56885 to *Parksosaurus warreni*.

3.6.1. UALVP 56885

UALVP 56885 is unlike other thescelosaurids (Calvo et al., 2007; Gilmore, 1915; Krumenacker, 2017; Makovicky et al., 2011; Scheetz, 1999; Varricchio et al., 2007), basal neornithischians (non-cerapodan) (Barrett et al., 2005; Coria and Calvo, 2002; Coria and

Salgado, 1996; Galton, 1974a; Godefroit et al., 2014; Han et al., 2012), and Late Cretaceous cerapodans (Arbour and Currie, 2013; Averianov et al., 2006; Bertozzo et al., 2017; Campione, 2014; Chapman and Brett-Surman, 1990; Coombs, 1979; Currie et al., 2016; Dodson et al., 2004; Galton and Sues, 1983; He et al., 2015; Holmes and Ryan, 2013; Holmes, 2014; Maidment and Barrett, 2011a; Morschhauser et al., 2019; Maryańska and Osmolska, 1974, 1984; Maryańska et al., 2004; Prieto-Marquez, 2006; Slowiak et al., 2019; You and Dodson, 2004) but has identically distinct morphologies as the *Parksosaurus* ROM 804 holotype. Thus, this partial skeleton can confidently be referred to as a new specimen to *Parksosaurus warreni*. UALVP 56885 represents the only *Parksosaurus* specimen to have been discovered within the last century. The morphologies that were in common with *Parksosaurus* ROM 804 are the shape and orientation of the brevis fossa; the concavity of the ischial mid-shaft (which may represent a local autapomorphic feature); the morphology of the obturator process and the distal ischia; the dorsal marginal shape of the postacetabular process (may be an ontogenetically dependent character or may represent individual variation in *Parksosaurus*); the obturator process position on the ischial shaft; and the lack of fusion in the caudal vertebrae between the neural arches, transverse processes, and centra. Furthermore, both *Parksosaurus* specimens (ROM 804 and UALVP 56885) can be placed within the *Hypacrosaurus altispinus – Saurolophus osborni* biozone which further supports that *Parksosaurus* was endemic to this zone (Eberth et al., 2013; Larson et al., 2010).

Muscle scars and depressions on the ilium are interpreted as the areas of origination for hindlimb musculature. The dorsal margin of the iliac blade in lateral view has dorsoventral striations and is interpreted as the origin point for the iliotibialis, a flexor and abductor muscle

for the hind limb (Maidment and Barrett, 2011b; Maidment et al., 2014). In birds, crocodilians, and theropods, the iliotibialis is divided into three parts with separate sites of origin along the iliac blade (Carrano and Hutchinson, 2002; Maidment and Barrett, 2011b; Rhodes et al., 2020, 2021). In ornithischians there is no evidence for division of the iliotibialis (Maidment and Barrett, 2011b). It is likely that UALVP 56885 had no division of the iliotibialis but this is uncertain given that the anterior portions of both ilia are missing. The concavity on the posterior end of the postacetabular process can be interpreted as the insertion of the iliofibularis which acts as an extensor the hindlimb. The concave feature on the iliac blade above the acetabulum is the origination point for the iliofemoralis, which acted to flex and abduct the hindlimb. The brevis shelf acts as the origination point for the caudofemoralis brevis, which is an extensor of the hindlimb (Maidment and Barrett, 2011b; Maidment et al., 2014).

With the musculature interpretation of UALVP 56885, the pelvic girdle of *Parksosaurus warreni* appears to be derived as it lacks many plesiomorphic features present in other thescelosaurids. It is likely that the unique adaptations present in the ilia and ischia of *Parksosaurus* represent a divergence from the typical locomotor adaptations present in thescelosaurids. It appears that *Parksosaurus* is specialized in the pelvic girdles whereas other thescelosaurids are specializing in their pectoral girdle (*Koreanosaurus* and *Oryctodromeus*) or their teeth, skull, and hindlimbs (*Thescelosaurus*) (Boyd, 2014; Galton, 1974b; Huh et al., 2011; Varricchio et al., 2007). For example, *Thescelosaurus* possesses a derived skull compared to *Parksosaurus*, whereas the pelvic girdle in *Thescelosaurus* is plesiomorphic compared to the derived one in *Parksosaurus*. It appears that thescelosaurids are not specialized into a single ecological role but rather specializing into multiple ecological roles.

3.6.2. New Pelvic Autapomorphies in *Parksosaurus warreni*

No autapomorphies have previously been explicitly identified in the ilia and ischia of *Parksosaurus* despite the long history of descriptive work on this taxon (Boyd et al., 2009; Galton, 1995; Parks, 1926; Sternberg, 1940). The ilia and ischia of *Parksosaurus* have new autapomorphies when compared with non-thescelosaurid neornithischians such as *Agilisaurus* (Barrett et al., 2005), *Anabisetia* (Coria and Calvo, 2002), *Gasparinisaura* (Coria and Salgado, 1996), *Hexinlusaurus* (Barrett et al., 2005), *Hypsilophodon* (Galton, 1974a), *Jeholosaurus* (Han et al., 2012), and *Kulindadromeus* (Godefroit et al., 2014; Godefroit et al., 2020), and with thescelosaurids such as Haya (Makovicky et al., 2011), *Macrogryphosaurus* (Calvo et al., 2007), *Orodromeus* (Scheetz, 1999), *Oryctodromeus* (Krumenacker, 2017; Varricchio et al., 2007), and *Thescelosaurus* (Fisher et al., 2000; Gilmore, 1915).

The posterior part of the dorsal margin of the ilium differs slightly in shape between the *Parksosaurus* specimens ROM 804 and UALVP 56885. The posterior part of the dorsal margin of the ilium is more convex in *Parksosaurus* ROM 804 than in other thescelosaurids. However, this part of the dorsal margin in lateral view is nearly straight in UALVP 56885, becoming rounded only at the posterodorsal corner of the bone (Fig. 3.3, 3.6). This shape difference could represent an indication that UALVP 56885 belongs to a species distinct from *Parksosaurus warreni*. For example, *Thescelosaurus neglectus* and *Thescelosaurus assiniboiensis* differ from one another in the shape of the postacetabular process of the ilium. This has not been pointed out by other authors, who have relied on cranial characters to formally diagnose these taxa (Brown, 2009; Brown et al., 2011; Gilmore, 1915). Nevertheless, a more conservative interpretation is that the difference in the curvature of the dorsal margin of the ilium between ROM 804 and

UALVP 56885 represents individual or ontogenetic variation, as UALVP 56885 is smaller than ROM 804 (Fig. 3.3, 3.6).

In some basal neornithischians, previous work has investigated ontogenetic changes in the skulls and the osteohistology of *Jeholosaurus* and *Oryctodromeus* (Barrett and Han, 2009; Han et al., 2020; Krumenacker, 2017), and it has suggested that they underwent some ontogenetic changes in postcranial morphology (Barrett and Han, 2009; Han et al., 2020; Krumenacker, 2017). For instance, multiple specimens of *Orodromeus* and *Thescelosaurus* show variability in the shape of the dorsal margin of the postacetabular process (Brown, 2009). Ontogeny could explain the differences in the dorsal margin curvature of the postacetabular processes in ROM 804 and UALVP 56885. A major caveat in testing ontogenetically dependent postcrania in thescelosaurids is that their data sets are based on few postcranial skeletons and lack the statistical significance to be robustly supported. In other ornithischians, the postacetabular process is highly variable in shape, a pattern that has been attributed to individual variation (e.g., *Camptosaurus aphanoecetes*, *Iguanodon bernissartensis*, and *Iguanodon galvensis*) (Carpenter and Lamanna, 2015; Verdu et al., 2012). In contrast, little variation in the dorsal margin shape is seen in some ornithischians, such as *Camptosaurus dispar* (Carpenter and Lamanna, 2015) and *Mantellisaurus* (McDonald, 2012). Verdu et al. (2012) also suggest that the variation in the ilia of *Iguanodon* is not ontogenetically dependent as a similar range of morphologies is observed in juvenile specimens. Given this, no studies have rigorously tested whether postcranial differences seen in various thescelosaurid species are linked with ontogenetic change or with individual variation. Thus, the differences between the curvature of

margins of the ventral postacetabular processes in the *Parksosaurus* specimens cannot be used as a diagnostic feature at the species level.

The shapes and orientations of the brevis fossae in ROM 804 and UALVP 56885 are similar and appear to be unique among thescelosaurids, in which this character is highly variable (Fisher et al., 2000; Gilmore, 1915; Han et al., 2012; Krumenacker, 2017; Makovicky et al., 2011; Scheetz, 1999; Varricchio et al., 2007). The brevis fossa has a narrow oval facet that extends posteroventrally along the ventral margin of the postacetabular process that is present in both specimens of *Parksosaurus* (Fig. 3.7). This feature appears to be unique among other thescelosaurids and ornithischians, which either lack a brevis fossa or possess one that is broad and elongate, broad and sub-rectangular, or broad and triangular; these are along the ventral margin of the postacetabular process and can be oriented either posteroventrally or ventrally (Fig. 3.7). The orientation of the brevis shelf is likely not an autapomorphy for *Parksosaurus*, as it difficult to determine its orientation with certainty in the holotype (ROM 804). Furthermore, a medioventral orientation of the brevis shelf is common throughout Thescelosauridae, except for *Orodromeus* (Gilmore, 1915; Han et al., 2012; Krumenacker, 2017; Makovicky et al., 2011, Parks, 1926; Scheetz, 1999). The brevis shelf size differences between ROM 804 and UALVP 56885 can likely be explained as individual or ontogenetic variation, as UALVP 56885 is smaller than ROM 804.

The dorsal margin at mid-shaft of the ischium of *Parksosaurus* (ROM 804 and UALVP 56885) is likely unique for the taxon as its dorsal margin is concave. In most other thescelosaurids (except *Macrogryphosaurus*), it is straight in lateral view. However, the concave dorsal margin is present in other neornithischians outside Thescelosauridae (e.g., *Agilisaurus*,

Anabisetia, *Gasparinisaura*, *Hexinlusaurus*, *Kulindadromeus*, and *Lesthosaurus*) (Fig. 3.3, 3.6, 3.8 and Table 3.3) (Barrett et al., 2005; Coria and Calvo, 2002; Calvo et al., 2007; Galton, 1978; Godefroit et al., 2014; Maidment and Barrett, 2011b). This character may be a local autapomorphy for *Parksosaurus* within Thescelosauridae, but given that it is present in the basal neornithischian *Lesthosaurus* it might also be the pleisomorphic condition for ornithischians (Baron et al., 2017; Galton, 1978). Depending on the phylogenetic analysis, *Macrogryphosaurus* (Elasmaria in general) is not typically placed within Thescelosauridae (Boyd, 2015; Madzia et al., 2018). Other ischial morphologies of *Macrogryphosaurus* are not similar to *Parksosaurus* (Calvo et al., 2007). Thus, it is likely that this character may have evolved independently in both taxa. The occurrence of the concave dorsal margin in *Macrogryphosaurus* may be unique within Elasmaria. However, this is difficult to confirm because of the clade's weak support, with taxa shifting to positions within or outside of Elasmaria, and because of the lack of comparable material. Thus, the concave dorsal margin at mid-shaft on the ischium of *Parksosaurus* should be regarded as a local autapomorphy within Thescelosauridae that was acquired independently.

ROM 804 and UALVP 56885 both possess paddle-shaped expansions of the distal ends of the ischia. This feature clearly represents an autapomorphy of *Parksosaurus* that is not present in other thescelosaurids, or in cerapodans. In medial view, the obturator process is mound-like and is found at the proximal expansion of the paddle-shaped portion of the ischium. The obturator process is present in most basal neornithischians, but typically has the form of a tab that curls around (but does not contact) the pubic shaft. However, it is a roughened tuberosity in *Parksosaurus* (Fig. 3.8).

Previous phylogenetic studies have identified autapomorphies in *Parksosaurus*, most of which pertained to the skull, teeth, and hindlimbs (Boyd, 2015; Brown et al., 2013b; Madzia et al., 2018). Few were identified in the ilium and ischium. Within the character matrices analyzed, none of the character states reflect the shape of the distal part of the ischium. As recovered in the matrix of Brown et al. (2013b), two character states are shared between ROM 804 and UALVP 56885; the ischium possesses an obturator process 60% of the way down the shaft, and the dorsal margin of the ischial shaft is posterodorsally concave at mid-length. The latter was also recovered in Boyd (2015). The position of the obturator process relative to the ischial shaft may represent an autapomorphy for *Parksosaurus*, and the curvature of the dorsal marginal of the mid-shaft of the ischium further supports this character as an autapomorphy for *Parksosaurus*. However, the obturator process position is problematic as an autapomorphy for *Parksosaurus*, because it has also been recovered as a synapomorphy of Thescelosaurinae (*Notohypsilophodon* and *Thescelosaurus*) (Madzia et al., 2018). Re-evaluating this character by taking measurements by hand for *Notohypsilophodon* and *Thescelosaurus* revealed that the obturator process is not 60% of the way down the ischial shaft in *Thescelosaurus* and the ischia is not preserved in *Notohypsilophodon*. This presumed error in character scoring calls into question the validity of Madzia et al.'s (2018) phylogenetic result and the present chapter's analysis using this character matrix. This character may be an autapomorphy for *Parksosaurus* based on the scoring error. However, this character is questionable in any case, as it is dependent on arbitrary delineation of character states within a continuous data distribution (Type II A error of Simoes et al., 2017). I tentatively consider the position of the obturator process as an autapomorphy for *Parksosaurus*, while noting that this character needs reevaluation.

The aforementioned characters have not been identified as autapomorphies for *Parksosaurus* in previous studies (Boyd et al., 2009; Galton, 1995; Sternberg, 1940). In addition, adding new characters to current matrices would be necessary to capture the unique ischial morphology present in *Parksosaurus*. Here, I propose that these autapomorphies in the postcrania of *Parksosaurus warreni* represent new autapomorphies that further distinguish the taxon from other ornithischians. These autapomorphies include a paddle-shaped, sheet-like, dorsoventrally thin expansion of the distal portion of the ischium; a concave dorsal margin of the mid-shaft region of the ischium; a mound-like obturator process situated at the level of the proximal end of the paddle-shaped portion of the ischium; and a narrow, oval brevis fossa that extends anteroposteriorly along the ventral margin of the postacetabular process. I tentatively consider the position of the obturator process to be an additional autapomorphy of *Parksosaurus*, but this awaits further testing.

3.6.3. Phylogenetic Analysis

UALVP 56885 was recovered in a polytomy with *Hypsilophodon*, *Parksosaurus* ROM 804, Orodrominae, Ornithopoda, and Thescelosaurinae using Brown et al.'s (2013b) matrix; in a polytomy with a range of Late Cretaceous North American thescelosaurines (*Notohypsilophodon*, *Parksosaurus*, *Thescelosaurus assiniboiensis*, *T. garbanii*, and *T. neglectus*) using Madzia et al.'s (2018) matrix; and as sister taxon to *Parksosaurus* (ROM 804) using Boyd's (2015) matrix (Fig. 3.9-3.11). UALVP 56885 is a new specimen of *Parksosaurus warreni* based on the following suite of characters in common with the holotype (ROM 804): the ischium possesses an obturator process that is 60% down the ischial shaft (Brown et al., 2013b); the dorsal margin of the ischial shaft is posterodorsally concave at mid-length in lateral view

(Boyd, 2015). In the Madzia et al.'s (2018) analysis, UALVP 56885 shares a synapomorphy with Thescelosaurinae (*Notohypsilophodon*, *Parksosaurus* holotype, *Thescelosaurus assiniboiensis*, *T. garbanii*, and *T. neglectus*), in that an obturator process is present 60% of the way down the ischial shaft. In the analysis based on the matrix of Boyd (2015), however, this feature emerged not as a synapomorphy of Thescelosaurinae but rather as a synapomorphy of *Parksosaurus* and UALVP 56885. This character may not be an autapomorphy and needs further analysis. Tentatively it is considered an autapomorphy for *Parksosaurus*. Character codings for ROM 804 and UALVP 56885 were identical in Boyd, (2015) and Madzia et al. (2018) character matrices, reinforcing the conclusion that UALVP 56885 is referable to *Parksosaurus warreni*. Character codings for UALVP 56885 and ROM 804 were not identical in Brown et al.'s (2013b) character matrix as the character codings were apparently outdated in the analysis (Boyd, 2015). Future work on thescelosaurid phylogenetics should focus on identifying and establishing autapomorphies and synapomorphies, assessing patterns of character variation, and developing new characters pertaining to the postcranium in particular.

3.7. Conclusions

New postcranial autapomorphies were identified in the ilium and ischium of *Parksosaurus warreni* by considering ROM 804 and UALVP 56885 together. The autapomorphies presented are unique among basal neornithischians. These features include a dorsoventrally thin distal ischium that is paddle-shaped and expands mediolaterally as a sheet of bone; the dorsal margin of the ischial mid-shaft is posterodorsally concave; the obturator process is mound-like and marks the proximal start of the paddle-shaped ischium; the brevis fossa is a narrow, oval facet that extends anteroposteriorly along the ventral margin of the postacetabular

process; and the tentatively useful position of the obturator process being 60% down the ischial shaft. Given the distinct morphologies in the ilium and ischium of the *Parksosaurus* holotype, the aforementioned characters in the ilium and ischium are considered to represent additional diagnostic features for the taxon.

The newly described UAVLP 56885 is assigned to *Parksosaurus warreni* based on the presence of the autapomorphic features seen in the ilium and the ischium of the holotype (ROM 804). Its referral to the genus is based on anatomical comparisons (postcranial autapomorphies and identical character coding) with the holotype (Fig. 3.12). UALVP 56885 represents the only *Parksosaurus* specimen to have been discovered within the last century. Phylogenetic analyses recover UALVP 56885 as being sister to *Parksosaurus* ROM 804, or in a large polytomy with it. The synapomorphies that support the sister relationship between *Parksosaurus* ROM 804 and UALVP 56885 posited in one analysis include the obturator process being 60% down the ischial shaft, and the dorsal margin of the ischial shaft being dorsally concave at mid-length. Successful identification of new postcranial autapomorphies for *Parksosaurus* suggests that attempts to find diagnostic postcranial characters for other basal neornithischians may represent a promising line of inquiry for the future.

3.8. Tables and Figures

Table 3.1. Measurements of UALVP 56885.

Values left of "/" indicate left side and values to the right of "/" indicate right side.

UALVP 56885 Measurements	Value (mm)
Sacral Centra Length (Anteroposterior)	
Sacral 1	26.6
Sacral 2	28.4
Sacral 3	24.9
Sacral 4	21.9
Sacral Centra Transverse Width	
Sacral 1	19.1
Sacral 2	18.4
Sacral 3	20.5
Sacral 4	25.2
Sacral Centra Height	
Sacral	23.4
Sacral Neural Spines Length (Anteroposterior)	
Sacral 1	17.2
Sacral 2	20.7
Sacral 3	20.8
Sacral 4	-
Sacral Neural Spines Transverse Width	
Sacral 1	4.0
Sacral 2	2.7
Sacral 3	3.9
Sacral 4	-
Sacral Neural Spines Height	
Sacral 1	37.6
Sacral 2	37.6
Sacral 3	-
Sacral 4	-

Sacral Neural Spine Angle	
Sacral 1	-
Sacral 2	69.4
Sacral 3	63.5
Sacral 4	-
Sacral Ribs Length (Anteroposterior)	
Sacral 1	28.0/13.0
Sacral 2	15.0/29.2
Sacral 3	18.2/23.5
Sacral 4	15.3/12.5
Sacral Ribs Transverse Width	
Sacral 1	28.0/30.5
Sacral 2	32.5/31.3
Sacral 3	32.9/29.6
Sacral 4	27.7/25.4
Sacral Ribs Height	
Sacral 1	17.3/10.0
Sacral 2	16.0/15.0
Sacral 3	12.0/11.6
Sacral 4	10.7/9.1
Caudal Centra Anteroposterior Length	
Caudal 1	23.1
Caudal 2	23.3
Caudal Centra Transverse Width	
Caudal 1	24.3
Caudal 2	-
Caudal Centra Height	
Caudal 1	18.1
Caudal 2	16.5
Caudal Neural Spines Anteroposterior Length	
Caudal 1	14.8
Caudal 2	-
Caudal Neural Spines Transverse Width	
Caudal 1	3.8
Caudal 2	-

Caudal Neural Spines Height	
Caudal 1	20.3
Caudal 2	
Caudal Transverse Process Anteroposterior Length	
Caudal 1	12.0/10.4
Caudal 2	13.7/-
Caudal Transverse Process Transverse Width	
Caudal 1	23.1/-
Caudal 2	11.2/10.3
Caudal Transverse Process Height	
Caudal 1	6.1/5.7
Caudal 2	8.0

Table 3.2. Measurements of the ilium and ischium in UALVP 56885 and other thescelosaurid specimens.

Values left of "/" indicate left side and values to the right of "/" indicate right side. MOR 1636 and 1642 represent ilium and ischium measurements, respectively. Abbreviations: IBH, ilium blade height above the ischiadic peduncle; IBTW, ilium blade transverse width; IPTW, ischiadic peduncle transverse width; ML, maximum length from iliac peduncle to distal end; IPOP, iliac peduncle to obturator process; MTW, maximum transverse width; MMTW, maximum mid-shaft transverse width; PPLIP; postacetabular process length to the ischiadic peduncle.

Measurement	UAVLP 56885	*Parksosaurus* (ROM 804)	*Thescelosaurus* (NCSM 15728)	*Haya* (IGM 100/2015)	*Orodromeus* (MOR 623)	*Oryctodromeus* (MOR 1636 and 1642)
Ilium						
MTW	128.4	-	-	-	-	-
IPTW	22.2/19.2	18.8/-	-	-/20.3	18.4/19.2	-
IBTW	8.1/7.6	7.6/-	-/14.6	-	2.7/3.7	-
IBH	41.5/35.3	67.5-	-/143.4	-/28.7	28.2/28.1	19.3/-
PPLIP	113.9/101.4	148.2/-	-/227.7	-/70.0	56.5/68.3	54.1/-
Ischium						
ML	119.4/112.6	-/193.6	-/395.8	-/141.6	-	-/169.5
IPOP	44.4/-	-/102.0	-	-/59.3	-	-/108.7
MMTW	12.5/13.0	-/15.6	-	-/8.3	-	-/16.8

Table 3.3. Ilium and ischium character comparisons with other neornithischians.

Comparisons with other basal neornithischians, iguanodontians, and thescelosaurids. Abbreviations: Thesc, Thescelosaurinae; Neo, Neornithischia; Igua, Iguanodontia; Elas, Elasmaria; Oro, Orodrominae; Hyp, Hypsilophodontidae; bso, brevis shelf orientation; bf, brevis fossa; idm, ischial mid-shaft dorsal margin; opp, obturator process position; ops, obturator process shape; dim, distal ischium morphology; ref, reference.

Taxa	Clade	Specimen	bso	bf	idm	opp	ops	dim	ref
Parksosaurus	Thesc	ROM 804	Either ventral or medioventral	Semioval	Concave	60% down the ischial shaft	Mound-like	Paddle-shaped and flat	This study
Parksosaurus	Thesc	UALVP 56885	Medioventrally	Semioval	Concave	60% down the ischial shaft	Mound-like	Paddle-shaped and flat	This study
Agilisaurus	Neo	ZDM T6011	Medioventrally	-	Concave	Less than 60% down the ischial shaft	Tab-shaped	Splint-shaped	Barrett et al., 2005
Anabisetia	Igua	MCF-PVPH-76	Either ventrally or medially	Broad	Concave	Less than 60% down the ischial shaft	Tab-shaped	Narrow with an anteroventrally directed foot	Coria and Calvo, 2002
Gasparinisaura	Igua	MUCPv-208	Either ventrally or medially	-	Concave	-	Tab-shaped	Splint-shaped	Coria and Salgado, 1996
Haya	Thesc	IGM 100/2019	Medioventrally	Broad rectangle	Straight	Less than 60% down the ischial shaft	Tab-shaped	Narrow and flat	Barta and Norell, 2021
Hexinlusaurus	Neo	ZDM T6001	Medially	-	Concave	Less than 60% down the ischial shaft	Tab-shaped	Narrow	Barret et al., 2005
Hypsilophodon	Hyp	BMNH R196	Medially	Broad rectangle	Proximally straight, concave distally	60% down the ischial shaft	Tab-shaped	Broad	Galton, 1974a
Jeholosaurus	Thesc(?)	IVPP V 15939	Ventrally	Broad rectangle	Straight	Less than 60% down the ischial shaft	Tab-shaped	Narrow and flat	Han et al., 2012
Kulindadromeus	Neo	INREC k3/109	Either ventrally or medially	-	Concave	-	Tab-shaped	Narrow and flat	Godefroit et al., 2014
Macrogryphosaurus	Elas	MUCPv-321	Medially	Narrow rectangle	Concave	-	-	Narrow with a distal foot	Calvo et al., 2007
Orodromeus	Oro	MOR 623	Ventrally	Narrow rectangle	Straight	Less than 60% down the ischial shaft	Tab-shaped	Narrow and flat	Scheetz, 1999
Oryctodromeus	Oro	MOR 1636 and 1642	Medioventrally	Narrow rectangle	Straight	Less than 60% down the ischial shaft	Tab-shaped	Narrow and flat	Krumenacker, 2017
Thescelosaurus	Thesc	USNM 7757	Medioventrally	Broad rectangle	Straight	Less than 60% down the ischial shaft	Tab-shaped	Narrow	Gilmore, 1915

Table 3.4. Phylogenetic statistical results.

UALVP 56885 from the three analyses. Abbreviations: MPT, most parsimonious trees; TL, tree length; CI, consistency index; RI, retention index; Bst, bootstrap analysis; Bs, Bremer support.

Character Matrix	MPT	TL	CI	RI	Bst	Bs	Sister taxa	Clade
Brown et al., 2013b	6	431	0.43	0.61	0	0	Polytomy with Orodrominae and Ornithopoda	Unresolved
Boyd, 2015	36	881	0.36	0.64	17	1	*Parksosaurus*	Thescelosaurinae
Madzia et al., 2018	16830	924	0.34	0.63	15	1	Polytomy within Thescelosaurinae	Thescelosaurinae

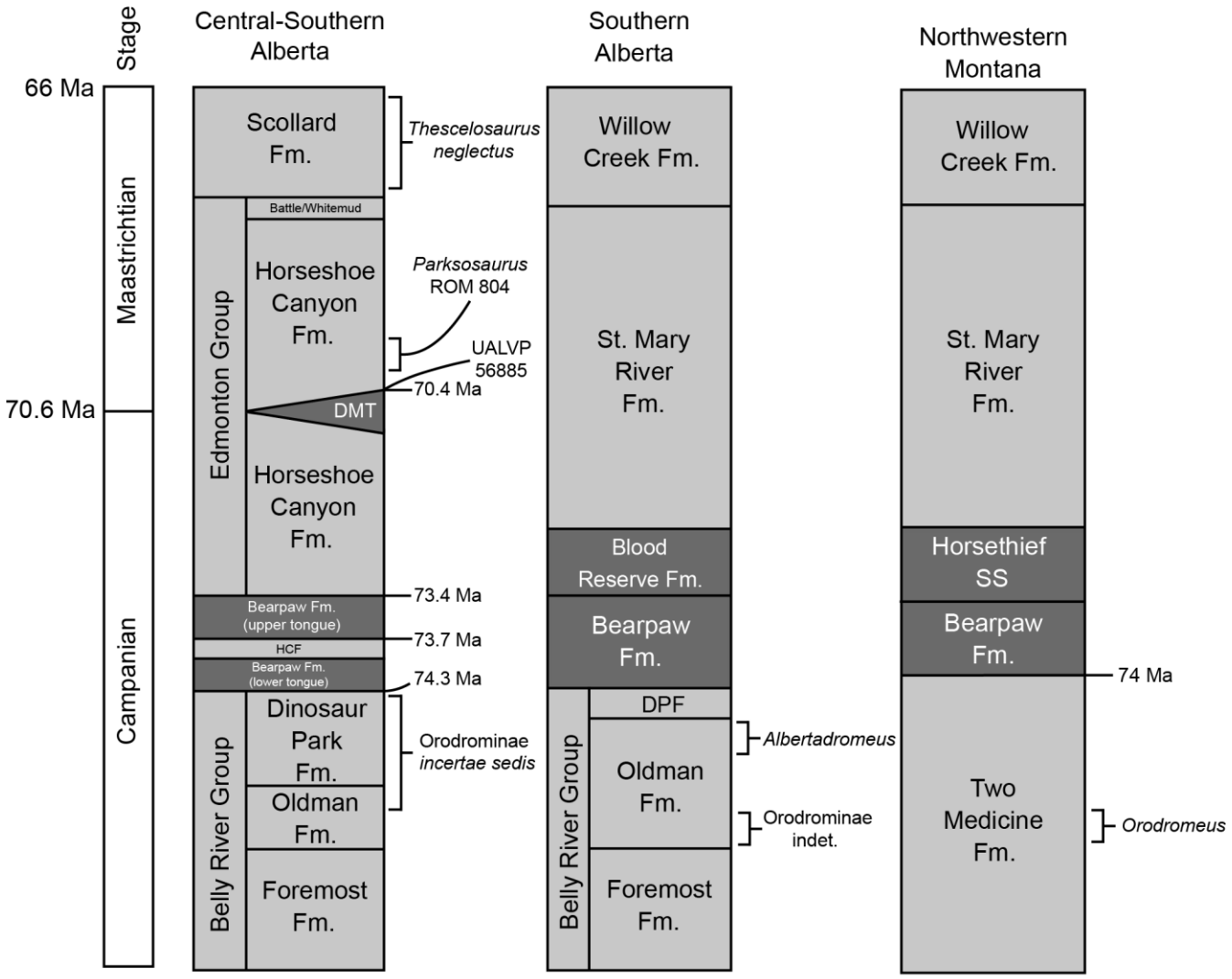

Figure 3.1. Approximate biostratigraphy and chronostratigraphy of Thescelosauridae occurrences in the Upper Cretaceous of Alberta and Montana with U-Pb dates.

Formations in light grey are terrestrial deposits, and those in dark grey are marine. Abbreviations: DMT, Drumheller Marine Tongue; DPF, Dinosaur Park Formation; HCF, Horseshoe Canyon Formation. Stratigraphy and radio-metric dates are from Brown et al. (2013b), Eberth et al. (2013), Eberth and Kamo (2019), and Fanti and Catuneanu (2010).

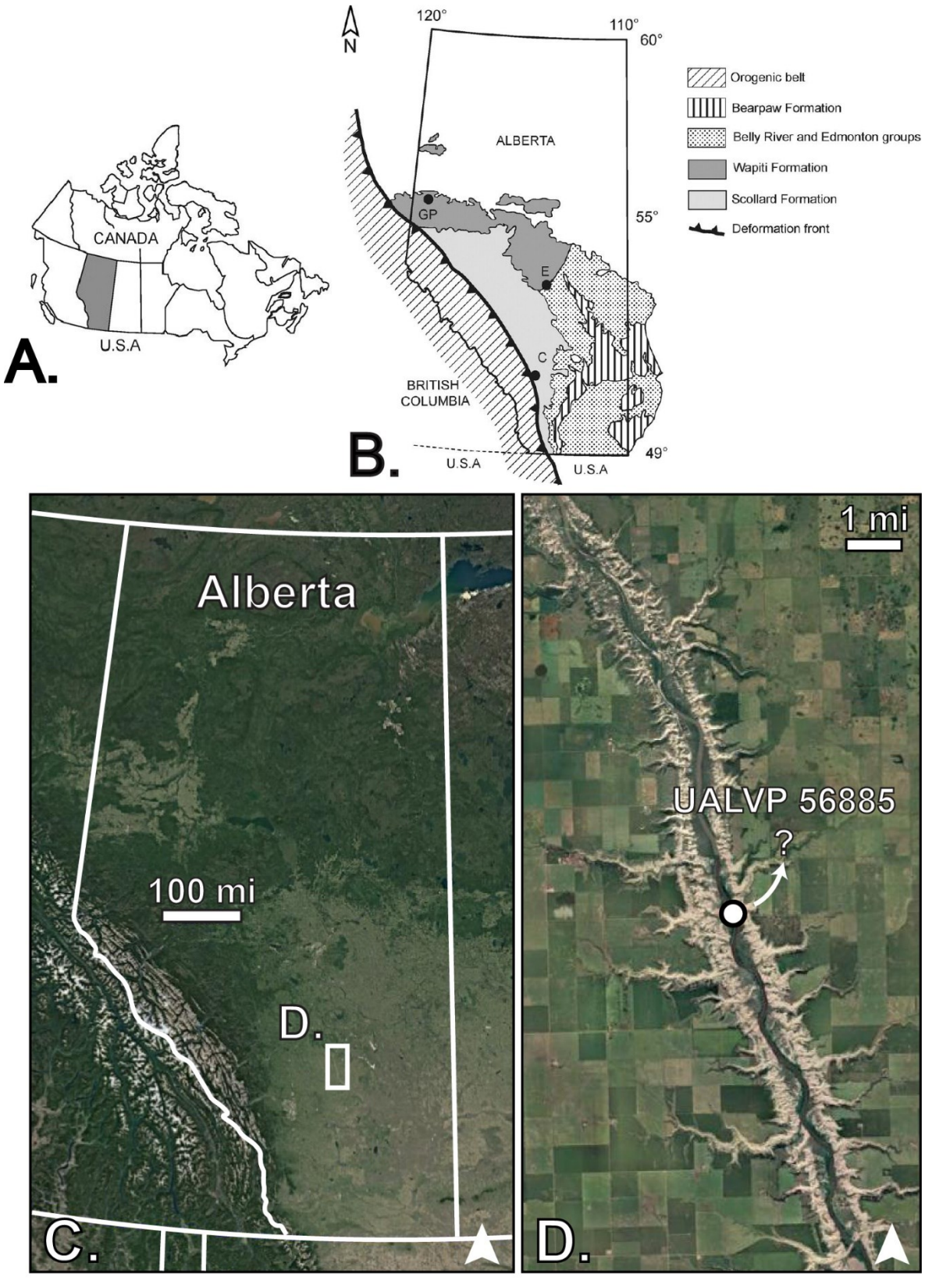
A.
CANADA
U.S.A
B.
N
120°
110°
60°
55°
49°
ALBERTA
GP
E
C
BRITISH
COLUMBIA
U.S.A
U.S.A
Orogenic belt
Bearpaw Formation
Belly River and Edmonton groups
Wapiti Formation
Scollard Formation
Deformation front
Alberta
100 mi
D.
C.
1 mi
UALVP 56885
?
D.

Figure 3.2. Geographic location for UALVP 56885 in Alberta, Canada.

Diagrammatic maps of Alberta, Canada (A, B) and map of Alberta with white rectangle showing general area from which UALVP 56885 was recovered (C). Enlarged map of the area between the Tolman and Morrin Bridges, with a circle indicating the approximate location where UALVP 56885 was found (D). White arrows indicate north. Abbreviations: C, Calgary; E, Edmonton; GP, Grande Prairie. Map based on Fanti and Catuneanu (2010).

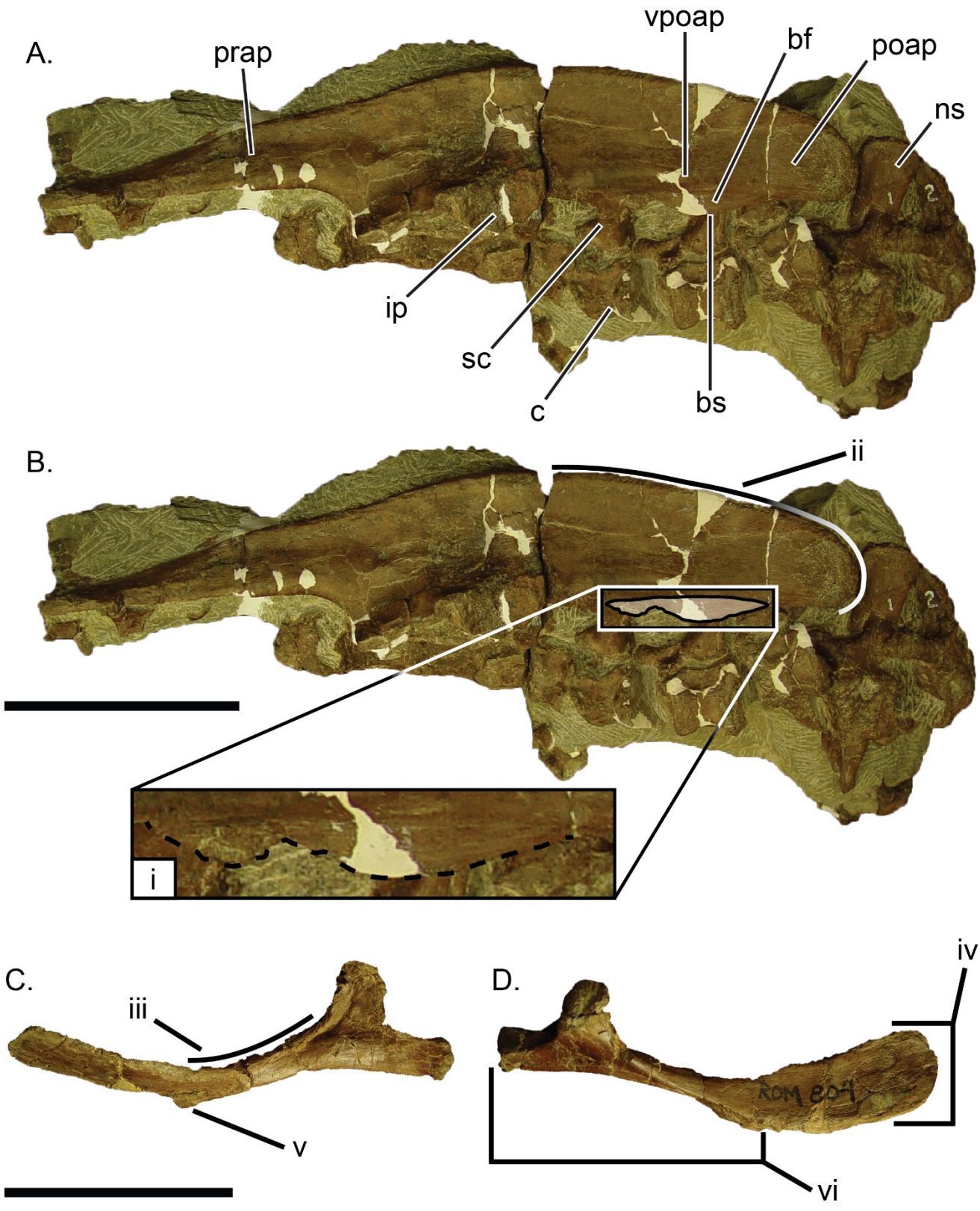
A.
prap
vpoap
bf
poap
ns
ip
sc
c
bs
B.
ii
i
C.
iii
v
D.
iv
vi

Figure 3.3. Ilium and ischium autapomorphies of *Parksosaurus warreni*.

The left ilium is shown in lateral view with articulated sacrals in lateroventral view (A, B). Right ischium in right lateral view (C) and in a dorsal, slightly medially tilted view (D). Six postcranial autapomorphies of *Parksosaurus warreni* present in the ilium (B) and the ischium (C, D) of ROM 804. The brevis fossa is a narrow semioval shaped feature that that extends anteroposteriorly along the ventral margin of the postacetabular process (i); the posterior part of the dorsal margin of the postacetabular process is rounded, however, this feature may not represent an autapomorphy but may be an ontogenetic dependent character or represents individual variation within the taxon (see discussion) (ii); the dorsal margin of the ischial mid-shaft is posterodorsally concave (iii); the obturator process is about 60% down the ischial shaft (identified in phylogenetic analysis and present in other thescelosaurids) (iv); the obturator process is mound-like and marks the proximal start of the distal paddle-shaped ischium (v); a dorsoventrally thin paddle-shaped feature at the distal end of the ischium expands mediolaterally as a sheet of bone (vi). Abbreviations: bf, brevis fossa; bs, brevis shelf; c, centrum; ip, ischial peduncle; poap, postacetabular process; prap, preacetabular process; ns, neural spine; sc, sacral rib; vpoap; ventral margin of the postacetabular process. Scale bar = 10 cm.

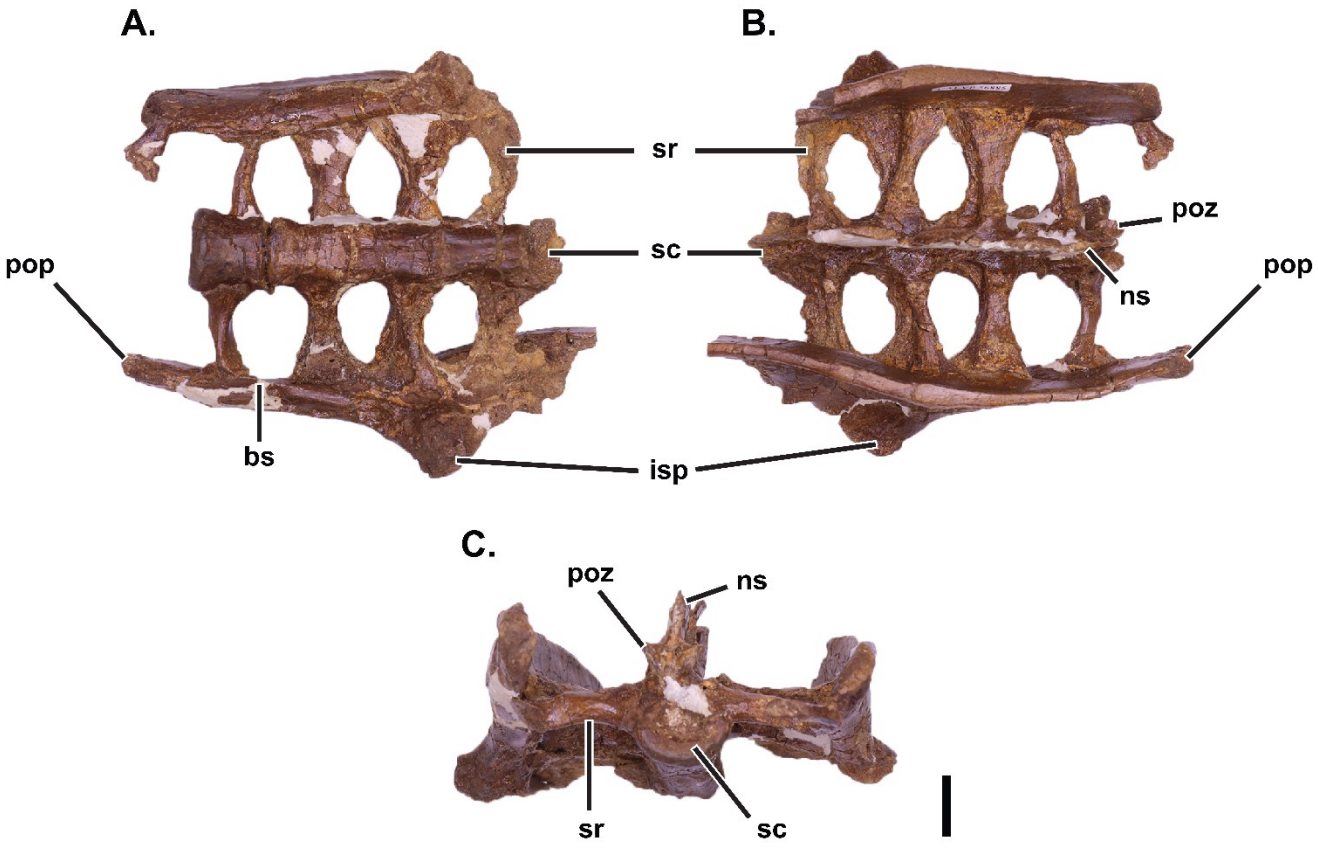

Figure 3.4. Partial ilia with articulated sacral vertebrae (UALVP 56885).

Ilia with articulated sacral vertebrae in ventral (A), dorsal (B) and posterior (C), views. Abbreviations: bs, brevis shelf; isp, ischial peduncle; ns, neural spine; pop, postacetabular process; poz, postzygapophysis; sc, sacral centrum; sr, sacral rib. Scale bar = 20 mm.

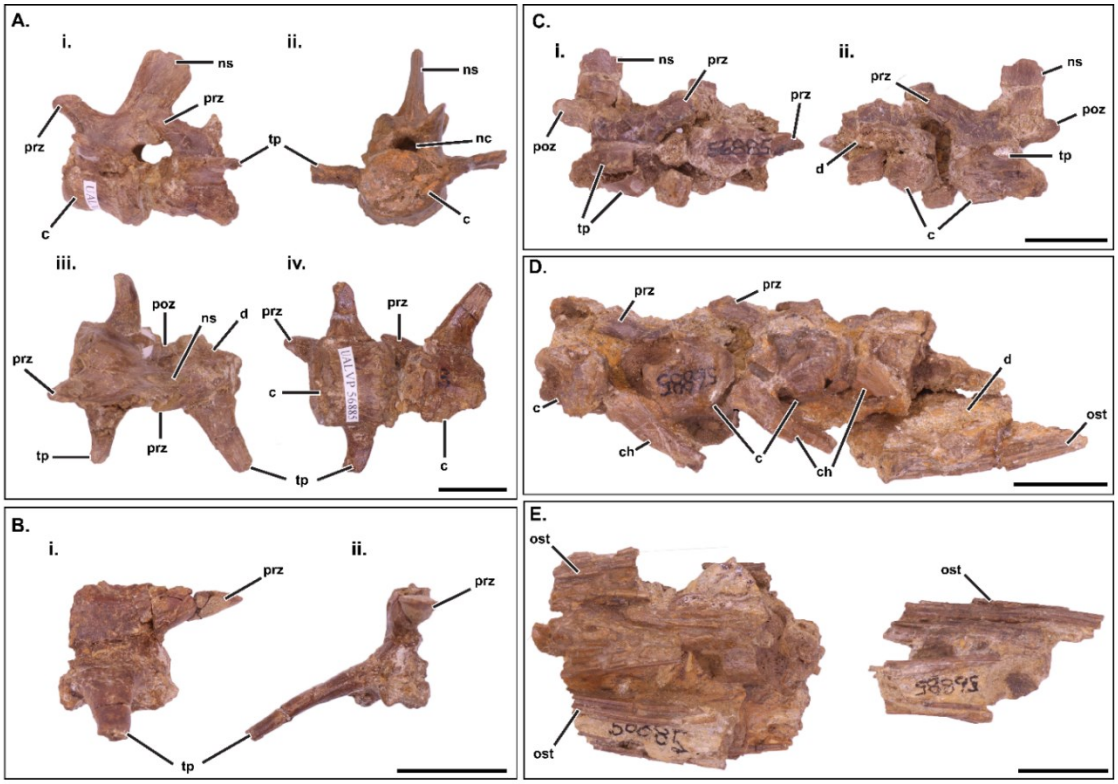
A.
i.
ns
prz
prz
tp
c
ii.
ns
nc
c
iii.
poz
ns
d
prz
tp
prz
iv.
prz
prz
c
tp
c
B.
i.
prz
tp
ii.
prz
C.
i.
ns
prz
prz
poz
tp
ii.
prz
ns
poz
d
tp
c
D.
prz
prz
d
c
ch
c
ch
ost
E.
ost
ost
ost

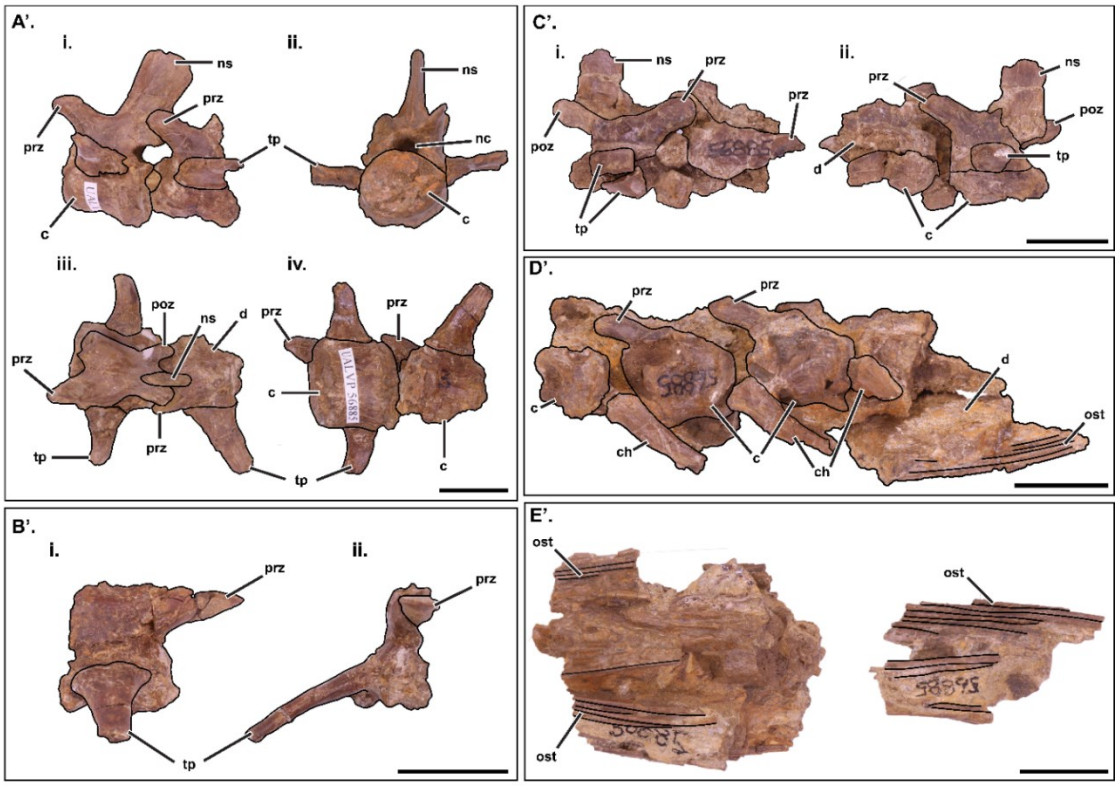
A'.
i.
ns
prz
prz
tp
c
ii.
ns
nc
c
iii.
poz
ns
d
prz
tp
prz
iv.
prz
prz
c
tp
c
B'.
i.
prz
tp
ii.
prz
C'.
i.
ns
prz
prz
poz
tp
ii.
prz
ns
poz
d
tp
c
D'.
prz
prz
d
c
ch
c
ch
ost
E'.
ost
ost
ost

Figure 3.5. Caudal vertebrae and ossified tendons of UALVP 56885.

Articulated caudal vertebrae (A) in left lateral view (i), anterior view (ii), ventral view (iii), and dorsal view (iv). Partial caudal vertebra (B) in right lateral view (i) and anterior view (ii). Partial articulated caudal vertebrae (C) in right (i) and left (ii) lateral view. Articulated caudal vertebrae in left lateral view (D). Ossified caudal tendons, orientation uncertain (E). Primes are the outline interpretation of anatomical features in the associated caudal vertebrae (A'-E'). Abbreviations: c, centrum; ch, chevron; d, damage; nc, neural canal; ns, neural spine; ost, ossified tendons; poz, postzygapophysis; prz, prezygapophysis; tp, transverse process. Scale bar = 20 mm.

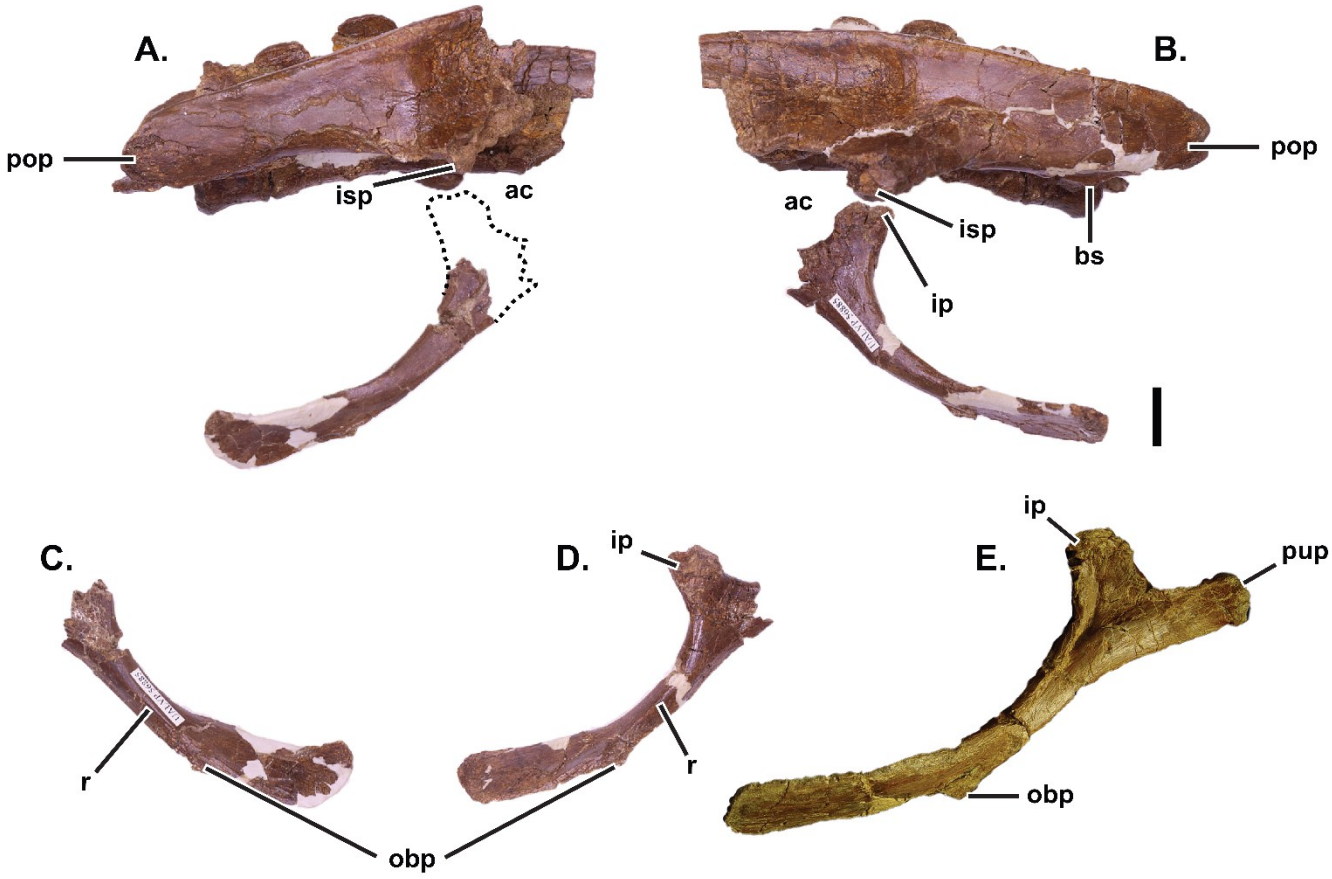

Figure 3.6. Partial ilia with articulated sacral vertebrae, partial left and right ischia, and ischium comparison (UALVP 56885).

Lateral views of iliosacral complex with right (A), and left (B) ischia; medial views of right (C) and left (D) ischia; with right ischium of *Parksosaurus* (ROM 804) in lateral view for comparison with UALVP 56885 (H). Dotted line represents the reconstructed partial outline, based on the left ischium, of the proximal portion of the right ischium. Abbreviations: ac, acetabulum; bs, brevis shelf; ip, ilium peduncle; isp, ischial peduncle; obp, obturator process; pop, postacetabular process; pup, pubic peduncle. Scale bar = 20 mm.

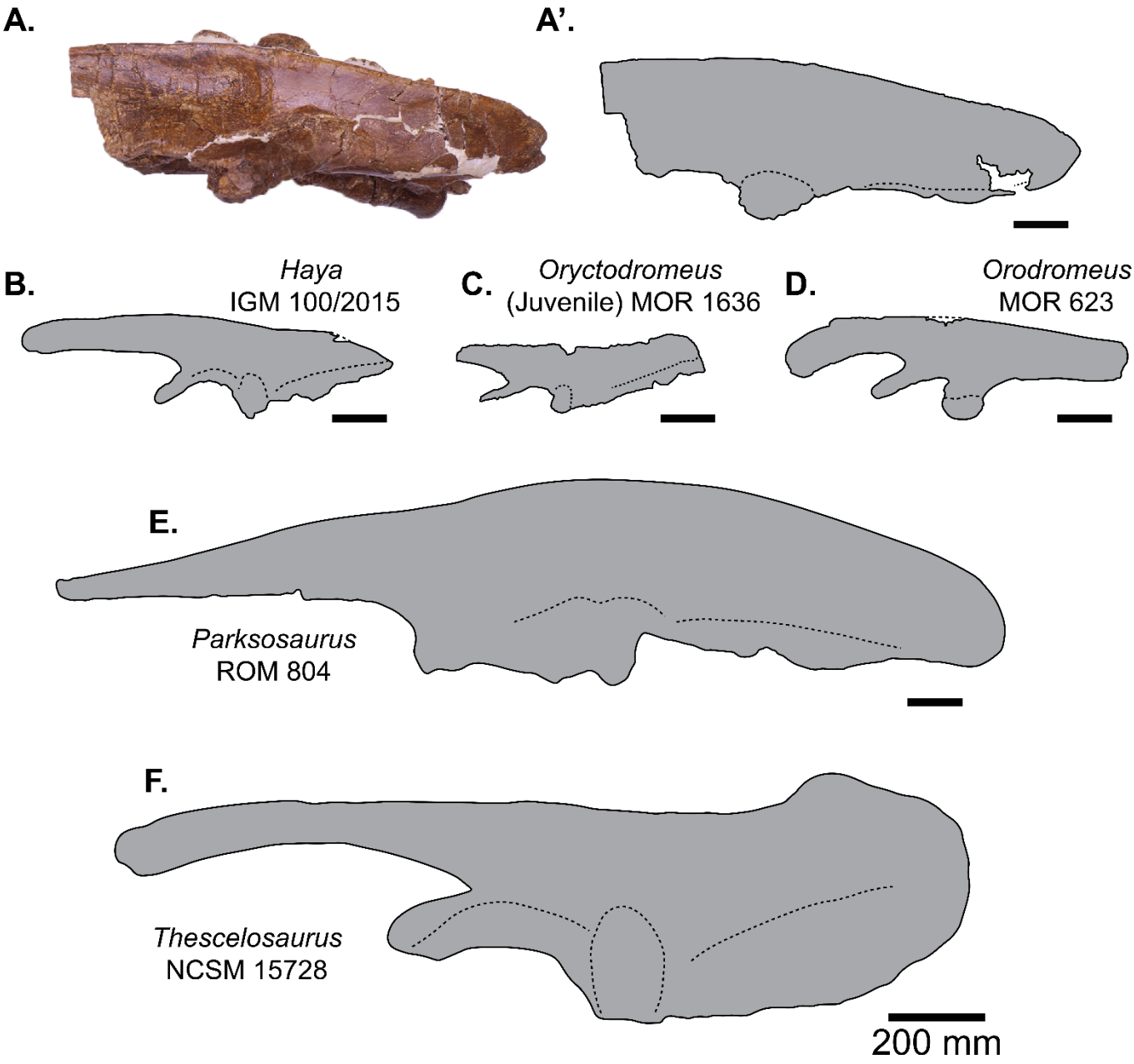
A.
A'.
B.
Haya
IGM 100/2015
C.
Oryctodromeus
(Juvenile) MOR 1636
D.
Orodromeus
MOR 623
E.
Parksosaurus
ROM 804
F.
Thescelosaurus
NCSM 15728
200 mm

Figure 3.7. Representative thescelosaurid ilia in lateral view.

Photo (A) and sketch (A') of left ilium of UALVP 56885 in lateral view, and sketches in lateral view of left ilia of various thescelosaurids: *Haya* (IGM 100/2015) (B), juvenile O*ryctodromeus* (MOR 1636) (C), *Orodromeus* (MOR 623) (D), *Parksosaurus* (ROM 804) (E), *Thescelosaurus* (NCSM 15728) (F). Dotted lines indicate the acetabulum, brevis shelf, and ischial peduncle. Scale bar = 20 mm, unless stated otherwise.

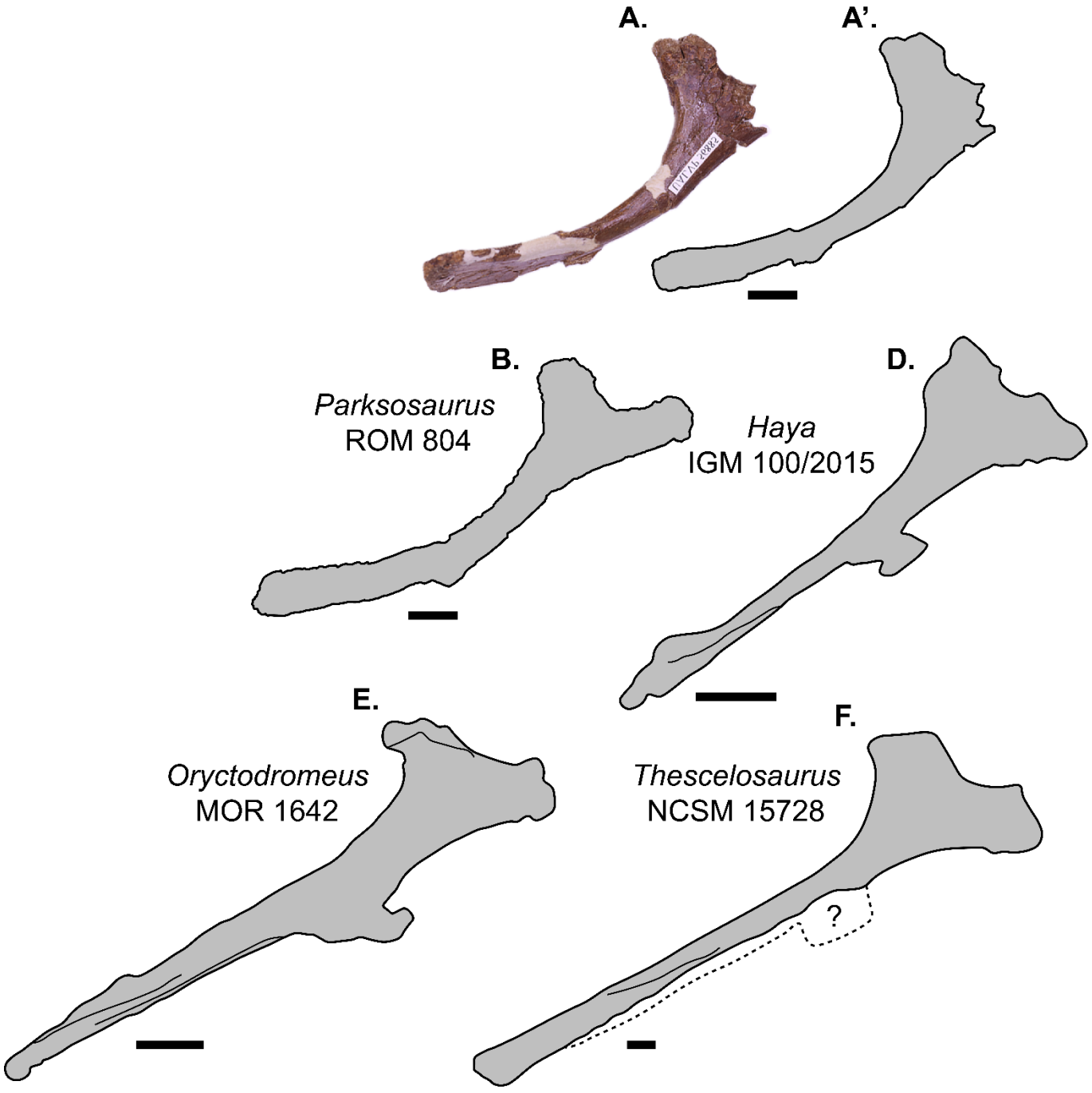
A.
A'.
B.
Parksosaurus
ROM 804
D.
Haya
IGM 100/2015
E.
Oryctodromeus
MOR 1642
F.
Thescelosaurus
NCSM 15728
?

Figure 3.8. Representative thescelosaurid ischia in lateral view.

Photo (A) and sketch (A') of left ischium (reversed) of UALVP 56885 in lateral view, and sketches in lateral view of right ischia of various thescelosaurids: *Parksosaurus* (ROM 804) (B); *Haya* (IGM 100/2015) (C); *Oryctodromeus* (MOR 1642) (D); and *Thescelosaurus* (NCSM 15728) (E). Dotted line represents the inferred outline of the *Thescelosaurus* ischial shaft and obturator process, which are obscured by an ironstone concentration, based on other *Thescelosaurus* specimens in which the ischial shaft and obturator process are exposed. Scale bar = 20 mm.

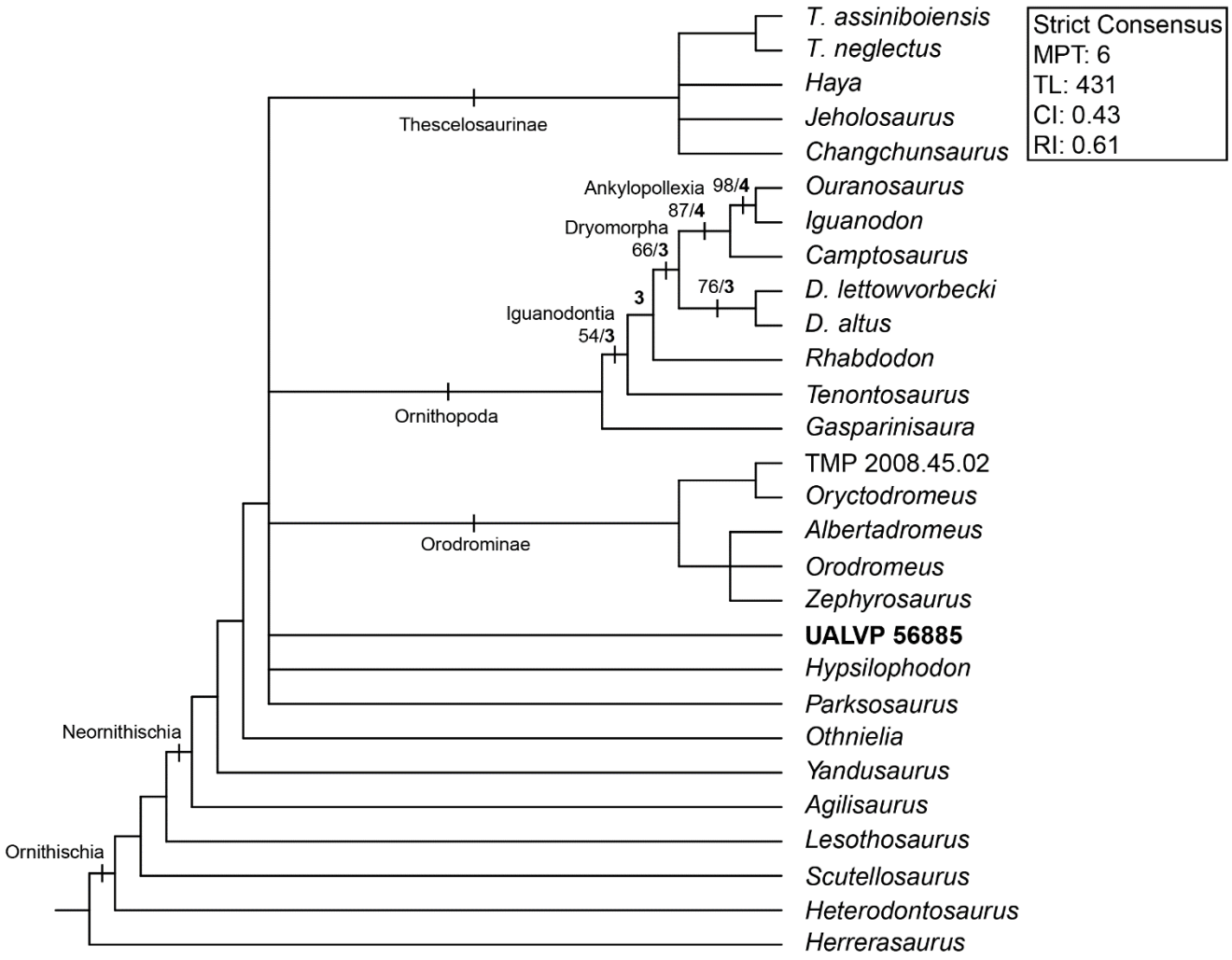

Figure 3.9. Strict consensus from phylogenetic analysis using matrix of Brown et al. (2013b).

Strict consensus tree resulting from addition of the new *Parksosaurus* specimen (UALVP 56885) to Brown et al.'s (2013b) character matrix. Most parsimonious trees (MPT) = 6, tree length (TL) = 431 steps, consistency index (CI) = 0.43, and retention index (RI) = 0.61. Bold numbers are Bremer support values >1, and plain text numbers are bootstrap support values >50%.

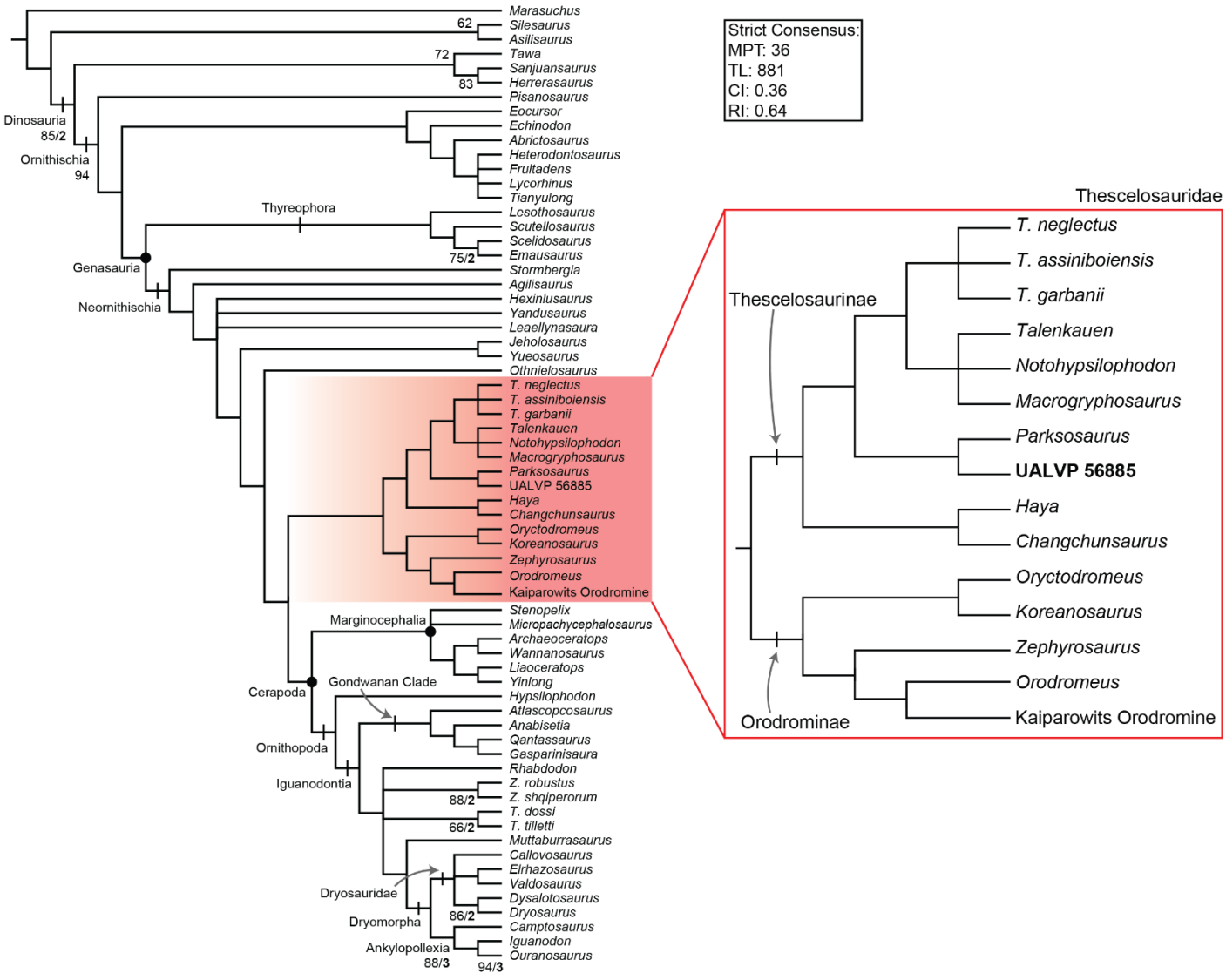
Strict Consensus:
MPT: 36
TL: 881
CI: 0.36
RI: 0.64
Marasuchus
Silesaurus
Asilisaurus
Tawa
Sanjuansaurus
Herrerasaurus
Pisanosaurus
Eocursor
Echinodon
Abrictosaurus
Heterodontosaurus
Fruitadens
Lycorhinus
Tianyulong
Lesothosaurus
Scutellosaurus
Scelidosaurus
Emausaurus
Stormbergia
Agilisaurus
Hexinlusaurus
Yandusaurus
Leaellynasaura
Jeholosaurus
Yueosaurus
Othnielosaurus
T. neglectus
T. assiniboiensis
T. garbanii
Talenkauen
Notohypsilophodon
Macrogryphosaurus
Parksosaurus
UALVP 56885
Haya
Changchunsaurus
Oryctodromeus
Koreanosaurus
Zephyrosaurus
Orodromeus
Kaiparowits Orodromine
Stenopelix
Micropachycephalosaurus
Archaeoceratops
Wannanosaurus
Liaoceratops
Yinlong
Hypsilophodon
Atlascopcosaurus
Anabisetia
Qantassaurus
Gasparinisaura
Rhabdodon
Z. robustus
Z. shqiperorum
T. dossi
T. tilletti
Muttaburrasaurus
Callovosaurus
Elrhazosaurus
Valdosaurus
Dysalotosaurus
Dryosaurus
Camptosaurus
Iguanodon
Ouranosaurus
62
72
83
Dinosauria
85/2
Ornithischia
94
Thyreophora
75/2
Genasauria
Neornithischia
Marginocephalia
Cerapoda
Gondwanan Clade
Ornithopoda
Iguanodontia
88/2
66/2
Dryosauridae
Dryomorpha
86/2
Ankylopollexia
88/3
94/3
Thescelosauridae
Thescelosaurinae
Orodrominae
T. neglectus
T. assiniboiensis
T. garbanii
Talenkauen
Notohypsilophodon
Macrogryphosaurus
Parksosaurus
UALVP 56885
Haya
Changchunsaurus
Oryctodromeus
Koreanosaurus
Zephyrosaurus
Orodromeus
Kaiparowits Orodromine

Figure 3.10. Strict consensus from phylogenetic analysis using matrix of Boyd (2015).

Strict consensus tree resulting from addition of the new Parksosaurus specimen (UALVP 56885) to Boyd (2015) character matrix. Most parsimonious trees (MPT) = 36, tree length (TL) = 881 steps, consistency index (CI) = 0.36, retention index (RI) = 0.64. Bold numbers are Bremer support values >1, and plain text numbers are bootstrap support values >50%.

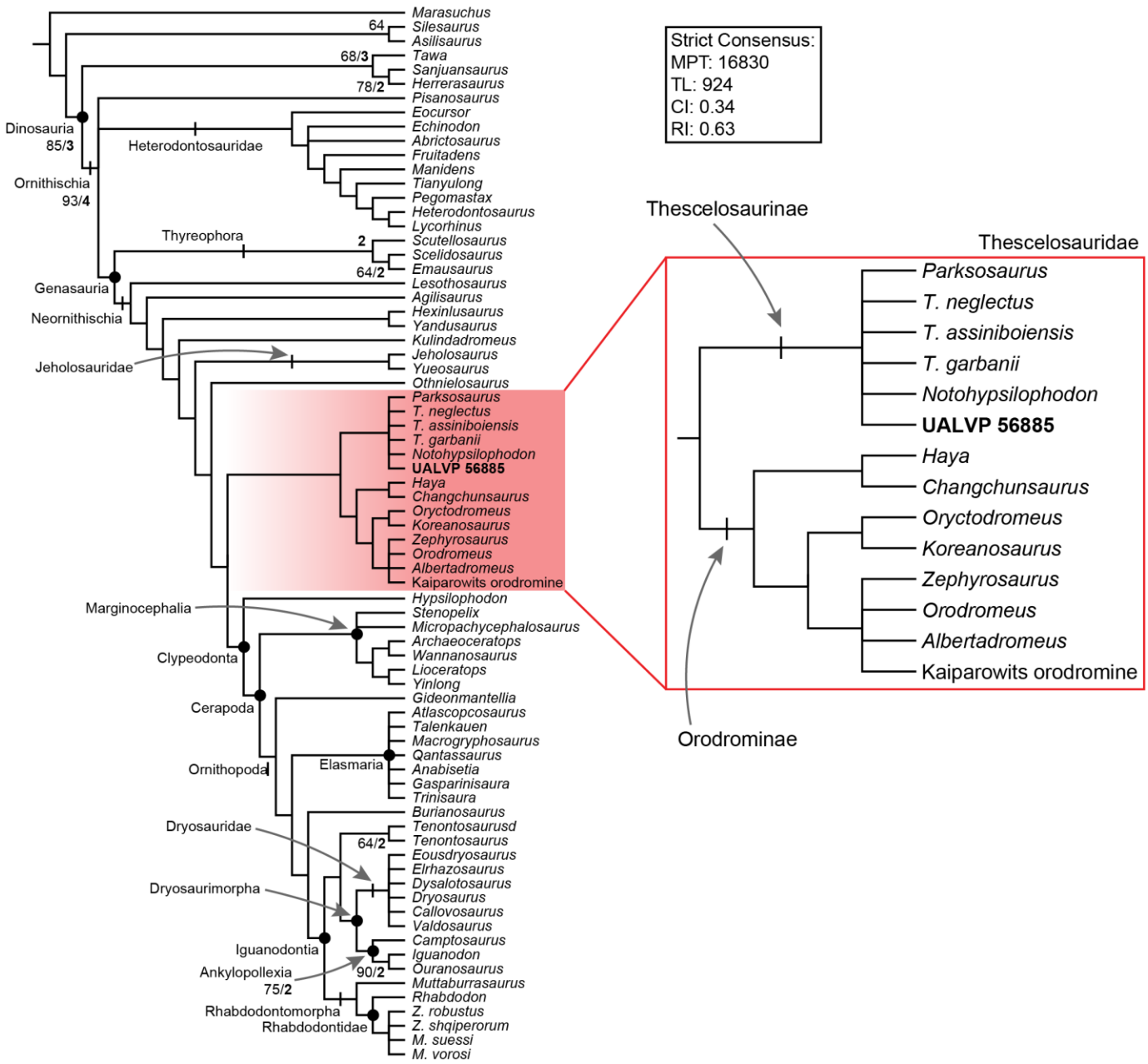
Strict Consensus:
MPT: 16830
TL: 924
CI: 0.34
RI: 0.63
Marasuchus
64
Silesaurus
Asilisaurus
68/3
Tawa
Sanjuansaurus
78/2
Herrerasaurus
Pisanosaurus
Dinosauria
85/3
Eocursor
Heterodontosauridae
Echinodon
Abrictosaurus
Fruitadens
Ornithischia
93/4
Manidens
Tianyulong
Pegomastax
Heterodontosaurus
Lycorhinus
Thyreophora
2
Scutellosaurus
Scelidosaurus
64/2
Emausaurus
Genasauria
Lesothosaurus
Agilisaurus
Neornithischia
Hexinlusaurus
Yandusaurus
Kulindadromeus
Jeholosauridae
Jeholosaurus
Yueosaurus
Othnielosaurus
Parksosaurus
T. neglectus
T. assiniboiensis
T. garbanii
Notohypsilophodon
UALVP 56885
Haya
Changchunsaurus
Oryctodromeus
Koreanosaurus
Zephyrosaurus
Orodromeus
Albertadromeus
Kaiparowits orodromine
Marginocephalia
Hypsilophodon
Stenopelix
Micropachycephalosaurus
Archaeoceratops
Wannanosaurus
Clypeodonta
Lioceratops
Yinlong
Gideonmantellia
Cerapoda
Atlascopcosaurus
Talenkauen
Macrogryphosaurus
Elasmaria
Qantassaurus
Ornithopoda
Anabisetia
Gasparinisaura
Trinisaura
Burianosaurus
Dryosauridae
Tenontosaurusd
64/2
Tenontosaurus
Eousdryosaurus
Elrhazosaurus
Dryosaurimorpha
Dysalotosaurus
Dryosaurus
Callovosaurus
Valdosaurus
Camptosaurus
Iguanodontia
Iguanodon
Ankylopollexia
90/2
Ouranosaurus
75/2
Muttaburrasaurus
Rhabdodon
Rhabdodontomorpha
Z. robustus
Rhabdodontidae
Z. shqiperorum
M. suessi
M. vorosi
Thescelosaurinae
Thescelosauridae
Parksosaurus
T. neglectus
T. assiniboiensis
T. garbanii
Notohypsilophodon
UALVP 56885
Haya
Changchunsaurus
Oryctodromeus
Koreanosaurus
Zephyrosaurus
Orodromeus
Albertadromeus
Kaiparowits orodromine
Orodrominae

Figure 3.11. Strict consensus from phylogenetic analysis using matrix of Madzia et al. (2018).

Strict consensus tree resulting from addition of the new Parksosaurus specimen (UALVP 56885) to Madzia et al. (2018) character matrix. Most parsimonious trees (MPT) = 16830, tree length (TL) = 924, consistency index (CI) = 0.34, retention index (RI) = 0.63. Bold numbers are Bremer support values >1, and plain text numbers are bootstrap support values >50%.

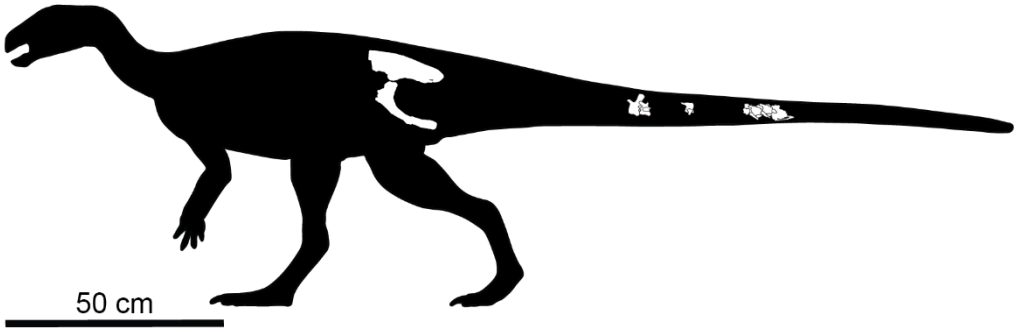

Figure 3.12. Skeletal reconstruction of the new *Parksosaurus* (UALVP 56885) specimen from the Horseshoe Canyon Formation.

Known skeletal elements are shown in white. Silhouette was modified from Scott Hartman.

Chapter 4. Osteology, Histology, and Phylogenetic Affinities of New Thescelosaurid (Dinosauria: Ornithischia) Material from the Wapiti and Dinosaur Park Formations (Campanian) of Alberta, with Implications for the Stratigraphic Separation Between Orodromine and Thescelosaurine Thescelosaurids in North America

4.1. Introduction

The Upper Cretaceous dinosaur-bearing Edmonton and Belly River Groups of southern Alberta are richly fossiliferous and intensely studied, and neornithischians were a major component of the dinosaur dominated ecosystems preserved in these deposits. Among the neornithischians represented is the Thescelosauridae, a poorly studied clade of small, cursorial, herbivorous bipeds that flourished from the Aptian to the Maastrichtian. Their fossil record is sparse, and interrupted by large ghost lineages (Boyd, 2015). Thescelosauridae can be divided taxonomically into two major subclades, Orodrominae and Thescelosaurinae (Fig. 4.1). Thescelosaurid interrelationships are contentious, as is the phylogenetic position of the group within Ornithischia, but thescelosaurids are widely considered to be basal (non-cerapodan) neornithischians, and in fact the sister taxon to Cerapoda (Brown et al., 2013b; Boyd, 2015; Dieudonné et al., 2020; Madzia et al., 2018). The various phylogenetic analyses have often disagreed regarding the position of Thescelosauridae and its two major subfamilies, especially with respect to the placement of Early Cretaceous Asian forms.

4.1.1. Geologic Context

Deposited in the Campanian (between 80 and 75 Ma), the Belly River Group is part of the Judith River clastic wedge, and comprises the Foremost, Oldman, and Dinosaur Park

Formations (Fig. 4.2). The Judith River clastic wedge is over- and underlain by the transgressive marine shales of the Bearpaw and Pakowki Formations, respectively. The Dinosaur Park Formations forms the upper portion of the Judith River clastic wedge, was deposited on the western margin of the Western Interior Seaway, and is characterized by inclined heterolithic stratification of fine to medium grained sandstones, with ~10% volcanics. The Dinosaur Park Formation depositional environment has been interpreted as containing a series of broad alluvial fans, in addition to a high sinuosity fluvial/estuarine coastal plain with swamp and lagoonal environments (Eberth and Hamblin, 1993; Eberth, 2005). Various UALVP orodromine specimens have been recovered from unknown stratigraphic horizons at various locations within the Dinosaur Park Formation of southern Alberta (Fig. 4.2, 4.3), and are difficult to pinpoint stratigraphically in relation to the megaherbivore assemblage zones (MAZ) that have been defined for the Dinosaur Park Formation (Mallon et al., 2012).

Deposited between 74.9 and 66.8 Ma in southern Alberta (Campanian-Maastrichtian), the Horseshoe Canyon Formation is a clastic wedge in the Western Canada Sedimentary Basin that represents coastal plain strata consisting of coal beds, sandstone, siltstone, and mudstone (Eberth and Braman, 2012; Eberth and Kamo, 2019; Heller et al., 1988; Ogg and Hinnov, 2012) (Fig. 4.2). Sediment supply and accumulation of the Horseshoe Canyon Formation is interpreted to be tectonically controlled by the two-phased foreland-basin sequence stratigraphy model (Eberth and Braman, 2012; Heller et al., 1988). The accretion of the Insular and Intermontane Superterranes onto the western coast of Laramidia (Eberth and Braman, 2012) caused uplift, forming the young Rocky Mountains, and was followed by subsidence as a result of tectonic

quiescence. Sediment accumulation of the Horseshoe Canyon Formation was facilitated by subsidence during the Late Cretaceous.

Overlying the Dinosaur Park Formation and largely underlying the Horseshoe Canyon Formation, the Bearpaw Formation is a marine interval that was deposited between 74.3 to 73.4 Ma and consists of lower and upper tongues that bound the Strathmore Member of the Horseshoe Canyon Formation (Fig. 4.2) (Currie and Koppelhus, 2005; Eberth and Braman, 2012; Eberth and Hamblin, 1992; Eberth and Kamo, 2019; Eberth et al., 2013). The Bearpaw Formation is restricted to southern Alberta and causes a crucial gap in the Late Cretaceous terrestrial fossil record, obscuring thescelosaurid evolution. The thescelosaurid subfamilies are stratigraphically divided, in that orodromines occur in the older Belly River Group and thescelosaurines occur in the younger Edmonton Group (Fig. 4.2) (Brown et al., 2013b; Hudgins et al., 2020a). Orodromines were the dominant small-bodied ornithischians during most of the Late Cretaceous in North America until their disappearance prior to, during, or after the onset of the Bearpaw Formation in Canada and the United States (Brown et al., 2013b; Hudgins et al., 2020a). The reasons for this stratigraphic separation of the main thescelosaurid groups in the North American record, and for the rise of thescelosaurines to dominance by Horseshoe Canyon times, are uncertain.

4.1.2. Current Study

The Bearpaw Formation is absent in northern Alberta, but northern regions of the province offer a continuous record of terrestrial, fossil-bearing rocks that has the potential to provide insight into thescelosaurid evolution and shed light on the stratigraphic separation between thescelosaurines and orodromines (Fig. 4.2). Specifically, the Wapiti Formation of the

Grande Prairie region in northwestern Alberta, Canada, is Campanian to Maastrichtian in age and rich in fossiliferous localities (Fanti et al., 2015), and includes a terrestrial interval corresponding to the southern Alberta marine Bearpaw Formation. The Wapiti Formation of northern Alberta overlies the marine Puskwaskau Formation and underlies the terrestrial Scollard Formation (Fanti and Catuneanu, 2009, 2010). Deposited ~80-67 Ma, the Wapiti Formation is a nonmarine alluvial clastic wedge that is subdivided into five distinct lithostratigraphic units (Fig. 4.2) and represents an extensive lowland environment near the paleo-shoreline of the Western Interior Seaway (Fanti and Catuneanu, 2009, 2010). However, previously reported hypsilophodontid material from the Wapiti Formation is limited to an isolated tooth and a questionable caudal centrum, which cannot be reliably referred to either Orodrominae or Thescelosaurinae. However, it was noted that the size and morphology of the tooth resembles those of *Parksosaurus* and *Thescelosaurus* (Fanti and Miyashita, 2009).

Here I describe new thescelosaurid body fossils from the Wapiti Formation, which represent the first diagnostic thescelosaurid elements ever collected from this stratigraphic unit and from anywhere in northern Alberta. These fossils are unassociated bones and teeth from the Dinosaur-Chelonian (DC) Bonebed near Grande Prairie. This multitaxic bonebed has yielded a substantial sample of well-preserved, rare small-bodied vertebrates, together with plant material, and lies within Unit 3 of the Wapiti Formation (Fig. 4.2, 4.3). Lithologically, the DC Bonebed is characterized by mud-dominated facies, bentonitic layers, well-developed coal seams, and peat deposits. Overall, the Wapiti Formation is interpreted as having been deposited in a low-energy, lowland alluvial system that supported swampy environments (Fanti and Catuneanu, 2009, 2010; Fanti and Miyashita, 2009; Koppelhus and Fanti, 2019). The DC Bonebed is an isolated channel

deposit with vertically stacked point bars of mudstones and siltstones interbedding with minor channel sandstones and lenticular coal seams. The depositional environment is interpreted as a channel system with low rates of migration and avulsion. U-Pb geochronology using chemical abrasion isotope dilution thermal ionization mass spectrometry (CA-ID-TIMS) on bentonite zircons and palynological assemblages, the DC Bonebed is ~73.5 Ma and is roughly equivalent to the Bearpaw Formation and the Strathmore Member of the Horseshoe Canyon Formation (Fig. 4.2) (Eberth et al., 2013; Eberth and Kamo, 2019; Fanti and Catuneanu, 2010). Excavation in the DC Bonebed has yielded new thescelosaurid fossils that include a number of disarticulated and unassociated cranial and postcranial elements.

Here I describe new orodromine material from the Dinosaur Park Formation, and compare it with multiple ornithischian groups. I also describe the new thescelosaurid material (Wapiti thescelosaurid) from the DC Bonebed, and compare it with other basal neornithischians, thescelosaurids, and cerapodans to test whether this material represents an orodromine, a thescelosaurine, another ornithischian group, or a combination of the former. A reduced major axis (RMA) analysis including the femur (UALVP 1849) and a ternary diagram including the premaxillary tooth of the Wapiti thescelosaurid were used to compare these elements to their equivalents in other thescelosaurids. Furthermore, the Wapiti thescelosaurid was histologically sectioned to evaluate its maturity and growth, and phylogenetic analyses were conducted using previous published character matrices to understand its evolutionary relationships amongst multiple thescelosaurid phylogenies (Brown et al., 2013b; Boyd, 2015; Madzia et al., 2018).

The Wapiti thescelosaurid represents the first specimens and the northern-most occurrence of thescelosaurine body fossils from the Wapiti Formation. With the occurrence of

orodromines in the Dinosaur Park Formation and the stratigraphic correlation of the DC Bonebed with the Bearpaw Formation, the Wapiti thescelosaurid can provide insight into the evolution of thescelosaurids during this time interval and can potentially help indicate why the stratigraphic separation between older orodromines and younger thescelosaurines occurred.

4.2. Materials and Methods

4.2.1. Anatomical Comparisons

The unassociated specimens from the Dinosaur Park Formation includes UALVP 5449, pedal phalanx; UALVP 48812 and 53744, right femora; UALVP 52839, basioccipital; and UALVP 60985, caudal vertebra. The unassociated fossils from the DC Bonebed includes UALVP 1849, right femur; UALVP 23088 and 59803, caudal vertebrae; UALVP 23089, dorsal vertebra; UALVP 23111 and 59506, phalanges; UALVP 23114, left quadrate; UALVP 50999 and 59855, right fibulae; UALVP 59471, cervical vertebra; UALVP 59483, left metatarsal II; UALVP 59834, right metatarsal I; and UALVP 59863; premaxillary tooth crown. Specimens were described and compared to other Late Cretaceous ornithischians, and a number of skeletal measurements were taken. Digital calipers, measuring tape, and the line tool in ImageJ software were used to take linear measurements of specimens (Table 4.1-3). ImageJ allows for accurate measurements of specimens that are too fragile or small to be measured directly, or of specimens that are not accessible physically (Schneider et al., 2012). In this study, the ImageJ line tool was used to measure specimens that were not physically available. The body mass of the Wapiti thescelosaurid was estimated by applying Campione et al.'s (2014) body mass estimation equation for non-avian bipeds (Equation 1) to the minimal femoral circumference of UALVP

1849. The equation is phylogenetically corrected and derived from body mass estimation for non-avian quadrupeds (Campione and Evans, 2012):

$$log_{10}BM_{bip} = 2.754 \cdot log_{10}(C_{femur}) - 0.683 \qquad (1)$$

where BM_{bip} is the body mass of a biped and C_{femur} is the minimal femoral circumference. The body mass estimate for UALVP 1849 was compared with those obtained for other thescelosaurids (Table 4.3).

4.2.2. Osteohistological Sectioning

I histologically sectioned a partial right fibula (UALVP 50999) to assess the ontogenetic status of the Wapiti thescelosaurid and compare its osteohistological features with those of other basal (non-cerapodan) and derived (cerapodan) neornithischians. A mid-shaft section was detached from the remainder of the specimen by using acetone to dissolve the glue holding together a break in the shaft. The section of bone was vacuum-embedded in Castolite AC polyester resin to minimize air bubbles. An Isomet 1000 Precision Sectioning Saw was used to make an initial cut midway through the embedded specimen. The Castolite AC polyester resin was vacuum-embedded into the cut surface, eliminating any remaining air pockets and stabilizing the surface for mounting. Excess resin was ground away using a Hillquist Thin Section Machine, before mounting the billet on a plexiglass slide using 3M Cyanoacrylate glue. The billet was cut off the slide using an Isomet 1000 Precision Sectioning Saw, and the slide was ground thin by hand on a glass plate using progressively finer grits. The resulting slide was imaged using plane polarized (ppl) and cross-polarized (x-pol) light using a Nikon Eclipse 80i upright microscope with an attached Nikon DS-Ri1 digital camera and a Nikon Eclipse

E600POL trinocular polarizing microscope with an attached Nikon DS-Fi3 digital camera. Panoramas of the fibula thin-section in plane-polarized and cross-polarized light were stitched together using the multipoint captured images function in NIS-element software. Osteohistological features were assessed through direct observation of slides in plane and cross-polarized light. Histological terminology follows Padian and Lamm (2013). Cross-sectional and medullary cavity diameter and cortical thickness were measured along the anteroposterior and lateromedial axes using ImageJ (Schneider et al., 2012) (Table 4.4).

4.2.3. Statistical Analyses

Four linear femoral measurements were taken using digital calipers, measuring tape, or ImageJ (Schneider et al., 2012) from a total of 16 thescelosaurid femora (Table 4.3). Femur length is defined as the maximum proximodistal length in anterior view. Femur width is the mid-shaft anteroposterior diameter. Lesser trochanter width is the maximum width of the lesser trochanter in lateral view. Intertrochanteric notch is the proximodistal length of the cleft in the lateral side of the femur that separates the lesser and greater trochanters. Bivariate analyses of femur width, lesser trochanter width, and intertrochanteric notch versus femur length were performed in order to compare the femoral proportions of the Wapiti thescelosaurid with those of other basal neornithischians (Table 4.3). The Asian neornithischian category (*Changchunsaurus*, *Haya*, and *Jeholosaurus*) in the analysis consists of Lower Cretaceous forms that have been placed in Thescelosauridae by at least some analyses, but which cannot be clearly associated with Orodrominae or Thescelosaurinae.

The set of tooth measurements used in this chapter is modified from Buckley et al. (2010) and Hendrickx et al. (2015) (Table 4.6), and includes three measurements (two linear and one

angular) that were taken from 31 in situ premaxillary teeth of *Changchunsaurus* (1), *Haya* (10), *Jeholosaurus* (4), *Orodromeus* (2), *Thescelosaurus* (8), *Zephyrosaurus* (5), and one isolated premaxillary tooth from the DC Bonebed (Table 4.5). Measurements were taken using ImageJ (Schneider et al., 2012) from photos of the premaxillary teeth in lateral view, in order to compare the proportions of the DC Bonebed isolated premaxillary tooth with those of other basal neornithischians. Crown height is defined as the maximum apicobasal distance from the base of the cingulum to the apex of the crown. Crown base length is the maximum mesiodistal length of the cingulum. Crown angle is the angle between the crown base length and the apical length (the maximum length of the mesial margin of the crown, measured obliquely from the mesial end of the cingulum to the apex of the crown) (Table 4.6). In previous studies (Buckley et al., 2010; Hendrickx et al., 2015), crown angle was calculated using the laws of cosine, but in this analysis, crown angle was measured using the angle tool in ImageJ by obtaining the angle between the crown base length and the crown height (Schneider et al., 2012). Any missing data in the premaxillary tooth dataset were estimated by imputation using the R package "missMDA" (Husson and Josse, 2016; R Core Team, 2013). The imputation method accurately estimates missing data by utilizing the regularized iterative principal components analysis algorithm, which substitutes the column mean and iteratively runs the principal components analysis to improve estimates (Husson and Josse, 2012; Josse et al., 2012; R Core Team, 2013; Strauss et al., 2003). The premaxillary data set was more than 90% complete, with crown height accounting for most of the missing observations.

Measurements were log transformed for standardization, but it is nevertheless worth noting that each of the four femoral variables was normally distributed. The femoral bivariate

analysis was performed using the model linear bivariate function of Paleontological Statistics Software (PAST) (Hammer et al., 2001). Reduced major axis (RMA) regression was used to obtain a Pearson's correlation with an associated p-value for the relationship between each pair of measurements, and to determine the nature of the correlation between them. RMA was preferred over ordinary least squares regression because the former assumes that the X and Y variables are susceptible to error (Smith, 2009). The premaxillary tooth dataset was plotted as a ternary diagram that was performed in PAST using the plot ternary plot function (Hammer et al., 2001).

4.2.4. Phylogenetic Analysis

Three phylogenetic analyses, using the character matrices of Brown et al. (2013b), Boyd (2015), and Madzia et al. (2018), were separately performed to assess the phylogenetic position of the Wapiti thescelosaurid. All of the thescelosaurid fossils from the DC Bonebed were assumed to belong to a single species for purposes of these analyses, and were therefore scored into each matrix as one operational taxonomic unit. Dieudonné et al.'s (2020) character matrix was not used, because it was rampant with scoring errors and fixing the character matrix is not within the scope of this paper. The three data sets chosen for this part of the study were initially developed to analyze patterns of relationships in various parts of the neornithischian tree.

Brown et al.'s (2013b) character matrix was modified from Boyd et al. (2009) and was developed to resolve the relationships amongst thescelosaurids, but included a number of non-thescelosaurid taxa (*Dryosaurus*, *Herrerasaurus*, *Iguanodon*, and *Scutellosaurus*). The version analyzed here of the Brown et al. (2013b) matrix contained 28 operational taxonomic units and 137 characters. *Herrerasaurus* was set as the outgroup taxon. The character matrix from Boyd

(2015) was modified from various previously published matrices (Butler et al., 2008; Scheetz, 1999; Weishampel and Heinrich, 1992; Weishampel et al., 2003) and was developed to resolve the relationships of basal neornithischians. Boyd's (2015) character matrix extensively sampled thescelosaurids and the analysis included operational taxonomic units that were non-thescelosaurid (Thyreophora, Marginocephalia, and Ornithopoda). The version analyzed here of the matrix from Boyd (2015) contained 66 operational taxonomic units and 255 characters with *Marasuchus* set as the outgroup taxon. Madzia et al.'s (2018) character matrix was modified from Boyd (2015) and was developed to assess the phylogenetic relationships of *Burianosaurus* amongst non-ankylopollexian ornithopods. The version of the matrix analyzed here contained 75 operational taxonomic units and 255 characters, with *Marasuchus* as the outgroup taxon. Madzia et al.'s (2018) operational taxonomic units included non-thescelosaurid clades in the analysis (Thyreophora, Marginocephalia, and Ornithopoda). Although the matrices vary in character and taxon sampling, they essentially represent different versions of one another, and using the different matrices should give an increasing phylogenetic resolution for the Wapiti thescelosaurid. Under the aforementioned assumptions, the character matrices make it possible to test the phylogenetic position of the Wapiti thescelosaurid, determine whether Thescelosauridae and its main constituent clades are recovered when the new material is included in each analysis, and compare phylogenetic statistical results.

The three character matrices were compiled in Mesquite v.3.6 (Maddison and Maddison, 2009), then exported as TNT files and separately analyzed in Tree analysis using New Technology (TNT) phylogenetic software (Goloboff et al., 2008). Characters were run as unordered and the traditional search option was used. A traditional search was run using Wagner

trees and the tree bisection reconnection swapping algorithm, utilizing 1,000 replicates and saving 100 trees per replication. Branches were collapsed if their minimum length was equal to zero. Most parsimonious trees were held in memory and subjected to a second run of the tree bisection reconnection swapping algorithm to optimize the total number of most parsimonious trees. A standard bootstrap analysis of 1,000 replicates was performed, and Bremer support values were calculated by using tree bisection reconnection from existing trees. A strict consensus tree was recovered from the analyses, and a majority rule tree was also generated using a 50% cutoff in order to improve the level of phylogenetic resolution.

4.3. Systematic Paleontology

DINOSAURIA Owen, 1842

ORNITHISCHIA Seeley, 1887

NEORNITHISCHIA Cooper, 1985 (sensu Butler et al., 2008)

ORNITHOPODA Marsh, 1881 (sensu Butler et al., 2008)

THESCELOSAURIDAE Sternberg, 1937

Phylogenetic Definition- The most recent common ancestor of *Thescelosaurus neglectus* Gilmore, 1913 and *Orodromeus makelai* Horner and Weishampel, 1988, and all of its descendants.

Comments- Initially erected by Sternberg (1937), Thescelosauridae is used to differentiate *Thescelosaurus* and *Hypsilophodon*. Recent research advancements in non-iguanodontian phylogenetics has revealed Thescelosauridae monophyly (Boyd et al., 2009; Boyd, 2015; Brown et al., 2013b; Madzia et al., 2018). The stem-based clade Thescelosauridae

was described by Buchholz (2002) and included *Parksosaurus*, but not *Dryosaurus*, *Hypsilophodon*, or *Iguanodon*. Brown et al. (2013b) used the phylogenetic definition of Thescelosauridae to recognize its monophyly by preserving its original intention to differentiate *Thescelosaurus* and closely related taxa from *Hypsilophodon* and to reflect the increasing diversity of small-bodied non-cerapodans in the Late Cretaceous. Boyd (2015) recovered Thescelosauridae (=Parksosauridae) in the analysis with the original fourteen taxa and the clades within, similar to Brown et al. (2013b). However, the evolutionary relationships of basal neornithischians are strongly debated with different studies resulting in disparate phylogenetic topologies (Dieudonné et al., 2020; Herne et al., 2019; Madzia et al., 2018; Rozadilla et al., 2016).

ORODROMINAE Brown et al., 2013b

Phylogenetic Definition- A stem-based clade including all neornithischians more closely related to *Orodromeus makelai* Horner and Weishampel (1988) than to *Thescelosaurus neglectus* Gilmore (1913) or *Parasaurolophus walkeri* Parks (1922).

Comments- Orodrominae was erected to differentiate *Orodromeus* from *Thescelosaurus* (Brown et al., 2013b). Brown et al. (2013b) defined orodromines as a stem-based clade and established its phylogenetic definition to reflect the increasing diversity of small-bodied basal non-cerapodans in the Late Cretaceous.

ORODROMINAE

Gen. et sp. indet.

Referred specimens- UALVP 52839, braincase; UALVP 48812 and 53744, right femora; UALVP 54497, phalanx; UALVP unnamed, caudal vertebrae.

Locality- UALVP 48812 was collected from the Dinosaur Park Formation in Dinosaur Provincial Park at Locality 34. UALVP 54497 was collected in the Dinosaur Park Formation in Dinosaur Provincial Park at the 'Happy Jacks' locality. UALVP 53744 was collected from the Dinosaur Park Formation in Dinosaur Provincial Park. UALVP 52839 was collected in west-central Alberta from the Dinosaur Park Formation. Refer to figure 4.3 for specimen localities.

Horizon- Exact horizon is unknown, but the specimens were collected at various locations in the Dinosaur Park Formation. Dinosaur Park Formation, Alberta (Campanian; 76 - 75 Ma) (Eberth and Hamblin, 1993; Ogg and Hinnov, 2012).

THESCELOSAURINAE Sternberg, 1940

Phylogenetic Definition- Thescelosaurinae is a stem-based clade including all neornithischians more closely related to *Thescelosaurus neglectus* Gilmore (1913) than to *Orodromeus makelai* Horner and Weishampel (1988) or *Parasaurolophus walkeri* Parks (1922).

Comments- Thescelosaurinae was originally proposed by Sternberg (1940) to differentiate *Thescelosaurus* from *Dysalotosaurus*, *Hypsilophodon*, and *Parksosaurus*. Brown and Druckenmiller (2011) defined Thescelosaurinae as a stem-based clade. Brown et al. (2013b), Boyd (2015), Madzia et al. (2018) recovered Thescelosaurinae as a subclade in Thescelosauridae. Evolutionary relationships of basal neornithischians are strongly debated where different studies result in disparate phylogenetic topologies where thescelosaurine taxa

shift in and out of Thescelosauridae (Brown et al., 2013b; Boyd, 2015; Dieudonné et al., 2020; Herne et al., 2019; Madzia et al., 2018; Rozadilla et al., 2016).

THESCELOSAURINAE

Gen. et sp. indet.

Referred Specimens- All specimens are unassociated bones or teeth from the DC Bonebed, unit 3 of the Wapiti Formation. UALVP 1849, right femur; UALVP 59512, UALVP 59855, right fibulae; UALVP 59483, left metatarsal II; UALVP 59834 right metatarsal I; UALVP 59471, cervical vertebra; UALVP 23089, dorsal vertebra; UALVP 23088, UALVP 59803, caudal vertebrae; UALVP 23114, left quadrate; UALVP 23111, UALVP 59506, pedal phalanges; UALVP 59863; premaxillary tooth crown.

Locality- The Dinosaur-Chelonian Bonebed, 10 km southeast of Grande Prairie along the south bank of the Wapiti River.

Horizon- Unit 3 of the Wapiti Formation, Alberta (Campanian; ~73.5 Ma) (Ogg and Hinnov, 2012) (Fig. 4.3).

4.4. Description of New Thescelosaurid Material from the Dinosaur Park Formation

4.4.1. Basioccipital

A partial basioccipital (UALVP 52839) is preserved with only the left ventral portion missing (Fig. 4.4). Overall, the specimen has a similar morphology with thescelosaurid basioccipitals. Given this, bone contact interpretations of the basioccipital are based on basal neornithischian braincase anatomy (Norman et al., 2004b). UALVP 52839 has a similar morphology with *Zephyrosaurus*, but direct comparisons with *Changchunsaurus*, *Jeholosaurus*,

and *Parksosaurus* are limited because comparable views are obscured by bone/matrix or are significantly damaged (Barrett and Han, 2009; Jin et al., 2010; Parks, 1926). The anterior margin of the basioccipital would have contacted the basisphenoid, and the dorsolateral margins would have likely contacted the exoccipitals, which would have formed the rest of the occipital condyle. UALVP 52839 is an occipital condyle that is bulbous and u-shaped in posterior view, similar to those of *Changchunsaurus*, *Jeholosaurus*, *Orodromeus*, *Oryctodromeus*, *Thescelosaurus*, and *Zephyrosaurus* (Barrett and Han, 2009; Boyd, 2014; Brown et al., 2011; Jin et al., 2010; Krumenacker, 2017; Scheetz, 1999; Sues, 1980). In contrast, the occipital condyles of *Haya* and *Hypsilophodon* are either a bilobed u-shape or a broad v-shape, respectively (Galton, 1974a; Makovicky et al., 2011). In lateral view, the occipital condyle forms a comma-shape, similar to *Zephyrosaurus* but unlike the circular condyle in *Haya*, *Oryctodromeus*, *Orodromeus*, and *Thescelosaurus* (Boyd, 2014; Brown et al., 2011; Krumenacker, 2017; Makovicky et al., 2011; Scheetz, 1999; Sues, 1980). Transversely wider than dorsoventrally tall, the occipital condyle's dorsal surface forms a concave border for the foramen magnum (Table 4.1). In dorsal view, the foramen magnum forms a straight trough unlike the hourglass shape seen in *Thescelosaurus* (Boyd, 2014; Brown et al., 2011). Foramen magnum shape comparisons with other thescelosaurids are difficult as they are obscured by overlapping bone or matrix (Barrett and Han, 2009; Krumenacker, 2017; Makovicky et al., 2011; Scheetz, 1999; Sues, 1980). Eroded meandering dorsolateral sutural scars are present and would likely form the contacts of the exoccipital. In posterior view, the basioccipital constricts to a midline midpoint that is dorsal to the occipital condyle (Fig. 4.4). The constriction subsequently broadens laterally around the basioccipital keel where its margin forms a saw tooth sutural surface that would have

contacted the basisphenoid. However, the sutural surface for the contact of the basisphenoid is damaged on the left lateral side. The saw tooth sutural surface forms an anteroventral directed v-shape that would have inserted into the basisphenoid in posterior view. The v-shape ventral contact between the basioccipital and the basisphenoid is present in *Thescelosaurus neglectus* but it is a broad u-shape in each of *Haya*, *T. assiniboiensis*, and *Zephyrosaurus* and is an inverted T-shape in *Oryctodromeus* (Boyd, 2014; Brown et al., 2011; Krumenacker, 2017; Makovicky et al., 2011; Sues, 1980). The basioccipital keel forms a prominent ventrally extended medial ridge, similar to *Changchunsaurus*, *Haya*, *Hypsilophodon*, *Jeholosaurus*, *Thescelosaurus*, *Oryctodromeus*, *Orodromeus*, and *Zephyrosaurus* (Barrett and Han, 2009; Boyd, 2014; Brown et al., 2011; Galton, 1974a; Jin et al., 2010; Krumenacker, 2017; Makovicky et al., 2011; Scheetz, 1999; Sues, 1980). Immediately lateral to the basioccipital keel, there are small, asymmetrical foramina along the lateral margins. Three small foramina are present dorsal to the basioccipital keel, whereas in *Thescelosaurus* there is a single foramen (Boyd, 2014; Brown et al., 2011). In anterior view, a T-shaped feature is present at the midline of the element where it would have likely contacted the basisphenoid, and the dorsal portion of this feature would have likely supported the floor of the braincase. Despite minor discrepancies in dimensions, the morphology of the occipital condyle, and the contacts with other braincase bones, the basioccipital has a similar morphology with other basal neornithischians such as *Gasparinisaura* (Coria and Salgado, 1996), *Hypsilophodon* (Galton, 1974a), and *Jeholosaurus* (Barrett and Han, 2009). Overall, the basioccipital is similar with other thescelosaurids such as *Changchunsaurus*, *Haya*, *Orodromeus*, *Oryctodromeus*, *Thescelosaurus assiniboiensis*, *Thescelosaurus neglectus*, and especially *Zephyrosaurus* (Boyd, 2014; Brown et al., 2011; Coria and Calvo, 2002; Galton,

1973; Jin et al., 2010; Krumenacker, 2017; Makovicky et al., 2011; Scheetz, 1999; Sues, 1980). The basioccipitals in derived Late Cretaceous ornithischians are distinct from UALVP 52839 in that the occipital condyles have differing morphologies on how much participate in the foramen magnum, and the contacts with other braincase bones (Arbour and Currie, 2013; Averianov et al., 2006; Currie et al., 2016; Dodson et al., 2004; Evans, 2009; Galton and Sues, 1983; Godefroit et al., 2004; Hailu and Dodson, 2004; Holmes et al., 2020; Horner et al., 2004; Lull, 1933; Maryańska and Osmolska, 1974; Maryańska et al., 2004; Sereno et al., 1988; Sullivan, 2006; Vickaryous et al., 2004).

4.4.2. Caudal Vertebra

UALVP 60985 is an isolated caudal centrum that is missing neural arch and transverse processes. The exact placement of the centrum is uncertain but has a similar morphology with basal neornithischian mid-series vertebrae (12^{th} - 25^{th}) (Barta and Norell, 2021; Brown et al., 2011; Coria and Salgado, 1996; Galton, 1974a; Gilmore, 1915; Han et al., 2012; Ibiricu et al., 2014; Krumenacker, 2017; Makovicky et al., 2011; Martinez, 1998; Norman et al., 2004a, b; Parks, 1926; Sheetz, 1999) but is different than other Late Cretaceous ornithischians (Arbour and Currie, 2013; Campione, 2015; Holmes, 2014; Xing et al., 2010). (Fig. 4.4). The centrum is anteroposteriorly longer than dorsoventrally tall (Table 4.1) and the centrum is spool shaped with the concave lateral and ventral surfaces. In ventral view, there is a midline depression that extends anteroposteriorly and connects the anteroventrally and posteroventrally directed chevron facets. The centrum is amphicoelous, typical of the proximal and middle portions of caudal vertebrae (Krumenacker, 2017). The neural arch is present but damaged and if the neural arch was there, then it would have been fused with the centrum based on the lack of sutures present

between it and the centrum. In ventral view, the neural canal has an hourglass shape, and damaged dorsolaterally directed transverse processes are present.

4.4.3. Femur

Two partial and isolated femora (UALVP 48812 and 53744) are preserved, although the mid-shaft regions are missing in both specimens (Fig. 4.5). The right femur (UAVLP 48812) is larger and preserves the femoral head, a damaged greater trochanter, and the lateral and medial condyles, whereas the smaller specimen (UALVP 53744) preserves a partial femoral head, a damaged greater trochanter, a partial medial condyle, the incipient base of the lesser trochanter, and the proximal margin of the fourth trochanter (Fig. 4.5). Femoral morphology is similar to other basal neornithischians (Coria and Calvo, 2002; Galton, 1974a; Gilmore, 1915; Han et al., 2012; Huh et al., 2010; Ibiricu et al., 2014; Krumenacker, 2017; Makovicky et al., 2011; Norman et al., 2004b; Parks, 1926; Sheetz, 1999) but has a close resemblance with orodromines from the Dinosaur Park Formation (Brown et al. 2013b).

The proximal portion of UALVP 48812 measures 46.8 mm and 27.9 mm in anteroposterior length and transverse width (Table 4.1). In posterior view, the femoral head is perpendicular to the femoral shaft where a neck constriction separates them from the greater and lesser trochanters. A distinctive bulbous femoral head is present, which is a common shape in other thescelosaurids (Boyd, 2015; Butler et al., 2011; Gilmore, 1915; Han et al., 2012; Krumenacker, 2017; Makovicky et al., 2011; Parks, 1926; Sheetz, 1999). The femoral head bows posteriorly in medial view. In anterior view, a deep ligament sulcus is present on the posterior portion of the femoral head where it is directed towards the femoral shaft. This marks the insertion of the iliotrochantericus (Maidment and Barrett, 2011b) and is similar in other

thescelosaurids (Butler et al., 2011; Gilmore, 1915; Huh et al., 2010; Krumenacker, 2017; Makovicky et al., 2011; Scheetz, 1999). In dorsal view, the femur is constricted anteroposteriorly between the head medially and the region that expands into the greater and lesser trochanter. In posterior view, ventral to the femoral head, a shallow depression is present that runs parallel to the ridge of the greater trochanter. Although damaged, the greater trochanter preserves the flat lateral margin that is a synapomorphy for Thescelosauridae (Brown et al., 2013b; Butler et al., 2011; Gilmore, 1915; Han et al., 2012; Krumenacker, 2017; Makovicky et al., 2011; Parks, 1926; Scheetz, 1999). The distal end of the UALVP 48812 is 39.7 mm in anteroposterior length (Table 4.1). In lateral view, the femoral shaft appears to bow anteriorly. There is no anterior intercondylar groove. These features commonly occur in thescelosaurids (Brown et al., 2013b; Butler et al., 2011; Gilmore, 1915; Han et al., 2012; Huh et al., 2010; Makovicky et al., 2011; Parks, 1926; Scheetz, 1999) and is the basal condition for Ornithischia (Norman et al., 2004b). A deep posterior intercondylar groove is present where it separates the medial and bilobed lateral condyles. The inner condyle is anteroposterioly larger than the outer condyle but the outer condyle is transversely wider than the inner condyle.

The length of the proximal part of UALVP 53744 is 25.6 mm (Table 4.1). In medial view, the femoral head is damaged but bows anteriorly. The distal portion of the damaged greater trochanter is flat (Fig. 4.5). On the anterior margin of the greater trochanter, the incipient start of the lesser trochanter is present where it forms a pronounced ridge. The proximal portion of the fourth trochanter is present with a relatively large nutrient foramen occurring on the proximal margin of the posterior side. A shallow pit is present on the anterior margin of the fourth trochanter where it forms the insertion of the caudofemoralis longus and

puboischiofemoralis internus (Maidment and Barrett, 2011b; Maidment et al., 2014). The femoral shaft presumably bows anteriorly in lateral and medial views, based on the curvature of the distal anterior portion. There is a shallow anterior intercondylar groove distally, but damage makes it impossible to know how deep it may have been. The presence of one is unlike in thescelosaurids and other basal neornithischians (Brown et al., 2011; Coria and Salgado, 1996; Galton, 1974a; Gilmore, 1915; Han et al., 2012; Huh et al., 2010; Makovicky et al., 2011; Parks, 1926; Scheetz, 1999). An anterior intercondylar groove is present in *Anabisetia* (Coria and Calvo, 2002), *Notohypsilophodon* (Ibiricu et al., 2014), and *Oryctodromeus* (Krumenacker, 2017). A deep posterior intercondylar groove separates the damaged medial and lateral condyles.

Overall, UALVP 44812 and 53744 have similar shapes and proportions that do not differ from named orodromines (Brown et al., 2013b; Huh et al., 2011; Krumenacker, 2017; Scheetz, 1999) and are distinct in size proportions and morphology from other Late Cretaceous ornithischians (Butler and Zhao, 2009; Campione, 2015; Carpenter, 2003; Coombs, 1979; Farke and Yip, 2019; Galton and Sues 1983; He et al., 2015; Holmes, 2014; Maidment and Barrett, 2011a; Maryańska and Osmolska, 1974; Maryańska et al., 2004; Prieto-Marquez, 2014; Xu et al., 2010).

4.4.4. Pedal Phalanx

UALVP 54497 is a non-ungual phalanx that measures 57 mm and 25 mm in anteroposterior length and transverse width, respectively (Table 4.1). The overall shape is consistent with those of other thescelosaurids (Fig. 4.3) in that it is wider than tall, longer than wide, has a midshaft constriction, and a concave proximal articular surface. Two distal condyle surfaces are present and are divided into the lateral and medial ginglymi. Ligament pits are

present on the medial and lateral sides of the distal condyles. The ventral margin of the phalanx is dorsally concave. The articular surface on the proximal end is keeled suggesting that the element experienced weight bearing and lateral displacement. The pedal phalanx is similar in size and shape with those of other thescelosaurids such as *Haya* and *Jeholosaurus* (Barta and Norell, 2021; Han et al., 2012; Makovicky et al., 2012) and other basal neornithischians (*Gasparinisaura*, Coria and Salgado, 1996; and *Hypsilophodon*, Galton, 1974a). In contrast, the pedal phalanx is more robust compared to those of *Changchunsaurus* (Butler et al., 2011), *Orodromeus* (Scheetz, 1999), and *Oryctodromeus* (Krumenacker, 2017) but more gracile compared to *Thescelosaurus* (Brown et al., 2011; Gilmore, 1915). The pedal phalanges of other Late Cretaceous dinosaurs are distinct in sizes and shapes from UALVP 54497 (Averianov et al., 2006; Campione, 2014; Clark et al., 2004; Currie et al., 2016; Funston, 2020; Hailu and Dodson, 2004; Holmes, 2014; Holtz, 2004; Makovicky et al., 2004; Norell and Makovicky, 2004; Osmolska et al., 2004; Park et al., 2021; Prieto-Marquez, 2014; Smith and Galton, 1990; Vickaryous et al., 2004).

4.5. Description of New Thescelosaurid Material from the Wapiti Formation

The new thescelosaurid material from the Wapiti Formation comprises a small collection of unassociated, fragmentary elements. The specimens are from a single locality but are not otherwise associated. The minimum number of individuals in the sample is two because two right fibulae are present. The specimens are more or less proportionate in size to one another. The morphology is distinctive of a thescelosaurine with features similar to *Changchunsaurus*, *Haya*, and *Thescelosaurus* but is not sufficiently diagnostic to serve as the basis for erecting as a new taxon. The cervical vertebra has been crushed diagenetically. All of the Wapiti

thescelosaurid material is distinct from other Late Cretaceous cerapodans (Arbour and Currie, 2013; Averianov et al., 2006; Butler and Zhao, 2009; Campione, 2014; Carpenter, 2003; Carpenter et al., 2008; Chinnery and Weishampel, 1998; Coombs, 1979; Currie et al., 2016; Farke and Yip, 2019; Galton and Sues, 1983; He et al., 2015; Holmes, 2014; Maidment and Barrett, 2011a; Maryańska and Osmolska, 1974; Maryańska et al., 2004; Wu et al., 2007; Xing et al., 2010; Xing et al., 2017; Xu et al., 2010).

4.5.1. Premaxillary Tooth

A single isolated premaxillary crown (UALVP 59863) has been recovered and has similar premaxillary crown proportions as thescelosaurines such as *Changchunsaurus* (Jin et al., 2010), *Haya* (Makovicky et al., 2011), *Jeholosaurus* (Barrett and Han, 2009), and *Thescelosaurus* (Boyd, 2014). UALVP 59863 possesses a bulbous morphology that is longer than tall and slightly buccolingually compressed, with a pointed and recurved apex. The base of the crown lacks a cingulum, but forms a bulbous swelling, basal to which is a constricted neck (Fig. 4.6 and Table 4.5). The crown height, crown base length, and crown angle values are 3.6 mm, 4.2 mm, and 48.2°, respectively (Table 4.5; consult this table for other average tooth measurements with other thescelosaurids). Premaxillary crowns in *Changchunsaurus* and *Haya* are apicobasally tall and peg-shaped, whereas the crown of UALVP 59863 is similar to those of *Thescelosaurus* (Boyd, 2014) and *Jeholosaurus* (Barrett and Han, 2009), where they are short and stout. The apex of the crown is blunt and recurves presumably distally as in other thescelosaurines (Boyd, 2014; Jin et al., 2010; Makovicky et al., 2011). Ornamentation on the premaxillary crown consists of numerous fine ridges that extend from the apex to the bulbous base, which is diagnostic in *Thescelosaurus* (Boyd, 2014) and absent in other thescelosaurines

(Jin et al., 2010; Makovicky et al., 2011) (Fig. 4.6). Fine apicobasal ridges are usually not seen in the premaxillary teeth of orodromines, such as *Orodromeus* and *Zephyrosaurus* (Scheetz, 1999; Sues, 1980). It is unknown if *Parksosaurus* possessed the fine, apicobasal oriented ridges as the holotype lacks premaxillary teeth (Parks, 1926). The Prince Creek Formation may potentially yield premaxillary teeth of *Parksosaurus,* but it is pending on taxonomic verification (Brown and Druckenmiller, 2011). Denticles are absent on the mesial and distal margins, similar to other thescelosaurines (Boyd, 2014; Jin et al., 2010; Makovicky et al., 2011; Sues, 1980). The root cross-section is elliptical. This suggests its tooth position maybe anterior based on the root cross-section because in *Thescelosaurus* the root cross-sections change from circular posteriorly to elliptical anteriorly (Boyd, 2014). In contrast, the root cross-sections are elliptical throughout the premaxillary tooth row in various basal neornithischians (Barrett and Han, 2009; Jin et al., 2010; Makovicky et al., 2011), or are circular throughout the premaxillary tooth row as in *Zephyrosaurus* (Sues, 1980). The apex likely preserves a single wear facet where it is presumed to be on the buccal side and likely contacted either hard food or the lower predentary. This wear facet pattern is similar to those of other thescelosaurines (Barrett and Han, 2009; Boyd, 2014; Jin et al., 2010; Makovicky et al., 2011). However, the wear facet and apicobasal ridges of the crown appear to be eroded and it is likely that the crown was ingested by breaking off during mastication and swallowed, or the result of postmortem processes (e.g., abrasion or erosion).

4.5.2. Quadrate

A three-dimensionally preserved left quadrate is damaged dorsally, and has a damaged pterygoid wing (Fig. 4.7). UALVP 23114 has an anteroposterior length of 12 mm. The shaft of the quadrate arcs posterodorsally in left lateral view, a condition seen in basal ornithischians and

thescelosaurids (Boyd, 2014; Krumenacker, 2017; Jin et al., 2010; Norman et al., 2004b). The cross-section of the quadrate at mid-length is triangular. The ventral condyles of the quadrate are concave ventrally in lateral view, whereas the ventral condyles in *Thescelosaurus* are concave dorsally (Boyd, 2014). The anterior lateral condyle is slightly rounded and extends further ventrally than the slightly flattened posterior medial condyle in lateral view. In medial view, the ventral condyles form a "s" shape where the anterior ventral condyle is slightly rounded anteriorly, then flattens posteriorly, and then curves dorsally to the posterior condyle where it flattens posteriorly (Fig. 4.7). A small depression slightly separates the ventral condyles in medial view.

The lateral contact surface for the quadratojugal is present on the anterior ventral corner as a depression and terminates as a ridge posteriorly. The quadrate suture with the quadratojugal and its position on the quadrate is a basal ornithischian condition (Norman et al., 2004b). A well-defined ridge is present on the anterolateral mid-shaft surface that is dorsally above the lateral quadratojugal contact. In lateral view, the quadratojugal suture on the quadrate starts just dorsal to the anterior condyle and extends ventrally below the midshaft ridge. The ridge gradually shallows along the anterior margin of the lateral surface and terminates below the damaged dorsal portion. The ridge forms a continuous contact with the quadratojugal and wraps around the quadrate shaft onto the medial side. A similar dorsally extended quadratojugal suture and a well-defined midshaft ridge on the anterolateral surface is present in other thescelosaurines such as *Changchunsaurus* (Jin et al., 2010), *Haya* (Makovicky et al., 2011) and *Thescelosaurus* (Fig. 4.7) and the basal neornithischian *Jeholosaurus* (Barrett and Han, 2009).

On the lateral surface, a quadrate foramen is present posterior to the quadratojugal contact, similar to the situation in *Haya* (Makovicky et al., 2011), *Parksosaurus* (Boyd, 2014), and *Thescelosaurus* (Boyd, 2014). The quadratic foramen passes through the base of the jugal wing and exits on the anteromedial side of the quadrate. Although damaged anteriorly, the jugal wing is present. It is mediolaterally thin where it originates on the anterolateral margin of the quadrate shaft, similar to *Thescelosaurus* (Boyd, 2014). The jugal wing is further up the quadrate shaft in *Oryctodromeus* compared to its lower position in thescelosaurines (Fig. 4.7). The pterygoid wing is damaged but emerges posteromedially on the quadrate shaft, dorsally above the ventral condyles and ventrally below the quadratic foramen (Fig. 4.7). A fossa is present on the pterygoid wing in posterior view and its position is dorsally above the emergence of the pterygoid wing, similar to *Jeholosaurus* (Barrett and Han, 2009), *Orodromeus* (Boyd, 2009), *Parksosaurus* (Boyd, 2009), *Thescelosaurus* (Boyd, 2014), and *Zephyrosaurus* (Sues, 1980).

4.5.3. Cervical Vertebra

An isolated cervical vertebra (UALVP 59471) has been crushed postmortem and is incomplete; features above the neurocentral line are missing. The missing features include the neural spine, the diapophyses, and the pre- and postzygapophyses. UALVP 59471 measures 46 mm and 37 mm in anteroposterior length and transverse width, respectively (Table 4.2). The centrum is amphicoelous, longer than wide, and spool-shaped (Fig. 4.8). Lateral sides of the centrum are concave just below the neuro-central line with a saw tooth suturing pattern present. In dorsal view, the neural canal is exposed and depressed medially inward and then expands laterally outward anteroposteriorly, giving an hourglass shape. The lateral expansion of the neural canal is greater posteriorly than it is anteriorly. The ventral side of the centra is keeled

with the ventral margins being rugose and crenulated. These features are typical of other thescelosaurid cervical vertebrae (Butler et al., 2011; Gilmore, 1915; Han et al., 2012; Krumenacker, 2017; Makovicky et al., 2011; Scheetz, 1999). The parapophysis is a pronounced process on each side of the most anterior portion of the centrum and is located on and below the neurocentral line. The articular surfaces of the parapophyses face laterally and are damaged at their distal ends. The position of the parapophysis suggests that the centrum and the neural arch contributes to this process. Based on thescelosaurids, the position in the vertebral column of UALVP 59471 is posteriorly placed (cervical vertebrae 4-9) (Butler et al., 2011; Gilmore, 1915; Han et al., 2012; Krumenacker, 2017; Makovicky et al., 2011; Scheetz, 1999).

4.5.4. Dorsal vertebra

UALVP 23089 is a three-dimensionally partially preserved isolated dorsal vertebra that is of an unknown position in the vertebral series and the features above the neurocentral line are missing. The dorsal vertebra measures 43 mm and 36 mm in anteroposterior length and transverse width, respectively (Table 4.2). The centra is amphicoelous and spool-shaped and has a similar morphology with *Thescelosaurus* (Fig. 4.8). The lateral sides of the centrum are concave just below the neuro-central line with a saw tooth suturing pattern present. In dorsal view, the neural canal is exposed and pinches medially inward and then expands laterally outward anteroposteriorly, giving an hourglass shape. Based on thescelosaurids, the lateral expansion of the neural canal is greater posteriorly than it is anteriorly. The ventral side of the centra is keeled but not at the degree of the cervical vertebra, and the ventral anterior and posterior margins are rugose and crenulated. UALVP 23089 lacks a parapophysis process on the centrum and would suggest that the process would be placed on the neural arch.

4.5.5. Caudal Vertebrae

Two three-dimensional, partially preserved isolated caudal vertebrae are known (UALVP 23088 and 59803) (Fig. 4.8). UALVP 23088 is more anteriorly positioned whereas UALVP 59803 is positioned posteriorly in the tail. The centrum is amphicoelous in UALVP 23088, and UALVP 59803 is slightly platycoelus to acoelus. Both specimens are longer than wide, and wider than high. UALVP 23088 is spool shaped and UALVP 59803 is cylindrical. The neurocentral line is fused in both specimens.

Articulations for the chevrons are present on the ventral anterior and posterior margins in UALVP 23088. UALVP 23088 is measured 40 mm and 29 mm in anteroposterior length and transverse width, respectively (Table 4.2). The facets for chevron are typically present in the most anterior caudal vertebrae in other thescelosaurids (Gilmore, 1915; Han et al., 2012; Makovicky et al., 2011). Damaged left and right lateral transverse processes are present in UALVP 23088, but the right one is more heavily damaged. Caudal vertebrae with transverse processes are typically found in the first fourteen caudals and progressively become shorter posteriorly (Gilmore, 1915; Han et al., 2012; Makovicky et al., 2011). The vertebrae do not preserve the zygapophyses. An incomplete and laterally compressed neural spine with an oval cross-section inclines posteriorly at 45º.

The posteriorly positioned caudal vertebra UALVP 59803 has a cylinder-like morphology (Fig 4.8). Articulations for chevron facets are not present on the either anterior and posterior margins of the ventral side of the centrum. UALVP 59803 measures 40 mm and 22 mm in anteroposterior length and transverse width (Table 4.2). However, a strong lateral keel is present that depresses medially inward. The neural spine, transverse processes, and

zygapophyses are not present, although, a “shelf” is present were the neurocentral line would have been positioned.

4.5.6. Femur

UALVP 1849 is a partial, three-dimensionally preserved right femur that includes a partially damaged femoral head, but is missing the distal end of the fourth trochanter and the distal inner and outer condyles (Fig. 4.9). It measures 237 mm, 35 mm, and 122 mm in proximodistal length, transverse proximal width, and circumference, respectively (Table 4.2, 4.3). Using the body mass estimation calculation from Campione et al. (2014), UALVP 1849 had an estimated body mass of 115 ± 29 kg, comparable to that of *Thescelosaurus assiniboiensis* (113 ± 28 kg) despite the latter having a greater femoral length. See Table 4.3 for estimated body mass comparisons in basal Neornithischia. The femur is bowed anteriorly in lateral view, a characteristic of basal neornithischians (Norman et al., 2004b) and thescelosaurids (Brown et al., 2013b; Gilmore, 1915; Han et al., 2012; Huh et al., 2011; Makovicky et al., 2011; Scheetz, 1999). The mid-shaft of the femur has a sub-oval cross-section. Posteriorly, the femoral head is partially destroyed and is approximately perpendicular to the femoral shaft where the neck forms a distinctive constriction as seen in all thescelosaurids (Butler et al., 2011; Gilmore, 1915; Makovicky et al., 2011; Han et al., 2012; Huh et al., 2011; Scheetz, 1999). The head in posterior view possesses a shallow depression between the lateral side of the fourth trochanter to the femoral head's proximal base, where it extends and terminates at the greater trochanter. A smaller depression is present in *Thescelosaurus neglectus* (Gilmore, 1915). A ligament sulcus is present posterior to the femoral head where the sulcus is directed towards the femoral shaft, similar to *Changchunsaurus* (Butler et al., 2011), *Haya* (Makovicky et al., 2011), *Jeholosaurus*

(Han et al., 2012), *Koreanosaurus* (Huh et al., 2010), *Orodromeus* (Scheetz, 1999), and *Thescelosaurus* (Gilmore, 1915). In dorsal view, the femoral head is directed anteromedially and in posterior view, a broad, shallow depression (fossa trochanteris) separates the femoral head from the greater trochanter. The fossa trochanteris is present in other thescelosaurids (Butler et al., 2011; Gilmore, 1915; Huh et al., 2010; Makovicky et al., 2011; Scheetz, 1999) but it is absent in basal neornithischians (Butler et al., 2012; He and Cai, 1984; Santa Luca, 1980; Thulborn, 1972).

The dorsal margin of the greater trochanter is flat and expands anteroposteriorly with shallow dorsoventrally extending striations on the lateral surface, similarly to *Jeholosaurus* (Han et al., 2012) and *Thescelosaurus* (Gilmore, 1915). A depressed intertrochanteric notch extends dorsoventrally on the femur's proximal lateral surface, separating the greater and lesser trochanters. In lateral view, the intertrochanteric notch originates proximally at the femur and terminates medially at the mid-shaft. Dorsoventral striations are present within the intertrochanteric notch. A similar intertrochanteric notch is present in *Changchunsaurus* (Butler et al., 2011), *Jeholosaurus* (Han et al., 2012), an indeterminate orodromine (Brown et al., 2013b), *Oryctodromeus* (Krumenacker, 2017), and *Thescelosaurus* (Gilmore, 1915), but are shallow in *Haya* (Makovicky et al., 2011), and absent in *Parksosaurus* (Parks, 1926). The intertrochanteric notch appears to be deeper and longer than in other thescelosaurid taxa previously described. In lateral view, the lesser trochanter is a finger-like process with a D- to sub-oval shaped cross-section, and the proximal margin terminates below the dorsal margin of the greater trochanter. The lesser trochanter is large in width and length compared to other

thescelosaurids, relative to the size of the femur (Fig. 4.9 and Table 4.3). Striations extend dorsoventrally on the proximal lateral surface of the lesser trochanter.

A pendant fourth trochanter is present on the posteromedial margin of the femoral shaft. The proximal base of the fourth trochanter is positioned on the proximal half of the femur, and the base ends at the femoral mid-shaft. The proximal margin of the fourth trochanter to the femur proximal end is 32% of the total length of the femur, and the distal base to the distal margin is 48%. The pendant fourth trochanter is common in other small-bodied basal neornithischians (Barrett and Han, 2009; Gilmore, 1915; Han et al., 2012, Krumenacker, 2017; Norman et al., 2004; Persons and Currie, 2020). The convex fourth trochanter is robust compared to other thescelosaurid taxa (Fig. 4.9). A sub-oval depression is present on the medial side of the fourth trochanter and is interpreted as the insertion of the caudofemoralis longus and puboischiofemoralis internus (Maidment and Barrett, 2011b) (Fig. 4.10). The distal condyles of UALVP 1849 have been damaged and do not preserve the condyles or intercondylar groove; however, the distal end is expanded mediolaterally in anterior view.

4.5.7. Fibula

Two right fibulae are preserved: UALVP 59855 is a complete three-dimensionally preserved, unassociated fibula, and is a long and slender element (264 mm); UALVP 50999 preserves the three-dimensional distal end of the element (Table 4.2 and Fig. 4.11).

In lateral view, UALVP 59855 has a shallow sinusoidal shape. The proximal end is convex and the distal end is concave, similar to *Changchunsaurus* (Butler et al., 2011), *Parksosaurus* (Parks, 1926), *Notohypsilophodon* (Ibiricu et al., 2014), and *Thescelosaurus*

(Gilmore, 1915) (Table 4.2, 4.3). However, other thescelosaurids have straight and slender fibulae with little sinuosity, including *Haya* (Makovicky et al., 2011), *Orodromeus* (Scheetz, 1999), *Oryctodromeus* (Krumenacker, 2017), and *Talenkauen* (Novas et al., 2004) (Fig. 4.12). In addition, other basal neornithischians such as *Gasparinisaura* (Coria and Salgado, 1996), *Jeholosaurus* (Han et al., 2012), and the heterodontosaurid *Heterodontosaurus* (Galton, 2014), have straight and slender fibulae. The proximal end is mediolaterally compressed with an elongated rectangular cross-section, an oval cross-section at the mid-shaft, and a "D" shaped cross-section at the distal end. The proximal end is anteroposteriorly expanded compared to the fibular shaft and is deeper with respect to the mediolaterally compressed transverse width. The proximal articular surface has a convex shallow depression that extends anteroposteriorly where it starts proximally wide and then narrows distally on the fibular shaft. The convex depression shallows in depth and tapers distally until an abrupt termination at the mid-shaft. The convex medial proximal end articulated with the fibular condyle of the tibia, similar to *Jeholosaurus* (Han et al., 2012) and *Thescelosaurus* (Gilmore, 1915). In medial view, the fibular mid-shaft is flat and would have been appressed to the tibia, unlike the condition with *Albertadromeus* (Brown et al., 2013b). In lateral view, the distal end of UALVP 50999 is concave, similar to *Changchunsaurus* (Butler et al., 2011) and *Thescelosaurus* (Gilmore, 1915).

UALVP 59855 and 50999 have identical intermuscular lines (which are ridges that extend proximodistally on the fibular shaft) and facets on the fibular shaft (Fig. 4.11). The intermuscular lines extend dorsoventral on the mid-shaft in anterior view. In medial view, both specimens have a dorsoventrally directed, thin intermuscular line on the distal fibular shaft that terminates ventrally at a posteromedially directed, flat, and oval tibial facet. In posterior view,

intermuscular lines extend dorsoventrally but curve around the oval tibular facet. The distal ends of the fibulae possess large “tear-drop” facets that would have contacted the distal surface of the tibia. In lateral view, a single dorsoventrally extended intramuscular line is present in both specimens but the distal extent of it is damaged in UALVP 50999. Contacting the tibia anteromedially and the calcaneum distally, the distal margins of the fibulae are tear-drop shaped in anterior and posterior views, and comma shaped in lateral and medial views.

4.5.8. Metatarsals

Two associated metatarsals include the left metatarsal 1 and the weight-bearing right metatarsal 2 and are three-dimensionally preserved (UALVP 59834 and 59483) (Fig. 4.13). Metatarsal 1 is smaller than metatarsal 2 and is very similar to those of *Changchunsaurus* (Butler et al., 2011), and *Thescelosaurus* (Gilmore, 1915). Metatarsal 2 is similar in morphology to those of *Changchunsaurus* (Butler et al., 2011), *Haya* (Makovicky et al., 2011), *Jeholosaurus* (Han et al., 2012), and *Thescelosaurus* (Gilmore, 1915).

Metatarsal 1 measures 73 mm in proximodistal length and is concave throughout its length in anterior view, where the maximum bend occurs at its mid-section (Table 4.2). Metatarsal 1 is dorsoventrally taller than it is mediolaterally wide. The distal end is wider than its proximal end where the element gradually expands distally to form a bulbous, convex articular surface. The mid-shaft has an oval cross-section but gradually becomes D-shaped distally. The anterior distal end has a shallow depression. Two damaged condyles are present on the distal end of metatarsal 1 and have a convex lateral surface, and a flat medial surface where it would contact metatarsal 2.

Metatarsal 2 measures 112 mm in proximodistal length and is dorsoventrally straight, unlike in *Thescelosaurus* (Gilmore, 1915), but similar in *Jeholosaurus* (Han et al., 2012) and *Haya* (Makovicky et al., 2011) (Fig. 4.13 and Table 4.2, 4.3). The element is mediolaterally compressed with a cross-section at the proximal end being rectangular and gradually becomes "D" shaped towards the mid-shaft and to the distal end. The proximal articular surface is mediolaterally compressed with a flat medial surface that forms the articulation with metatarsal 3 and the lateral surface articulates with metatarsal 1 forming a dorsoventrally long shallow depression. The distal surface is expanded with a convex articular surface with two damaged condyles and ligament pits on the lateral and medial surfaces.

4.5.9. Pedal phalanges

Two three-dimensional pedal phalanges are preserved that are morphologically similar with one another but have slight variations in proportions and features (Fig. 4.14). Both phalanges are longer than wide, and wider than tall (Table 4.2). The overall shape of each is consistent with phalanges in thescelosaurids and other dinosaurs by possessing a constricted shaft, an expanded concave proximal articular surface, and the distal surface that has two condyles that are divided into lateral and medial ginglymi. Ligament pits are present on the lateral and medial sides of the distal condyles. In lateral view, the ventral margins are curved and the dorsal margin is concave. The proximal articular surface of UALVP 23111 is vertically keeled, and UALVP 59506 is not. This suggests that UALVP 23111 was weight-bearing and experienced lateral displacement where UALVP 59506 did not. This would suggest that UALVP 59506 is the most proximal of the phalanges, whereas the other is more distal.

4.6. Wapiti Thescelosaurid Osteohistology

The distal part of the shaft of the partial fibula UALVP 50999 was thin sectioned transversely (Fig. 4.15). The resulting cross-section is subcircular and measures 12.7 mm and 10.7 mm in anteroposterior and lateromedial diameter, respectively. The medullary cavity is also subcircular, with respective anteroposterior and lateromedial diameters of 2.4 mm and 2.3 mm (Table 4.4). The cortical bone is thickest on the lateral margin of the cross-section, and grows thinner anteriorly and medially, and thicker posteriorly. Along the posterior medial margins of the cross-section, the cortex is truncated internally by encroaching Haversian bone (Fig. 4.15). However, the cortical bone thins progressively medially to the Haversian bone. The densely remodeled Haversian bone is packed with secondary osteons that overlap previously deposited ones. The primary bone tissue consists of fibrolamellar, woven, and parallel-fibered bone, with longitudinal and lamellar vasculature, and primary and secondary osteons, present throughout (Fig. 4.15, 4.16). In plane-polarized (ppl) and cross-polarized (x-pol) light, the internal and external portions of the primary cortical bone are different colors, which suggests a shift in bone matrix texture. The inner primary cortical bone is lighter in color and thicker compared to the outer. The inner cortex is composed of parallel-fibered and woven bone, which transitions into the fibrolamellar and parallel-fibered bone of the outer cortex. The transition in bone matrix texture may have been linked to the onset of sexual maturity (Erickson et al., 2007, 2009; Lee and Werning, 2008). Vasculature is for the most part randomly distributed and oriented throughout the cortex, although a concentric band of longitudinal vasculature is associated with each line(s) of arrested growth (LAG). The secondary osteons are randomly distributed throughout the cortex, although they decrease periosteally. However, there is a higher density

distribution in secondary osteon on the posteromedial side where it is dominated by Haversian bone, and at the time of death must have been undergoing reworking that was cutting through LAGs, osteocyte lacunae, and vasculature. The Haversian bone abruptly stops before the periosteum. The osteocyte lacunae are aligned parallel to the periosteal margin of the bone, and to the longitudinal and lamellar vasculature. Seven LAGs are visible, and their spacing decreases towards the periosteum (Fig. 4.15, 4.16). An interval of rapid growth appears to have taken place following deposition of the fifth LAG, although growth abruptly slowed again with deposition of the last two LAGs. LAGs are not present near the medullary cavity, and it is unlikely that any previously existing LAGs in that area were obliterated, as there are no signs of extensive remodeling in the bone that forms the walls of the medullary cavity. Primary osteons are present between the LAGs that are close to the periosteum. Although the LAGs become more closely spaced periosteally, there is no external fundamental system (EFS) present around the periosteal surface. When present, the EFS (which is indicative of skeletal maturity) is typically avascular and composed of either parallel-fibered or lamellar bone (Woodward et al., 2011). The interior wall of the medullary cavity has been remodeled and is lined with endosteal lamellar bone. Bone architecture surrounding the medullary cavity differs between the anterolateral, anteromedial, and posteromedial sides. Fine cancellous bone is present on the anterolateral and anteromedial sides, and extensively remodeled coarse cancellous bone is present on the posteromedial side.

4.7. Results

4.7.1. Statistical Analyses

4.7.1.1. Femur Length/Femur Width

Based on 15 thescelosaurids, femoral length versus width (the mid-shaft anteroposterior diameter) bivariate analysis ($r = 0.99$; $p(a) < 0.01$) has a positive reduced major axis (RMA) regression line and can be described by the equation $y = 1.18x-1.33$ with small residuals around the trend line. Femoral linear measurements of Orodrominae (blue), Thescelosaurinae (red), and Asian neornithischians (purple) cluster along the trend line with orodromines in the middle, Asian taxa possessing smaller dimensions, and North American thescelosaurines being robust (Fig. 4.17A and Table 4.7).

Orodromines cluster close to the center of the regression with *Koreanosaurus*, *Orodromeus*, and indeterminate orodromines possessing medium sized femoral dimensions. However, *Oryctodromeus* has femoral dimensions similar to North American thescelosaurines (*Parksosaurus*) (Fig. 4.17A). Thescelosaurines have robust femoral dimensions with *Parksosaurus* being the smallest and Asian taxa having the smallest femoral dimensions in the plot (Fig. 4.17A). The Wapiti thescelosaurid (green) groups with the North American thescelosaurids; closely positioned between the thescelosaurine *Parksosaurus* and the orodromine *Oryctodromeus* (Fig. 4.17A). femoral width/femoral length ratios in orodromines are smaller than in thescelosaurines (Fig. 4.17B). The two small femoral width/femoral length values in *Jeholosaurus* are juvenile representatives and the linear pattern of *Jeholosaurus* in the RMA regression represents an ontogenetic sequence where the smaller individual is a juvenile (Fig.

4.17A, B). *Thescelosaurus assiniboiensis*, *Thescelosaurus neglectus*, and the CMN 8537 *Thescelosaurus* have large femoral width/femoral length values whereas *Parksosaurus* has the smallest femoral width/femoral length ratio relative to thescelosaurines (Fig. 4.17B). Asian taxa, excluding juvenile *Jeholosaurus* specimens, have comparable femoral width/femoral length values with those of thescelosaurines (Fig. 4.17B). The Wapiti thescelosaurid has a noticeably large femoral width/femoral length ratio that clusters with Thescelosaurinae and is more robust than *Thescelosaurus* (NCSM 15728) (Fig. 4.17B).

4.7.1.2. Lesser Trochanter Width/Femur Length

The log-transformed lesser trochanter width (maximum width of the lesser trochanter in lateral view) and femoral length bivariate analysis on 12 thescelosaurids has a positive RMA regression line ($r = 0.82$; $p(a) < 0.01$) and can be described by the equation $y = 1.62x-2.73$ with large residuals in Asian taxa and some residuals in orodromines (Fig. 4.17C and Table 4.7). Linear femoral measurements of Orodrominae (blue), Thescelosaurinae (red), and Asian neornithischian taxa (purple) plot along the trend line with orodromines roughly in the middle, Asian taxa possessing smaller dimensions, and North American thescelosaurines being robust (Fig. 4.17C).

Among Orodromines, *Koreanosaurus* and the indeterminate orodromines cluster in the center of the regression plot as a result of possessing moderate femoral lengths and moderate lesser trochanter dimensions. *Oryctodromeus* has femoral and lesser trochanter dimensions that are similar to North American thescelosaurines (*Parksosaurus*). However, *Orodromeus* plots distantly from other orodromines where it has femoral lengths similar to Asian taxa and smaller lesser trochanter widths (Fig. 4.17C). Thescelosaurines have large femoral lengths and lesser

trochanter widths compared to other thescelosaurids. Asian taxa occupy the smaller dimension plot space with larger lesser trochanter widths and smaller femoral lengths. The Wapiti thescelosaurid (green) groups with the North American thescelosaurids where it is closely positioned between the thescelosaurine *Parksosaurus* and the orodromine *Oryctodromeus* (Fig. 4.17C). The Wapiti thescelosaurid has a femoral length that is similar to that of *Oryctodromeus* but has a lesser trochanter width that is similar to that of *Thescelosaurus* (Fig. 4.17C). Lesser trochanter width/femoral length ratios in *Orodromeus* are smaller compared to other orodromines (*Koreanosaurus*, *Oryctodromeus*, and the indeterminate orodromines). *Koreanosaurus*, *Oryctodromeus*, and the indeterminate orodromine have values that are comparable with thescelosaurines and Asian taxa (Fig. 4.17D). The Wapiti thescelosaurid possesses a robust lesser trochanter width/femoral length ratio that plots closely but is larger than values of Thescelosaurinae and Asian taxa (Fig. 4.17D).

4.7.1.3. Intertrochanteric Notch Length/Femur Length

The bivariate analysis of log-transformed intertrochanteric notch lengths (the proximodistal length of the cleft in the lateral side of the femur that separates the lesser and greater trochanters) and femoral lengths of 11 thescelosaurids has a positive RMA regression line ($r = 0.88$; $p(a) < 0.01$) and can be described by the equation $y = 1.66x-2.39$ with large residuals in Asian taxa and *Parksosaurus* (Fig. 4.17E and Table 4.7). Linear femoral measurements of Orodrominae (blue), Thescelosaurinae (red), and Asian neornithischian taxa (purple) plot along the trend line. *Koreanosaurus* and the indeterminate orodromines plot roughly in the middle. Asian taxa possess smaller dimensions and *Orodromeus* plots closely with them. *Oryctodromeus* and the Wapiti thescelosaurid cluster together, and *Thescelosaurus* has the

largest femoral dimensions (Fig. 4.17E). Intertrochanteric notch length/femoral length ratios are scattered amongst Thescelosauridae in general (Fig. 4.17F). The largest values are present in *Thescelosaurus* and the Wapiti thescelosaurid but USNM 7757 has the largest value. *Orodromeus* has the smallest values amongst thescelosaurids.

4.7.2. Premaxillary Teeth Ternary Diagram

The ternary diagram of the proportions of 31 *in situ* log-transformed premaxillary teeth produced a distinct cluster for each taxon (Fig. 4.18 and Table 4.5; refer to this table for average measurements of premaxillary teeth). *Changchunsaurus* is characterized by high crown angle values and low crown height and crown base length values. *Haya*, *Jeholosaurus*, and *Orodromeus* have moderate crown base length and crown angle, and low crown height values. *Thescelosaurus* is characterized by relatively high crown height and crown base length values, and low crown angle values. The premaxillary teeth of *Zephyrosaurus* possess high crown height values and low crown base length and crown angle values. The Wapiti thescelosaurid premaxillary tooth shows a moderate crown height, relatively high crown base length, and low crown angle (Fig. 4.18). *Thescelosaurus*, *Zephyrosaurus*, and the Wapiti thescelosaurid cluster together in the ternary diagram, as do *Haya*, *Jeholosaurus*, *Orodromeus*, and to some extent *Changchunsaurus*.

4.7.3. Phylogenetic Results

4.7.3.1. Brown et al., 2013b

Addition of the Wapiti thescelosaurid to Brown et al.'s (2013b) data matrix resulted in two most parsimonious trees, with a tree length of 405 steps, a consistency index of 0.46, and a

retention index of 0.66. Bootstrap values (>50) and Bremer support (>1) are shown at the nodes and stems of the strict consensus tree (Fig. 4.19). The resulting topology diverges slightly from that obtained in the original analysis, and the inclusion of the Wapiti thescelosaurid has resulted in decreased phylogenetic resolution and lower levels of node support. This is likely due to the incompleteness of the specimen. However, clade support increased for Ankylopollexia, Dryomorpha, Iguanodontia, Neornithischia, but decreases in Ornithopoda. The Thescelosauridae and its major subclades (Orodrominae and Thescelosaurinae) were recovered in the analysis, but the pattern of thescelosaurid relationships exhibited minor differences from the results of previous studies. The clade Orodrominae consists of *Albertadromeus*, *Orodromeus*, *Oryctodromeus*, *Zephyrosaurus*, and an indeterminate orodromine (TMP 2008.45.02), whereas the clade Thescelosaurinae is comprised of *Changchunsaurus*, *Haya, Jeholosaurus*, *Parksosaurus*, and *Thescelosaurus*. Key differences between Brown et al.'s (2013b) results and the current analysis include the result that the addition of the Wapiti thescelosaurid recovered *Jeholosaurus* as sister to *Thescelosaurus*, and a polytomy was recovered between *Changchunsaurus*, *Haya*, and the clade comprising of *Jeholosaurus* and *Thescelosaurus*. The paper by Brown et al. (2013b) recovered a polytomy with *Changchunsaurus*, *Haya*, *Jeholosaurus*, and *Thescelosaurus*. The original analysis recovered three most parsimonious trees whereas in this analysis two most parsimonious trees were recovered. Retention index and consistency index values between the two analyses are approximately the same (Fig. 4.19 and Table 4.8). The Wapiti thescelosaurid was recovered in the Thescelosaurinae clade, sister to *Haya*, in all most parsimonious trees (Fig. 4.19), but no autapomorphies were recovered for it.

Thescelosauridae is supported in this analysis by the length of the articulation of the quadratojugal where the length of the quadrate is between 25% and 50% (character 3, convergent in *Rhabdodon*); the presence of a receipt for the anterolateral boss on the maxilla (character 29), the basioccipital tubera are level with the basisphenoid (character 74, convergent in *Camptosaurus*); and the greater trochanter is laterally flattened (character 109, convergent in *Gasparinisaura*).

Orodrominae is supported by a foramen magnum that is 20-30% of the occipital condyle width (character 71); the pubis is supported by a sacral centrum (character 84, convergent in *Rhabdodon*); the presence of a sharp and pronounced scapular spine (character 89); the acetabulum is vertically low and anteroposteriorly long (character 98, convergent in *Agilisaurus*); and the fibular shaft is D-shaped in cross-section (character 115).

Thescelosaurinae is supported in this analysis by the jugal wing ending above the distal condyles (character 9, reversed in the Wapiti thescelosaurid); the dentaries are straight in dorsal views (character 61, convergent in *Tenontosaurus*); the post-coronoid elements make up 25-35% of the total length of the lower jaw (character 62, convergent in *Hypsilophodon*); and the iliac peduncle of the ischium is larger or as large as the pubic peduncle (character 103, convergent in *Scutellosaurus*).

4.7.3.2. Boyd, 2015

Addition of the Wapiti thescelosaurid into the Boyd (2015) data matrix resulted in 72 most parsimonious trees, with a tree length of 401 steps, a consistency index of 0.36, and a retention index of 0.63 (Table 4.8). Bootstrap values (>50) and Bremer support (>1) are shown at

the nodes and stems of the strict consensus tree (Fig. 4.20). The resulting topology is identical to Boyd (2015), but the inclusion of the Wapiti thescelosaurid resulted in decreased phylogenetic resolution and lower levels of node support, likely due to the specimen's incompleteness. There are some instances where Bootstrap support increases for clades such as Ankylopollexia, and the clades comprised of the following pairings: *Dryosaurus* and *Dysalotosaurus*; *Scelidosaurus* and *Emausaurus*; *Tenontosaurus dossi* and *Tenontosaurus tilletti*; and *Zalmoxes robustus* and *Zalmoxes shqiperorum* (Fig. 4.20). Thescelosauridae (=Parksosauridae) and subclades within (Elasmaria, Orodrominae, and Thescelosaurinae) are recovered in this analysis. The clade Orodrominae consists of *Koreanosaurus*, *Orodromeus*, *Oryctodromeus*, *Zephyrosaurus*, and the Kaiparowits Orodromine. The clade Thescelosaurinae is comprised of *Changchunsaurus*, *Haya, Parksosaurus*, and *Thescelosaurus*. The South American clade, Elasmaria, was recovered and contains *Macrogryphosaurus*, *Notohypsilophodon*, and *Talenkauen*.

In all most parsimonious trees, the Wapiti thescelosaurid was recovered in the Thescelosaurinae where it forms a polytomy with Asian thescelosaurines (*Changchunsaurus* and *Haya*) (Fig. 4.20). The Wapiti thescelosaurid possesses an autapomorphy where the anteroposterior length of the quadratojugal contact on the quadrate makes up less than 50% of the total anteroposterior length of the quadrate (character 44, convergent in *Changchunsaurus*). A 50% majority rule consensus of the most parsimonious trees placed the Wapiti thescelosaurid in the same position as did the strict consensus.

Thescelosauridae is supported in this analysis by an everted oral margin on the lateral surface of the premaxillae (character 5, reversed in *Haya* and *Zephyrosaurus*, and convergent in *Agilisaurus*); the presence of a receipt for the anterolateral boss on the maxilla (character 14); a

braincase angle less than 35 degrees between the base and the long axis (character 98, convergent in *Hypsilophodon*); the pubis is supported by at least one sacral centrum (character 193); there is a flattened lateral surface of the greater trochanter (character 213); the distal tarsal is square (character 242, reversed in the Kaiparowits Orodrominae); and the premaxillae is unfused (character 255, reversed in *Haya*).

Similar to Boyd (2015), Elasmaria is recovered as an inclusive clade within Thescelosauridae and is supported by an epipophysis on the third cervical vertebra (character 145); a reduction of the deltopectoral crest on the humerus (character 168); a mediolaterally flattened prepubic process (character 197); and an ovoid to a subcylindrical ischial shaft (character 205, convergent in *Zephyrosaurus*).

The clade Orodrominae is supported in the analysis by possessing basioccipital tubera that are level with the basisphenoid (character 108, convergent in *Othnielosaurus*); there are denticles on the dentary teeth but they lack supporting ridges (character 114, convergent in *Changchunsaurus* and *Wannanosaurus*); each cervical vertebra has a sharp ventral keel (character 143, convergent in the Wapiti thescelosaurid); the sacrum is composed of seven or more fused vertebral centra (character 148); there is a pronounced and sharp scapular spine (character 158); and the shaft of the fibula is D-shaped in cross-section throughout its length (character 233).

Thescelosaurinae is supported by possessing two or more supraorbitals (character 23, convergent in *Agilisaurus* and *Wannanosaurus*); the supraorbital extends along at least 71% of the maximum anteroposterior length of the orbit (character 25, convergent in *Agilisaurus*); a quadrate notch is present between the jugal wing of the quadrate and the quadratojugal (character

51); a dorsally directed, finger-like process is present on the surangular (character 86); and the angle between the femoral neck of the femoral head and the femoral shaft is less than or equal to 100 degrees (character 210).

4.7.3.3. Madzia et al., 2018

Addition of the Wapiti thescelosaurid into the Madzia et al. (2018) character matrix resulted in 2400 most parsimonious trees, with a tree length of 934 steps, a consistency index of 0.31, and a retention index of 0.62. Bootstrap values (>50) and Bremer support (>1) are shown at the nodes and stems of the strict consensus tree (Fig. 4.21 and Table 4.8). The resulting topology does not change the topology found by Madzia et al. (2018), but Bootstrap and Bremer support for clades were not reported in the original analysis and cannot be compared with the results of this study. Overall, Bootstrap and Bremer support in this analysis is weak but has strong clade support for Dinosauria, Ornithischia, and Ankylopollexia (Fig. 4.21). Thescelosauridae, Orodrominae and Thescelosaurinae are recovered but the latter two are in a polytomy with one another and three other taxa. Thescelosaurinae is made up of *Notohypsilophodon*, *Parksosaurus*, and *Thescelosaurus* and Orodrominae consists of *Albertadromeus*, *Koreanosaurus*, *Orodromeus*, *Oryctodromeus*, *Zephyrosaurus*, and the Kaiparowits orodromine (Fig. 4.21). Asian representatives (*Changchunsaurus* and *Haya*) are in a polytomy with Thescelosaurinae and Orodrominae. Weak Bootstrap and Bremer support for the Wapiti thescelosaurid was recovered and the analysis placed it in a polytomy with *Changchunsaurus*, *Haya*, Orodrominae, and Thescelosaurinae (Fig. 4.21). A 50% majority rule consensus of the most parsimonious trees placed the Wapiti thescelosaurid, *Changchunsaurus*, and *Haya* into Orodrominae 58% percent of the time. The *Notohypsilophodon*, *Parksosaurus*, and *Thescelosaurus* polytomy was in the same

position as the strict consensus and the North American orodromines formed a clade at 100%. The Wapiti thescelosaurid possesses two autapomorphies (the distal condyles of the quadrate are horizontal (character 52, convergent with Clypeodonta) and the minimum diameter of the femur is greater than 15% of the total femur length (character 208, convergent with Dryosauridae and Iguanodontia)).

Thescelosauridae is supported in this analysis by the presence of an anterolateral boss of the maxilla (character 14); the presence of a quadrate notch (character 51, convergent in *Muttaburrasaurus*); there is an anteriorly directed process into orbit along the orbital edge of the postorbital (character 59, reversed in *Changchunsaurus*); the frontals are dorsally flat (character 65, reversed in *Orodromeus*); four to five teeth are present in each premaxilla (character 112, convergent in *Agilisaurus*); the angle between the neck of the femoral head and the femoral shaft is less than or equal to 100 degrees (character 210, reversed in *Notohypsilophodon* and *Zephyrosaurus*); the lateral surface of the greater trochanter of the femur is flat (character 213, convergent in *Eousdryosaurus* and *Gasparinisaura*); the lateral distal tarsal is square (character 242); and the premaxillae are fused (character 255, reversed in *Orodromeus*).

Orodrominae consists of *Albertadromeus*, *Koreanosaurus*, *Orodromeus*, *Oryctodromeus*, *Zephyrosaurus*, and the Kaiparowits Orodromine. It is supported in the analysis by lack of a foramen between the jugal wing of the quadrate and the quadratojugal (character 51); the foramen magnum extends between 20% and 30% of the dorsal margin of the occipital condyle (character 108, convergent in *Othnielosaurus*); simple denticles are present on the dentary teeth but supporting ridges are absent (character 114, convergent in *Changchunsaurus* and *Wannanosaurus*); sharp keels are present on the ventral surfaces of the cervical vertebrae

(character 143, convergent in *Valdosaurus*); the scapular spine is sharp and pronounced (character 158); and the fibular shaft is D-shaped in transverse section throughout its length (character 233).

Thescelosaurinae is supported by a groove on the base of the posterior side of the pterygoid wing of the quadrate (character 55, convergent in *Dysalotosaurus*); the frontal participates in less than 25% of the orbital margin (character 63, convergent in *Muttaburrasaurus* and *Wannanosaurus*); the supraoccipital contributes less than 5% of the margin of the foramen magnum (character 102); the post-temporal foramen is positioned at the boundary between the parietal and the paraoccipital process (character 103); post-temporal foramen is associated with a dorsally open groove (character 104); the length of the basisphenoid is less than the length of the basioccipital (character 109); each anterior cervical centrum is at least 1.5 times longer than tall (character 144, convergent in the Kaiparowits orodromine); there is partial ossification of the sternal segments of the anterior dorsal ribs (character 157); the obturator process is within the distal 60% of the ischium (character 204, convergent in *Hypsilophodon* and *Jeholosaurus*); the femoral shaft is distinctly bowed in anterior view (character 209, convergent *Dryosaurus*, *Dysalotosaurus*, and *Eousdryosaurus*); the fourth trochanter is at or below midshaft of the femur (character 221); presence of the anterior intercondylar groove on the distal end of the femur (character 222, convergent *Orodromeus* and *Oryctodromeus*); there is one lateral proximal condyle on the tibia (character, 228); and the epaxial tendons are longitudinally arranged into a single layer (character 252).

4.8. Discussion

All of the orodromine specimens are indistinguishable from previously named orodromine material from the Dinosaur Park Formation and other time equivalent formations (Fig. 4.4-5). Although fragmentary and unassociated, the material of the DC Bonebed can be diagnosed as belonging to an indeterminate thescelosaurine (Fig. 4.6-14 and 4.22), based on the close morphological resemblance of the premaxillary crown, quadrate, cervical vertebrae, femur, and fibula to equivalent characters in *Changchunsaurus*, *Haya*, *Parksosaurus*, and *Thescelosaurus*. The femur of the Wapiti thescelosaurid has unique features compared with other thescelosaurids including a high femoral width/femoral length value, a large lesser trochanter, and a deep intertrochanteric notch (Fig. 4.17). It is likely that the Wapiti thescelosaurid represents a new thescelosaurid from the Wapiti Formation based on the aforementioned characters, but the unassociated and incomplete nature of the sample is not enough to support a new taxon. The osteohistological and growth rate comparisons of the Wapiti thescelosaurid are similar with *Oryctodromeus* (Fig. 4.15-16). Three separate character matrices were analyzed with the Wapiti thescelosaurid added in as an operational taxonomic unit and in each case the specimen was recovered in association with Asian thescelosaurids (*Changchunsaurus* and *Haya*) (Fig. 4.19-21).

4.8.1. Further Dinosaur Park Orodrominae Comparisons

All specimens are from different geographic locations within the Dinosaur Park Formation possess morphological features that are indistinguishable from previously named orodromine material from the Dinosaur Park Formation and other time equivalent formations. Without any diagnostic characters, the isolated material can be referred to as indeterminate

orodromines. This further reinforces the idea that Orodrominae is the only occurrence of a small-bodied non-cerapodan neornithischian from the Dinosaur Park Formation (Brown et al., 2013b; Hudgins et al., 2020a).

A phylogenetic analysis was not performed on Dinosaur Park Formation material due to the paucity of character data. Based on size and the relatively few characters that can be assessed, the elements can be referred to Orodrominae, but remain indeterminate within that clade. The basioccipital is similar in its morphology and contacts with neighboring bones to those of previously described orodromines (especially *Zephyrosaurus*). Specific resemblances include the morphology of the occipital condyle, and how much this structure contributes to the ventral margin of the foramen magnum; the positions of contacts between the exoccipitals, basioccipital and basisphenoid; the morphology of the contact of the basioccipital with the basisphenoid; and the presence of a large, posteriorly directed tubercle in posterior view (Fig. 4.4). The caudal vertebra and the phalanx are similar in size, proportions and overall morphology to those of previously described orodromines. Femoral similarities between UALVP 44812 and 53744 and previously described orodromines include the presence of a proximodistally flat greater trochanter, size proportions differences between the distal condyles, and the proximal position of the fourth trochanter (Fig. 4.5). The femur UALVP 44812 also displays one orodromine synapomorphy: the angle between the femoral head and shaft is less than or equal to 100º (Boyd, 2015).

4.8.2. Further Wapiti Thescelosaurid Comparisons

All specimens from the DC Bonebed (unit 3 of the Wapiti Formation) are unassociated bones or teeth. The Wapiti thescelosaurid possesses many morphological features shared with

other thescelosaurines (*Changchunsaurus*, *Haya*, and *Thescelosaurus*). The Wapiti thescelosaurid possess apicobasal extending ridges on the premaxillary crown, a feature present in only *Thescelosaurus* (Boyd, 2014; Brown and Druckenmiller, 2011). There are no apicobasal ridges on premaxillary teeth of *Changchunsaurus*, *Haya*, *Jeholosaurus*, *Orodromeus*, and *Zephyrosaurus* (Barrett and Han, 2009; Jin et al., 2011; Makovicky et al., 2011; Scheetz, 1999; Sues, 1980). They may be present in *Parksosaurus*, but this needs confirmation from unidentified, isolated material in the Prince Creek Formation (Boyd, 2014; Brown and Druckenmiller, 2011). The nature of the possible wear facet is difficult to determine in UALVP 59863 as the isolated premaxillary crown is extremely worn and possibly underwent either a significant amount of abrasion during the fossilization process, was broken off and ingested during mastication, or a combination of the two. In the ternary diagram, the isolated premaxillary tooth of the Wapiti thescelosaurid plots close to *Thescelosaurus* and *Zephyrosaurus* (Fig. 4.18), corroborating the similarity to *Thescelosaurus* in crown ornamentation. The proximity in the plot of the Wapiti thescelosaurid to *Zephyrosaurus* partly reflects the lack of size correction in the analysis. In addition, Zephyrosaurus lacks common qualitative features with the Wapiti thescelosaurid crown because its teeth are peg-like and lack apicobasal ridges. The position of the parapophysis on the cervical centrum and the broad ventral keel are similar to thescelosaurines and Asian representatives, and the latter is distinct from the orodromine synapomorphy of a sharp ventral keel (Boyd, 2015; Gilmore, 1915; Madzia et al., 2018; Krumenacker, 2017; Scheetz, 1999). The quadrate is smaller than those of at least some thescelosaurines (*Changchunsaurus* and *Thescelosaurus*) but is larger than orodromine quadrates, and is morphologically distinct from *Oryctodromeus*, *Orodromeus*, and

Zephyrosaurus (Boyd, 2014; Jin et al., 2010; Krumenacker, 2017; Scheetz, 1999) (Fig. 4.7). The quadrate has a posterior deflection on the shaft, a quadrate foramen, a jugal wing in close proximity with the ventral condyles, and a pronounced ridge on the lateral wing of the anterior margin that extends dorsoventrally. These characters are similar in *Changchunsaurus*, *Haya*, and *Thescelosaurus*, and are distinct from those in orodromines (*Oryctodromeus*) (Boyd, 2014; Jin et al., 2010; Krumenacker, 2017; Makovicky et al., 2011; Scheetz, 1999; Sues, 1980). The Wapiti thescelosaurid femur (UALVP 1849) has features typical of thescelosaurid femora, including a proximally positioned pendant fourth trochanter, posteriorly directed femoral shaft in lateral view, and an intertrochanteric notch between the greater and lesser trochanters. The position of the lesser trochanter relative to the greater trochanter (Fig. 4.9) is also similar to thescelosaurids femora. UALVP 1849 has a large femoral width over length ratio, a robust lesser trochanter, and a long, deep intertrochanteric notch compared to other thescelosaurids. The Wapiti thescelosaurid fibula (UALVP 59855) has a similar morphology to those of other thescelosaurid fibulae in terms of shape and dimensions (Fig. 4.11, 4.12). UALVP 59855 is about the same size as a *Thescelosaurus* fibula, is morphologically similar to North American thescelosaurines, and is larger than Asian representatives (*Changchunsaurus* and *Haya*) (Butler et al., 2011; Gilmore, 1915; Han et al., 2012; Makovicky et al., 2011; Parks, 1926). However, skeletal proportions vary within *Thescelosaurus* because of ontogenetic and individual variation (Brown, 2009; Verdu et al., 2012). The fibula is morphologically similar to those of *Parksosaurus* and *Thescelosaurus*.

4.8.3. Musculature and Locomotion

As indicated by the reduced major axis (RMA) regression results, UALVP 1849 is exceptionally robust for a thescelosaurid femur. This likely correlates with an increase in muscle

attachment sites as suggested by the large lesser trochanter, the deep intertrochanteric notch, and the well-defined muscle scar medial to the fourth trochanter (Fig. 4.9, 4.10 and Table 4.3). The lesser trochanters in other thescelosaurids are proportionally smaller when corrected for size (Brown et al., 2013b; Gilmore, 1915; Han et al., 2012; Krumenacker, 2017; Jin et al., 2010; Scheetz, 1999) (Fig. 4.17C, D and Table 4.3). Muscle association with the lesser trochanters in basal and derived ornithischians have been inferred to be for the insertion of the iliofemoralis (Maidment and Barrett, 2011b; Maidment et al., 2014). Reconstructions suggest the iliofemoralis originates on the iliac blade, and it has been interpreted as a major flexion and abduction muscle for the femur in basal ornithischians and *Edmontosaurus* (Maidment and Barrett, 2011b; Maidment et al., 2014). The robust lesser trochanter in UALVP 1849 suggests larger flexion and abduction muscles for the femur compared to other thescelosaurids. The intertrochanteric notch probably allows for deeper muscle insertions for the puboischiofemoralis externus, the ischiotrochantericus, and the iliofemoralis. The puboischiofemoralis likely originated on the lateral surface of the ischial blade and inserted onto the greater trochanter. The ischiotrochantericus is reconstructed as originating on the medial surface of the ischial blade and inserting onto either the greater or lesser trochanters (Maidment and Barrett, 2011b). The puboischiofemoralis and ischiotrochantericus are major adductor muscles for the femur (Maidment et al., 2014). The large muscle attachment sites and the deep intertrochanteric notch present in UALVP 1849 suggests larger insertion sites for adduction compared with other thescelosaurids. The well-defined muscle scar medial to the fourth trochanter in UALVP 1849 is present. This muscle scar is interpreted as being the insertion point for the caudofemoralis longus and the puboischiofemoralis internus, which are major femoral flexion and extension muscles

(Maidment and Barrett, 2011b; Maidment et al., 2014). The robust features in UAVLP 1849 with its relatively small size suggests that this animal had powerful hindlimb extension and flexion compared to other larger thescelosaurids. This suggests that this animal could produce quick and sustained bursts of speed. The robust features of UALVP 1849 could potentially indicate the presence of a new thescelosaurid in the Wapiti Formation, but the incompleteness and lack of diagnostic features in the unassociated material does not provide enough support to establish a new thescelosaurid taxon.

Assuming that the bones represent an animal of comparable size and growth stage, and that the Wapiti thescelosaurid material is from a single individual, and that the length of the fibula is a good estimate for the length of tibia, the fibula is much longer proximodistally than the femur. This suggests that the unnamed taxon was likely highly cursorial (Table 4.3). Although it is difficult to define cursoriality, hindlimb proportions are a reliable predictor of locomotion style (cursorial and graviportal) among living mammals (Garland and Janis, 1993) and extinct archosaurs (Carrano, 1999; Kubo and Kubo, 2012). Despite the underlying assumptions, the proportions between the femur and the fibula in the Wapiti thescelosaurid are on par with those of *Jeholosaurus*, *Koreanosaurus*, and *Parksosaurus*, whereas in *Thescelosaurus* the femur is longer than the fibula. This contrast in hindlimb proportions between *Thescelosaurus* and other thescelosaurids was identified by Galton (1974), who suggested that *Thescelosaurus* should be placed within Iguanodontia (e.g., *Camptosaurus* and *Iguanodon*). However, a single ratio-based character is inadequate as a basis for placing *Thescelosaurus* in Iguanodontia, and is contradicted by a large amount of other evidence (Boyd et al., 2009; Boyd, 2015; Brown et al., 2013b; Madzia et al., 2018; Simoes et al., 2016).

Orodromines maintain relatively high cursorial adaptations despite the fossorial ecological interpretation, although *Koreanosaurus* is an exception (Fearon and Varricchio, 2015 and 2016; Krumenacker et al., 2019; Varricchio et al., 2011). The dichotomy between the hindlimb proportions in *Thescelosaurus* and those of other thescelosaurids suggest a shift from cursorial locomotion in earlier taxa (e.g., *Haya*, *Orodromeus*, *Oryctodromeus*, and *Parksosaurus*) to more graviportal locomotion, similar to that inferred for Iguanodontia, in *Thescelosaurus* (Galton, 1974b).

4.8.4. Osteohistology

There has been an extensive amount of research on long bone osteohistology in many ornithopods (*Dryosaurus*, *Dysalotosaurus*, *Edmontosaurus*, *Hypacrosaurus*, *Maiasaura*, *Mochlodon*, *Rhabdodon*, and *Tenontosaurus*). Adults are characterized by complex vascularization in the cortical bone, extensive remodeling, and a steady decrease in growth after rapid growth earlier in life (Horner et al., 2009; Chinsamy, 1995; Reid, 1985; Cooper et al., 2008; Horner et al., 1999, 2000, 2009; Ősi et al., 2012; Reid, 1985; Werning, 2012). However, long bone osteohistological descriptions of Late Cretaceous basal neornithischians are relatively uncommon. Only a few studies have been carried out, including *Haya* (Barta and Norell, 2021); *Hypsilophodon* (Chinsamy et al., 1998), *Jeholosaurus* (Han et al., 2020), *Orodromeus* (Horner et al., 2009; Scheetz, 1999), and *Oryctodromeus* (Krumenacker, 2017).

The osteohistology of a fibula (UALVP 50999) demonstrates that seven lines of arrested growth (LAG) were deposited. LAGs are thin, semi-translucent to opaque bands of bone tissue that forms concentric rings around the circumference of the cortical bone (Padian and Lamm, 2013) and the number of LAGs has been correlated with the age of the individual (de Buffrenil

and Castanet, 2000; Hutton, 1986; Snover and Hohn, 2004). Whether the formation of LAGs is due to metabolic processes (Castanet, 1994) or environmental cues (Castanet et al., 2004) is still debated within the literature, but both have convincing arguments and experiments (Kohler et al., 2012; Marangoni et al., 2009). This suggests that UALVP 50999 was at least 7 years old at the time of death. The individual had likely reached sexual maturity based on prior growth models of reptiles and dinosaurs, although this is difficult to determine with certainty (Erickson et al., 2007, 2009; Lee and Werning, 2007; Padian et al., 2001). The onset of sexual maturity coincides with bone texture changes from the inner to outer cortex, growth deceleration reflected in narrowing inter-LAG spaces towards the periosteum, and the presence of extensive secondary remodeling (Fig. 4.15, 4.16). Given this, the individual represented by UALVP 50999 had not reached skeletal maturity at the time of death, based on vasculature near the periosteum and the absence of an EFS (diagnostic for skeletal maturity) (Woodward et al., 2011). This inference is consistent with prior research indicating that dinosaurs reached sexual maturity before skeletal maturity (Erickson et al., 2007, 2009; Lee and Werning, 2008). However, the decreasing LAG spacing is likely an unreliable indicator of skeletal maturity (Woodward et al., 2020) and some authors have urged caution in using it to infer maturity (Cullen et al., 2014). Furthermore, the presence of medullary bone can suggest that an individual has reached sexual maturity as this bone type is consistent in sexually mature extant Aves (Lee and Werning, 2008). Nevertheless, previous work has questioned whether this bone tissue is correctly identified within Dinosauria (Chinsamy et al., 2016). There is no medullary bone present in UALVP 50999, however, so using this approach is irrelevant. The interpretations of sexual maturity in Dinosauria based on osteohistological features should be made with caution as small sample sizes integrated with

intraspecific variation and contentious interpretations may be misleading (Gee et al., 2020; Griffin et al., 2021). Thus, osteohistological comparisons between taxa using different anatomical elements should be made with caution as direct comparisons can be misleading (Cullen et al., 2014).

Growth in UALVP 50999 was rapid early on and then continued at a slower rate later in life, based on LAG spacing. Rapid growth early in life followed by a declined asymptotic growth is common in dinosaurs (Padian et al., 2001). As the animal grew, the increased secondary remodeling and Haversian bone on the posteromedial side is likely due to biomechanical stresses from locomotor behaviors throughout the animal's life (Kuehn et al., 2019). UAVLP 50999 has similar growth features and bone textures when compared with *Haya*, *Jeholosaurus*, *Orodromeus*, and *Oryctodromeus*, but is unlike derived ornithopods. UALVP 50999 has a higher LAG count (seven) compared to *Haya* (six), *Jeholosaurus* (four), *Orodromeus* (two), and *Oryctodromeus* (six to seven). Similar to *Oryctodromeus*, the onset of sexually and skeletal maturity occurred later in UALVP 50999 compared to other thescelosaurids and *Jeholosaurus*. The histology of the partial fibula suggests that the growth rate of the Wapiti thescelosaurid was similar to those of *Haya*, *Jeholosaurus*, and *Oryctodromeus*, faster than that of *Orodromeus*, and slower than those of *Hypsilophodon* and derived ornithischians (Barta and Norell, 2021; Chinsamy et al., 1998; Han et al., 2020; Horner et al., 2009; Krumenacker, 2017; Reid, 1985; Werning, 2012).

In the Wapiti thescelosaurid, an interval of rapid growth appears to have taken place following the deposition of the fifth LAG, although growth abruptly slowed again with the deposition of the last two. This LAG spacing variability appears to be consistent in some

specimens of *Haya* and *Jeholosaurus* where 'moderate' growth occurring in early life, followed by a period of rapid growth, and then slow growth later in life (Barta and Norell, 2021; Han et al., 2020) (Fig. 4.15, 4.16). Furthermore, skeletal immaturity at the time of death appears to be a common trend in sampled thescelosaurids (perhaps in basal neornithischians in general) and may represent a growth strategy (see subsequent discussion), a taphonomic bias, or a random signal (Brown et al., 2013a; Erickson et al., 2009; Woodward et al., 2015). It is unclear what the mechanism was for this pattern.

The variable LAG spacing is unusual in dinosaurs but is present in at least some other basal neornithischians (Barta and Norell, 2021; Han et al., 2020), ornithopods (Cullen et al., 2014), and theropods (Cullen et al., 2014; Woodward et al., 2020; Zanno et al., 2019). Here, I propose for this observed growth pattern several explanations, including changing environmental conditions, reproduction strategy, sexual dimorphism, parental care, bone pathology, niche partitioning between juveniles and adults, or random variation.

The closely packed LAGs might indicate harsh environmental conditions. The relatively high growth rate towards the end of the individual's life and after the fifth LAG may indicate a year with more stable environmental conditions and more abundant, accessible resources (Kohler et al., 2012).

Another explanation for this growth pattern observed in the Wapiti thescelosaurid, *Haya*, and *Jeholosaurus* may relate to a reproduction strategy, such as an r-strategist (Paul, 1994). R-strategists are characterized by reaching sexual maturity early in life; having a short lifespan; having high mortality rates; and having population sizes that are below carrying capacity (Vladstein et al., 1993). It is difficult to determine population size in the aforementioned taxa due

to low sample sizes. However, the other r-strategy characteristics seem to be consistent with the observed histological features. Depending on the taxa, thescelosaurids seem to have a short lifespan where they reach sexual maturity early in life. This seems to corroborate with the observation that nearly all thescelosaurids never reach skeletal maturity.

Sexual dimorphism is extremely difficult to demonstrate in dinosaurs (Hone and Mallon, 2017; Mallon, 2017) and potentially medullary tissue identification is the only method for distinguishing dinosaur sexes (Lee and Werning, 2008). However, medullary tissue identification is contentious in Dinosauria (Chinsamy, 2016). Sexual size dimorphism can be identified in growth trajectories and has been observed in some extant reptiles and avians (Andrews, 1982; Hone and Mallon, 2017). The histological patterns observed in the Wapiti thescelosaurid, *Haya*, and *Jeholosaurus* may represent a sexual dimorphic signal in thescelosaurids. However, until a larger in-group sample size exists, it is futile to determine sexual dimorphism in this clade based on the osteohistological observations and patterns.

Parental care may explain the observed growth pattern after reaching sexual maturity in the Wapiti thescelosaurid, *Haya*, and *Jeholosaurus*. Parental care can consume a large amount of energy and could potentially narrow the spacing between subsequent LAGs and reduce growth rates (Gittleman and Thompson, 1988; Zhao et al., 2014). Parental care has been considered in ornithischians (e.g., *Maiasaura*, *Oryctodromeus*, and *Psittacosaurus*) and could explain the observed pattern in thescelosaurids (Horner and Makela, 1979; Meng et al., 2004; Varricchio et al., 2007). Although, it is poorly known how parental care affects bone tissue across multiple tetrapod clades (Zhao et al., 2014).

External osteological pathologies have been examined in fractured long bones of *Psittacosaurus* (Hedrick et al., 2016) and the observed LAG spacing could be pathological in origin. However, the examination of these specimens shows that there are no external or internal pathologies that are similar to other described pathological bone tissues (Griffin, 2018).

Niche partitioning between juveniles and adults of the Wapiti thescelosaurid, *Haya*, and *Jeholosaurus* may explain this growth pattern (Barta and Norell, 2021; Han et al., 2020). Variable LAG spacing has been reported in ornithopods (Cullen et al., 2014), ornithomimids (Cullen et al., 2014), and tyrannosaurids (Woodward et al., 2020; Zanno et al., 2019). In *Tyrannosaurus rex*, the variable LAG spacing has been associated with niche partitioning between large adults and smaller juveniles where juveniles eat different foods from the adults (Woodward et al., 2020). This has been observed in extant reptiles (e.g., *Alligator mississipiensis* and *Varanus komodoensis*) where different food sources and foraging strategies are exploited throughout ontogeny (Dodson, 1975; Purwandana et al., 2016). However, this pattern could also be explained by fluctuating resource abundances in their ecosystems. Nevertheless, it is likely, but untested, that the variable LAG spacing in thescelosaurids is related to niche partitioning between younger and older individuals.

Intraspecific variation in growth that is unrelated to skeletal maturity and environmental constraints could explain the LAG spacing variability. Intraspecific developmental variation does affect growth rates in extant reptiles (Lagarde et al., 2001). Unfortunately, there is no evidence that suggests that individual developmental variation can generate the closely packed LAGs in thescelosaurids (Han et al., 2020).

4.8.5. Phylogenetics

The Wapiti thescelosaurid was recovered in Thescelosaurinae, sister to *Haya* using Brown et al.'s (2013b) matrix; in a polytomy with *Changchunsaurus* and *Haya* within Thescelosaurinae using Boyd's (2015) matrix; and in a polytomy with *Changchunsaurus* and *Haya* within Thescelosauridae using Madzia et al.'s (2018) matrix (Fig. 4.19-21). Using the matrix of Brown et al. (2013b) did not recover autapomorphies for the Wapiti thescelosaurids. However, autapomorphies were recovered using the matrices of Boyd (2015) and Madzia et al. (2018). Asian thescelosaurids (*Changchunsaurus* and *Haya*) are either placed in Orodrominae or Thescelosaurinae based on previous analyses, which does not improve the phylogenetic resolution of the Wapiti thescelosaurid because it has a close phylogenetic relationship to them (Brown et al., 2013b; Boyd, 2015; Madzia et al., 2018) (Fig. 4.19-21). However, this close relationship may be an artefact in any case. Recovering the Wapiti thescelosaurid as a basal member of Thescelosauridae, and the contrasting phylogenetic placement of it between Thescelosaurinae or Orodrominae, is likely an artefact due to the fragmentary nature of the specimen. It is also possible that the assumption is incorrect that all thescelosaurid fossils from the DC quarry represent a single individual. It might well be that they represent multiple individuals of the same taxon at different stages of growth, or even multiple individuals of different taxa. It is essential to recover more diagnosable thescelosaurid material from the Wapiti Formation. Despite these uncertainties, at least a few synapomorphies may be present that could tie the Wapiti thescelosaurid to Late Cretaceous derived thescelosaurids. Even so, the Wapiti Formation has no time-equivalent formation in North America that preserves thescelosaurid material to compare with the Wapiti thescelosaurid. The consistent basal position of the Wapiti

thescelosaurid is unusual as its morphology is similar to Late Cretaceous derived thescelosaurids (*Parksosaurus* and *Thescelosaurus*) and Asian thescelosaurids (*Changchunsaurus* and *Haya*). Given this, the unassociated and fragmentary nature of the material, and the assumptions made when performing the phylogenetic analyses, the fossils should not be diagnosed as a new species. If the material were designated as a new taxon, either the quadrate or the femur would be the holotype. The evolutionary relationships of basal neornithischians will become better resolved with the discovery of more specimens, and with new research. The systematic placement of the Wapiti thescelosaurid, as well as the placement of *Changchunsaurus* and *Haya* may change when this happens.

4.8.6. Pattern of Thescelosauridae Diversity and Evolution in North America

In terms of specimen count and taxa diversity, southern Alberta is rich in dinosaur fossil localities that are dominated by large-bodied ornithischians, particularly hadrosaurids and ceratopsids. Small-bodied thescelosaurids, by contrast, are rarely recovered. Despite the paucity of the thescelosaurid fossil record in southern Alberta, however, this taxon exhibits a clearly partitioned stratigraphic distribution in the Campanian and Maastrichtian of southern Alberta; orodromines typically occur in the Belly River Group and thescelosaurines in the younger Edmonton Group (Brown et al., 2013b; Hudgins et al., 2020a) (Fig. 4.2). These two stratigraphic groups are separated by deposits of the Bearpaw Formation that was laid down by the transgression of the Western Interior Seaway during the Campanian. The orodromine affinities of the specimens from the Dinosaur Park Formation described in this paper further reinforce the interpretation that a stratigraphic separation between the thescelosaurid subclades occurred in Alberta; orodromines are the only small-bodied non-cerapodan neornithischians from the

Dinosaur Park Formation (Brown et al., 2013b; Hudgins et al., 2020a). However, the stratigraphic position of the Wapiti thescelosaurid shows that thescelosaurines were present in North America by the time of the Bearpaw/Horseshoe Canyon Formation transition. Higher resolution of the thescelosaurid fossil record is needed to elucidate the mechanism and timing of the stratigraphic separation of the thescelosaurid subclades, and the disappearance of orodromines. Given this, it is not certain what the stratigraphic separation mechanism was and if the disappearance of orodromines occurred during, prior to, or after the deposition of the Bearpaw Formation in Alberta.

As the most northerly known thescelosaurid body fossil occurrence in Canada, and the geologically oldest occurrence of Thescelosaurinae in North America (~73.5 Ma), the Wapiti thescelosaurid extends the known range of thescelosaurines spatially into northern Alberta. It also stratigraphically extends thescelosaurines into beds approximately equivalent to the Bearpaw Formation (Fanti and Catuneanu, 2010) (Fig. 4.2, 4.22). The oldest previously known North American Thescelosaurinae was *Parksosaurus* from the Tolman member of the Horseshoe Canyon Formation (Eberth et al., 2013; Parks, 1926), whereas *Albertadromeus* from the Oldman Formation is the youngest named North American orodromine. Specimens from the Dinosaur Park Formation include the youngest, albeit indeterminate, evidence of orodromines in North America (Brown et al., 2013b). The Wapiti thescelosaurid may represent the product of a migration from Asia based on its close relationship between *Changchunsaurus* and *Haya* (Fig. 4.19-21). However, its phylogenetic placement may also be an artefact due to its fragmentary nature.

In principle, possible reasons for the stratigraphic separation between orodromines and thescelosaurines in North America may be related to any combination of changing climatic conditions, changing habitat preferences, taphonomic biases, migrations into and out of changing paleoenvironments, or anagenetic evolution (Behrensmeyer et al., 1979; Brown et al., 2013a, b; Eberth and Braman, 2012; Eberth and Hamblin, 1993; Eberth et al., 2013; Mallon et al., 2012; Woodward et al., 2005). Eberth et al. (2013) argued that the changing biozonation of dinosaur fossil assemblages in the Horseshoe Canyon Formation was due to migratory events into or out of the area. The lithographic variation of the Horseshoe Canyon Formation stratigraphic members was influenced by climate change and the boundaries between dinosaur assemblage zones coincide with the climate related paleoenvironmental changes. Eberth et al. (2013) proposed that Campanian climate change was likely the primary cause of the faunal turnovers observed between successive Horseshoe Canyon Formation stratigraphic members. This conclusion was based on the observation that assemblage zone dinosaur taxa have long stratigraphic ranges when their occurrences are considered in other formations. Dinosaur taxa appear to express habitat preference as they occur in earlier or later formations that are characterized by similar environments (Eberth et al., 2013).

Mallon et al. (2012) identified two megaherbivore assemblage zones (MAZ) in the orodromine dominated Dinosaur Park Formation and originally hypothesized that this faunal turnover was the result of climatic events. However, the MAZs could not be explained by the turnover pulse hypothesis but rather by a simple time gradient. Uncertain of the mechanism that caused changes to the MAZs, Mallon et al. (2012) suggested two possible mechanisms that require further testing: migratory and anagenetic events. Older MAZ taxa have been considered

transitional or intermediate to younger MAZ taxa given the apparent stratigraphic separation between them (*Chasmosaurus russelli* and *Chasmosaurus belli*). The centrosaurine *Spinops* has been considered an intermediate morphological form between *Centrosaurus* and *Styracosaurus* (Currie and Russell, 2005; Mallon et al., 2012). Given the stratigraphic separations of MAZ taxa and the difficulties distinguishing between taxa due to their morphological continuity, it is difficult to determine anagenetic events in the fossil record (Carr et al., 2017; Krishtalka, 1993; Rose and Bown, 1986; Scannella et al., 2014; Stroz and Allen, 2013).

Given the lack of compelling evidence that the MAZ taxa underwent anagenesis, Mallon et al. (2012) suggested that the stratigraphic separation was likely due to migratory events. The lower and upper Dinosaur Park Formation were alluvial and coastal plain settings, respectively, and taxa found in the lower and upper portions of the formation should occur in similar paleoenvironments outside the Dinosaur Park Formation. Although easier to test, few dinosaur taxa occur outside the Dinosaur Park Formation, except for *Centrosaurus apertus*, making the migration hypothesis difficult to test. Dinosaur taxa being endemic to specific formations is a common pattern across Late Cretaceous North American deposits and has led some authors to consider extreme provincialism in dinosaurs (Lehman, 1987). In contrast, Eberth et al. (2013) suggested that large herbivorous dinosaurs had habitat preferences and would follow them over geologic time.

The proposed mechanisms for the stratigraphic separation of thescelosaurid clades, such as changing climatic conditions, differences in habitat preference, or migration events, are not well supported (Table 4.9). Nearly all North American thescelosaurids are recovered from formations that are warm with seasonally hot and dry periods. An exception is *Parksosaurus*

(ROM 804; UALVP 56885), which lived in a cool environment with seasonally hot and dry periods (Eberth et al., 2013). In addition, the paleoenvironment climatic conditions have not been interpreted for the Wapiti thescelosaurid. Furthermore, the ideas that orodromines and thescelosaurines had differing habitat preferences and/or migratory behaviors are not supported as almost all thescelosaurids – except for *Orodromeus* and *Oryctodromeus* – are consistently found in sandstone deposits. *Orodromeus* was recovered from mudstone and siltstone interbedded with limestone in the Two Medicine Formation (Freimuth and Varricchio, 2019; Scheetz, 1999). *Oryctodromeus* was recovered from sandstone, siltstone, and mudstone deposits of the Wayan Formation (Krumenacker et al., 2019). The consistent recovery of thescelosaurid material from sandstone deposits with similar warm and seasonally variable paleoenvironments suggests there were no significant differences in habitat preferences between orodromines and thescelosaurines. Orodromines and thescelosaurines do not replace each other in the stratigraphic record when the lithology changes. Thus, there is no need for migrations to their preferred habitats when the environment changes.

Lyson and Longrich (2011) noticed that *Thescelosaurus* commonly occur in sandstone deposits and suggested that this animal preferred an environment near river channels. Given this, the near consistent pattern of thescelosaurids recovered in sandstone deposits suggests that, in general, thescelosaurids may have habitat preferences that were near river channels. The Lyson and Longrich (2011) study has low statistical power to determine the pattern of habitat preferences in *Thescelosaurus*. However, the near consistency of thescelosaurids recovered from sandstone deposits may reveal such pattern (Table 4.9). Additionally, there are conflicting results from other workers on *Thescelosaurus* habitat preferences where they concluded that

Thescelosaurus preferred flood plains (Carpenter and Young, 2002). The consistent recovery of thescelosaurids from similar lithological rock units suggests that their stratigraphic separation and the disappearance of orodromines was not induced by a changing climate. The depositional environment pattern could also be explained taphonomically (Behrensmeyer et al., 1979; Brown et al., 2013a, b) such as the transportation of the body by water after death (Boaz and Behrensmeyer, 1976), and subsequent burial in the river channels. Further investigations should test the taphonomic processes involved in the fossilization of neornithischians in general.

The process of anagenesis may explain the taxonomic separation between orodromines and thescelosaurines but it is unlikely. Granted, there are currently no anagenetic studies suggesting orodromines are a transitional grade to thescelosaurines. However, an anagenetic event is unlikely because (1) the anatomical features between orodromines and thescelosaurines are distinct and suggest a basal split in the Early Cretaceous, (2) Asian thescelosaurines (*Changchunsaurus* and *Haya*) are equivalent in time with other Orodromines (*Koreanosaurus* and *Zephyrosaurus*), and (3) the phylogenetics and biogeography of basal neornithischians suggest that orodromines are not transitional to thescelosaurines (Boyd, 2015, Brown et al., 2013b; Madzia et al., 2018). A basal split within Thescelosauridae occurred in the Early Cretaceous and gave rise to Orodrominae and Thescelosaurinae. Boyd (2015) suggested that the occurrence of younger North American thescelosaurines could be explained by a migratory event from Asia into North America and a subsequent radiation. However, Boyd (2015) had conflicting results within the study about the biogeographic history of thescelosaurids as some analyses had the ancestral geographic area being either North or South America. Despite the results from the ancestral biogeography of thescelosaurines, it still does not explain why

orodromines disappear after or during the onset of the Bearpaw Formation. Given this, more data and work needs to be done on the biogeography and ancestral reconstruction of neornithischians.

Small-bodied dinosaurs are generally rare amongst dinosaur bearing fossil assemblages that are dominated by large dinosaur taxa (Brown et al., 2013a; O'Gorman and Hone, 2012; White et al., 1998). Dominance of large body taxa in dinosaur fossil communities are counterintuitive compared to modern day ecosystems (Woodward et al., 2005; Behrensmeyer et al., 1979) and clearly indicate preservational biases in favor of larger individuals in many Mesozoic paleoenvironments. The taxonomic segregation of thescelosaurids in southern Alberta could be explained by the taphonomic bias against small-bodied taxa in dinosaur dominated ecosystems where their abundance and diversity were likely much higher. However, this explains the rarity of small bodied orodromines but does not explain the complete absent of thescelosaurines in the Belly River Group. It is difficult to determine if the stratigraphic separation between orodromines and thescelosaurines is real or an artefact because of geologic phenomena (e.g., the deposition of the Bearpaw Formation), taphonomic processes (e.g., preservational bias toward larger specimens), and their poor fossil record obscures any pattern. Additionally, there is a younger ~3 Ma gap between the Wapiti thescelosaurid and *Parksosaurus* and an older ~1 Ma gap between *Albertadromeus* and the Wapiti thescelosaurid (Fig 4.2). With these relatively large thescelosaurid fossil gaps, I cannot be certain what exactly caused the stratigraphic separation between orodromines and thescelosaurines until more of their fossils are recovered in North America. It is difficult to pinpoint the mechanism and timing of the stratigraphic separation between thescelosaurid clades and whether it occurred during, after, or prior to the onset of the Bearpaw Formation.

4.8.7. Limitations

Whether the Wapiti thescelosaurid fossils represent one taxon of multiple individuals at various ontogenetic stages, or multiple taxa is currently unknown based on the existing material. The conclusions about the Wapiti thescelosaurid paleobiology and evolutionary relationships are under the assumption that the material represents a single taxon of one individual. Until more fossils of a small-bodied basal neornithischian are recovered from the Wapiti Formation, not much about the material's paleobiology can be concluded with confidence. At this time, the unassociated and fragmentary material of the Wapiti thescelosaurid can be confidently referred to only as indeterminate thescelosaurines.

4.9. Conclusions

The isolated UALVP 48812, 52839, 53744, 54497, and 60985 from the Dinosaur Park Formation are indistinguishable from the morphology of named orodromine material from the Dinosaur Park Formation and other time equivalent formations. Without any diagnostic characters preserved that can be designated to a taxon, the isolated material is referred to as indeterminate orodromines.

The Campanian aged DC Bonebed yields the first and most northern Canadian occurrence of thescelosaurine material from the Wapiti Formation. The skeletal material has similar morphologies with *Changchunsaurus*, *Haya*, and *Thescelosaurus*; similar growth rates with *Oryctodromeus*; and a potentially close phylogenetic relationship with Asian thescelosaurids (*Changchunsaurus* and *Haya*). Similar features between the Wapiti thescelosaurid and *Changchunsaurus*, *Haya*, and *Thescelosaurus* are present in the premaxillary

tooth, cervical vertebra, quadrate, femur, and fibula. Robust features in the femur UALVP 1849 and the length ratio between the femur and fibula suggests that the Wapiti thescelosaurid was cursorial with powerful hindlimbs that could produce quick and sustained bursts of speed. In addition, the hindlimb of the Wapiti thescelosaurid suggests a locomotion shift from cursorial adapted Campanian thescelosaurids to more graviportal Maastrichtian thescelosaurines. UALVP 50999 osteohistology suggests that the individual was at least seven years old at the time of death, had similar growth rates to *Oryctodromeus*, and had likely reached sexual maturity but not skeletal maturity. Three phylogenetic analyses place the Wapiti thescelosaurid in either a polytomy within Orodrominae (Madzia et al., 2018) or Thescelosaurinae (Boyd, 2015; Brown et al., 2013b) with a close relationship with Asian thescelosaurids (*Changchunsaurus* and *Haya*). Autapomorphies were identified in the quadrate and femur using the matrices of Boyd (2015) and Madzia et al. (2018), respectively. The morphological similarities between Asian taxa and the Wapiti thescelosaurid suggest a thescelosaurid migration from Asia into North America occurred during the Campanian. Given this, it is likely that the phylogenetic placement of the Wapiti thescelosaurid may be an artefact due to its fragmentary skeleton and the assumptions made prior to the analyses. The phylogenetic analyses may not be currently informative until more material is recovered from a single individual. Whether the Wapiti thescelosaurid represents one taxon or multiple taxa is unknown. Given this, the Wapiti thescelosaurid lacks clear diagnosable material and therefore a new taxon cannot be erected. However, the Wapiti Formation may ultimately produce new associated thescelosaurid material that could be diagnosable in the future. At this time, the unassociated and fragmentary material is referred to as indeterminate thescelosaurines.

The mechanism for the stratigraphic separation between orodromines and thescelosaurines in southern Alberta cannot be explained by changing climatic conditions, habitat preference, migration, or an anagenetic event but it could likely be explained by taphonomic biases. Even with an occurrence of a thescelosaurine during Bearpaw equivalent times, it is unresolved why orodromines disappear just before, after, or during the onset of the Bearpaw Formation, and why thescelosaurines are dominate thereafter. Future work should investigate taphonomic processes of thescelosaurids such as looking at modern analogs of similar sized animals to test how burial and water transportation processes differentiate their elements.

4.10. Tables and Figures

Table 4.1. Measurements of UALVP 54497, 52839, 48812, 53744, 60985.

Measurement	Value (mm)
Phalange UALVP 54497	
Anteroposterior Length	57.4
Mid-Transverse Width	24.7
Height	25.2
Proximal End Width	30.5
Distal End Width	28.6
Basioccipital UALVP 52839	
Anteroposterior Length	26.7
Transverse Width	24.6
Height	38.5
Occipital Condyle Length	17.0
Occipital Condyle Width	18.1
Occipital Condyle Height	15.3
Femur UALVP 48812	
Transverse Width	27.9
Proximal Transverse Width	46.8
Distal Transverse Width	39.8
Femur UALVP 53744	
Proximal Transverse Width	25.6
Caudal Centra UALVP 60985	
Anteroposterior Length	24.7
Transverse Width	12.0
Height	22.4

Table 4.2. Measurements of the Wapiti thescelosaurid.

Measurement	Value (mm)
Quadrate UAVLP 23114	
Mid shaft length	11.6
Caudal Vertebra UAVLP 59471	
Maximum length	45.8
Mid shaft length	27.8
Mid shaft circumference	75.0
Dorsal Vertebra UALVP 23089	
Maximum length	42.5
Mid shaft length	24.7
Mid shaft circumference	97.0
Proximal end maximum length	36.2
Distal end maximum length	34.3
Caudal Vertebra UAVLP 23088	
Maximum length	39.8
Mid shaft length	120.0
Mid shaft circumference	23.2
Proximal end maximum length	28.4
Distal end maximum length	29.0
Caudal Vertebra UALVP 59803	
Maximum length	39.8
Mid shaft length	17.1
Mid shaft circumference	65.0
Proximal end maximum length	21.6
Distal end maximum length	20.7
Femur UALVP 1849	
Proximal end maximum length	69.7
Distal end maximum length	58.6
See Table 4.3 for additional measurements	
Fibula UALVP 59855	
Maximum length	264.3
Mid shaft length	13.2

Mid shaft circumference	55.0
Proximal end maximum length	41.9
Distal end maximum length	14.4
Fibula UALVP 50999	
Distal end maximum length	18.9
Metatarsal II UALVP 59483	
Mid shaft length	20.4
Mid shaft circumference	60.0
Proximal end maximum length	44.5
Distal end maximum length	22.7
Metatarsal I UALVP 59834	
Maximum length	73.3
Mid shaft length	9.2
Mid shaft circumference	32.0
Proximal end maximum length	20.5
Distal end maximum length	10.0
Phalanx UALVP 59506	
Maximum length	28.0
Mid shaft length	18.2
Mid shaft circumference	59.0
Proximal end maximum length	23.5
Distal end maximum length	20.3
Phalanx UALVP 23111	
Maximum length	19.9
Mid shaft length	16.4
Mid shaft circumference	56.0
Proximal end maximum length	19.8
Distal end maximum length	19.3

Table 4.3. Hindlimb measurements, ratios, and body mass estimations of thescelosaurids in millimeters and kilograms.

Abbreviations: FL, femur length; FW, femur width; FC, femur circumference; LTW, lesser trochanter width; ITN, intertrochanteric notch length; FiL, fibula length; MIL, metatarsal I length; MIIL, metatarsal II length; FW/FL, femur width/femur length; FiL/FL, fibula length/femur length.

Taxa	FL (mm)	FW (mm)	FC (mm)	LTW (mm)	ITN (mm)	FiL (mm)	MIL (mm)	MIIL (mm)	FW/FL	FiL/FL	Est. Body Mass (kg)	Body Mass Error (kg)	Specimen
Wapiti thescelosaurid	237	35	122	20	44	264	73	112	0.15	1.12	114.8	28.7	Various UALVP
Koreanosaurus	165	18	-	6	19	175	-	-	0.11	1.07	-	-	KDRC-BB3
Notohypsilophodon	-	-	-	-	-	192	-	-	-	-	-	-	UNPSJB-PV 942
Orodromeus	142	17	-	3	10	146	28	80	0.12	1.03	-	-	MOR 623
Orodromeus	139	15	-	3	10	-	-	-	-	-	-	-	MOR 473
Oryctodromeus	240	29	-	14	31	-	36	112	0.12	-	-	-	MOR 1642
Orodromine	178	21	-	8	16	-	-	-	0.12	-	-	-	TMP 1979.011. 0032
Orodromine	167	19	-	-	-	-	-	-	0.11	-	-	-	TMP 1990.036. 0065
Jeholosaurus	88	8	-	5	14	111	-	53	0.09	1.26	-	-	IVPP V12529
Jeholosaurus	51	5	-	-		61	15	31	0.11	1.20	-	-	IVPP V15719
Jeholosaurus	128	18	50	8	23	154	32	66	0.14	1.20	10.0	2.5	IVPP V15939
Haya	126	16	-	8	12	152	50	81	0.13	1.21	-	-	IGM 100/2013
Parksosaurus	270	33	103	14	-	305	88	135	0.12	1.13	72.5	18.1	ROM 804
T. assiniboiensis	301	39	121	-	-	261	63	102	0.13	0.87	113.0	28.2	RSM P 1225.1
T. neglectus	378	48	-	26	98	290	65	112	0.13	0.77	-	-	USNM 7757
T. neglectus	428	62	-	25	84	-	-	-	0.15	-	-	-	NCSM 15728
***Thescelosaurus* sp.**	335	47	137	-	-	288	-	94	0.14	0.86	159.1	39.8	CMN 8537

Table 4.4. Osteohistological measurements of the cross-sectional and medullary cavity diameter in anteroposterior and lateromedial directions.

Osteohistological Thin Section	Anteroposterior (mm)	Lateromedial (mm)
Cross-Sectional Diameter	12.7	10.7
Medullary Cavity Diameter	2.4	2.3

Table 4.5. Average values of the crown height (CH), crown base length (CBL), and crown angle (CA) for thescelosaurid premaxillary teeth.

Taxa	CH	CBL	CA
Thescelosaurinae (UALVP 59863)	3.6	4.2	48.2
***Changchunsaurus* (JLUM L0403-j-Zn2)**	2.0	1.4	59.0
***Haya* (IGM 100/2017)**	3.1	2.0	65.0
***Jeholosaurus* (IVPP V15716)**	2.0	3.1	46.7
***Orodromeus* (MOR 294)**	2.5	2.7	51.2
***Thescelosaurus* (NCSM 15728)**	5.0	5.2	52.3
***Zephyrosaurus* (MCZ 4392)**	6.0	4.0	69.0

Table 4.6. Morphometric measurements taken in this study on the premaxillary teeth of thescelosaurids.

Measurements and Abbreviation	Definitions
Crown Height (CH)	The maximum apicobasal length from the base of the cingulum to the apex of the crown
Crown Base Length (CBL)	The maximum mesiodistal length of the cingulum
Crown Angle (CA)	The angle between the line segments that define CBL and AL

Table 4.7. Statistical results of the reduced major axis regressions for femoral morphologies in Thescelosauridae.

Abbreviations: FW, femur width; LTW, lesser trochanter width; ITNL, intertrochanteric notch length.

Independent Variable (x)	Dependent Variable (y)	*n*	Slope Interval	Intercept Interval	Pearson's r	p(a)
Femur Length	FW	15	(1.09, 1.28)	(-1.57, -1.11)	0.99	0.0001
Femur Length	LTW	12	(0.82, 2.17)	(-4.07, -0.84)	0.82	0.001
Femur Length	ITNL	11	(1.13, 2.08)	(-3.38, -1.12)	0.89	0.0002

Table 4.8. Phylogenetic results of the Wapiti thescelosaurid from three character matrices.

Abbreviations: MPT, most parsimonious trees; TL, tree length; CI, consistency index; RI, retention index; Bst, bootstrap analysis; Bs, Bremer support.

Character Matrix	MPT	TL	CI	RI	Bst	Bs	Sister taxa	Clade
Brown et al., 2013b	2	405	0.46	0.66	0	1	*Haya*	Thescelosaurinae
Boyd, 2015	72	884	0.36	0.63	1	0	Polytomy with *Changchunsaurus* and *Haya*	Thescelosaurinae
Madzia et al., 2018	2400	934	0.34	0.62	0	0	Polytomy with Orodrominae and Thescelosaurinae	?

Table 4.9. Albian to Maastrichtian North American thescelosaurids occurrences with their associated geologic formations, lithology, and paleoclimate interpretations.

Abbreviations: CFm, Cloverly Formation; DPF, Dinosaur Park Formation; FFm, Frenchman Formation; HCF, Horseshoe Canyon Formation; HCFm, Hell Creek Formation; LFm, Lance Formation; OFm, Oldman Formation; SFm, Scollard Formation; TMFm, Two Medicine Formation; WF, Wapiti Formation; WFm, Wayan Formation; Oro, Orodrominae; Thesc, Thescelosaurinae; lms, limestone; mds, mudstone; slts, siltstone; and SS, sandstone.

Taxon	Specimen	Clade	Formation	Lithology	Paleoclimate	References
T. assiniboiensis	RSMP 1225.1	Thesc	FFm.	Unconsolidated SS	Warm, seasonally wet/dry	Bamforth et al., 2014; Brown et al., 2011; McIver, 2002
T. garbanii	LACM 33542	Thesc	HCFm.	SS	Warm	Bamforth et al., 2014; Lyson and Longrich, 2011; Morris, 1976
T. neglectus	USNM 7757	Thesc	LFm.	SS	Warm	Bamforth et al., 2014; Gilmore, 1915; Lyson and Longrich, 2011
***Thescelosaurus* sp.**	CMN 8537	Thesc	SFm.	SS	Warm, seasonally wet/dry	Eberth et al., 2013; Sternberg, 1940
Parksosaurus	ROM 804	Thesc	HCF.	?	Cool, seasonally wet/dry	Eberth et al., 2013; Parks, 1926
Parksosaurus	UALVP 56885	Thesc	HCF.	Fine to very fine SS	Cool, seasonally wet/dry	This study; Eberth et al., 2013
Thescelosaurine indet.	Various UALVP specimens	Thesc	WF	SS, slts, and mds	?	This study
Orodromine indet.	UALVP 48812	Oro	DPF.	?	Warm, wet	This study; Eberth et al., 2013
Incertae sedis orodromines	Various TMP specimens	Oro	DPF and OFm.	?	Warm, wet	Brown et al., 2013b; Eberth et al., 2013
Orodromine indet.	TMP 2008.045.0002	Oro	OFm.	Medium SS	Warm, seasonally wet/dry	Brown et al., 2013b; Eberth et al., 2013
Orodromeus	MOR 294	Oro	TMFm.	lms with interbedded mds and slts	Warm, seasonally wet/dry	Eberth et al., 2013; Freimuth and Varricchio, 2019; Scheetz, 1999
Albertadromeus	TMP 2009.037.0044	Oro	OFm.	Fine to very fine SS	Warm, seasonally wet/dry	Brown et al., 2013b; Eberth et al., 2013
Oryctodromeus	Various IMNH specimens	Oro	WFm.	SS, slts, and mds	Seasonally wet/dry	Krumenacker et al., 2019; Varricchio et al., 2007
Zephyrosaurus	MCZ 4392	Oro	CFm.	Silty SS	?	Sues, 1980

(A.) Brown et al., 2013
MPT: 3
TL: 401
CI: 0.47
RI: 0.66

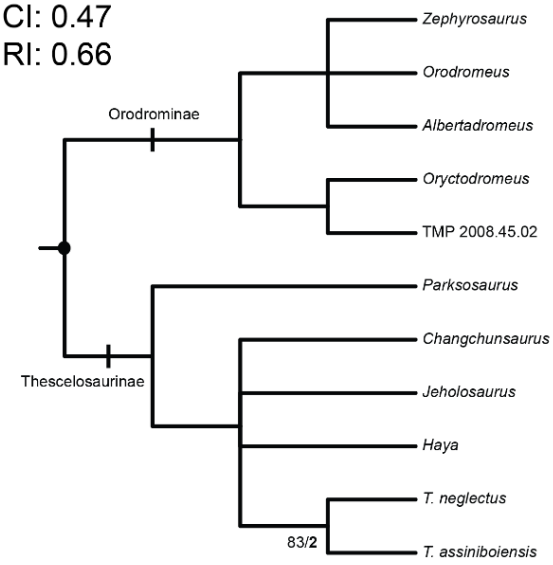

(B.) Boyd, 2015
MPT: 36
TL: 868
CI: 0.37
RI: 0.65

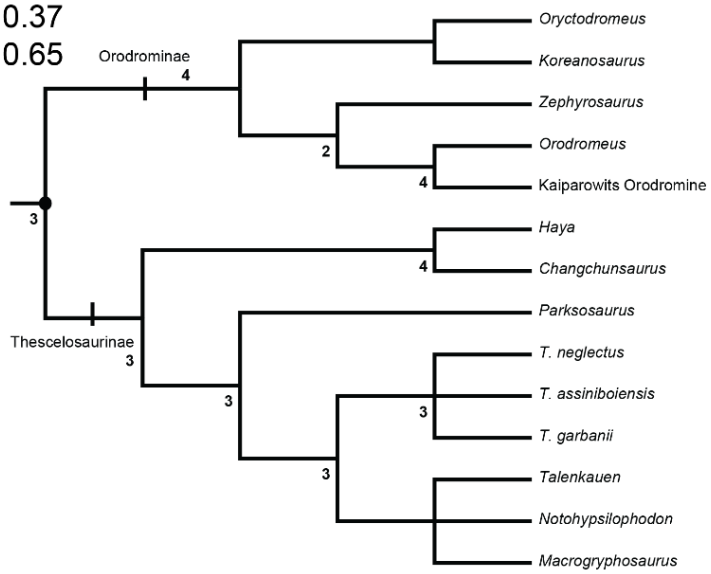

(C.) Madzia et al., 2018
MPT: 13,547
TL: 905
CI: unreported
RI: unreported

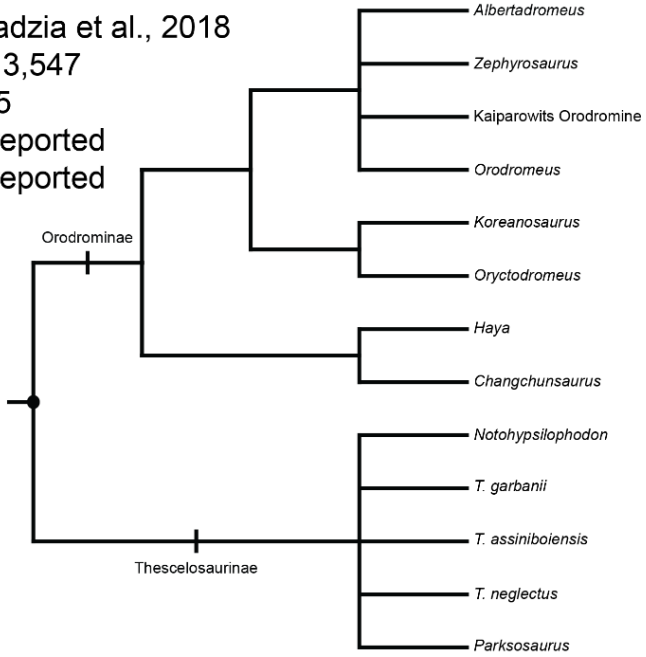

Figure 4.1. Results of three analyses of thescelosaurid phylogeny.

Brown et al. (2013b) (A), Boyd, (2015) (B), Madzia et al. (2018) (C). Bold numbers are Bremer support values >1 whereas numbers in plain text are bootstrap support values >50%. Abbreviations: MPT, most parsimonious tree; TL, tree length; CI, consistency index; RI, retention index.

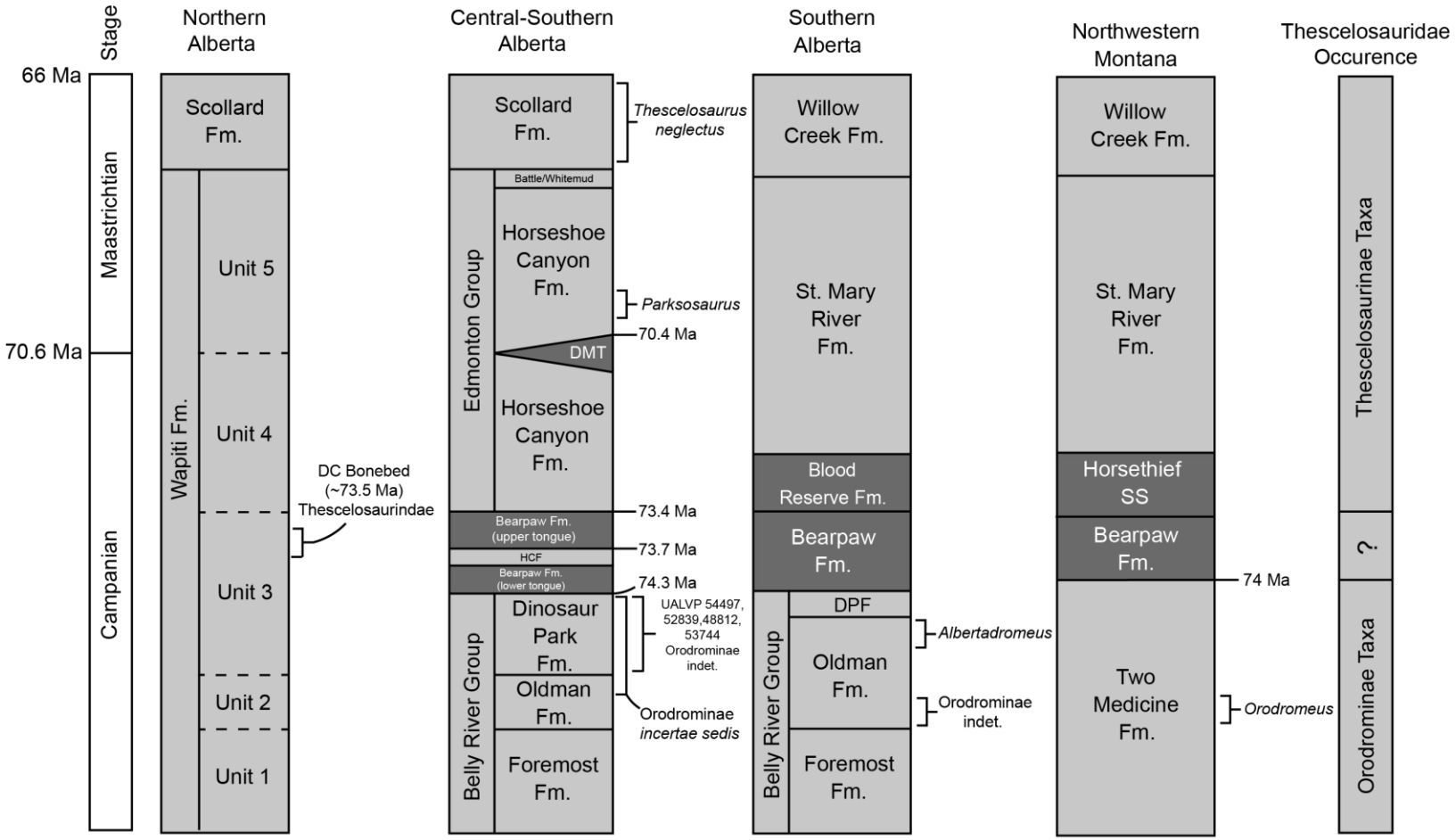
Stage
Northern Alberta
Central-Southern Alberta
Southern Alberta
Northwestern Montana
Thescelosauridae Occurence
66 Ma
70.6 Ma
Maastrichtian
Campanian
Scollard Fm.
Wapiti Fm.
Unit 5
Unit 4
Unit 3
Unit 2
Unit 1
DC Bonebed (~73.5 Ma) Thescelosaurindae
Edmonton Group
Battle/Whitemud
Horseshoe Canyon Fm.
DMT
70.4 Ma
Parksosaurus
Thescelosaurus neglectus
73.4 Ma
Bearpaw Fm. (upper tongue)
73.7 Ma
HCF
Bearpaw Fm. (lower tongue)
74.3 Ma
Belly River Group
Dinosaur Park Fm.
Oldman Fm.
Foremost Fm.
UALVP 54497, 52839,48812, 53744 Orodrominae indet.
Orodrominae incertae sedis
Willow Creek Fm.
St. Mary River Fm.
Blood Reserve Fm.
Bearpaw Fm.
DPF
Albertadromeus
Orodrominae indet.
Horsethief SS
74 Ma
Two Medicine Fm.
Orodromeus
Thescelosaurinae Taxa
?
Orodrominae Taxa

Figure 4.2. Approximate biostratigraphy and chronostratigraphy of Thescelosauridae occurrences in the Late Cretaceous of Alberta and Montana with U-Pb dates.

Formations in light grey are terrestrial deposits, and those in dark grey are marine. Abbreviations: DMT, Drumheller Marine Tongue; DPF, Dinosaur Park Formation; HCF, Horseshoe Canyon Formation. Stratigraphy and radio-metric dates from Brown et al. (2013b), Eberth et al. (2013), Eberth and Kamo (2019), and Fanti and Catuneanu (2010).

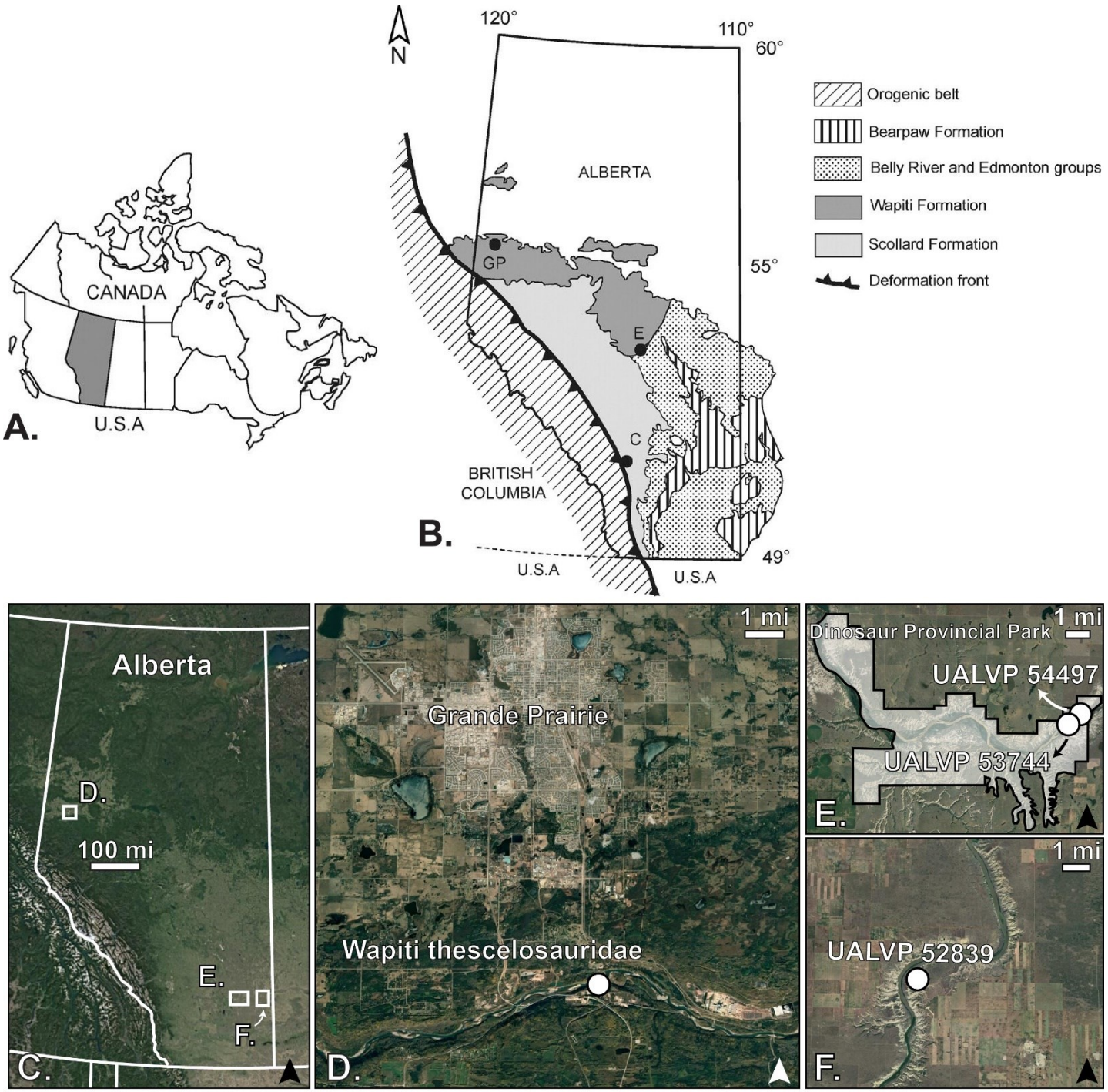
A.
CANADA
U.S.A
B.
N
120°
110°
60°
55°
49°
ALBERTA
GP
E
C
BRITISH
COLUMBIA
U.S.A
U.S.A
Orogenic belt
Bearpaw Formation
Belly River and Edmonton groups
Wapiti Formation
Scollard Formation
Deformation front
C.
Alberta
D.
100 mi
E.
F.
D.
1 mi
Grande Prairie
Wapiti thescelosauridae
E.
1 mi
Dinosaur Provincial Park
UALVP 54497
UALVP 53744
F.
1 mi
UALVP 52839

Figure 4.3. Geographic location of the Wapiti thescelosaurid from the Wapiti Formation and orodromine material from the Dinosaur Park Formation in Alberta, Canada.

Map of Alberta, Canada with highlighted specimen locations (A, B, C). (D) Enlarged map of the Grande Prairie Area with the approximate geographic location of the Dinosaur-Chelonian Bonebed, indicated by the white circle. (E) Map of the Dinosaur Provincial Park in Alberta, Canada is highlighted, showing the locations of UALVP 53744 and 54497 with GPS certainty. UALVP 54497 is within the 'Happy Jacks' locality. UALVP 48812 (not pictured here) was recovered at 'Locality 34' within the Dinosaur Provincial Park. Map of west-central Alberta showing the location of UALVP 52839 (F). Black and white arrows indicate the direction of north. Abbreviations: C, Calgary; E, Edmonton; GP, Grande Prairie. Map based on Fanti and Catuneanu (2010).

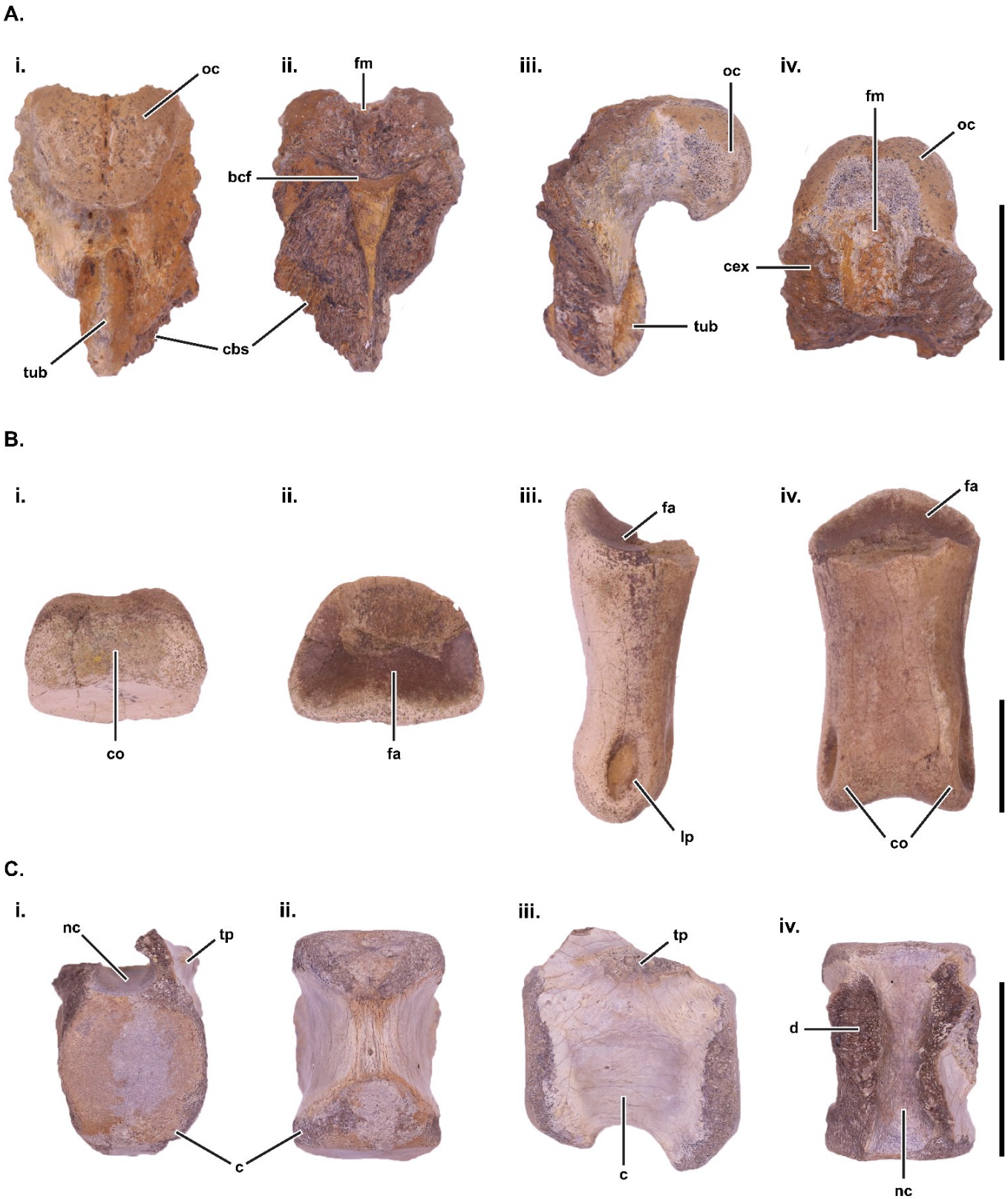
A.
i.
oc
tub
ii.
fm
bcf
cbs
iii.
oc
tub
iv.
fm
oc
cex
B.
i.
co
ii.
fa
iii.
fa
lp
iv.
fa
co
C.
i.
nc
tp
c
ii.
iii.
tp
c
iv.
d
nc

Figure 4.4. Unassociated braincase (UALVP 52839) (A), pedal phalange (UALVP 54497) (B), and caudal vertebra (UALVP 60985) (C) from southern Alberta.

Braincase in posterior view (i), anterior view (ii), left lateral view (iii), and ventral view (iv). Pedal phalange at the distal end surface (i), proximal end surface (ii), lateral view (iii), and ventral view (iv). Caudal vertebra in anterior view (i), ventral view (ii), lateral view (iii), and dorsal view (iv). Abbreviations: bcf, braincase floor; c, centrum; cbs, contact of the basisphenoid; cex, contact of the exoccipital; co, condyle; d, damage; fa, facets; fm, foramen magnum; lp, ligament pits; nc, neural canal; oc, occipital condyle; tp; transverse process; tub, tubercle. Scale bar = 20 mm.


A.
fh
gt
?
mc
icg
lc
B.
fh
d
l
?
mc
C.
fh
d
gt
?
lc
D.
fh
l
?
mc
E.
l
fh
gt
F.
lc
icg
mc
G.
fh
d
nf
ft
?
d
mc
H.
d
fh
?
I.
d
gt
?
d
J.
fh
ft
?
mc
K.
lt
fh
gt
L.
d
mc

Figure 4.5. Right femora of UALVP 48812 and 53744.

Posterior view (A, G), anterior view (B, H), lateral view (C, I), medial view (D, J), ventral view (E, K) and dorsal view (F, L). The dotted lines represent reconstruction interpretation of the femora. Anatomical Abbreviations: d, damage; fh, femoral head; ft, fourth trochanter; gt, greater trochanter; icg, intercondylar groove; l, ligament; lc, lateral condyle; lt, lesser trochanter; nf, nutrient foramen; mc, medial condyle. Scale bar = 20 mm.

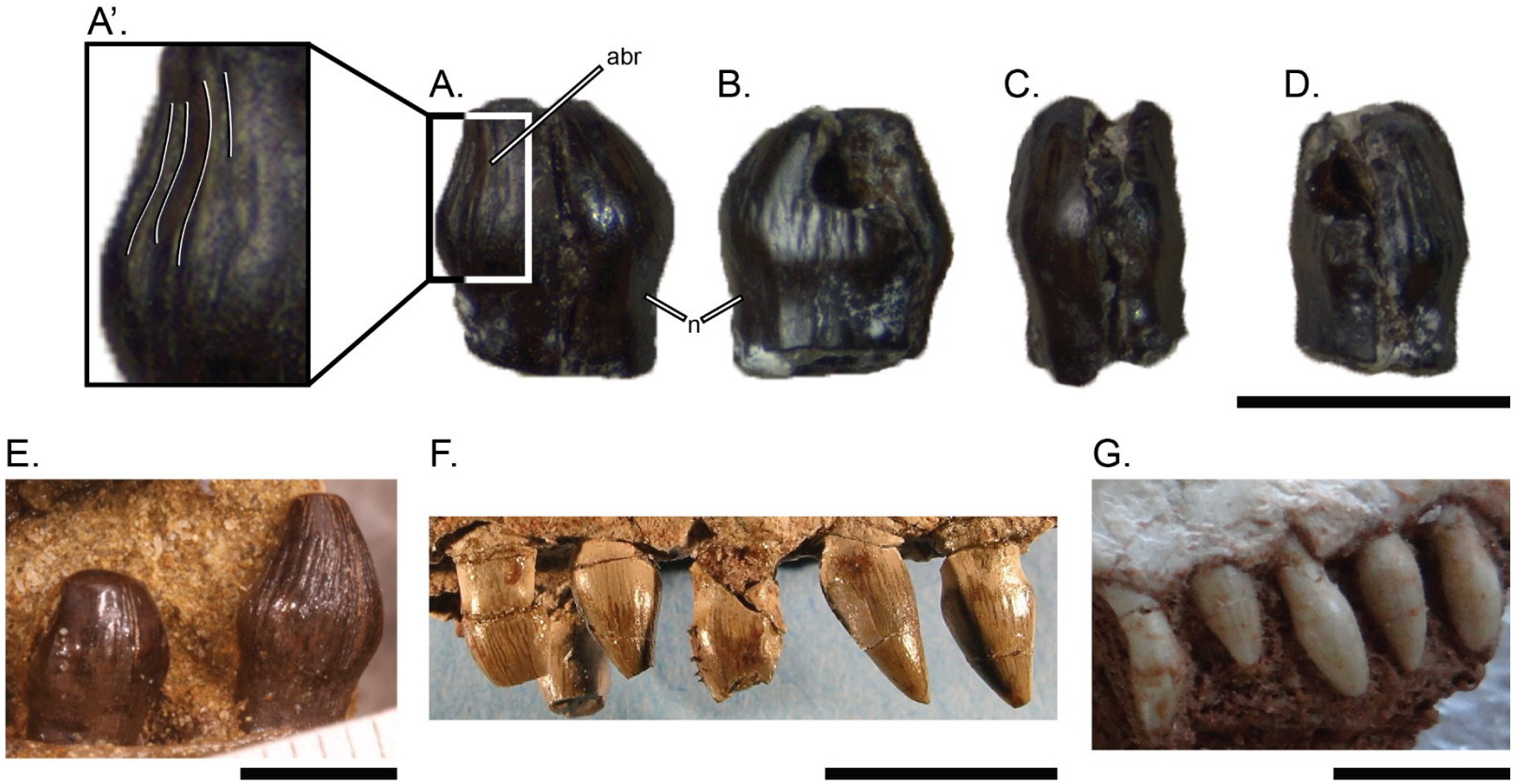
A'.
A.
abr
n
B.
C.
D.
E.
F.
G.

Figure 4.6. Wapiti thescelosaurid premaxillary tooth (UALVP 59863) compared with other thescelosaurids.

Wapiti thescelosaurid premaxillary tooth (UALVP 59863) in buccolingual view (A, B) and mesiodistal view (C, D). (A') The interpreted apicobasal oriented ridges on the buccolingual tooth margin. (E) *Thescelosaurus* (NCSM 15278) in left buccal view, (F) *Zephyrosaurus* (MCZ 4392) in left buccal view, and (G) *Haya* (IGM 100/2017) in right buccal view.

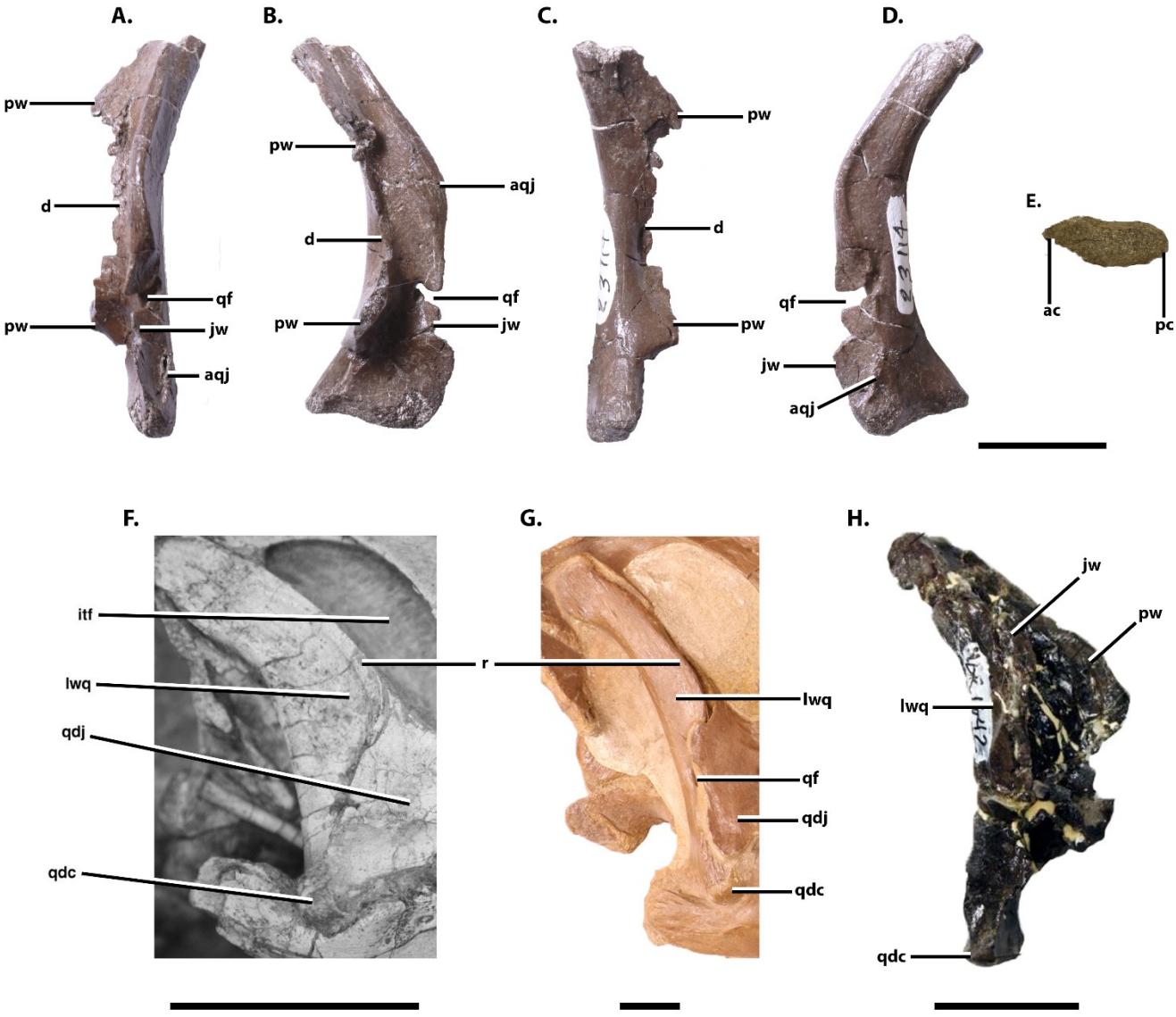
A.
pw
d
qf
pw
jw
aqj
B.
pw
aqj
d
qf
pw
jw
C.
pw
d
pw
D.
qf
jw
aqj
E.
ac
pc
F.
itf
r
lwq
qdj
qdc
G.
lwq
qf
qdj
qdc
H.
jw
pw
lwq
qdc

Figure 4.7. Left Quadrate of the Wapiti thescelosaurid UALVP 23114.

Left quadrate of the Wapiti thescelosaurid (UALVP 23114) in anterior view (A), medial view (B), posterior view (C), lateral view (D), ventral view (E). *Changchunsaurus* JLUM L0403-j-Zn2 (F), *Thescelosaurus* NCSM 15728 (G), and *Oryctodromeus* MOR 1642 quadrate comparisons in right lateral view. Anatomical Abbreviations: aqj, quadratojugal articulation; ac, anterior condyle; d, damage; itf, infratemporal fenestra; jw, jugal wing; lwq, lateral wing of quadrate; pc, posterior condyle; pw, pterygoid wing; qdc, lateral condyle of quadrate; qdj, quadratojugal; qf, quadratic foramen; r, ridge. Scale bar = 20 mm.


A.
nc
pp
B.
pp
c
cm
C.
pp
c
D.
pp
E.
c
nc
F.
cm
G.
c
H.
23089
I.
prz
tp
ns
J.
c
tp
K.
nc
c
L.
ns
prz
M.
nc
c
N.
O.
nc
c
P.

Figure 4.8. Cervical (A-D), dorsal (E-H), and caudal (I-P) vertebrae of the Wapiti thescelosaurid.

UALVP 59471 (A-D), 23089 (E-H), 23088 (I-L), and 59803 (M-P). Dorsal view (A, E, I, M), ventral view (B, F, N), anterior view (C, G, K, O), lateral view (D, H, L, P). Anatomical Abbreviations: c, centrum; cm, crenulated margin; pp, parapophysis; nc, neural canal; ns, neural spine; prz, prezygapophysis; tp, transverse process. Scale bar = 10 mm.

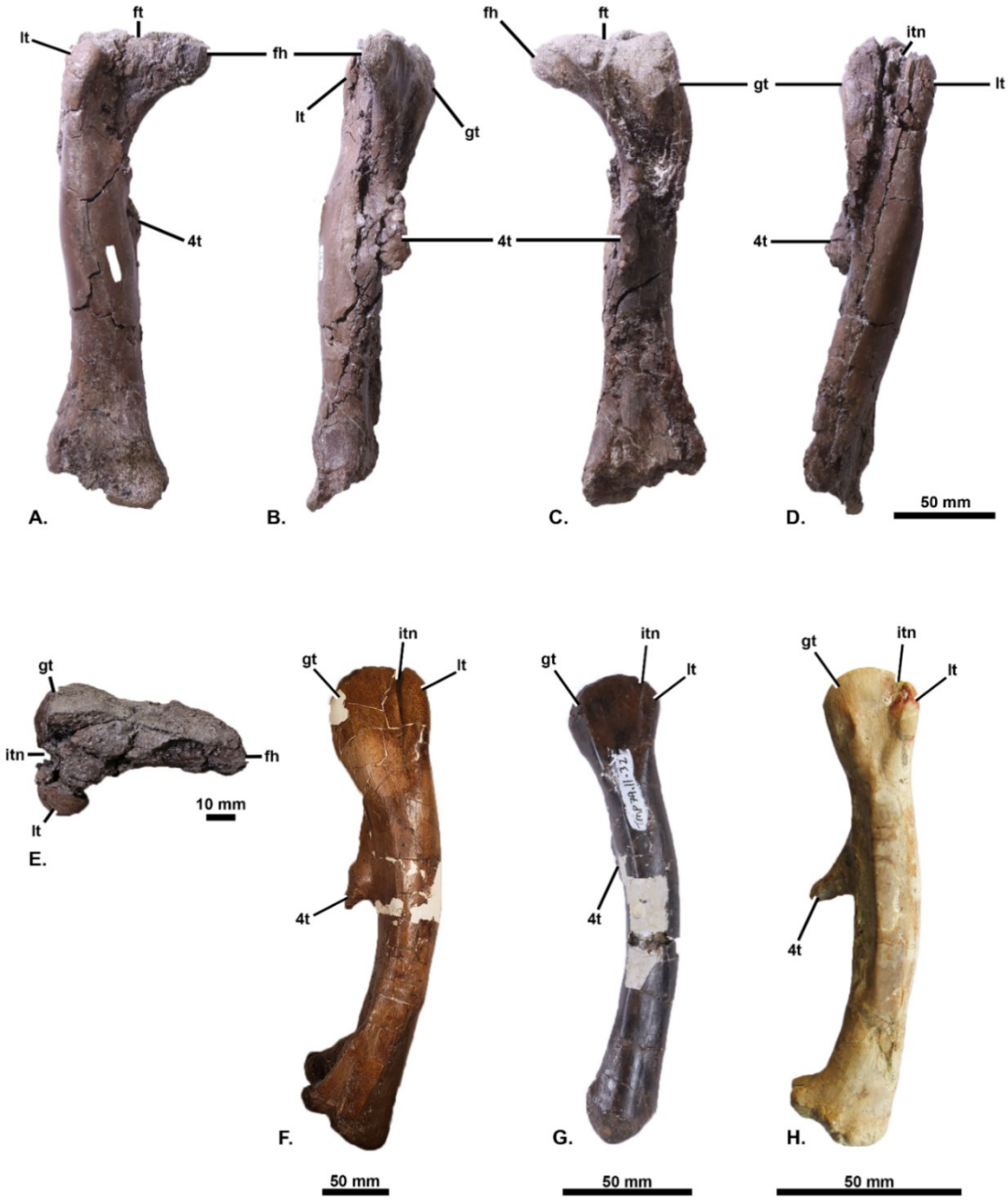
ft
lt
fh
4t
A.
fh
lt
gt
4t
B.
fh
ft
gt
4t
C.
itn
lt
4t
D.
50 mm
gt
itn
fh
lt
10 mm
E.
gt
itn
lt
4t
F.
50 mm
gt
itn
lt
4t
G.
50 mm
gt
itn
lt
4t
H.
50 mm

Figure 4.9. Right femur of the Wapiti thescelosaurid UALVP 1849.

Anterior view (A), medial view (B), posterior view (C), lateral view (D), dorsal view (E). Thescelosaurid femur comparisons in right lateral view. Right femur of *Thescelosaurus* USNM 7757 (F), right femur of an indeterminate Orodrominae TMP 1979.11.32 (G), right femur of *Jeholosaurus* IVPP V15939 (H). Anatomical Abbreviations: fh, femoral head; ft, fossa trochanteris; gt, greater trochanter; itn, intertrochanteric notch; lt, lesser trochanter; 4t, fourth trochanter.

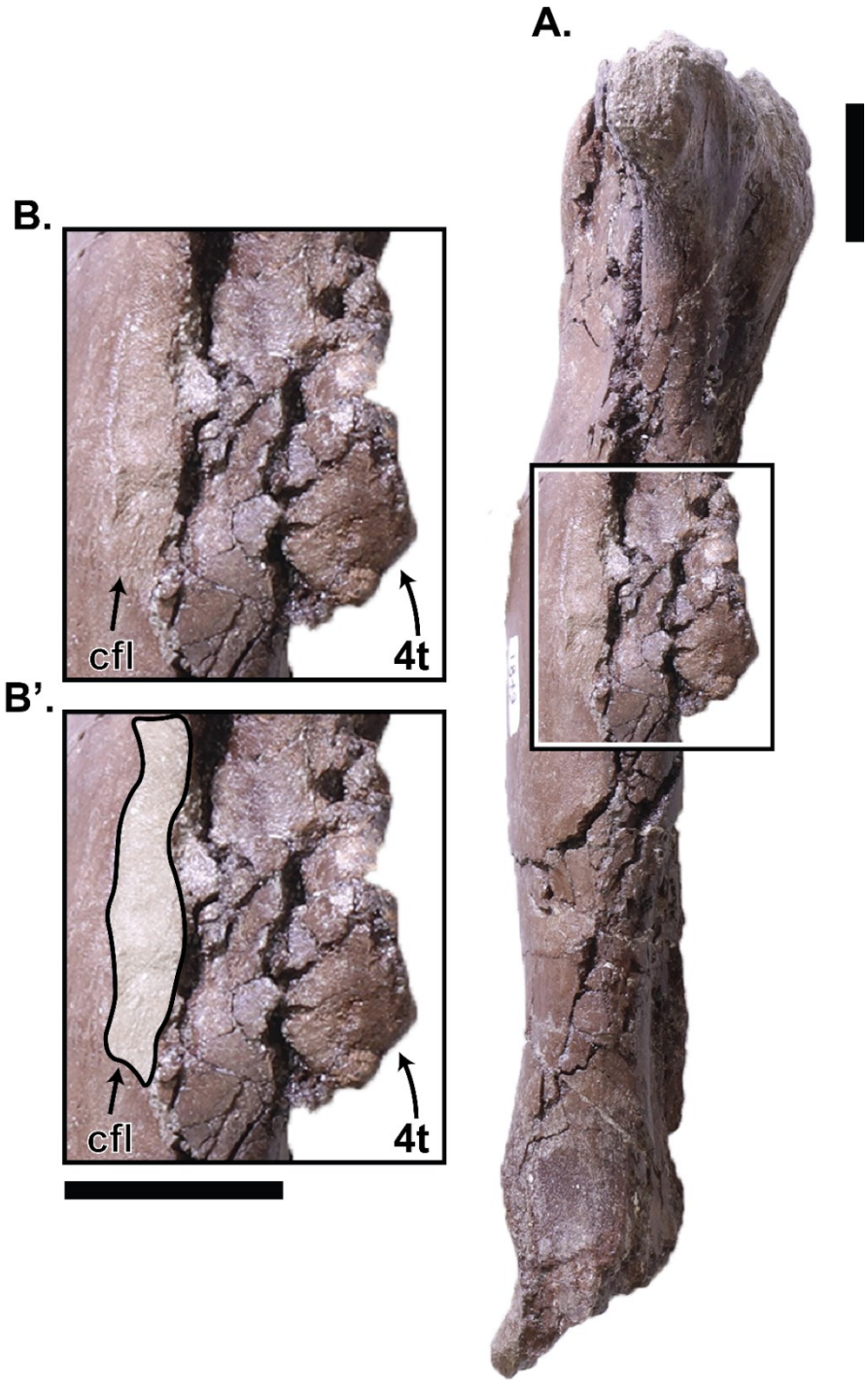
A.
B.
cfl
4t
B'.
cfl
4t

Figure 4.10. Close up of the fourth trochanter and muscle scar in Wapiti thescelosaurid femur.

Right femur of the Wapiti thescelosaurid UALVP 1849 in medial view (A) with close-up of the fourth trochanter and the caudofemoralis longus muscle scar (B). Highlighted region denotes the attachment area for the caudofemoralis longus (B'). Abbreviations: cfl, caudofemoralis longus; 4t, fourth trochanter. Scale bar = 25 mm.


A.
B.
C.
D.
E.
F.
G.
i
ii
iml
H.
i
ii
fa
iml
iml
I.
i
ii
iml
fa
J.
i
ii
iml

Figure 4.11. Right fibula of the Wapiti thescelosaurid UALVP 59855.

Posterior view (A), medial view (B), anterior view (C), lateral view (D), anterior view (E), medial view (F). Wapiti thescelosaurid right fibula distal end comparison between UALVP 59855 and 50999. Anterior view (G), medial view (H), posterior view (I), lateral view (J). Anatomical Abbreviations: fa, facet; iml, intermuscular lines. Scale bar = 20 mm.

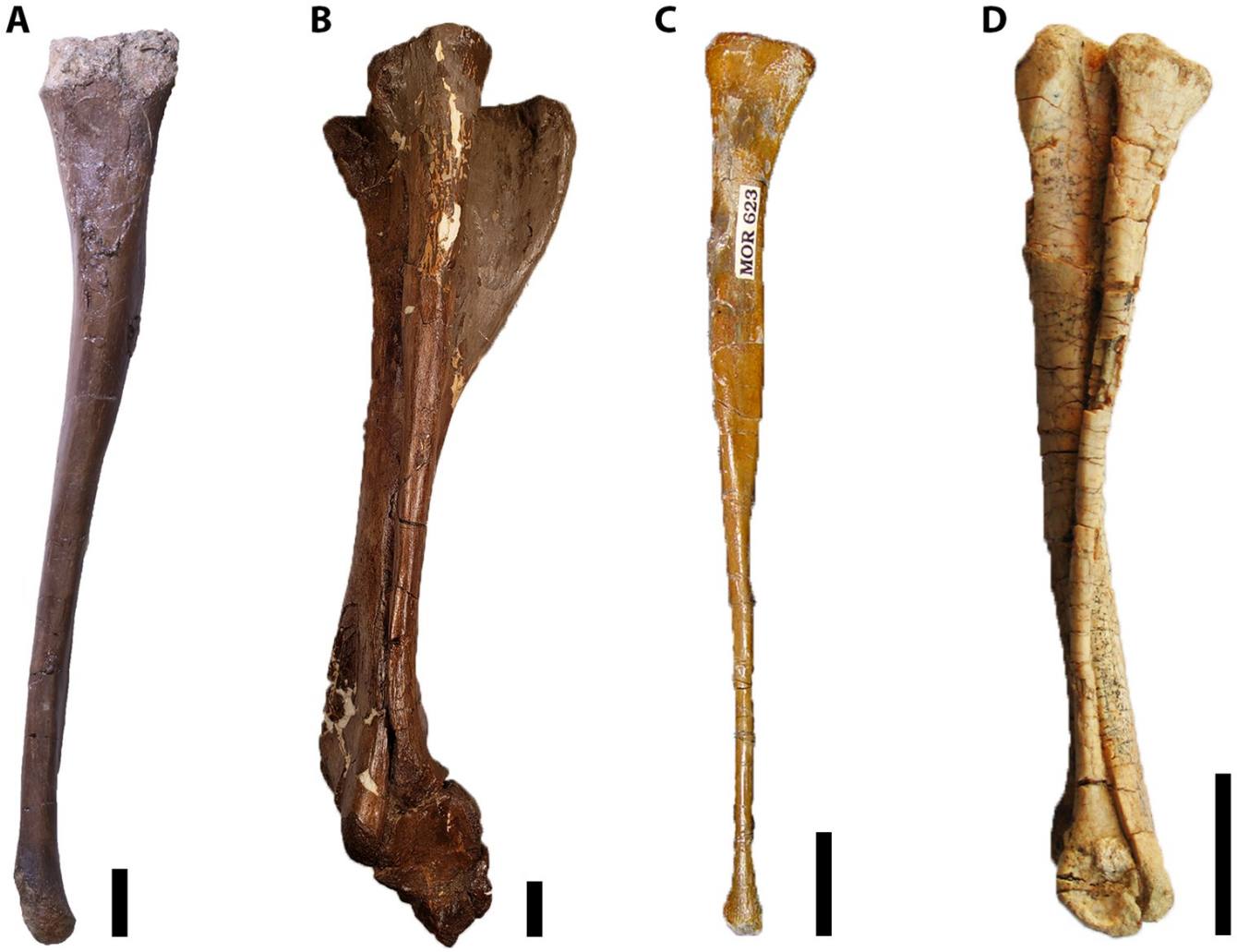
A
B
C
MOR 623
D

Figure 4.12. Thescelosauridae fibulae comparison with the Wapiti thescelosaurid (UALVP 59855).

Fibulae in lateral view. (A) UALVP 59855 from the DC Bonebed (right), (B) *Thescelosaurus* USNM 7757 (right), (C) *Orodromeus* MOR 623 (right), (D) *Jeholosaurus* IVPP V12529 (left). Scale bar = 20


A.
B.
C.
D.
E.
co
co
F.
G.
H.
I.
J.
fa
lp
co
de
co
lp

Figure 4.13. Left metatarsal 1 and right metatarsal 2 of the Wapiti thescelosaurid UALVP 59834.

Left metatarsal 1 in anterior view (A), medial view (B), posterior view (C), lateral view (D), ventral view (E). Right metatarsal 2 of the Wapiti thescelosaurid UALVP 59483. Anterior view (F), medial view (G), posterior view (H), lateral view (I), ventral view (J). Anatomical Abbreviations: co, condyles; de, depression; fa, facet; lp, lateral pit. Scale bar = 20 mm.

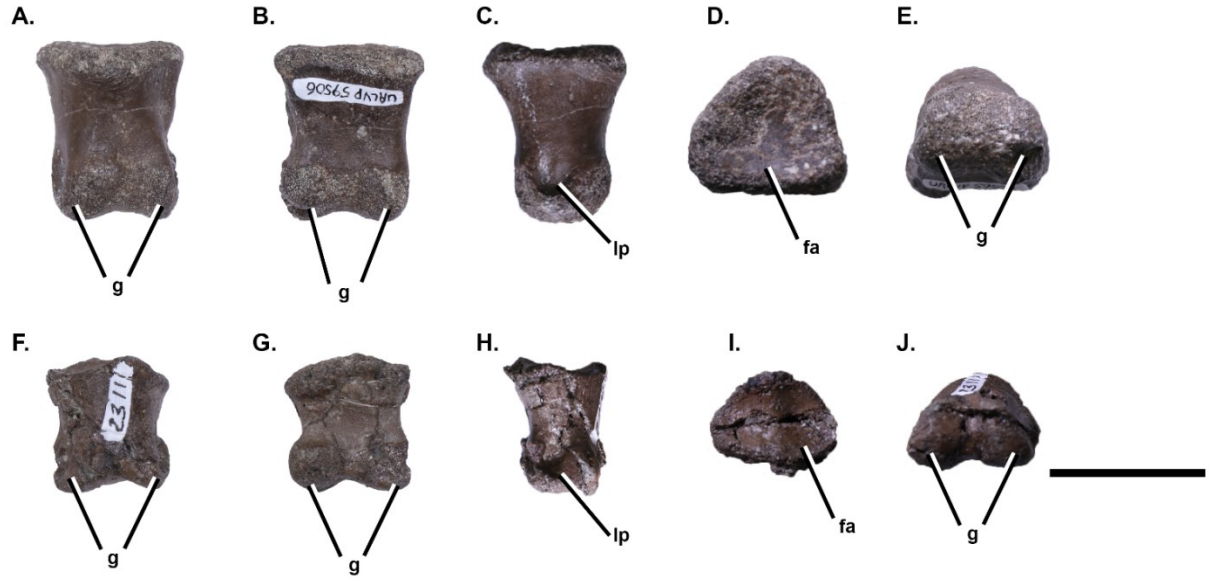

Figure 4.14. Pedal phalanges of the Wapiti thescelosaurid.

Pedal phalanges of the Wapiti thescelosaurid UALVP 59506 (A-E) and 23111 (F-J). Dorsal view (A, F), ventral view (B, G), lateral view (C, H), anterior view (D, I), and posterior view (E, J). Anatomical Abbreviation: fa, facet; g, ginglymi; lp, lateral pit. Scale bar = 25 mm.

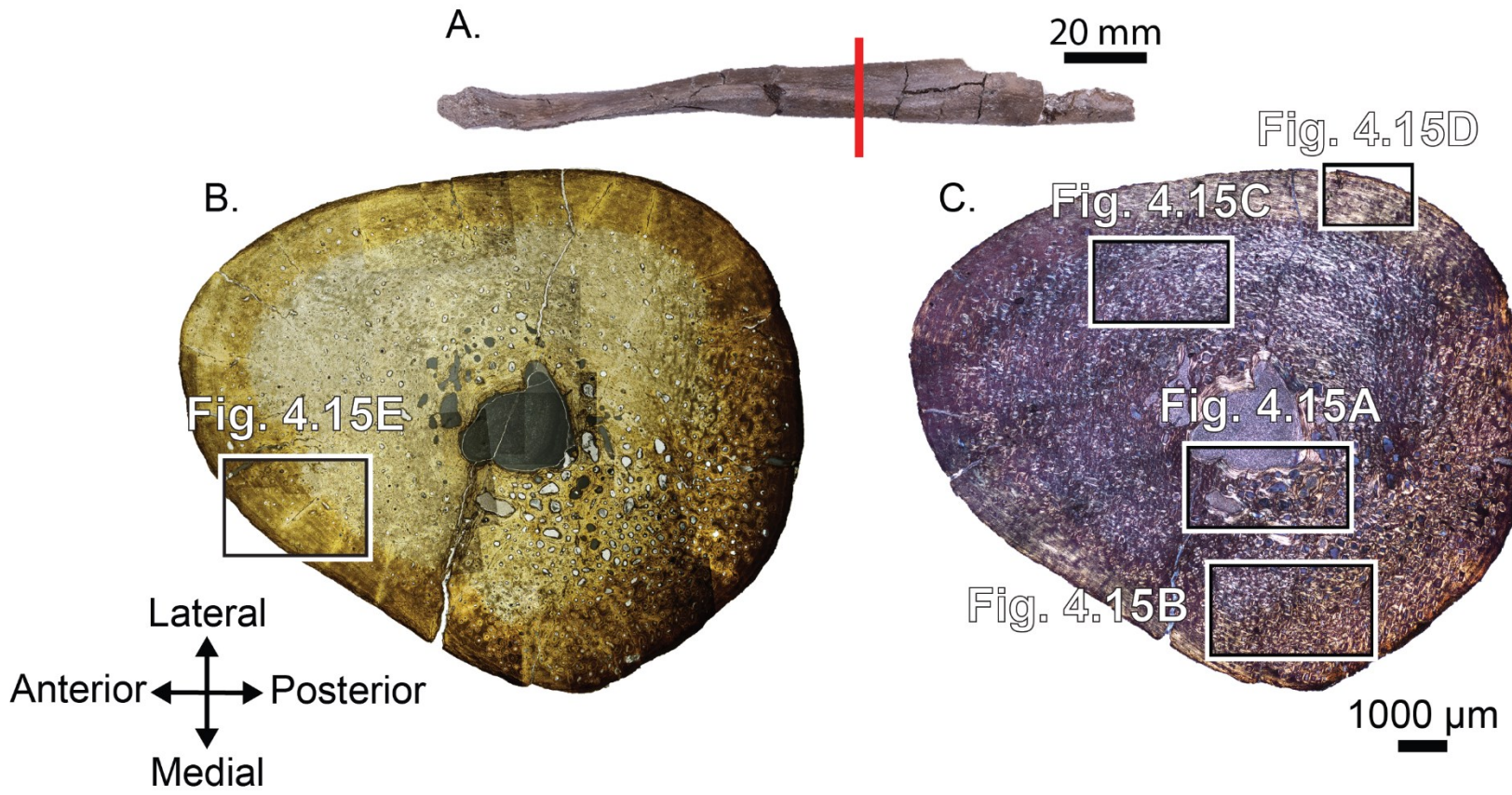
A.
20 mm
Fig. 4.15D
B.
C.
Fig. 4.15C
Fig. 4.15E
Fig. 4.15A
Fig. 4.15B
Lateral
Anterior
Posterior
Medial
1000 µm

Figure 4.15. Fibula osteohistology of the Wapiti thescelosaurid.

The location of the thin section as denoted by the red line on the fibula in medial view (A). Entire cross-section of UALVP 50999 in plane polarized light and cross polarized light and the close-up locations are in figure 4.13 (B, C).

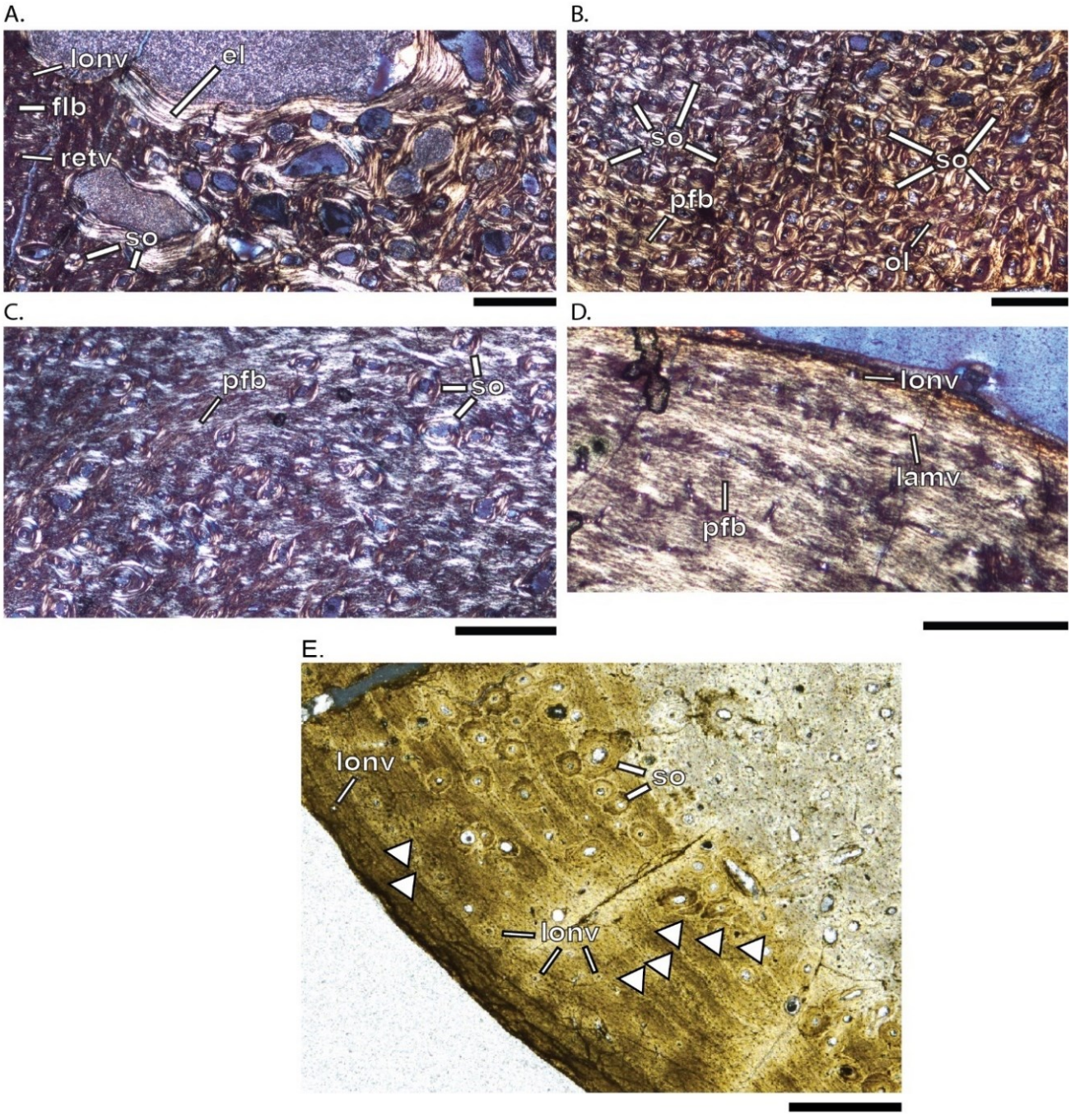
A.
lonv
el
flb
retv
so
B.
so
so
pfb
ol
C.
pfb
so
D.
lonv
lamv
pfb
E.
lonv
so
lonv

Figure 4.16. Osteohistological points of interests in the Wapiti thescelosaurid fibula.

Close-up of the medullary cavity of the fibula with endosteal lamellae, course cancellous bone, and well-developed secondary osteons in cross-polarized light (A). Well-developed dense Haversian bone in the posterior cortex of the fibula in cross-polarized light (B). Close-up of the inner cortical bone with well-developed secondary osteons on the lateral side of the fibula in cross-polarized light (C). Lateral margin of the outer cortex in cross-polarized light (D). Cortical bone with the distinctive color change from the outer and inner cortex on the anteromedial margin of the fibula under plane-polarized lights with LAGs, secondary osteons, vasculature (E). Abbreviations: el, endosteal lamellae; flb, fibrolamellar bone; lamv, lamellar vasculature; longv, longitudinal vasculature; ol, osteocyte lacunae; pfb, paralleled-fibered bone; retv, reticular vasculature; so, secondary osteons. Scale bar = 500 μm.

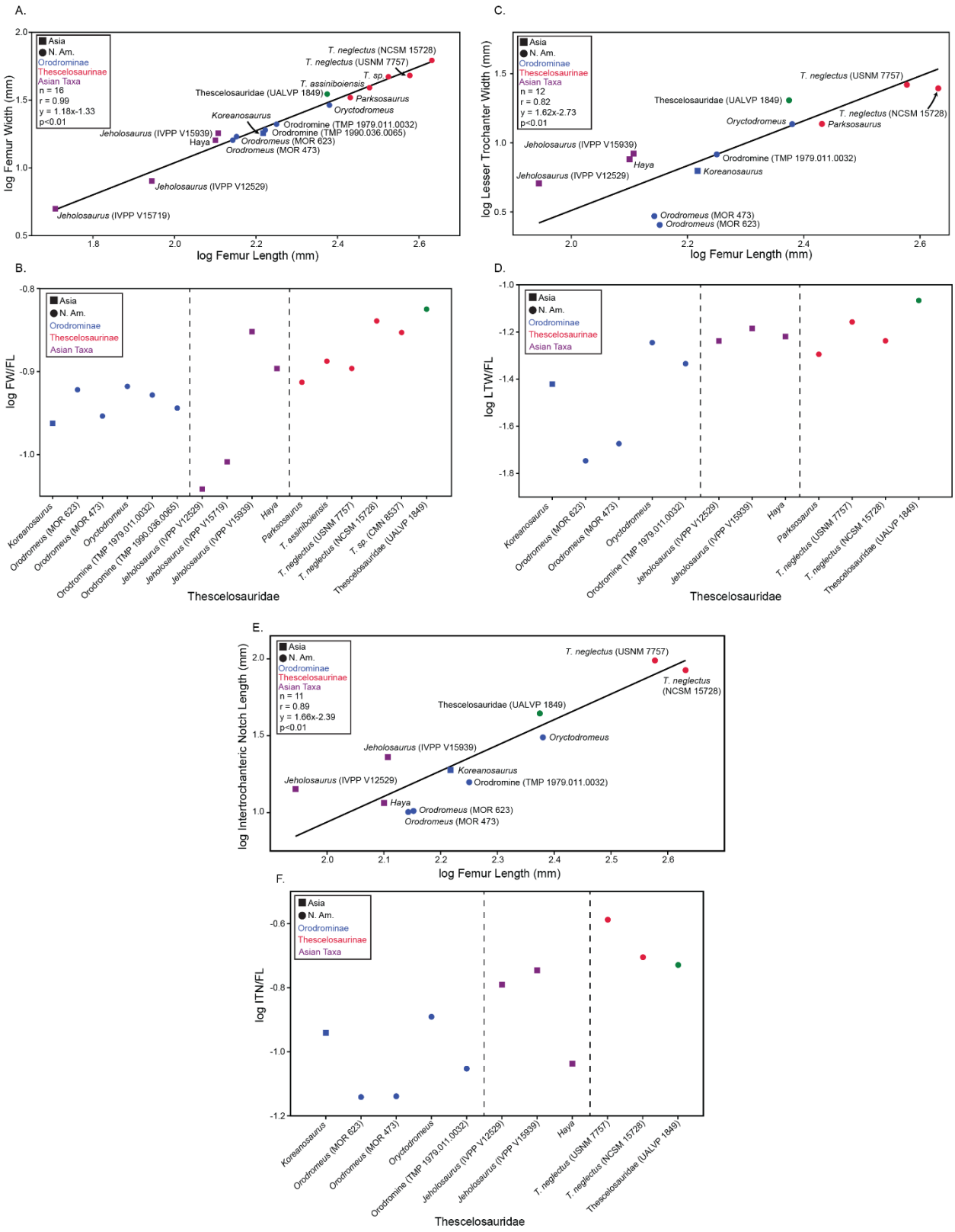
A.
Asia
N. Am.
Orodrominae
Thescelosaurinae
Asian Taxa
n = 16
r = 0.99
y = 1.18x-1.33
p<0.01
log Femur Width (mm)
log Femur Length (mm)
T. neglectus (NCSM 15728)
T. neglectus (USNM 7757)
T. sp.
T. assiniboiensis
Thescelosauridae (UALVP 1849)
Parksosaurus
Oryctodromeus
Koreanosaurus
Orodromine (TMP 1979.011.0032)
Orodromine (TMP 1990.036.0065)
Jeholosaurus (IVPP V15939)
Haya
Orodromeus (MOR 623)
Orodromeus (MOR 473)
Jeholosaurus (IVPP V12529)
Jeholosaurus (IVPP V15719)
C.
Asia
N. Am.
Orodrominae
Thescelosaurinae
Asian Taxa
n = 12
r = 0.82
y = 1.62x-2.73
p<0.01
log Lesser Trochanter Width (mm)
log Femur Length (mm)
T. neglectus (USNM 7757)
Thescelosauridae (UALVP 1849)
Oryctodromeus
T. neglectus (NCSM 15728)
Parksosaurus
Jeholosaurus (IVPP V15939)
Haya
Orodromine (TMP 1979.011.0032)
Jeholosaurus (IVPP V12529)
Koreanosaurus
Orodromeus (MOR 473)
Orodromeus (MOR 623)
B.
Asia
N. Am.
Orodrominae
Thescelosaurinae
Asian Taxa
log FW/FL
Thescelosauridae
Koreanosaurus
Orodromeus (MOR 623)
Orodromeus (MOR 473)
Oryctodromeus
Orodromine (TMP 1979.011.0032)
Orodromine (TMP 1990.036.0065)
Jeholosaurus (IVPP V12529)
Jeholosaurus (IVPP V15719)
Jeholosaurus (IVPP V15939)
Haya
Parksosaurus
T. assiniboiensis
T. neglectus (USNM 7757)
T. neglectus (NCSM 15728)
T. sp. (CMN 8537)
Thescelosauridae (UALVP 1849)
D.
Asia
N. Am.
Orodrominae
Thescelosaurinae
Asian Taxa
log LTW/FL
Thescelosauridae
Koreanosaurus
Orodromeus (MOR 623)
Orodromeus (MOR 473)
Oryctodromeus
Orodromine (TMP 1979.011.0032)
Jeholosaurus (IVPP V12529)
Jeholosaurus (IVPP V15939)
Haya
Parksosaurus
T. neglectus (USNM 7757)
T. neglectus (NCSM 15728)
Thescelosauridae (UALVP 1849)
E.
Asia
N. Am.
Orodrominae
Thescelosaurinae
Asian Taxa
n = 11
r = 0.89
y = 1.66x-2.39
p<0.01
log Intertrochanteric Notch Length (mm)
log Femur Length (mm)
T. neglectus (USNM 7757)
T. neglectus (NCSM 15728)
Thescelosauridae (UALVP 1849)
Oryctodromeus
Jeholosaurus (IVPP V15939)
Koreanosaurus
Jeholosaurus (IVPP V12529)
Orodromine (TMP 1979.011.0032)
Haya
Orodromeus (MOR 623)
Orodromeus (MOR 473)
F.
Asia
N. Am.
Orodrominae
Thescelosaurinae
Asian Taxa
log ITN/FL
Thescelosauridae
Koreanosaurus
Orodromeus (MOR 623)
Orodromeus (MOR 473)
Oryctodromeus
Orodromine (TMP 1979.011.0032)
Jeholosaurus (IVPP V12529)
Jeholosaurus (IVPP V15939)
Haya
T. neglectus (USNM 7757)
T. neglectus (NCSM 15728)
Thescelosauridae (UALVP 1849)

Figure 4.17. Reduced major axis regression bivariate plots of log-transformed femoral measurements.

Femoral length was compared with various femoral muscle attachment related variables between Asian Taxa (purple), Orodrominae (blue), Thescelosaurinae (red), and the Wapiti thescelosaurid (green). Log-transformed dependent variables include femur mid-shaft width (A), lesser trochanter width (C), and intertrochanteric notch length (E). Log-transformed ratio variation amongst thescelosaurids were compared between the denominator (femur length) and numerator variables including femur width (B), lesser trochanter width (D), and intertrochanteric notch length (F). Black line is the line of best fit. Shapes represent the biogeography of the taxa: Asia, squares; North America, circles. Vertical dotted lines separate Asian taxa, Orodrominae, and Thescelosaurinae in the ratio variation comparison.

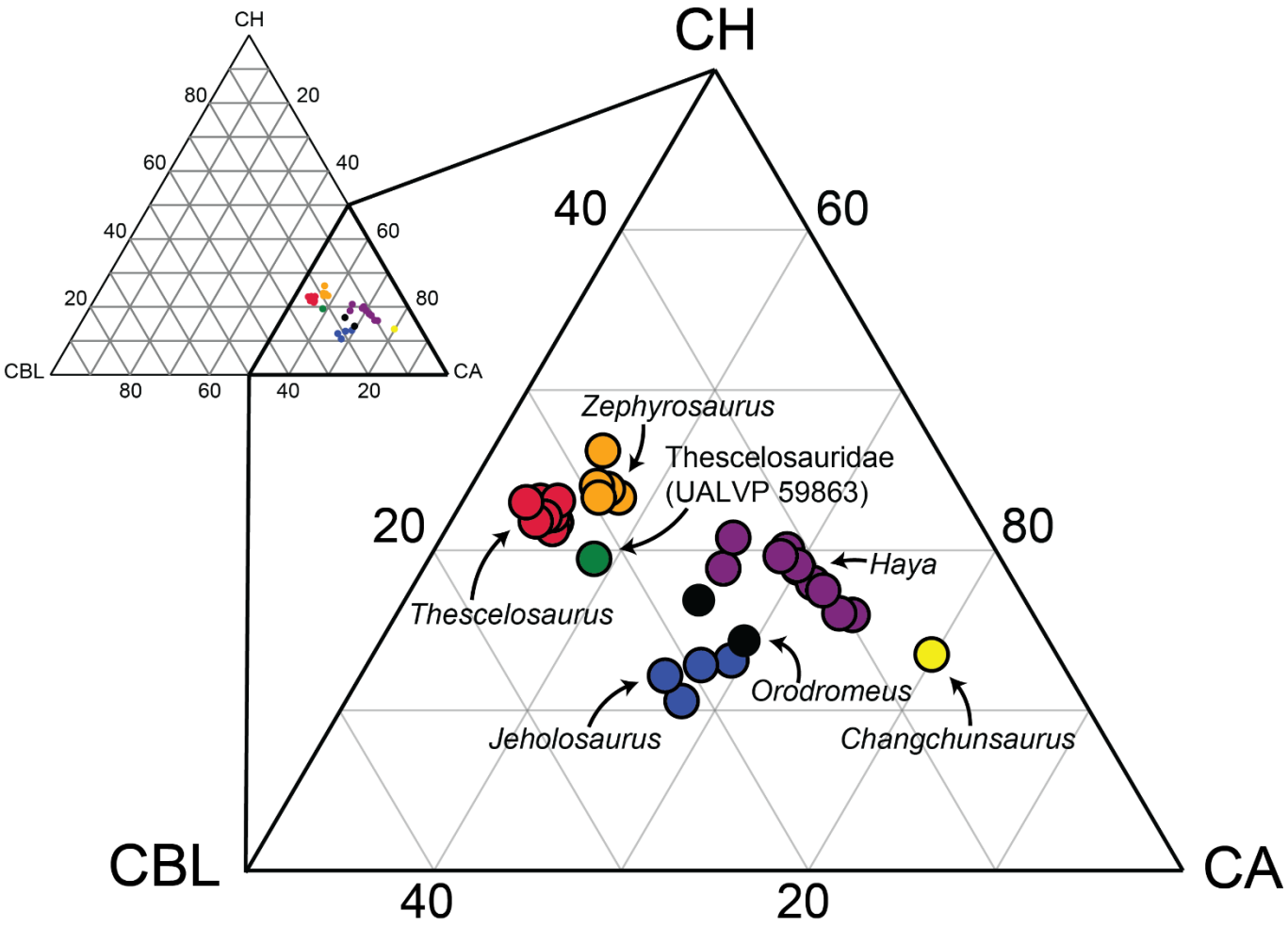

Figure 4.18. Ternary diagram of premaxillary tooth dimensions of the Wapiti thescelosaurid compared with other basal neornithischians.

Ternary diagram of premaxillary tooth dimensions of the Wapiti thescelosaurid (UALVP 59863; green) compared with other basal neornithischians. Tooth dimensions include the crown height, crown base length, and crown angle. *Changchunsaurus*, yellow; *Haya*, purple; *Jeholosaurus*, blue; *Orodromeus*, black; *Thescelosaurus*, red; *Zephyrosaurus*, orange.

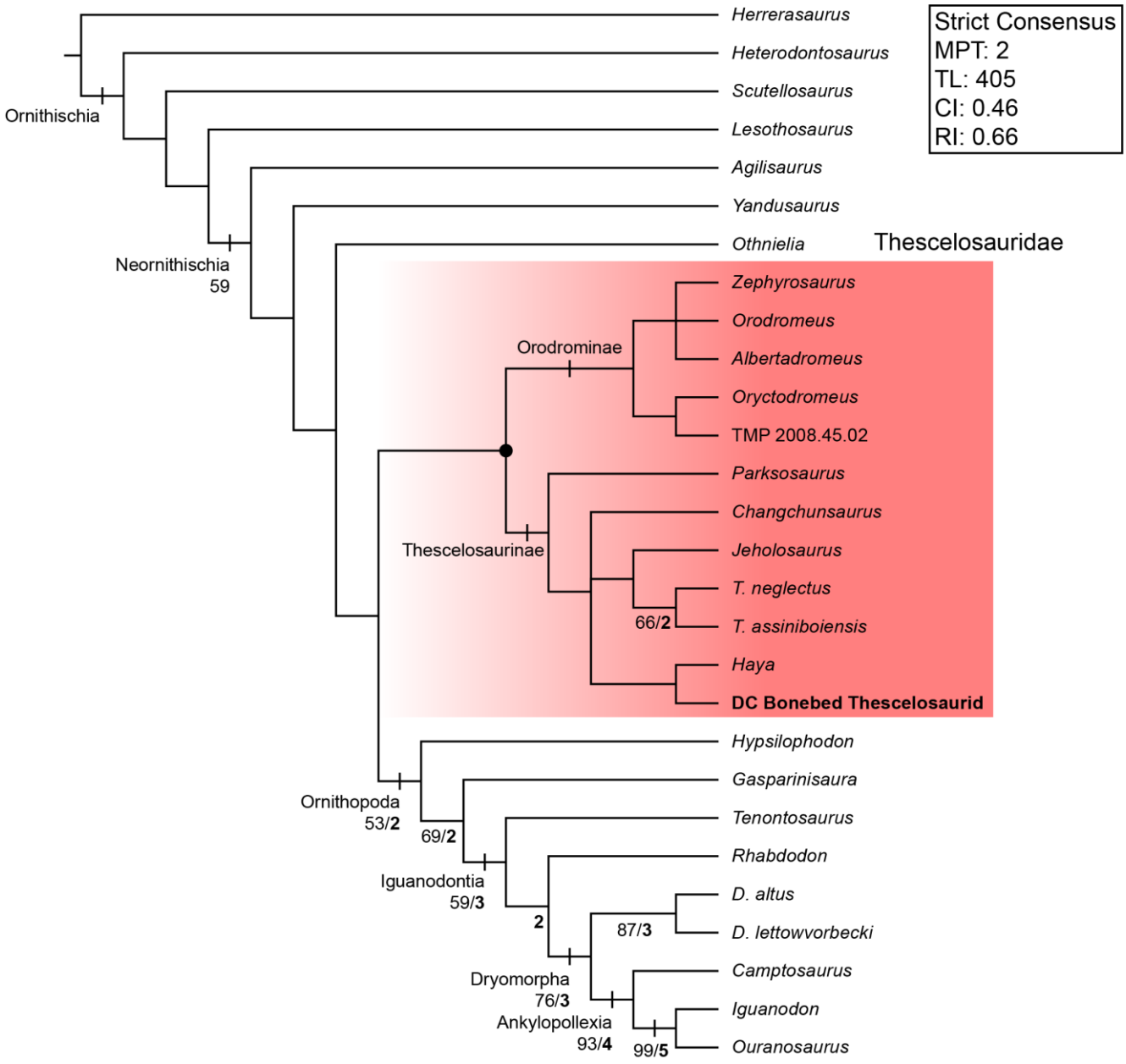
Strict Consensus
MPT: 2
TL: 405
CI: 0.46
RI: 0.66
Herrerasaurus
Heterodontosaurus
Scutellosaurus
Lesothosaurus
Agilisaurus
Yandusaurus
Othnielia
Thescelosauridae
Ornithischia
Neornithischia
59
Zephyrosaurus
Orodromeus
Albertadromeus
Oryctodromeus
TMP 2008.45.02
Parksosaurus
Changchunsaurus
Jeholosaurus
T. neglectus
T. assiniboiensis
Haya
DC Bonebed Thescelosaurid
Orodrominae
Thescelosaurinae
66/2
Hypsilophodon
Gasparinisaura
Tenontosaurus
Rhabdodon
D. altus
D. lettowvorbecki
Camptosaurus
Iguanodon
Ouranosaurus
Ornithopoda
53/2
69/2
Iguanodontia
59/3
2
87/3
Dryomorpha
76/3
Ankylopollexia
93/4
99/5

Figure 4.19. Strict consensus from phylogenetic analysis using matrix of Brown et al. (2013b).

Strict consensus tree that includes the Wapiti thescelosaurid into Brown et al. (2013b) character matrix. Most parsimonious trees (MPT) = 2, Tree length (TL) = 405 steps, consistency index (CI) = 0.46, and retention index (RI) = 0.66. Bold numbers are Bremer support values >1, and plain text numbers are bootstrap support values >50%.

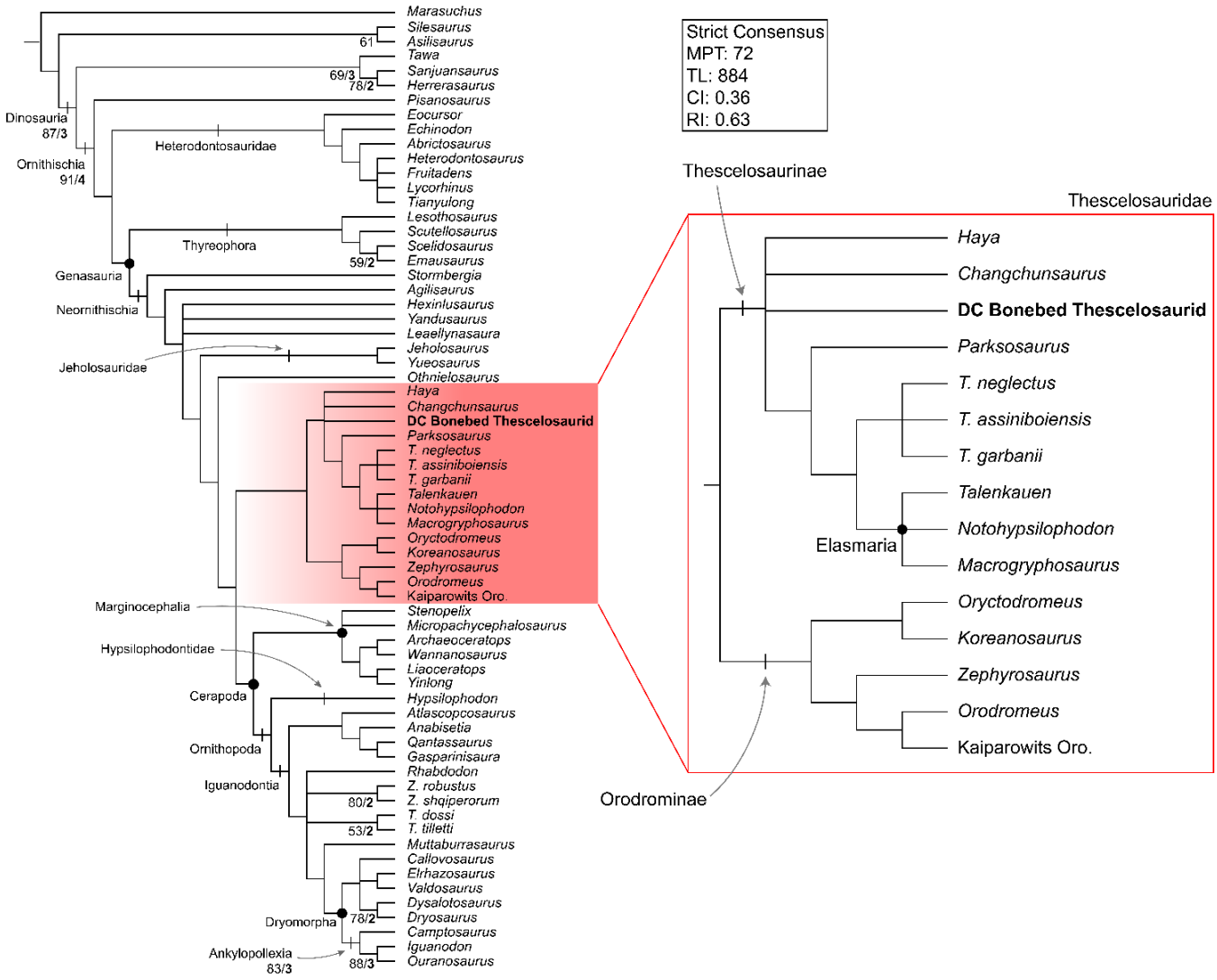
Marasuchus
Silesaurus
Asilisaurus
Tawa
Sanjuansaurus
Herrerasaurus
Pisanosaurus
Eocursor
Echinodon
Abrictosaurus
Heterodontosaurus
Fruitadens
Lycorhinus
Tianyulong
Lesothosaurus
Scutellosaurus
Scelidosaurus
Emausaurus
Stormbergia
Agilisaurus
Hexinlusaurus
Yandusaurus
Leaellynasaura
Jeholosaurus
Yueosaurus
Othnielosaurus
Haya
Changchunsaurus
DC Bonebed Thescelosaurid
Parksosaurus
T. neglectus
T. assiniboiensis
T. garbanii
Talenkauen
Notohypsilophodon
Macrogryphosaurus
Oryctodromeus
Koreanosaurus
Zephyrosaurus
Orodromeus
Kaiparowits Oro.
Stenopelix
Micropachycephalosaurus
Archaeoceratops
Wannanosaurus
Liaoceratops
Yinlong
Hypsilophodon
Atlascopcosaurus
Anabisetia
Qantassaurus
Gasparinisaura
Rhabdodon
Z. robustus
Z. shqiperorum
T. dossi
T. tilletti
Muttaburrasaurus
Callovosaurus
Elrhazosaurus
Valdosaurus
Dysalotosaurus
Dryosaurus
Camptosaurus
Iguanodon
Ouranosaurus
61
69/3
78/2
59/2
80/2
53/2
78/2
88/3
Dinosauria
87/3
Ornithischia
91/4
Heterodontosauridae
Thyreophora
Genasauria
Neornithischia
Jeholosauridae
Marginocephalia
Hypsilophodontidae
Cerapoda
Ornithopoda
Iguanodontia
Dryomorpha
Ankylopollexia
83/3
Strict Consensus
MPT: 72
TL: 884
CI: 0.36
RI: 0.63
Thescelosaurinae
Thescelosauridae
Haya
Changchunsaurus
DC Bonebed Thescelosaurid
Parksosaurus
T. neglectus
T. assiniboiensis
T. garbanii
Talenkauen
Notohypsilophodon
Macrogryphosaurus
Elasmaria
Oryctodromeus
Koreanosaurus
Zephyrosaurus
Orodromeus
Kaiparowits Oro.
Orodrominae

Figure 4.20. Strict consensus from phylogenetic analysis using matrix of Boyd (2015).

Strict consensus tree resulting from the addition of the Wapiti thescelosaurid to Boyd (2015) character matrix. Most parsimonious trees (MPT) = 72, tree length (TL) = 884 steps, consistency index (CI) = 0.36, and retention index (RI) = 0.63. Bold numbers are Bremer support values >1, and plain text numbers are bootstrap support values >50%.

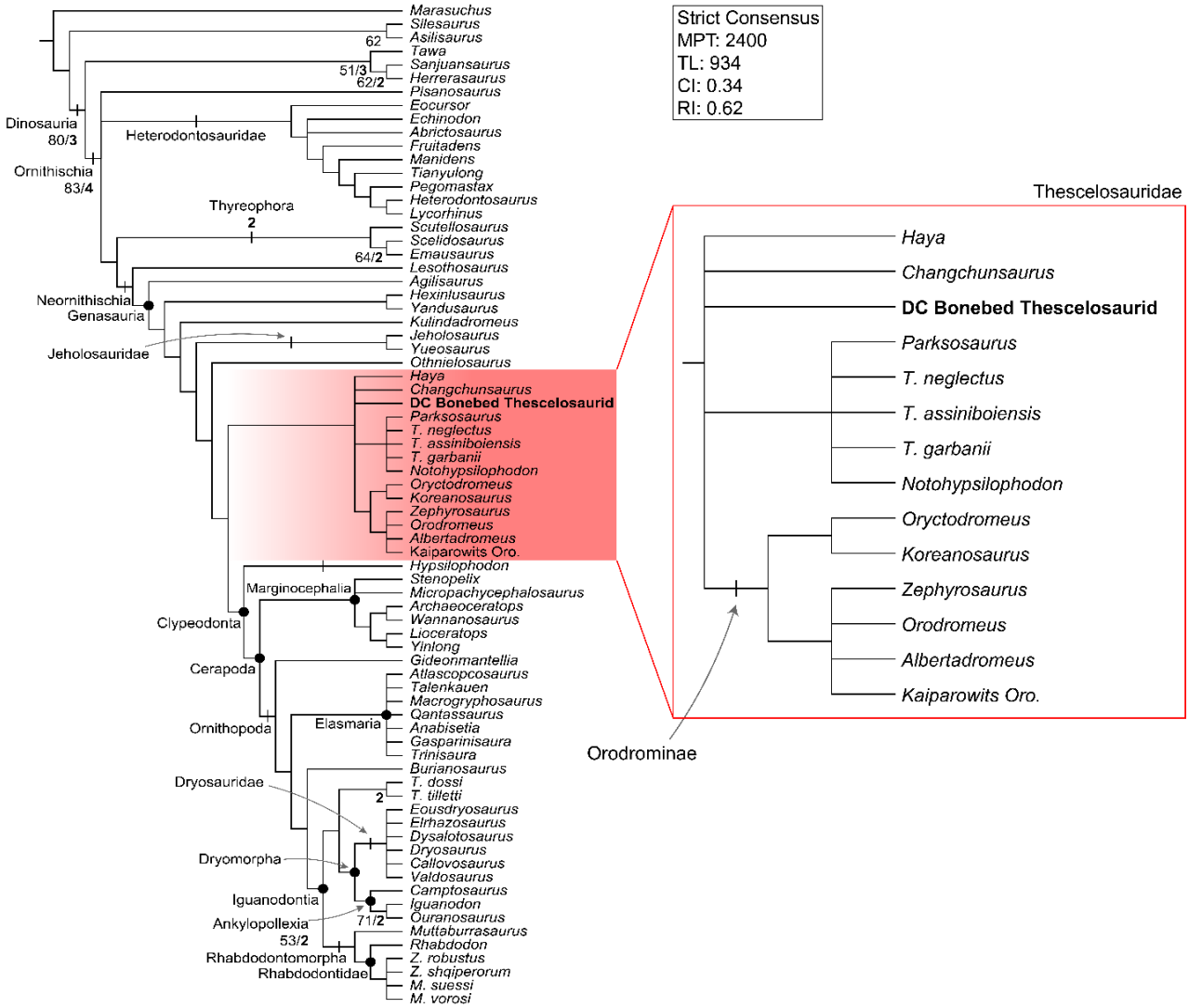
Strict Consensus
MPT: 2400
TL: 934
CI: 0.34
RI: 0.62
Marasuchus
Silesaurus
Asilisaurus
Tawa
Sanjuansaurus
Herrerasaurus
Pisanosaurus
Eocursor
Echinodon
Abrictosaurus
Fruitadens
Manidens
Tianyulong
Pegomastax
Heterodontosaurus
Lycorhinus
Scutellosaurus
Scelidosaurus
Emausaurus
Lesothosaurus
Agilisaurus
Hexinlusaurus
Yandusaurus
Kulindadromeus
Jeholosaurus
Yueosaurus
Othnielosaurus
Haya
Changchunsaurus
DC Bonebed Thescelosaurid
Parksosaurus
T. neglectus
T. assiniboiensis
T. garbanii
Notohypsilophodon
Oryctodromeus
Koreanosaurus
Zephyrosaurus
Orodromeus
Albertadromeus
Kaiparowits Oro.
Hypsilophodon
Stenopelix
Micropachycephalosaurus
Archaeoceratops
Wannanosaurus
Lioceratops
Yinlong
Gideonmantellia
Atlascopcosaurus
Talenkauen
Macrogryphosaurus
Qantassaurus
Anabisetia
Gasparinisaura
Trinisaura
Burianosaurus
T. dossi
T. tilletti
Eousdryosaurus
Elrhazosaurus
Dysalotosaurus
Dryosaurus
Callovosaurus
Valdosaurus
Camptosaurus
Iguanodon
Ouranosaurus
Muttaburrasaurus
Rhabdodon
Z. robustus
Z. shqiperorum
M. suessi
M. vorosi
62
51/3
62/2
Dinosauria
80/3
Heterodontosauridae
Ornithischia
83/4
Thyreophora
2
64/2
Neornithischia
Genasauria
Jeholosauridae
Marginocephalia
Clypeodonta
Cerapoda
Ornithopoda
Elasmaria
Dryosauridae
2
Dryomorpha
Iguanodontia
Ankylopollexia
71/2
53/2
Rhabdodontomorpha
Rhabdodontidae
Thescelosauridae
Haya
Changchunsaurus
DC Bonebed Thescelosaurid
Parksosaurus
T. neglectus
T. assiniboiensis
T. garbanii
Notohypsilophodon
Oryctodromeus
Koreanosaurus
Zephyrosaurus
Orodromeus
Albertadromeus
Kaiparowits Oro.
Orodrominae

Figure 4.21. Strict consensus from phylogenetic analysis using matrix of Madzia et al. (2018).

Strict consensus tree resulting from the addition of the Wapiti thescelosaurid to Madzia et al. (2018) character matrix. Most parsimonious trees (MPT) = 2400, tree length (TL) = 934 steps, consistency index (CI) = 0.34, and retention index (RI) = 0.62. Bold numbers are Bremer support values >1, and plain text numbers are bootstrap support values >50%.

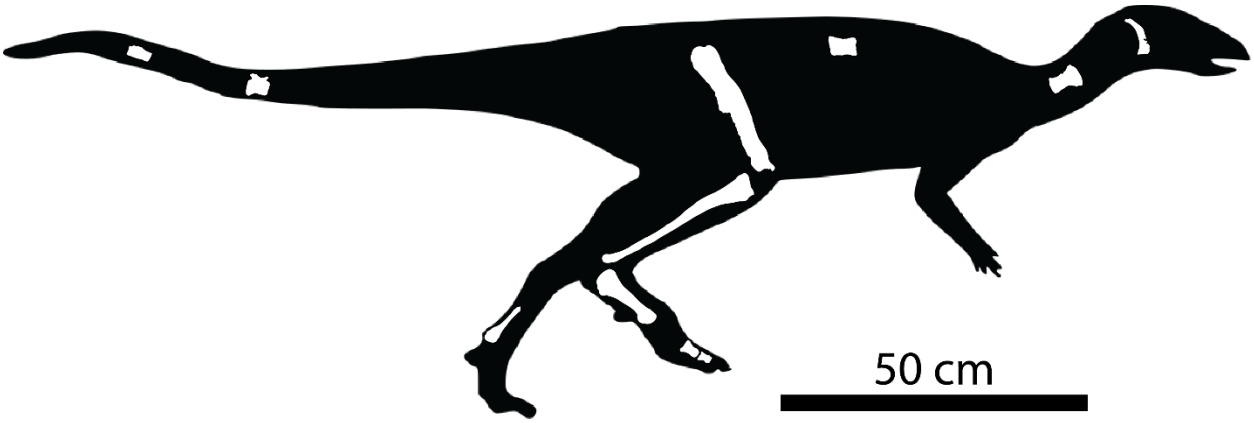

Figure 4.22. Skeletal reconstruction of the Wapiti thescelosaurid.

Known skeletal material is shown in white.

Chapter 5. Qualitative and Quantitative Assessment of Dental Differences between *Stegoceras validum* (Ornithischia: Pachycephalosauridae) and *Thescelosaurus neglectus* (Ornithischia: Thescelosauridae), with Implications for Paleoecology and Isolated Tooth Identification

5.1. Introduction

Vertebrate microfossil sites are taxonomically rich sources of fossilized vertebrate material from multiple individuals on the mm - cm scale. These assemblages have provided the basis for much of our understanding of extinct community level ecosystems (Eberth, 1990; Roger and Brady, 2010). Pachycephalosauridae and Thescelosauridae are clades of small ornithischian herbivores that co-occur in the Late Cretaceous of North America, but which are not especially closely related within Ornithischia (Boyd, 2015; Madzia et al., 2018) (Fig. 5.1). Pachycephalosaurids are derived cerapodan ornithischians and are consistently placed together with ceratopsids in the clade Marginocephalia (Boyd, 2015; Butler et al., 2008; Dieudonné et al., 2020; Madzia et al., 2018; Sereno, 1986). The phylogenetic position of thescelosaurids within Ornithischia is contentious, but they are considered basal neornithischians (non-cerapodans), sister to cerapodans (Boyd, 2015; Madzia et al., 2018).

Pachycephalosaurids and thescelosaurids have a comparatively sparse fossil record due to the vulnerability of their gracile skeletons to post-mortem destruction (Brown et al., 2013a; O'Gorman and Hone, 2012). However, the skulls of pachycephalosaurids, and particularly their thick frontoparietal domes, are disproportionally abundant in the fossil record compared to thescelosaurid cranial material (Brown et al., 2013a, b). Many isolated teeth belonging to these groups have been collected from Campanian-Maastrichtian microfossil localities in North

America, but are difficult to precisely identify owing to a lack of conspicuous diagnostic features. The teeth of pachycephalosaurids and thescelosaurids are difficult to tell apart because they show many plesiomorphic ornithischian features, with limited variation in dental morphology both within and between the two groups (Brown and Druckenmiller, 2011; Maryańska et al., 2004; Norman et al., 2004a, b). Brown and Druckenmiller (2011) have elucidated some of the minute differences and variation that exist among thescelosaurids, but no equivalent studies have examined pachycephalosaurids. Moreover, pachycephalosaurids and thescelosaurids occur together in multiple Upper Cretaceous formations in North America, including the Dinosaur Park Formation, Hell Creek Formation, Horseshoe Canyon Formation, and Prince Creek Formation (Table 5.1). Thus, isolated teeth from these units cannot typically be assigned to one group or the other based on provenance alone (Brown et al., 2011; Brown et al., 2013b; Eberth et al., 2013; White et al., 1998). The sympatric coexistence of similarly sized herbivorous dinosaur groups (Ankylosauria, Ceratopsidae, Hadrosauridae, Leptoceratopsidae, Pachycephalosauridae, and Thescelosauridae) in the Late Cretaceous has been explained by niche partitioning reflected in differences in craniodental morphology. However, differences in tooth structures have not been established in pachycephalosaurids and thescelosaurids (Mallon and Anderson, 2013; Wyenberg-Henzler, 2020). How pachycephalosaurids and thescelosaurids managed to limit the effects of mutual competition is poorly understood, but one possibility is that the two clades had divergent feeding strategies, which would presumably be indicated by identifiable albeit potentially subtle differences in their dentitions.

Given the problem of accurately identifying isolated pachycephalosaurid and thescelosaurid teeth, I set out to establish differences in dental morphology between the two

groups by qualitatively describing and quantitatively analyzing *in situ* tooth series preserved in specimens of the pachycephalosaurid *Stegoceras validum* and the thescelosaurid *Thescelosaurus neglectus*. *Stegoceras* and *Thescelosaurus* are excellent representatives of their respective clades for purposes of this study, as specimens with well-preserved dentitions are available (Fig. 5.2 and 5.3) (Eberth et al., 2013; White et al., 1998; Wyenberg-Henzler, 2020). Although *Stegoceras* and *Thescelosaurus* do not represent contemporaneous taxa, the former being Campanian in age and the latter Maastrichtian (Boyd, 2014; Eberth et al., 2013; Gilmore 1913; Ogg and Hinnov, 2012; Sullivan, 2003), this study has the potential to be a significant step towards establishing clade-level differences in dental morphology between pachycephalosaurids and thescelosaurids. The results have implications both for accurate identification of isolated small ornithischian teeth from the Late Cretaceous of North America, and for scientific understanding of pachycephalosaurid and thescelosaurid paleoecology.

5.2. Materials and Methods

5.2.1. Specimens and Description of Teeth

In situ teeth from well-preserved skulls of the pachycephalosaurid *Stegoceras validum* (UALVP 2) and the thescelosaurid *Thescelosaurus neglectus* (NCSM 15728) were examined in this study. Osteological descriptions and linear measurements were taken from five premaxillary, 20 maxillary, and five dentary teeth of *Stegoceras*, and from eight premaxillary, 15 maxillary, and six dentary teeth of *Thescelosaurus*. Terminology used in this paper to describe dental features is based on Boyd (2014), Hendrickx et al. (2015), Smith and Dodson (2003), and Sues and Galton (1987).

Stegoceras validum (UALVP 2) is a pachycephalosaurid from the Upper Campanian (76.9-75.8 Ma) Dinosaur Park Formation, Alberta, Canada (Fowler, 2016; Lambe, 1902; Ogg and Hinnov, 2012; Sues and Galton, 1987). Four dental morphotypes are identifiable in *Stegoceras*. The premaxillary (5) and maxillary (20) teeth are relatively uniform and are separated by a diastema. By contrast, distinct tooth morphotypes occupy different parts of the dentary, the anterior teeth (3) being distinct from the posterior ones (2) (Fig. 5.2). Wear facets occur on the premaxillary, maxillary, and dentary teeth, and reflect occlusal contacts during the animal's life. The maxillary and dentary teeth are arranged *en echelon*, and the distal margin of each tooth buccally overlaps the mesial margin of the next tooth in the sequence (Maryańska et al., 2004).

Thescelosaurus neglectus (NCSM 15728) is a relatively large-bodied neornithischian thescelosaurid from the Maastrichtian (72.1-66 Ma) Hell Creek Formation, Montana, USA (Boyd, 2014; Fisher et al., 2000; Ogg and Hinnov, 2012). *Thescelosaurus* possessed heterodont dentition, as in typical basal ornithischians (Norman et al., 2004b). Five dental morphotypes were identified in *Thescelosaurus*. The premaxillary teeth (8) are uniform, but the maxilla (15) and dentary (6) each bear teeth that can be separated into two wear stages with two morphotypes, which are interspersed along the length of the maxilla and dentary (Fig. 5.3). The maxillary and dentary tooth crowns are arranged *en echelon*, the distal margin of each tooth overlapping the mesial margin of the posteriorly adjacent tooth on the buccal side (Boyd, 2014).

5.2.2. Linear Measurements

Linear measurements of in situ teeth were taken using the software package ImageJ from images of the teeth in lateral view. ImageJ allows for accurate measurements of specimens that

are too fragile or small to be measured directly, or of specimens that are not accessible physically (Schneider et al., 2012). In the present study, dental measurements were taken using ImageJ software due to the small and fragile nature of the well-preserved pachycephalosaurid and thescelosaurid skulls containing the teeth of interest.

The set of tooth measurements used in this study is modified from Buckley et al. (2010) and Hendrickx et al. (2015) (Fig. 5.4 and Table 5.2), and includes 12 measurements (11 linear and one angular) that were taken from a combined total of 59 in situ teeth of *Stegoceras validum* (UALVP 2) and *Thescelosaurus neglectus* (NCSM 15728). Crown height is defined as the maximum apicobasal length from the base of the cingulum to the apex of the crown. Crown base length is the maximum mesiodistal length of the cingulum. Mid-crown length is the mesiodistal length of the tooth at mid-point of the crown height. Neck length is the mesiodistal length of the tooth at its point of maximal constriction basal to the cingulum, measured perpendicular to crown height. Apical length is the maximum apicobasal length of the mesial margin of the crown, measured obliquely from the mesial end of the cingulum to the apex of the crown. Mesial carina length is the apicobasal distance from the most basal mesial denticle to the most apical mesial denticle. Distal carina length is the maximum apicobasal distance from the most basal distal denticle to the most apical distal denticle. Mesial denticle height is the height of the denticle that is closest to the mid-length of the mesial margin of the crown. Mesial denticle length is the mesiodistal length of the denticle that is closest to the mid-length of the mesial margin of the crown. Distal denticle height is the height of the denticle that is closest to the mid-length of the distal margin of the crown. Distal denticle length is the mesiodistal length of the denticle that is closest to the mid-length of the distal margin of the crown. Crown angle is the

angle between the line segments that define crown base length and apical length. In previous studies (Buckley et al., 2010; Hendrickx et al., 2015) crown angle was calculated using the cosine law, but in this study crown angle was measured using the angle tool in ImageJ by obtaining the angle between the crown base length and the crown height (Schneider et al., 2012).

5.2.3. Multivariate Analysis

To correct the linear measurements for size and reduce the effects of allometry in the analysis, they were all divided by crown base length. The measurements were then log-transformed to standardize the dataset. However, the *Thescelosaurus* premaxilla had no denticles and the measurements could not be directly log-transformed because they were equal to zero. To overcome the error inherent in log-transforming data points equal to zero, I added 0.001 to each measurement prior to transformation (Corruccini, 1987). A principal components analysis (PCA), a linear discriminant analysis (LDA), Mann-Whitney *U* tests, and a PERMANOVA were performed using Paleontological Statistics (PAST) version 3.25 (Hammer et al., 2001) on the size-corrected, log-transformed linear measurements of *in situ* worn and unworn teeth of *Stegoceras* and *Thescelosaurus*. Each analysis was carried out both with and without worn teeth. However, the results of this study excluded worn teeth because they presented few differences when compared. This study uses the univariate and multivariate analyses of excluded worn teeth of *Stegoceras* and *Thescelosaurus* to prevent skewing of the data. The differences between univariate and multivariate results among the inclusion and exclusion of worn teeth is discussed further in the result section of the paper.

PCA was used to find mutually orthogonal axes that expressed as much of the variation within the data set as possible, and was performed using the multivariate ordination PCA

function in PAST (Hammer and Harper, 2006). A correlation matrix was produced during the analysis, which generated PC loadings, PC scores, and a scree plot with the broken stick model. Principal components that were smaller than the corresponding value in the broken stick model were regarded as insignificant (Jackson, 1993; see appendices).

LDA is based on the one-dimensional projection of a multivariate data set that maximizes the separation between two groups that have been defined *a priori*, and is an excellent method for testing hypotheses of similarity and difference between established groups (Hammer and Harper, 2006). An LDA was performed on the size-corrected and log-transformed linear tooth measurements from *Stegoceras validum* and *Thescelosaurus neglectus* using the multivariate ordination LDA function in PAST, and a confusion classification matrix was produced. Significant separation was assessed in terms of the percentage of specimens accurately assigned to *Stegoceras* and *Thescelosaurus* based on their position on the discriminant axis, and using Hotelling's t^2. For example, had the two groups not overlapped at all on the LDA axis, the data set would have been considered 100% correctly classified within the confusion classification matrix, with a statistically significant Hotelling's t^2 test. Classification of specimens with 90% accuracy was accepted as the threshold for statistical recognition of two distinct groups (Hammer and Harper, 2006). Non-parametric statistical analyses, namely the Mann-Whitney *U* test and the multivariate PERMANOVA analysis, were performed on size corrected, log-transformed measurements. The PERMANOVA was performed on the linear measurements only, whereas the Mann-Whitney *U* test was performed on the entire data set including crown angle. The Mann-Whitney *U* test is used when the data are non-parametric and the sample size is small, and tests for univariate median differences between two a priori groups (Hammer and Harper, 2006).

The PERMANOVA is a statistical test used when sample sizes are small, non-normally distributed, and tests for differences between two or more groups of multivariate data (Hammer and Harper, 2006). The Mahalanobis similarity index, as opposed to the traditional Euclidean similarity index, was used for the PERMANOVA because the former is more suitable for non-spherically symmetric data (Mahalanobis, 1936). Statistical significance was estimated using a permutation of 10,000 replicates across *a priori* groups. The PERMANOVA test performed a F-test and calculated the pairwise comparison Bonferroni-corrected p-value to offset the probability of committing a type I error. The Mann-Whitney *U* test was performed using the univariate two-sample test function in PAST, and the PERMANOVA was analyzed using the multivariate test one-way PERMANOVA function (Hammer and Harper, 2006). The multivariate and univariate analyses were repeated with worn teeth of *Stegoceras* and *Thescelosaurus* excluded, but the results were similar to those obtained from the analysis of the full data set.

Multivariate analyses cannot be performed if data points are missing, a common problem in paleontological studies. Numerous methods, such as deletion, substitution, and averages of known observations, have been put forward by previous authors to address this issue (Brown et al., 2012). However, these methods tend to decrease the statistical power of analyses by introducing error, estimating invalid negative values of missing observations, biasing parameters, underestimating variance, and leading to inaccurate assessments of statistical significance (Brown et al., 2012; Strauss et al., 2003). In this study, missing data was estimated by imputation using the R package "missMDA" (Husson and Josse, 2016; R Core Team, 2013). The imputation method accurately estimates missing data by utilizing the regularized iterative principal

components analysis algorithm, which substitutes the column mean and iteratively runs the principal components analysis to improve estimates (Husson and Josse, 2016; Josse et al., 2012; R Core Team, 2013; Strauss et al., 2003). A number of tooth measurements were missing from both *Stegoceras validum* and *Thescelosaurus neglectus* owing to damage, hidden teeth, and limited image quality, so that the combined *Stegoceras* and *Thescelosaurus* data set was missing 6.9% of the data. Specifically, the data set for *Stegoceras* was missing 8.3% of the data, mainly distal denticle height values. The *Thescelosaurus* data set was missing 5.5% of the data, mainly crown base length values.

5.3. Results

5.3.1. Descriptions

5.3.1.1. Premaxillary Teeth

The premaxillary tooth crowns of *Stegoceras* (UALVP 2) are characteristically taller than long and buccolingually compressed, with pointed and recurved apices (Fig. 5.2 and Table 5.3) (Sues and Galton, 1987) and average crown height, crown base length, and crown angle values of 5.1 mm, 4.3 mm, and 56.9°, respectively (Table 5.4; consult this table for other average measurements). *Stegoceras* possesses three teeth in each premaxilla, as in other pachycephalosaurids such as *Goyocephale* and *Prenocephale* (Maryańska et al., 2004). The base of the crown lacks a cingulum, but forms a bulbous swelling, basal to which is a constricted neck (Fig. 5.2). The crown thins buccolingually toward the apex to a greater degree than in *Thescelosaurus*, in which the apical portion of the crown is more robust, as noted by Boyd (2014). The lingual surface of the crown bears a central ridge that extends from the base of the

crown to the apex. The cross-sections of the root and crown are circular and oval, respectively, whereas that of the mid-crown is elliptical. The enamel surface texture is smooth and is the same on all sides of the crown. A wear facet is present on the apical part of the lingual side and can be interpreted as a result of biting hard food material or occluding with the predentary (Fig. 5.5) (Sues and Galton, 1983). The crowns each possess eight denticles on their mesial margins, and nine to eleven on their distal margins. Marginal denticles are also common in other pachycephalosaurids (Maryańska et al., 2004; Sues and Galton, 1987). Thescelosaurine premaxillary teeth typically lack denticulated crown margins, as exemplified by *Changchunsaurus*, *Haya*, *Jeholosaurus*, *Thescelosaurus*, and *Zephyrosaurus*, but denticles are present in the orodromine *Orodromeus* (Barrett & Han, 2009; Boyd, 2014; Jin et al., 2010; Makovicky et al., 2011; Scheetz, 1999).

NCSM 15728 possesses six teeth in each premaxilla, like the thescelosaurid *Jeholosaurus* (Barrett & Han, 2009), and the basal ornithischian *Lesothosaurus* (Sereno, 1991). Pachycephalosaurids, in contrast, have three teeth per premaxilla (Galton & Sues, 1983; Maryańska et al., 2004). Some thescelosaurids, such as *Changchunsaurus*, *Haya*, and *Zephyrosaurus*, reportedly have only five teeth in each premaxilla (Makovicky et al., 2011; Sues, 1980; Zan et al., 2005). However, the differences in premaxillary tooth count that have been documented in thescelosaurids are likely due to ontogeny, the specimens with lower tooth counts representing immature individuals (Boyd, 2014).

The premaxillary teeth of *Thescelosaurus* (NCSM 15728) are only exposed in buccal view, and are bulbous in shape. Their crowns have elliptical cross-sections (Table 5.3) but the cross-sections of the roots are elliptical anteriorly and become progressively more circular

posteriorly (Boyd, 2014). Among other thescelosaurids, the tooth roots of *Jeholosaurus* are elliptical throughout the premaxillary tooth series, whereas those of *Zephyrosaurus* are circular throughout (Barrett & Han, 2009; Sues, 1980). The crowns are slightly buccolingually compressed and slightly constricted at their bases, each forming a distinct neck (Fig. 5.3). Crown height is less than or approximately equal to crown base length, these measurements respectively averaging 5.0 mm and 5.2 mm (Table 5.4). In buccal view, the crown apices are blunt and recurved, with an average crown angle of 52.3°. The distal and mesial margins of the tooth crowns lack carinae and denticles, as in *Changchunsaurus*, *Haya*, and *Jeholosaurus* (Barrett & Han, 2009; Jin et al., 2010; Makovicky et al., 2011). By contrast, carinae and denticles are present in the orodromine *Orodromeus* (Scheetz, 1999) and the pachycephalosaurid *Stegoceras* (Galton and Sues, 1983). As in other thescelosaurids and the pachycephalosaurid *Stegoceras*, the base of the crown does not possess a cingulum (Barrett & Han, 2009; Galton & Sues, 1983; Jin et al., 2010; Makovicky et al., 2011). The enamel surface is ornamented with fine, apicobasally oriented ridges, and this texture is present on all sides of the crown (Fig. 5.3). The enamel ornamentation ridges appear unique to *Thescelosaurus*, and are absent in *Changchunsaurus*, *Jeholosaurus*, and *Zephyrosaurus* (Barrett & Han, 2009; Jin et al., 2010; Sues, 1980). Wear facets are present on the distal margins of the buccal surfaces of the crowns (Fig. 5.5).

5.3.1.2. Maxillary Teeth

The 20 maxillary crowns of *Stegoceras* (UALVP 2) appear broad and asymmetric in buccal view, and are buccolingually compressed like those of other pachycephalosaurids (Table 5.3) (Maryańska et al., 2004). The crowns are longer than tall, with pointed, posteriorly directed apices and average crown height, crown base length, and crown angle measurements of 3.9 mm,

4.6 mm, and 46°, respectively (Table 5.4). The buccal sides of the crowns are concave mesiodistally, with a central ridge oriented apicobasally, and the lingual sides are convex (Maryańska et al., 2004). On either side of the tooth, the bases of the crowns are inclined distobasally relative to the alveolar margin of the maxilla in lingual view, whereas the bulbous bases of the crowns are parallel with the alveolar margin in buccal view (Fig. 5.2). When unworn, the bulbous base of the crown is asymmetric in lingual view with the mesial half projecting further lingually than the distal half. The maxillary tooth roots are oval in cross-section, whereas the cross-sections of the crowns vary from oval to reniform (Sues and Galton, 1983). The lingual surfaces of the crowns bear either a single wear facet on the mesial side, or wear facets on both the mesial and distal sides (Fig. 5.5). In the crowns with two facets, the mesial facet is larger than the distal one (Sues and Galton, 1983). The wear facet pattern is not dependent on position in the tooth row; instead, distal facets tend to appear in more heavily worn teeth. The mesial facets were presumably produced by occlusion with the distal edges of the buccal sides of the dentary crowns (Maryańska et al., 2004). In addition, it appears that the maxillary distal wear facets of the lingual surface only occur at advanced wear stages (Fig. 5.5). These wear pattern are potentially unique among pachycephalosaurids. The maxillary crowns of *Goyocephale*, *Homalocephale*, and *Tylocephale* tend to have extensive wear along the lingual surfaces, which is interpreted as the result of a continuous occlusal plane over the maxillary series (Maryańska et al., 2004). In *Prenocephale*, a narrow wear facet is present along the basal margin of each maxillary crown (Maryańska et al., 2004).

In *Stegoceras*, a distinct neck constriction and cingulum are present at the base of each maxillary tooth crown, as in basal (non-genasaurian) ornithischians (Boyd, 2015; Norman et al.,

2004b). The enamel texture is smooth on all sides of the crown (Sues and Galton, 1983). Mesial and distal marginal denticles are present, and the largest denticle is at the apicobasal midpoint of each margin; every denticle continues as a weak ridge on the buccal surface (Maryańska et al., 2004; Sues and Galton, 1983). Unlike thescelosaurids, the ridges that are associated with the denticles do not extend to the base of the crown (Boyd, 2014; Barrett and Han, 2009; Jin et al., 2010; Parks, 1926; Sues, 1980). The number of denticles on each margin varies from six to eight, but the mesial margin usually bears one or two more denticles than the distal margin (Sues and Galton, 1983). At the base of the distal denticle margin, the carina turns mesially to extend across the distal portion of the lingual surface of the tooth, dorsal to the cingulum. The resulting features form a "ledge" on the distolingual surface. This feature, which some authors have described as a lingually curved distal carina, is observed in *Orodromeus* (Scheetz, 1999), *Zephyrosaurus* (Galton, 1999; Sues, 1980), and the Upper Jurassic ornithischian *Nanosaurus* (Scheetz, 1999). This feature is not always limited to the maxillary teeth, as it is present on the dentary teeth of an indeterminate orodromine (Brown et al., 2013b). It is unclear if NCSM 15278 (*Thescelosaurus*) had the lingually curved distal carina, as the lingual sides of the maxillary teeth are not exposed, but it is present in the *Thescelosaurus* specimens CMN 8537 and SDSM 7210 (Brown et al., 2013b; Galton, 1995; Galton, 1999; Sternberg, 1940). However, this feature is not observed in the dentary teeth of *Parksosaurus* (ROM 804), nor in isolated teeth potentially attributable to *Thescelosaurus* (UAMES 3567 and UAMES 7863) from the Prince Creek Formation (Brown and Druckenmiller 2011). The carinal ledge is not present in other pachycephalosaurid taxa (Maryańska et al., 2004; Maryańska and Osmólska, 1974) and makes

UALVP 2 the first pachycephalosaurid observed to have this feature despite previous descriptions (Bakker et al., 2006; Galton and Sues, 1983; Sullivan, 2006).

Overall, the maxillary teeth of *Thescelosaurus* (NCSM 15728) have the broad appearance typical in basal ornithischians (Norman et al., 2004b), appearing symmetrical in buccal view but with the apices shifted slightly posteriorly in worn teeth (Fig 5.3 and 5.5) (Boyd, 2014). Unfortunately, the lingual views of the maxillary teeth are obscured by skeletal elements. Based on CT scans presented by Boyd (2014), the unworn maxillary tooth roots are apicobasally straight, similar to other basal ornithischians (Norman et al., 2004b). Crown height is less than or approximately equal to crown base length, the two measurements averaging 4.4 mm and 5.4 mm respectively (Table 5.4). The crown apices are blunt and recurved, with an average crown angle of 41.4°. A cingulum is present at the base of the crown, as in basal neornithischians, pachycephalosaurids, and thescelosaurids (Barrett and Han, 2009; Galton & Sues, 1983; Jin et al., 2010; Maryańska et al., 2004; Scheetz, 1999). Basal to the crown is a constricted neck, as in the thescelosaurids *Changchunsaurus*, *Jeholosaurus*, *Orodromeus*, and *Zephyrosaurus* (Barrett & Han, 2009; Jin et al., 2010; Scheetz, 1999; Sues, 1980). Mesial and distal marginal denticles are present on the maxillary crowns, each associated with a pronounced crescentic ridge that converge with the other ridges as they extend to near the base of the crown. This is similar to the morphologies seen in *Changchunsaurus*, *Haya*, *Jeholosaurus*, *Parksosaurus*, and *Zephyrosaurus* (Barrett and Han, 2009; Makovicky et al., 2011; Jin et al., 2010; Parks, 1926, Sues, 1980). The mesial and distal margins consistently bear an equal number of denticles, ranging from four to six. The associated ridges are not as pronounced in *Changchunsaurus*, *Haya*, *Jeholosaurus*, and *Zephyrosaurus*, and are absent in the orodromine *Orodromeus* and the pachycephalosaurid

Stegoceras (Barrett and Han, 2009; Galton and Sues, 1983; Jin et al., 2010; Makovicky et al., 2011; Scheetz, 1999; Sues, 1980). The enamel is consistently smooth, and the distribution of enamel is even across the buccal surface of the crown. Although the lingual surfaces of the maxillary teeth are obscured, the pattern of wear can be inferred based on how the maxillary and dentary crowns likely occluded. Based on what can be observed in NCSM 15278, the lingual surface of each posterior maxillary tooth appears to have occluded with one dentary tooth, possibly forming a single wear facet on the entire lingual surface of the tooth row. The anterior maxillary teeth are offset with the dentary teeth, and would have formed wear facets on the mesial and distal margins of their lingual surfaces (Boyd, 2014).

In *Thescelosaurus* (NCSM 15728), worn maxillary crowns appear asymmetrical in buccal view, and lack the broad appearance typical of the maxillary teeth of basal ornithischians (Norman et al., 2004b). The average crown height of worn maxillary teeth is only 2.9 mm, significantly less than in unworn maxillary teeth, whereas the average crown base length of unworn maxillary teeth is similar to that of worn teeth at 4.9 mm. The crown angle of worn maxillary teeth averages 28.8°, which is substantially less than in unworn maxillary teeth.

5.3.1.3. Dentary Teeth

Seven dentary teeth are preserved in *Stegoceras* (UALVP 2), but only five were unworn, and were used in the multivariate analyses. Of the five, the three anterior members of the series appear to represent a different morphotype from the posterior two (Sues and Galton, 1983) (Fig. 5.2). Preservation of *in situ* dentary teeth is rare in pachycephalosaurids (Maryańska et al., 2004; Maryańska and Osmólska, 1974). However, heterodonty is present in the dentary tooth series of the pachycephalosaurids *Goyocephale* (Maryańska et al., 2004) and *Wannanosaurus* (Butler and

Zhao, 2009). The anterior part of the dentary possesses a similar morphology with premaxillary teeth. In buccal view, the anterior dentary teeth appear to have a "caniniform" morphology, being about equally tall and long, mediolaterally compressed, pointed, and recurved (Table 5.3), with average crown height, crown base length, and crown angle values of 5.0 mm, 5.1 mm, and 51.1° (Table 5.4). The posterior dentary teeth appear in buccal view to have the broad shapes of typical basal ornithischian teeth, being longer than tall and mediolaterally compressed, with blunt, vertically directed apices (Norman et al., 2004b) (Table 5.3). These posterior dentary crowns have average crown height, crown base length, and crown angle values of 4.1 mm, 5.3 mm, 49.8°, respectively (Table 5.4). As in basal ornithischians, both the anterior and posterior dentary teeth have constricted necks and cingula at a level just apical to their roots (Norman et al., 2004b). The cingula are more pronounced on the posterior teeth than on the anterior ones. A smooth, even enamel texture is distributed evenly on the buccal and lingual faces of the crowns (Sues and Galton, 1983). The roots of the anterior and posterior dentary teeth are oval, and the crown lenticular, in cross-section, (Sues and Galton, 1983). The anterior dentary teeth each possesses a single wear facet on the distal edge of the buccal surface. The wear facets on the posterior dentary teeth are on the mesial and distal edges of the buccal surfaces, with the distal facets being the larger. The anterior dentary teeth evidently each had a single continuous occlusal surface that contacted the corresponding maxillary crown, while each posterior dentary tooth occluded with two maxillary crowns. The wear facet patterns in the anterior dentary teeth are similar to those seen in the pachycephalosaurid *Goyocephale* (Maryańska et al., 2004), whereas those in the posterior dentary teeth are more reminiscent of the thescelosaurid *Thescelosaurus* (Boyd, 2014). The anterior dentary crowns bear 6-9 denticles on the mesial margin and nine on

the distal, while the posterior dentary crowns have 4-9 denticles on the mesial margin and nine on the distal. The denticles are associated with ridges that are similar to those in *Goyocephale*, but are not as pronounced as those in *Thescelosaurus* (Boyd, 2014; Maryańska et al., 2004).

The visibility of unworn dentary teeth is limited in *Thescelosaurus* (NCSM 15728) because of overlap by the maxillary crowns. Only three dentary teeth are visible on the right side, and nine on the left side. The unworn dentary teeth appear subtriangular to "caniniform" in buccal view, with crown base length exceeding crown height as in other basal ornithischians and thescelosaurids (Fig. 5.3) (Boyd, 2014; Norman et al., 2004b). Crown height averages 3.8 mm, and crown base length 4.2 mm (Table 5.4). Based on the CT scans of Boyd (2014), the roots of the dentary teeth are dorsoventrally straight, whereas in *Parksosaurus* they are curved along their dorsoventral heights (Galton, 1973; Galton, 1974b). The average crown angle of the dentary crowns is 55.9°. Similar to other known thescelosaurids, a distinct neck constriction is present apical to the root and basal to a weakly developed cingulum (Barrett and Han, 2009; Boyd, 2014, Jin et al., 2010; Makovicky et al., 2011; Parks, 1926). The mesial and distal margins of the dentary crowns bear denticles, which are associated with ridges that are relatively pronounced but not as prominent as those on the maxillary crowns (Boyd, 2014). There are 3-7 denticles on the mesial margins of the dentary crowns and 2-5 denticles on the distal margins. The first three dentary crowns do not have wear facets as they are aligned with the diastema between the premaxillary and maxillary teeth (Boyd, 2014). The two posteriorly positioned anterior dentary teeth have visible wear facets near the mesial and distal margins of the lingual side of the crown (Fig. 5.5). This wear pattern demonstrates that each anterior dentary crown occluded with two maxillary teeth. Because the posterior dentary crowns are obscured, it is uncertain whether they

exhibit two distinct wear facets as in the anterior dentary crowns, or a single continuous occlusal surface as in the posterior maxillary teeth (Boyd, 2014).

The first three dentary crowns in *Thescelosaurus* are unworn, and subtriangular to caniniform, with blunt, recurved apices. The worn, posteriormost dentary crowns are roughly triangular, with blunt, nearly vertical apices and denticles on the mesial and distal margins. As in unworn crowns, crown height is consistently smaller than crown base length, respective average values for these measurements being 3.5 mm and 4.6 mm. Average crown angle for worn crowns is 56.9°.

5.3.2. Principal Components Analysis

The two-dimensional morphometric principal components analysis (PCA) of unworn *in situ* teeth of *Stegoceras* and *Thescelosaurus* shows that 62% of the variation in the data set can be attributed to principal component 1 (PC1), and 17% to principal component 2 (PC2), as indicated in the scree plot (Fig. 5.6, Table 5.5). More positive PC1 values primarily indicate high denticle length, carina length and denticle height, and low neck length, but crown height, mid-crown length, and apical length also have small negative loadings on PC1 (Fig. 5.6). All linear measurements load positively on PC2, but the loadings associated with apical length, crown height, and neck length are considerably greater than those associated with the other variables (Fig. 5.6). PC2 can be regarded as primarily a measure of overall crown size. On the plot of PC loadings, measurements of the denticles and carinae are directed approximately to the right, and the dimensions of the crown are directed upward and slightly to the left (Fig. 5.6). Eigenvalues, percent variances, loadings, and PC scores can be viewed in supplemental material.

Premaxillary (triangles), maxillary (circles), and dentary (squares) teeth of *Stegoceras* (blue) and *Thescelosaurus* (red) are distinguished on the PC plot (Fig. 5.6). The maxillary and dentary tooth clusters overlap in *Stegoceras* despite their disparities in morphology. In addition, the premaxillary and maxillary tooth clusters slightly overlap in *Stegoceras*. In *Thescelosaurus*, the tooth types form separate clusters, the premaxillary teeth being widely separated on PC1 from all other teeth in the data set. Most of the overlap seen in *Stegoceras* involves the maxillary and dentary teeth, although one premaxillary teeth falls within the same area of morphospace as the maxillary cluster. The dentary teeth of *Thescelosaurus* overlap with the premaxillary, maxillary, and dentary teeth of *Stegoceras*, whereas the premaxillary and maxillary teeth of *Thescelosaurus* lack any overlap with *Stegoceras* (Fig. 5.6). The maxillary teeth of *Thescelosaurus* are positioned to the right of all other teeth on the plot, reflecting their large denticles and overall crown shape (Fig. 5.6). Repetition of the PCA with worn teeth included produced broadly similar results. However, worn maxillary teeth of *Thescelosaurus* extended the maxillary cluster both positively and negatively on PC2 in the expanded analysis, and dentary teeth of *Thescelosaurus* had a greater overlap with maxillary and dentary teeth of *Stegoceras*.

5.3.3. Linear Discriminant Analysis

The linear discriminant analysis (LDA) plot of *in situ Stegoceras* (blue) and *Thescelosaurus* (red) teeth reveals distinct separation between the two taxa, albeit with some overlap (Fig. 5.7). *Thescelosaurus* teeth are positioned positively on the discriminant function axis, whereas *Stegoceras* ones are negatively positioned. The LDA correctly classified 96.6% of *Stegoceras* and *Thescelosaurus* teeth, with a Hotelling's t^2 p(a) < 0.01 (Table 5.6). The excellent separation between *Stegoceras* and *Thescelosaurus* should make it possible to use LDA to

accurately distinguish their isolated teeth from one another. A PERMANOVA test indicated that the separation between the species was statistically significant ($F = 5.15$, $p(a) < 0.01$). To minimize the effects of type I error, a Bonferroni-correction was applied, which resulted a $p(a) < 0.01$ (Table 5.6). Adding worn teeth to the analysis resulted in a slight decrease in the level of separation between *Thescelosaurus* and *Stegoceras*, but 92.0% of teeth were still correctly classified, with Hotelling's t^2 $p(a) < 0.01$. A PERMANOVA test still indicated statistically significant separation ($F = 5.463$, $p(a) < 0.01$) even with a Bonferroni-correction ($p(a) < 0.01$). Regardless of whether worn teeth are excluded or included, LDA captures significant morphometric differences in dental morphology between the two taxa.

5.3.4. Mann-Whitney *U* Test

Average values of linear measurements for both species, and results of the Mann-Whitney *U* tests, are reported in Table 5.4. Based on raw data, the premaxillary and maxillary teeth are larger in *Thescelosaurus* than in *Stegoceras*, and the dentary teeth are smaller. Mann-Whitney *U* tests of size-corrected data also reveal differences in shape between the two species (Fig. 5.8). Specifically, the Mann-Whitney *U* tests of size-corrected measurements show that statistically significant differences between *Stegoceras* and *Thescelosaurus* are present for crown height, mesial carina length, distal carina length, mesial denticle height, mesial denticle length, distal denticle height, and distal denticle length in premaxillary teeth. Similarly, the differences are significant for apical length, neck length, mesial carina length, mesial denticle height, distal denticle height, and distal denticle length in maxillary teeth, and for the distal denticle height and distal denticle length in dentary teeth (Fig. 5.8). Crown angle was significantly lower in *Thescelosaurus* than in *Stegoceras* in the case of maxillary teeth, significantly higher in

Thescelosaurus than in *Stegoceras* in the case of dentary teeth, and not significantly different between the two species in the case of premaxillary teeth (Fig. 5.8). Inclusion of worn teeth did not substantially alter these *U* test results except that crown height and mid-crown length were identified as additional variables differing significantly between the two species in the case of maxillary teeth, while distal denticle height was no longer found to differ significantly in the case of dentary teeth.

5.4. Discussion

Both quantitative analyses and qualitative observations provide a basis for drawing clade-level comparisons and for differentiating between the dentitions of *Stegoceras* and *Thescelosaurus*. This suggests that even isolated pachycephalosaurid and thescelosaurid teeth may be readily distinguishable at the clade level. The PCA results alone are insufficient to distinguish between teeth from the two species considered in this analysis, given that they plot in overlapping areas of PC morphospace. However, *Stegoceras* and *Thescelosaurus* teeth can be accurately separated from one another based on a combination of LDA, PCA, and Mann-Whitney *U* test results, together with attention to qualitative morphological features. LDA provided especially clear separation between *Stegoceras* and *Thescelosaurus*, correctly classifying 96.6% of all unworn teeth in the sample. PERMANOVA confirmed the statistical significance of the LDA separation between the two species, and Mann-Whitney *U* tests identified significant differences between their premaxillary, maxillary, and dentary teeth with regard to specific measurements. Noteworthy qualitative morphological discrepancies between the teeth of *Stegoceras* and *Thescelosaurus* relate to root and crown cross-sections, crown

symmetry, crown ornamentation, apical geometry, wear facet patterns, and denticulation, and variance in nature among premaxillary, maxillary and dentary teeth.

5.4.1. Morphological Differences and Identification of Teeth from Microsites

Dental variability within pachycephalosaurids and thescelosaurids has never been extensively investigated, but the differences between premaxillary, maxillary and dentary teeth of *Stegoceras* and *Thescelosaurus* have been demonstrated (Figs. 5.2, 5.3 and 5.5). At least some of the differences established in this study may prove useful in distinguishing between pachycephalosaurid and thescelosaurid teeth in general.

5.4.1.1. Premaxillary Teeth

The premaxillary teeth of *Stegoceras* have pointed apices, while those of *Thescelosaurus* have blunt ones. The root and crown cross-sections are respectively circular and oval in *Stegoceras*. However, in *Thescelosaurus* the crowns are elliptical in cross-section throughout the premaxillary tooth row, and the root cross-section is elliptical in anterior premaxillary teeth but circular in posterior ones (Boyd, 2014). Crown ornamentation is absent in *Stegoceras*, whereas in *Thescelosaurus* the crowns bear fine, apicobasally oriented ridges. Such ridges are absent in other thescelosaurids (Barrett & Han, 2009; Jin et al., 2010; Makovicky et al., 2011; Sues, 1980), but less well-developed ones occur in the orodromine *Orodromeus* (Scheetz, 1999). The presence of ornamentation is uncertain in *Parksosaurus* because no definitively identified premaxillary teeth are available for assessment. The Prince Creek Formation of Alaska has yielded what may be premaxillary teeth of *Parksosaurus*, but this identification remains unverified (Brown and Druckenmiller, 2011). Wear facets are present on the distal margins of

the crowns in *Stegoceras*, but on the distal edges of the buccal surfaces of the crowns in *Thescelosaurus* (Fig. 5.5). The most important difference between the two species, however, is that denticles are present on the mesial and distal crown margins in *Stegoceras*, but are entirely absent in *Thescelosaurus*. The premaxillary teeth of most other thescelosaurids also lack denticles (Barrett & Han, 2009; Jin et al., 2010; Makovicky et al., 2011), although denticles are uniquely present in the orodromine *Orodromeus* (Scheetz, 1999). Marginal denticles are consistently present in pachycephalosaurids, as exemplified by *Goyocephale* and *Prenocephale*, but their occurrence is not restricted to this clade (Maryańska et al., 2004). In the PCA, the absence of denticles appears to largely account for the wide separation on PC1 between premaxillary teeth of *Thescelosaurus* and all other teeth included in the analysis (Fig. 5.6). Two-sample *U* tests revealed that crown base length, mid-crown length, and neck length values are significantly higher for *Thescelosaurus* than for *Stegoceras* (Fig. 5.8), a shape difference not captured by the PCA. An interesting feature of *Stegoceras*, which neither the PCA nor the *U* test captured successfully, is that the tooth is buccolingually thinner towards the apex. Buccolingual thinning of the crown also occurs in *Thescelosaurus*, but to a less extreme degree that allows the teeth to retain their bulbous shape throughout the crown. This feature potentially provides an excellent basis for distinguishing between pachycephalosaurid and thescelosaurid premaxillary teeth.

5.4.1.2. Maxillary Teeth

Maxillary tooth crowns of *Stegoceras* are asymmetrical, whereas those of *Thescelosaurus* are symmetrical. *Stegoceras* teeth bear 6-8 denticles on their mesial and distal margins, whereas *Thescelosaurus* teeth have 4-6 denticles. In *Thescelosaurus*, the denticles are continuous with

long ridges that extend to the base of the crown in a converging crescentic pattern, whereas corresponding ridges are lacking in *Stegoceras*. The differences in denticle morphology are captured by the PCA, which clearly separates maxillary teeth of two species (Fig. 5.6). The denticles are longer in *Thescelosaurus* than they are in *Stegoceras.* Large ridge-associated denticles are also present in other thescelosaurids, and are an important feature for identifying isolated teeth from microsites (Barrett & Han, 2009; Brown and Druckenmiller, 2011; Jin et al., 2010; Parks, 1926; Sues, 1980). Pronounced, central, apicobasally-oriented ridges are present in both species, but are better developed in *Stegoceras*. A particularly notable feature of *Stegoceras* is that on the lingual side of the crown, at the base of the distal denticle margin, the carina forms a "ledge" along the distal portion of the crown base length (Brown and Druckenmiller, 2011; Parks, 1926). This carinal ledge appears to be present in other neornithischian taxa (e.g., indeterminate orodromines (TMP 1986.043.0035, TMP 1987.034.0056, and TMP 2007.024.0054), *Nanosaurus*, *Orodromeus*, some specimens of *Thescelosaurus*, and *Zephyrosaurus*). However, it is lacking in other pachycephalosaurids and in isolated teeth that are potentially referable to *Parksosaurus* (Bakker et al., 2006; Brown and Druckenmiller, 2011; Brown et al., 2013b; Carpenter and Currie, 1992; Maryańska et al., 2004; Maryańska and Osmólska, 1974; Scheetz, 1999; Sullivan, 2006). Lightly worn *Stegoceras* teeth each have a single wear facet on the mesial side of the lingual surface, whereas more heavily worn ones bear a large facet on the mesial side together with a smaller one on the distal side (Fig. 5.5). The asymmetrical wear facet pattern is not dependent on maxillary tooth position, but rather is associated in the maxillary teeth with advanced wear with the dentary teeth. The distal wear facet would have been formed through contact with the posteriorly adjacent dentary tooth as wear

continued, whereas the mesial wear facet would have contacted the anteriorly adjacent dentary tooth. In *Thescelosaurus*, wear pattern is dependent on position within the maxillary tooth series. Although largely obscured by the dentary crowns, the anteriorly positioned maxillary teeth must bear wear facets of similar size on the mesial and distal sides of their lingual surfaces, based on the matching wear facets visible on the dentary crowns. Posteriorly positioned teeth instead each have a single wear facet covering their entire lingual surface, as can be observed in the articulated skull (NCSM 15728) (Boyd, 2014). Key differences between maxillary teeth of *Stegoceras* and *Thescelosaurus* are the presence of symmetrical tooth crowns and crescentic ridges associated with the denticles in the latter taxon, and the presence of a pronounced central apicobasal ridges and lingual swellings on the crown bases, in the former.

Statistically significant differences between the two species were identified using two-sample Mann-Whitney *U* tests, and the PC plot captured clear separation between the dentition of the two species (Fig. 5.6 and 5.8). Based on raw data, both worn and unworn crowns of *Thescelosaurus* are broader with larger denticles and have significantly greater average crown base length, apical length, mesial carina length, mesial distal height, mesial denticle length, distal denticle height, and distal denticle length values than do crowns of *Stegoceras*. Other thescelosaurid maxillary teeth have not been extensively investigated to determine to what degree they resemble their counterparts in *Thescelosaurus*, but prominent ridge-associated denticles do seem to be present in at least some other thescelosaurids (Barrett and Han, 2009; Jin et al., 2010; Makovicky et al., 2011; Parks, 1926; Scheetz, 1999; Sues, 1980).

5.4.1.3. Dentary Teeth

Differences in dentary tooth morphologies between *Stegoceras validum* and *Thescelosaurus* mostly pertain to overall crown shape, denticle ornamentation and morphology, and wear facet patterns (Figs. 5.2, 5.3, and 5.5). Anteriorly positioned dentary teeth have similar crown shapes in *Stegoceras* and *Thescelosaurus*, but the posteriorly positioned ones are broader in *Stegoceras* than in *Thescelosaurus*. The posterior dentary teeth in the specimen of *Thescelosaurus* examined in this study are extremely worn, and largely obscured by the maxillary teeth. In *Stegoceras*, the anterior dentary crowns bear weakly developed cingula, whereas posterior crowns bear pronounced ones in both *Stegoceras* and *Thescelosaurus*. In *Stegoceras*, the apices of the posterior dentary crowns are pointed, whereas those of the anterior dentary crowns are blunt. Anterior dentary teeth of *Stegoceras* possess 6-9 denticles on the mesial margin and nine denticles on the distal margin, whereas posterior ones possess 4-9 denticles on the mesial margin and nine on the distal margin. Only anterior dentary teeth are visible in *Thescelosaurus*, and these bear only 3-7 denticles on the mesial margin and 2-5 on the distal margin. In *Thescelosaurus*, but not in *Stegoceras*, the denticles are associated with weakly-developed ridges. The anterior teeth of *Stegoceras* display a single relatively small wear facet on the distal side of the buccal surface, whereas the posterior teeth have larger facets that are mesial positioned. In *Thescelosaurus* the anterior dentary crowns display wear facets on the mesial and distal sides of the buccal surface, but the wear facet pattern on the posterior crowns could not be observed in this study. Statistically significant differences in dentary tooth morphology between the two species were identified using the Mann-Whitney *U* test, and the PC plot showed some separation between the dentary teeth but failed to capture substantial differences (Fig. 5.8)

including larger average size-corrected, log-transformed distal denticle height and distal denticle length values in *S. validum.*

Both *Stegoceras* and *Thescelosaurus* teeth are quite different from those of ankylosaurids, which bear prominent cingula distinctly set off from the rest of the crown. Ankylosaurid dentary teeth also have apicobasally oriented denticle ridges, which are considerably better developed than in *Stegoceras* and *Thescelosaurus*, and do not extend to the cingulum (Coombs and Maryańska, 1992; Galton, 2007; Kirkland, 1998; Vickaryous et al., 2004). However, further studies of ankylosaurid, pachycephalosaurid, thescelosaurid teeth will be necessary to ensure that they can be accurately distinguished from one another when found in isolation.

5.4.2. Paleoecology

Pachycephalosauridae and Thescelosauridae co-occur in multiple Upper Cretaceous formations in North America (Table 5.1). In the Hell Creek Formation, pachycephalosaurids are represented by *Pachycephalosaurus* (Gilmore, 1931) and *Sphaerotholus* (Williamson and Carr, 2002), and thescelosaurids by *Thescelosaurus garbanii* (Morris, 1976) and *Thescelosaurus neglectus* (Boyd, 2014; Fisher et al., 2000). The Horseshoe Canyon Formation contains the pachycephalosaurid *Sphaerotholus*, although the material is not diagnostic to the species level, and the thescelosaurid *Parksosaurus* (Eberth et al., 2013), whereas the Dinosaur Park Formation has the pachycephalosaurid *Stegoceras* (Sullivan, 2003) and an indeterminate orodromine thescelosaurid (Brown et al., 2013b). As relatively small herbivores, pachycephalosaurids and thescelosaurids might be assumed to have competed for similar trophic resources. This raises questions as to how they were able to coexist in North America during the Late Cretaceous

without either clade driving the other to extinction. Several authors have suggested the possibility that pachycephalosaurids and thescelosaurids avoided competition as a result of different habitat preferences, which led to spatial niche partitioning. In the Hell Creek Formation, *Thescelosaurus* fossils commonly occur in channel sandstone deposits, whereas *Pachycephalosaurus* fossils occur in both channel sandstones and floodplain mudstone deposits (Lyson and Longrich, 2011; Pearson et al., 2002). This suggests that *Thescelosaurus* preferred the environment near river channels, while *Pachycephalosaurus* had an indiscriminate preference between channel-adjacent and floodplain habitats. Even if the postulated difference in habitat preference is valid, the two species could still have found themselves competing for resources in channel-adjacent areas that they both frequented. However, the Lyson and Longrich (2011) and Pearson et al. (2002) studies have low statistical power to determine patterns of habitat preference. The postulated difference in occurrence between the two species is likely due to taphonomic biases (Brown et al., 2013a, b; O'Gorman and Hone, 2012), and other workers have reached divergent conclusions regarding their habitat preferences (Carpenter and Young, 2002).

Stegoceras and *Thescelosaurus* appear to have occupied different ecomorphospaces, based on tooth enamel microstructure, wear facet patterns, and craniodental morphology (Mallon and Anderson, 2013; Virág and Ősi, 2017; Wyenberg-Henzler, 2020). Wyenberg-Henzler (2020) argued persuasively that this was likely facilitated by a discrepancy in feeding styles between the two groups, reflected in differences in cranial morphologies. The observed contrasting patterns of enamel microstructure and wear facet patterns in pachycephalosaurids and thescelosaurids imply differences in mastication styles (Teaford, 1994; Virág and Ősi, 2017).

Pachycephalosaurids were observed to have vertical wear facets that would have formed through orthal chewing with incipient columnar units that grade into parallel crystallite enamel, whereas thescelosaurids had oblique facets formed through orthal to slightly orthopalinal chewing with parallel crystallite enamel (Virág and Ősi, 2017). The PCA results obtained in the present study indicate strong heterodonty among the premaxillary, maxillary, and dentary teeth of *Thescelosaurus*, contrasting with more homodont teeth in *Stegoceras*. The differences in dental morphology between the two species suggest that they were characterized by divergent feeding modes.

Differences in rostrum shape between the two species further support the interpretation that they feed in distinct ways. Variation in the shape of the rostrum correlates with dietary adaptations in extant ruminants, where narrow rostra allow for selective feeding and wider rostra allows for unselective, indiscriminate feeding (Solounias et al., 1988). In extant ruminants, a narrow rostra facilitates selective feeding strategies on well-spaced food items, whereas a wide rostra facilitates indiscriminate bulk feeding on whatever vegetation is available, strategies that are respectively typical of browsers and grazers (Solounias et al., 1988). However, pure indiscriminant bulk feeding and selective feeding strategies represent endpoints on a continuum of dietary adaptation, and the shape of the rostrum reflects the animal's position on this spectrum (Hofmann, 1973; Solounias et al., 1988). Assuming that rostral shape had the same relationship to feeding behaviors in ornithischians as it does to extant ruminants, the fact that *Stegoceras* possesses a wider rostrum than *Thescelosaurus* suggests that the former species utilized a relatively indiscriminate feeding strategy potentially targeting lower-quality plant material, whereas the latter was more selective and may have targeted higher-quality material (Mallon and

Anderson, 2013). According to Mallon and Anderson (2013) and Wyenberg-Henzler (2020), tooth row length correlates negatively with bite force and presumably with ability to process mechanically resistant plants, suggesting the shorter-faced *Stegoceras* would have been more capable of biting more forcefully, and processing tougher plant material, than the longer-faced *Thescelosaurus*. The high level of heterodonty seen in *Thescelosaurus*, combined with the relatively narrow rostrum and long premaxilla and maxilla, thus suggests a specialized strategy of feeding selectively on less mechanically resistant plants. *Stegoceras* combines less pronounced heterodonty with a relatively wide rostrum and a short premaxilla and maxilla, suggesting more indiscriminate bulk-feeding on lower quality, mechanically resistant plant material. Although *Stegoceras* and *Thescelosaurus* are temporally separated taxa, the former being Campanian in age and the latter Maastrichtian, the inferred differences in feeding behavior between the two species may apply to pachycephalosaurids and thescelosaurids in general (Boyd, 2014; Eberth et al., 2013; Gilmore 1913; Ogg and Hinnov, 2012; Sullivan, 2003).

5.5. Future Work

Future studies will combine this data set with other pachycephalosaurids and thescelosaurids from other Cretaceous formations. Isolated pachycephalosaurid and thescelosaurid teeth will be included, to test how readily they can be distinguished using the data set. A comprehensive data set comparing the qualitative and quantitative features of pachycephalosaurid and thescelosaurid teeth will greatly improve the ability of researchers to differentiate between the two groups, and facilitate accurate identification of isolated teeth from microfossil sites. Future work should also focus on microwear pattern analysis of *Stegoceras* and *Thescelosaurus* to discern differences in jaw feeding kinematics that might indicate

paleoecological discrepancies. Further analyses will provide an improved basis for testing hypotheses on the biogeography, macroevolution, and temporal distribution of Pachycephalosauridae and Thescelosauridae using the microfossil record.

5.6. Conclusions

This analysis of two individual species represents a step towards a clearer understanding of the differences in dental morphology between pachycephalosaurids and thescelosaurids more generally. It should help to facilitate accurate identification of isolated teeth in museum collections and the field. In combination, quantitative analyses (linear discriminant analysis (LDA), principal components analyses (PCA), *U* tests and PERMANOVA) and examination of qualitative characters were found to provide a basis for distinguishing premaxillary, maxillary and dentary teeth of the pachycephalosaurid *Stegoceras* from those of the thescelosaurid *Thescelosaurus*. LDA was able to discriminate almost perfectly between teeth of the two genera, PERMANOVA confirmed the statistical significance of this separation, and *U* tests identified significant differences pertaining to individual tooth measurements. However, qualitative morphological features proved most informative in differentiating between *Stegoceras* and *Thescelosaurus* teeth, which were found to differ in denticle morphology, crown ornamentation, and wear facet patterns. The PCA revealed *Thescelosaurus* to be more heterodont than *Stegoceras*, but did not clearly distinguish between *Stegoceras* and *Thescelosaurus* maxillary and dentary teeth owing to a lack of wide separation in morphospace.

These findings allow accurate identification of isolated pachycephalosaurid and thescelosaurid teeth from microsites and museum collections and to test hypotheses of paleoecological differences between pachycephalosaurids and thescelosaurids from their teeth.

Further investigation will be needed to determine the extent to which the differences documented in this study between *Stegoceras* and *Thescelosaurus* apply to other pachycephalosaurids and thescelosaurids. Being able to reliably distinguish between the superficially similar teeth of these two groups when they are found in isolation will facilitate use of the microfossil record to test hypotheses pertaining to their biogeography, macroevolution, species diversity, and temporal distribution.

5.7. Tables and Figures

Table 5.1. Occurrences of currently known pachycephalosaurids and thescelosaurids from the Santonian to the Maastrichtian.

Co-occurrences of pachycephalosaurids and thescelosaurids are bolded. Abbreviations: A, Asia; Alb, Albian; BBFm, Bajo Barreal Formation; BFm, Baynshire Formation; BGFm, Barun Goyot Formation; BLFm, Black Leaf Formation; Camp, Campanian; Ceno, Cenomanian; CFm, Cloverly Formation; Coni, Coniacian; DPF, Dinosaur Park Formation; FFm, Foremost Formation; HCF, Horseshoe Canyon Formation; HCFm, Hell Creek Formation; JFm, Javkhlant Formation; Maas, Maastrichtian; MRFm, Milk River Formation; N. Am., North America; NFm, Nemegt Formation; OFm, Oldman Formation; PAFm, Pari Aike Formation; PCFm, Prince Creek Formation; PFm, Portezuelo Formation; ; QFm, Quantou Formation; S. Am., South America; Sant, Santonian; TMFm, Two Medicine Formation.

Geologic Formation	Biogeography	Pachycephalosaurids	Thescelosaurids	Age	References
HCFm	**N. Am.**	***Pachycephalosaurus* and *Sphaerotholus***	***Thescelosaurus***	**Maas.**	Fisher et al., 2000; Gilmore, 1931; Williamson and Carr, 2002
PCFm	**N. Am.**	***Alaskacephale***	**Thescelosaurinae Indet.**	**Maas.**	Brown and Druckenmiller, 2011; Sullivan, 2006
NFm	A	*Homalocephale* and *Prenocephale*	-	Maas.	Maryańska and Osmólska, 1974
PAFm	S. Am.	-	*Talenkauen*	Maas.	Novas and Cambiaso, 2004
HCF	**N. Am.**	***Spaerotholus sp.***	***Parksosaurus***	**Camp.-Maas.**	Eberth et al., 2013
DPF	**N. Am.**	***Stegoceras* and *Foraminacephale***	**Orodrominae Indet.**	**Camp.**	Brown et al., 2013b; Schott and Evans, 2016
OFm	**N. Am.**	***Foraminacephale***	***Albertadromeus***	**Camp.**	Brown et al., 2013b; Sullivan, 2006
BGFm	A	*Tylocephale*	-	Camp.	Sullivan, 2003
FFm	N. Am.	*Colepiocephale*	-	Camp.	Sullivan, 2003

TMFm	N. Am.	-	*Orodromeus*	Camp.	Horner and Weishampel, 1988
MRFm	N. Am.	*Acrotholus*	-	Camp.	Evans et al., 2013
BFm	A	*Amtocephale*	-	Camp.	Watabe et al., 2011
JFm	A	-	*Haya*	Sant.	Makovicky et al., 2011
PFm	S. Am.	-	*Macrogryphosaurus*	Coni.	Calvo et al., 2007
BBFm	S. Am.	-	*Notohypsilophodon*	Ceno.	Martinez, 1998
BLFm	N. Am.	-	*Oryctodromeus*	Ceno.	Varricchio et al., 2007
CFm	N. Am.	-	*Zephyrosaurus*	Alb.	Sues, 1980
QFm	A	-	*Changchunsaurus*	Ceno.	Jin et al., 2010; Zan et al., 2005

Table 5.2. Morphometric measurements taken in this study on the premaxillary, maxillary, and dentary teeth of *Stegoceras* and *Thescelosaurus*.

Measurements and Abbreviation	Definitions
Crown Height (CH)	The maximum apicobasal length from the base of the cingulum to the apex of the crown
Crown Base Length (CBL)	The maximum mesiodistal length of the cingulum
Mid-Crown Length (M-CL)	The mesiodistal length of the tooth at mid-point of the CH
Neck Length (NL)	The mesiodistal length of the tooth at its point of maximal constriction basal to the cingulum
Apical Length (AL)	The maximum apicobasal length of the mesial margin of the crown, measured obliquely from the mesial end of the cingulum to the apex of the crown
Mesial Carina Length (MCL)	The maximum apicobasal distance from the most basal mesial denticle to the most apical mesial denticle
Distal Carina Length (DCL)	The maximum apicobasal distance from the most basal distal denticles to the apical-most distal denticle
Mesial Denticle Height (MDH)	The height of the denticle that is closest to the mid-length of the mesial margin of the crown
Mesial Denticle Length (MDL)	The mesiodistal length of the denticle that is closest to the mid-length of the distal margin of the crown
Distal Denticle Height (DDH)	The height of the denticle that is closest to the mid-length of the distal margin of the crown
Distal Denticle Length (DDL)	The mesiodistal length of the denticle that is closest to the mid-length of the distal margin of the crown
Crown Angle (CA)	The angle between the line segments that define CBL and AL

Table 5.3. Qualitative morphological differences between the premaxillary (A), maxillary (B), and dentary (C) teeth of *Stegoceras* and *Thescelosaurus*.

A.

Premaxillary	Shape	Cingulum	Neck Constriction	Apex	Denticles	Root cross-section	Crown cross-section	Ornamentation	Enamel	Wear pattern
Stegoceras	Bulbous and buccolingually compressed	Absent	Present	Pointed and recurved	Mesial margin (8); distal margin (9-11)	Circular	Oval	Absent	Smooth	Apical portion of the lingual surface
Thescelosaurus	Bulbous and buccolingually compressed	Absent	Present	Blunt and recurved	Absent	Elliptical to Circular	Elliptical	Apicobasally extended ridges	Smooth	Distal margin of the buccal surface

B.

Maxillary	Shape	Cingulum	Neck Constriction	Apex	Denticles	Root cross-section	Crown cross-section	Ornamentation	Enamel	Wear pattern
Stegoceras	Broad and buccolingually compressed	Present	Present	Pointed and recurved	Mesial and distal margin (6-8)	Oval	Reniform to oval	Absent	Smooth	On the lingual surface, single wear facet on mesial side, and as wear increases, distal side forms
Thescelosaurus	Broad	Present	Present	Blunt and recurved	Mesial and distal margin (4-6)	Unknown	Unknown	Converging crescent pattern of ridge associated denticles	Smooth	Anterior: wear facet on the mesial and distal sides of the lingual surface. Posterior: single facet on the lingual surface

C.

Dentary	Shape	Cingulum	Neck Constriction	Apex	Denticles	Root cross-section	Crown cross-section	Ornamentation	Enamel	Wear pattern
Stegoceras	Anterior: caniniform Posterior: broad	Anterior: weakly pronounced Posterior: pronounced	Present	Anterior: pointed and recurved Posterior: pointed and vertical	Anterior: mesial margin (6-9), distal margin (9). Posterior: mesial margin (4-9), distal margin (9).	Oval	Lenticular	Small weak ridges	Smooth	Anterior: Single, distal edge facet on the buccal surface Posterior: facets on the mesial and distal edge of buccal surface
Thescelosaurus	Anterior: caniniform Posterior: subtriangular	Weakly pronounced	Present	Anterior: blunt and recurved Posterior: pointed and vertical	Mesial margin (3-7); distal margin (2-5)	Unknown	Unknown	Present. Denticles weakly associated by ridges	Smooth	Anterior: wear facets on the mesial and distal sides of the buccal surface. Posterior: Unknown

Table 5.4. Average values for measurements of unworn premaxillary, maxillary and dentary teeth of *Stegoceras validum* and *Thescelosaurus neglectus* (A), and results of *U* tests comparing the measurements between the two species (B).

Bolded values are significant. Average values for linear measurements are in millimeters, and crown angle values are in degrees. The *U* test results were calculated based on the size corrected, log-transformed morphometric measurements. Note that the premaxillary teeth of *Thescelosaurus* lack carinae and denticles. Abbreviations: AL, Apical Length; CA, Crown Angle; CBL, Crown Base Length; CH, Crown Height; DCL, Distal Carina Length; DDH, Distal Denticle Height; DDL, Distal Denticle Length; M-CL, Mid-Crown Length; MCL, Mesial Carina Length; MDH, Mesial Denticle Height; MDL, Mesial Denticle Length; NL, Neck length.

A.

Average *Stegoceras*	**CH**	**CBL**	**M-CL**	**AL**	**NL**	**MCL**	**DCL**	**MDH**	**MDL**	**DDH**	**DDL**	**CA**
Premaxillary	5.11	4.26	3.62	4.72	3.38	4.09	3.94	0.45	0.32	0.43	0.25	56.85
Maxillary	3.92	4.60	3.53	3.57	3.34	3.02	2.54	0.43	0.38	0.40	0.33	45.98
Dentary	4.61	5.19	3.21	4.38	3.40	3.75	4.12	0.41	0.37	0.44	0.35	50.57
Average *Thescelosaurus*	**CH**	**CBL**	**M-CL**	**AL**	**NL**	**MCL**	**DCL**	**MDH**	**MDL**	**DDH**	**DDL**	**CA**
Premaxillary	5.00	5.22	4.19	5.13	4.13	-	-	-	-	-	-	52.29
Maxillary	4.42	5.44	3.98	4.75	3.20	4.18	2.86	1.96	0.48	2.08	0.47	41.37
Dentary	3.81	4.23	3.07	4.13	3.13	3.08	3.15	0.49	0.28	0.68	0.45	55.87

B.

Stegoceras* vs *Thescelosaurus	**CH**	**M-CL**	**AL**	**NL**	**MCL**	**DCL**	**MDH**	**MDL**	**DDH**	**DDL**	**CA**
Premaxillary *u*-test	2.56	0.95	1.32	0.22	3.26	3.26	3.26	3.26	3.26	3.26	1.54
p(a)	**0.01**	0.34	0.19	0.83	**0.001**	**0.001**	**0.001**	**0.001**	**0.001**	**0.001**	0.12
Maxillary *u*-test	0.83	1.02	2.38	4.62	2.85	0.47	4.98	0.45	4.98	2.48	2.42
p(a)	0.41	0.31	**0.02**	**3.9E-06**	**0.004**	0.64	**6.3E-07**	0.65	**6.2E-07**	**0.013**	**1.6E-02**
Dentary *u*-test	0.01	1.92	1.92	1.55	0.09	0.09	0.46	0.09	2.47	2.01	2.10
p(a)	0.93	0.06	0.06	0.12	0.93	0.93	0.65	0.93	**0.01**	**0.04**	**0.04**

Table 5.5. Eigenvalues, percent variance, and descriptions of variation results from principal components analysis.

Results of principal components analysis on size corrected, log-transformed linear measurements of premaxillary, maxillary and dentary teeth of *Stegoceras* and *Thescelosaurus*, including the eigenvalue for each principal component and the percentage of variation in the sample that the principal component explains. For the three most important principal components, a description of the type of variation explained by the component is given as well.

PC	Eigenvalue	% Variance	Description of Variation
1	6.15	61.47	Size and shape of the denticles and length of the carina
2	1.74	17.42	Crown shape
3	1.00	9.99	Mid-crown length shape
4	0.69	6.94	-
5	0.27	2.71	-
6	0.08	0.80	-
7	0.03	0.32	-
8	0.02	0.22	-
9	0.01	0.10	-
10	0.00	0.03	-

Table 5.6. Confusion matrix, Hotelling's t^2, F-test, and Bonferroni-corrected p-value of linear discriminant analysis and PERMANOVA.

Confusion matrix and Hotelling's t^2 test for linear discriminant analysis (A) and PERMANOVA (B) of size corrected, log-transformed linear measurements of premaxillary, maxillary, and dentary teeth of *Stegoceras* and *Thescelosaurus*. PERMANOVA with F-test, and Bonferroni-corrected p-value of size corrected, log-transformed linear measurements of premaxillary, maxillary, and dentary teeth of *Stegoceras* and *Thescelosaurus* (B). The F-test confirms the significant separation obtained in the LDA.

A.

Classification	% Correctly Identified	Hotelling's t^2
Stegoceras* vs *Thescelosaurus	96.6	**1.00E-04**

B.

PERMANOVA		**Bonferroni-corrected p(a)**	*Stegoceras*	*Thescelosaurus*
F:	5.15	*Stegoceras*	-	**1.00E-04**
p (a):	**1.00E-04**	*Thescelosaurus*	**1.00E-04**	-

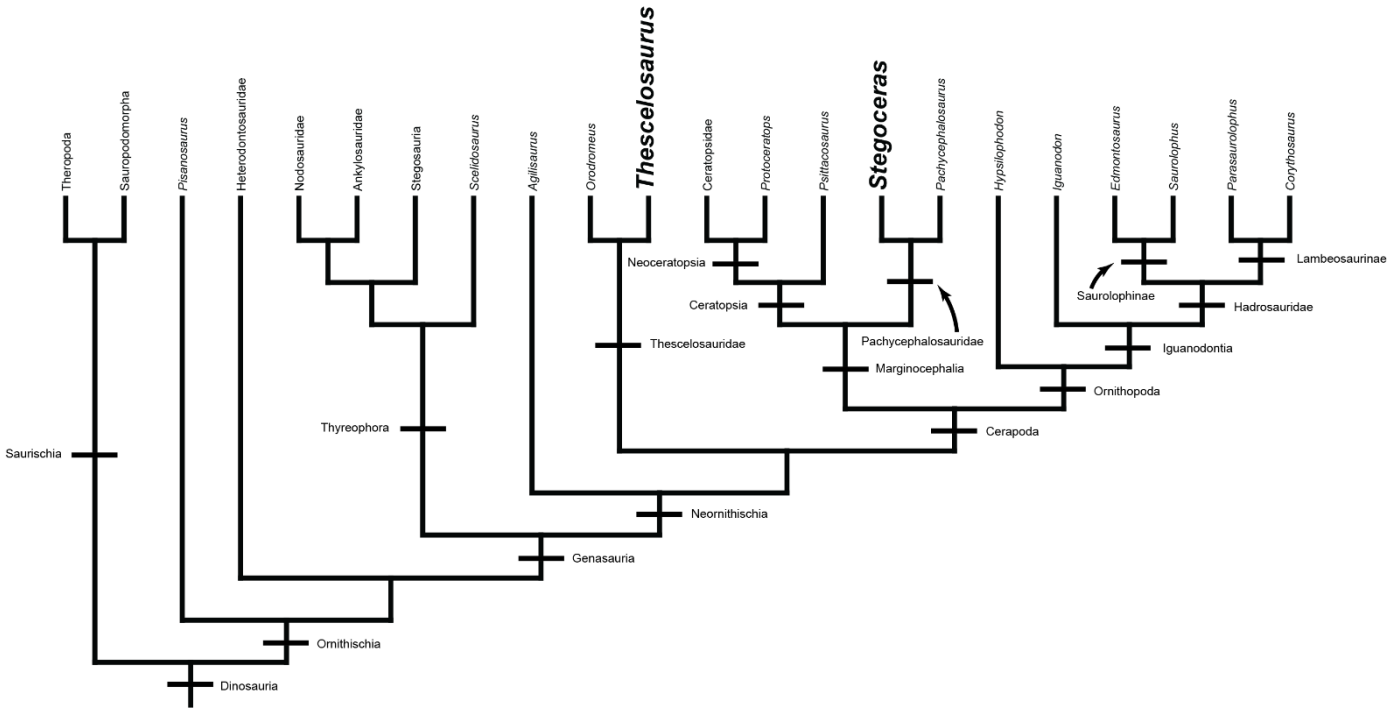

Figure 5.1. Phylogenetic overview of ornithischians.

Phylogenetic position of specimens used in this study are bolded.

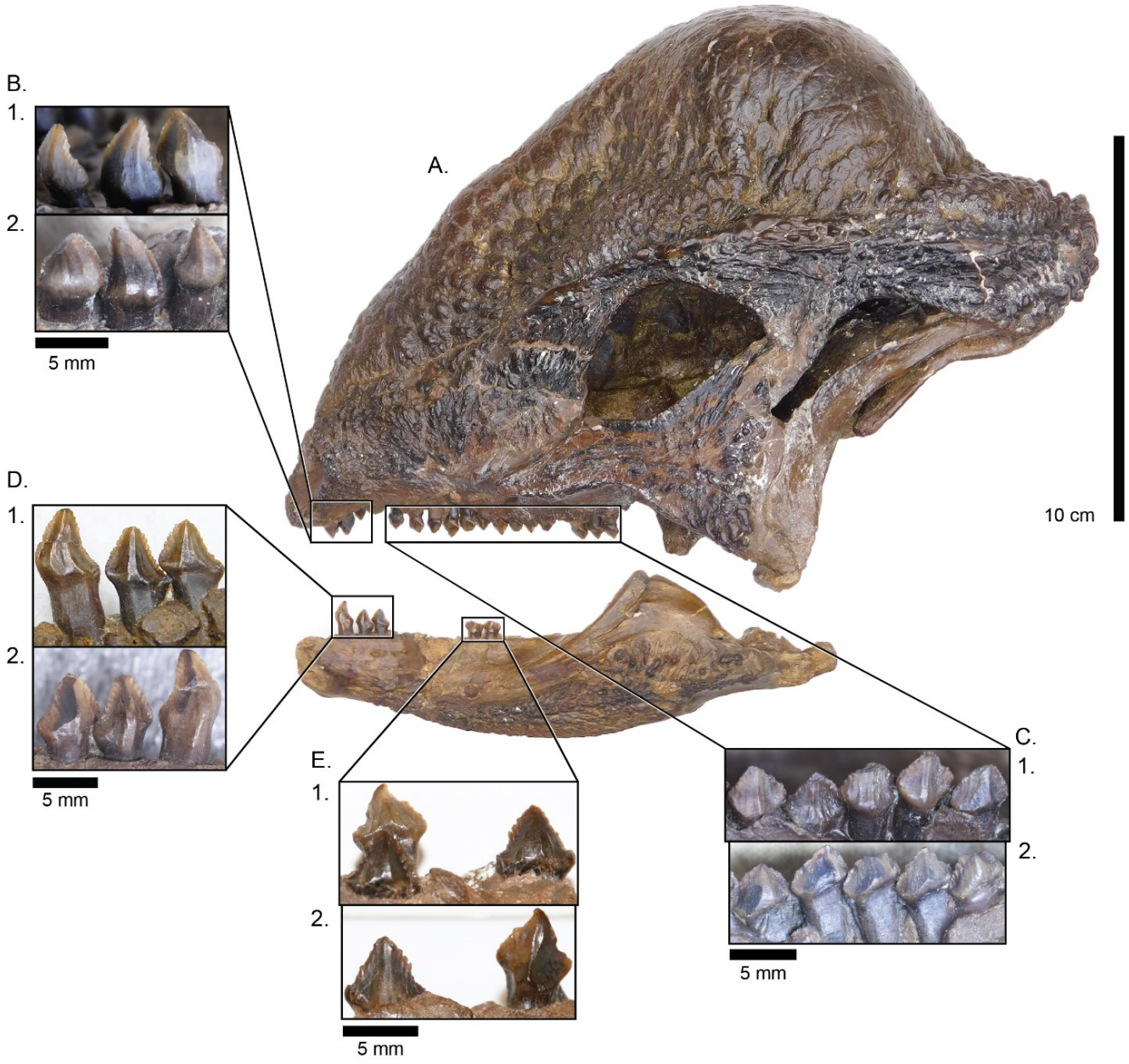
B.
1.
2.
5 mm
A.
10 cm
D.
1.
2.
5 mm
E.
1.
2.
5 mm
C.
1.
2.
5 mm

Figure 5.2. Premaxillary, maxillary, and dentary morphotypes of *Stegoceras* (UALVP 2).

Skull is in left lateral view and the dentary in right lateral view (inverted) (A). Right premaxillary teeth in buccal (B1) and lingual (B2) view. Left maxillary teeth in buccal (C1) and lingual view (C2). Right anteriorly positioned dentary teeth in buccal (D1) and lingual (D2) view. Left posteriorly positioned dentary in buccal (E1) and lingual (E2) view.

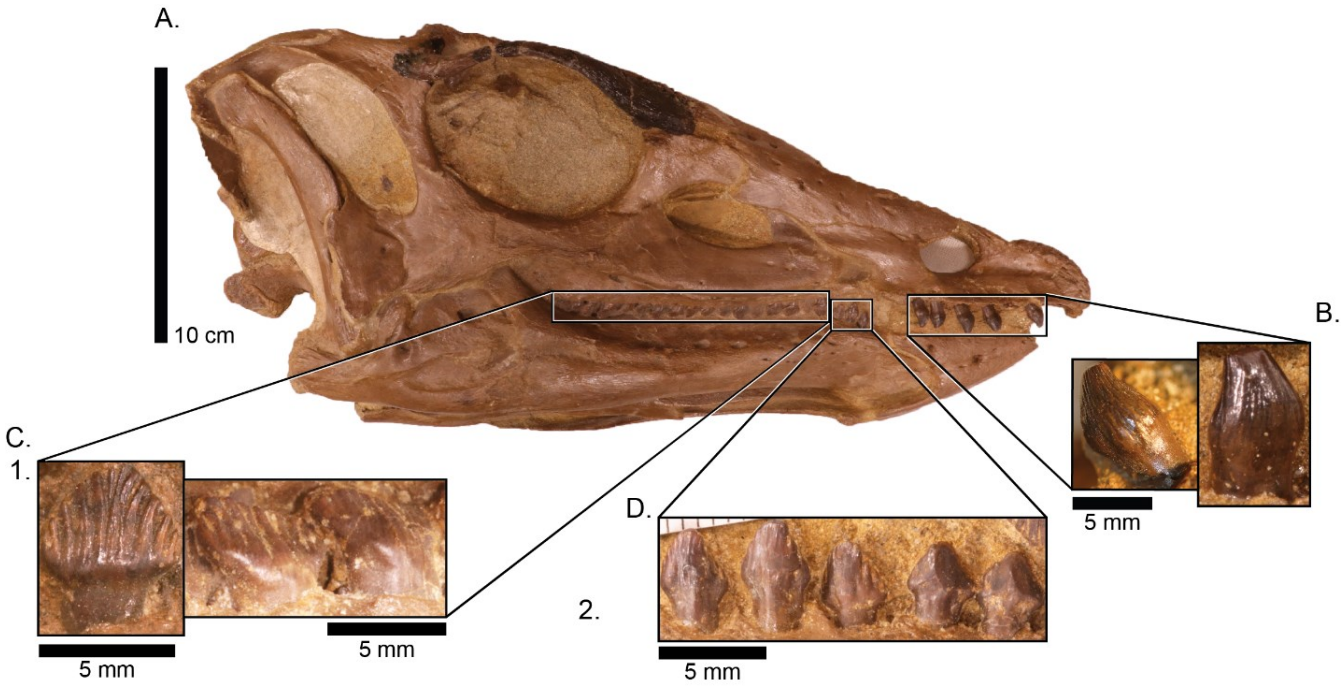

Figure 5.3. Premaxillary, maxillary, and dentary morphotypes of *Thescelosaurus* (NCSM 15728).

Premaxillary, maxillary, and dentary teeth of *Thescelosaurus* (NCSM 15728) in right lateral view (A). Premaxillary teeth in buccal view (B). Unworn (C1) and worn (C2) maxillary teeth in buccal view. Unworn (left) and worn (right) dentary teeth in buccal view (D).

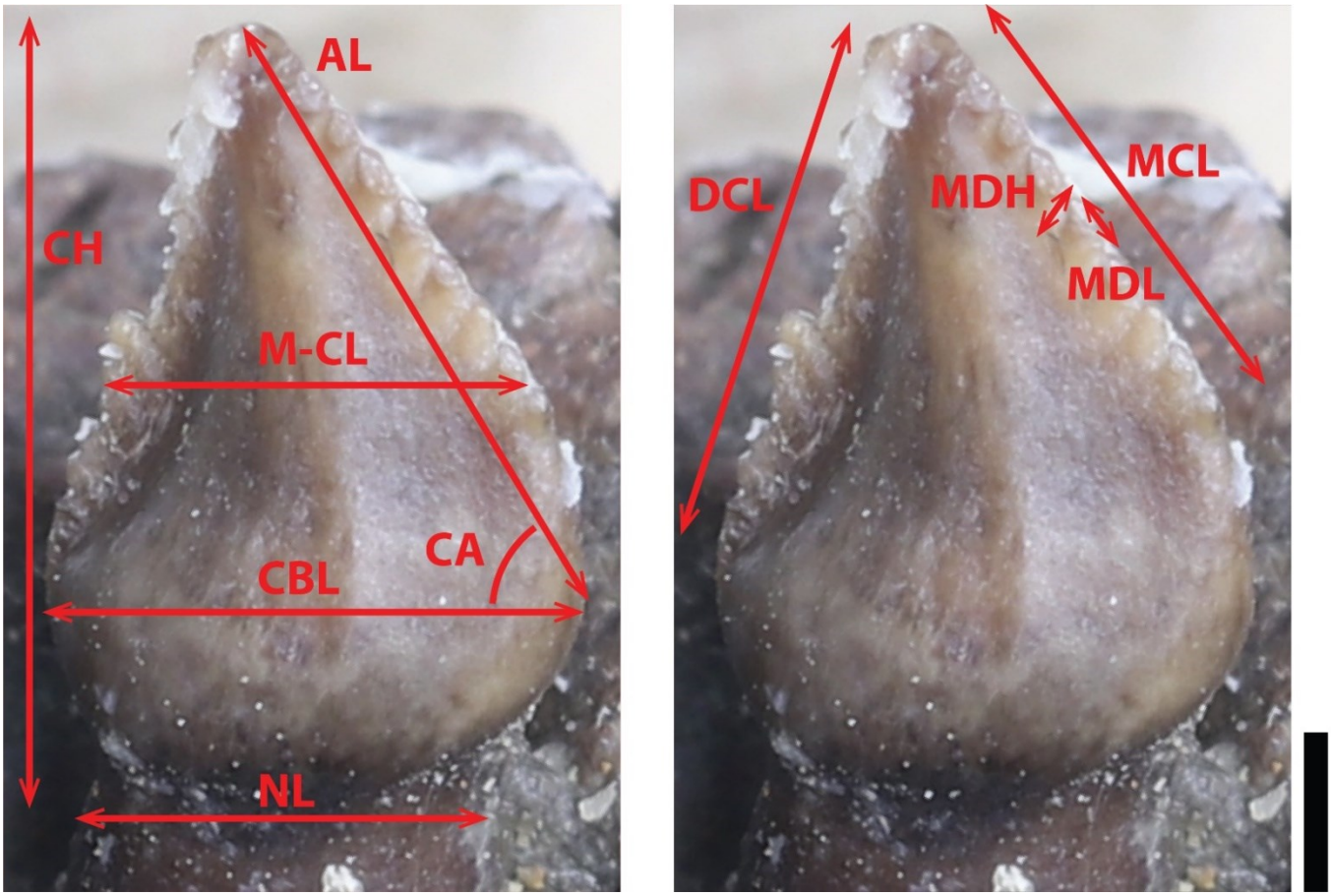

Figure 5.4. Morphometric measurements collected from in situ teeth of *Stegoceras* and *Thescelosaurus*, illustrated using a premaxillary tooth of *Stegoceras* in lingual view (UALVP 2).

Abbreviations: AL, apical length; CA, crown angle; CBL, crown base length; CH, crown height; DCL, distal carina length; DDH, distal denticle height; DDL, distal denticle length; M-CL, mid-crown length; MCL, mesial carina length; MDH, mesial denticle height; MDL, mesial denticle length; NL, neck length. Scale bar = 1 mm.

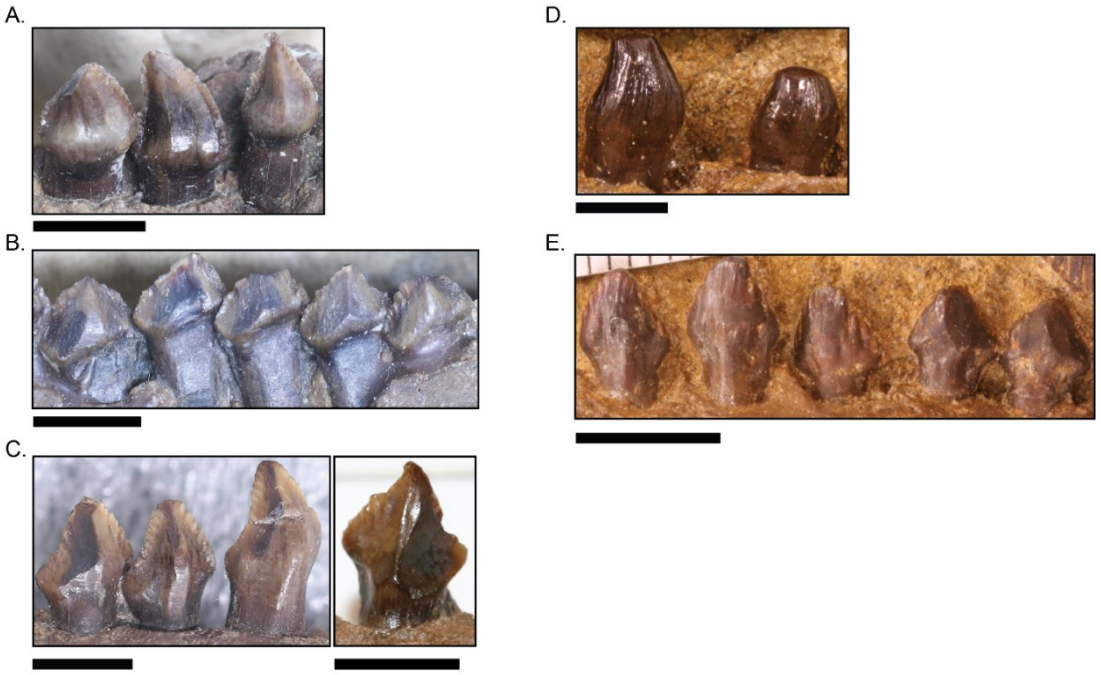
A.
B.
C.
D.
E.

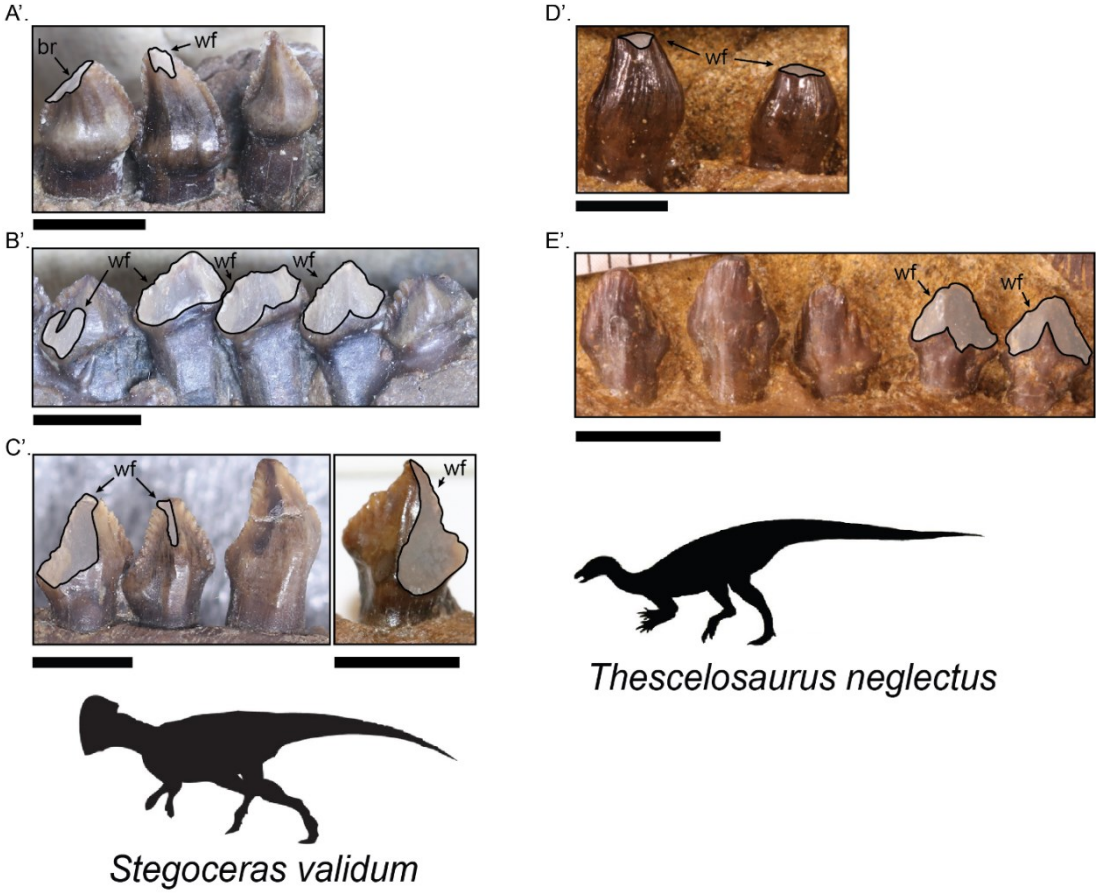
A'.
br
wf
B'.
wf
wf
wf
C'.
wf
wf
D'.
wf
E'.
wf
wf
Stegoceras validum
Thescelosaurus neglectus

Figure 5.5. Wear facet patterns of *Stegoceras* and *Thescelosaurus* teeth

In situ teeth of the premaxillary (lingual view), maxillary (lingual view), and dentary (buccal view) teeth of *Stegoceras* (UALVP 2) (A-C) and the premaxillary (buccal view) and dentary (buccal view) teeth of *Thescelosaurus* (NCSM 15728) (D-E). Primes indicate the interpreted wear facet patterns of the premaxillary, maxillary, and dentary teeth of *Stegoceras* (UALVP 2) (A'-C') and *Thescelosaurus* (NCSM 15728) (D'-E'). Premaxillary teeth in lingual view showing the wear facet pattern on the midline towards the apex (A'). Maxillary teeth in lingual view showing different asymmetrical wear stages with single and double wear facets on the teeth (B'). Anterior (left) and anterior (right) dentary teeth in lingual view showing wear facet patterns on the distal margin of the teeth (C'). Premaxillary teeth in buccal view showing wear facet pattern on the apical surface of the teeth (D'). Dentary teeth in buccal view displaying almost symmetrical wear patterns on the mesial and distal margins (E'). Abbreviations: br, breakage; wf, wear facets. Scale bar = 5 mm.

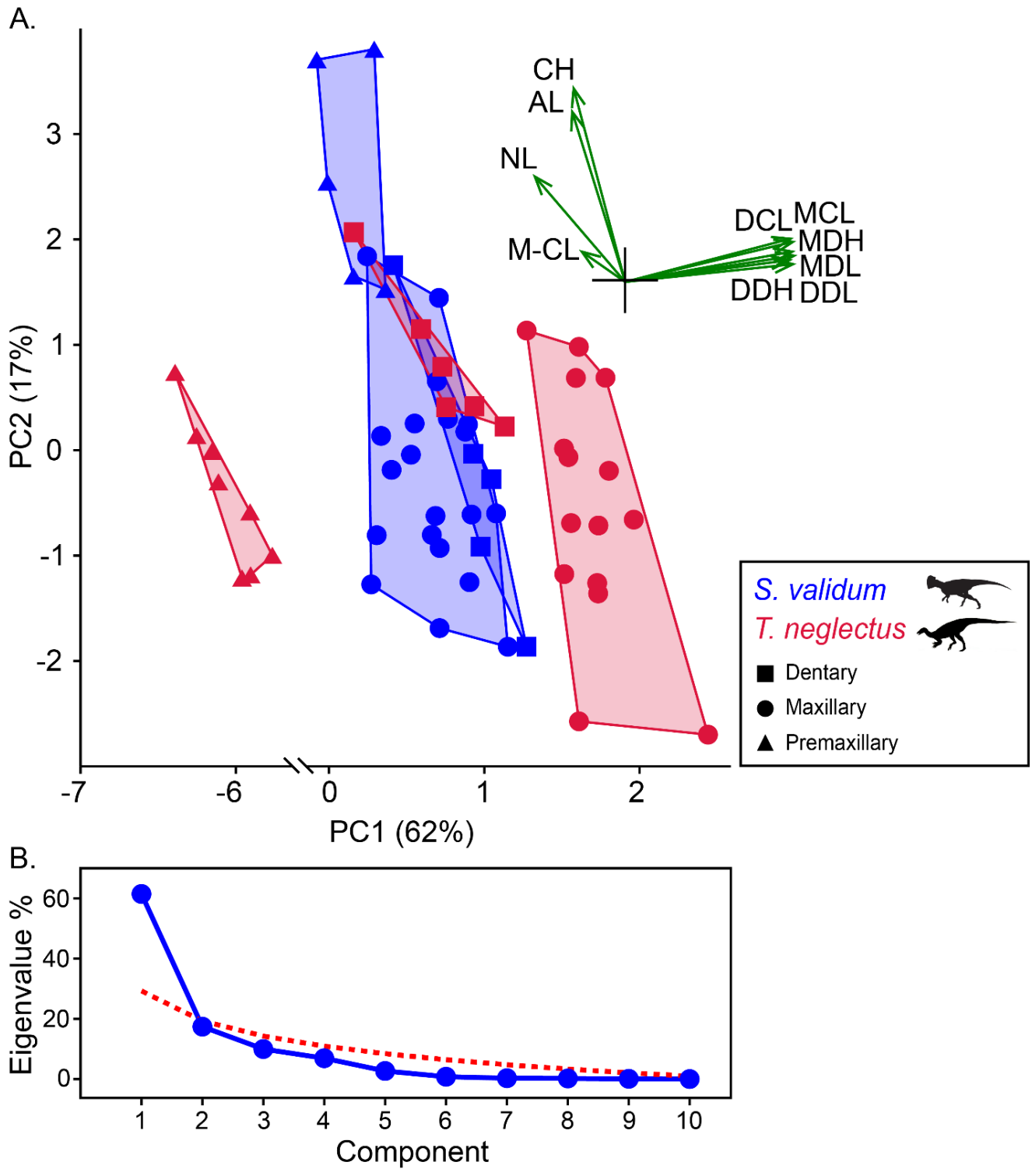
A.
CH
AL
NL
M-CL
DCL
MCL
MDH
MDL
DDH
DDL
PC2 (17%)
PC1 (62%)
S. validum
T. neglectus
Dentary
Maxillary
Premaxillary
B.
Eigenvalue %
Component

Figure 5.6. Results of PCA dentition of *Stegoceras* and *Thescelosaurus*.

Results of PCA on premaxillary (triangles), maxillary (circles), and dentary (squares) tooth series of *Stegoceras* (blue) and *Thescelosaurus* (red) (A). The biplot and eigenvectors (green) represent the direction and magnitude of morphometric measurements on the first and second principal components (A). Scree plot of principal components against eigenvalue percent variance and red dotted line is the broken stick model to determine significant principal components (B).

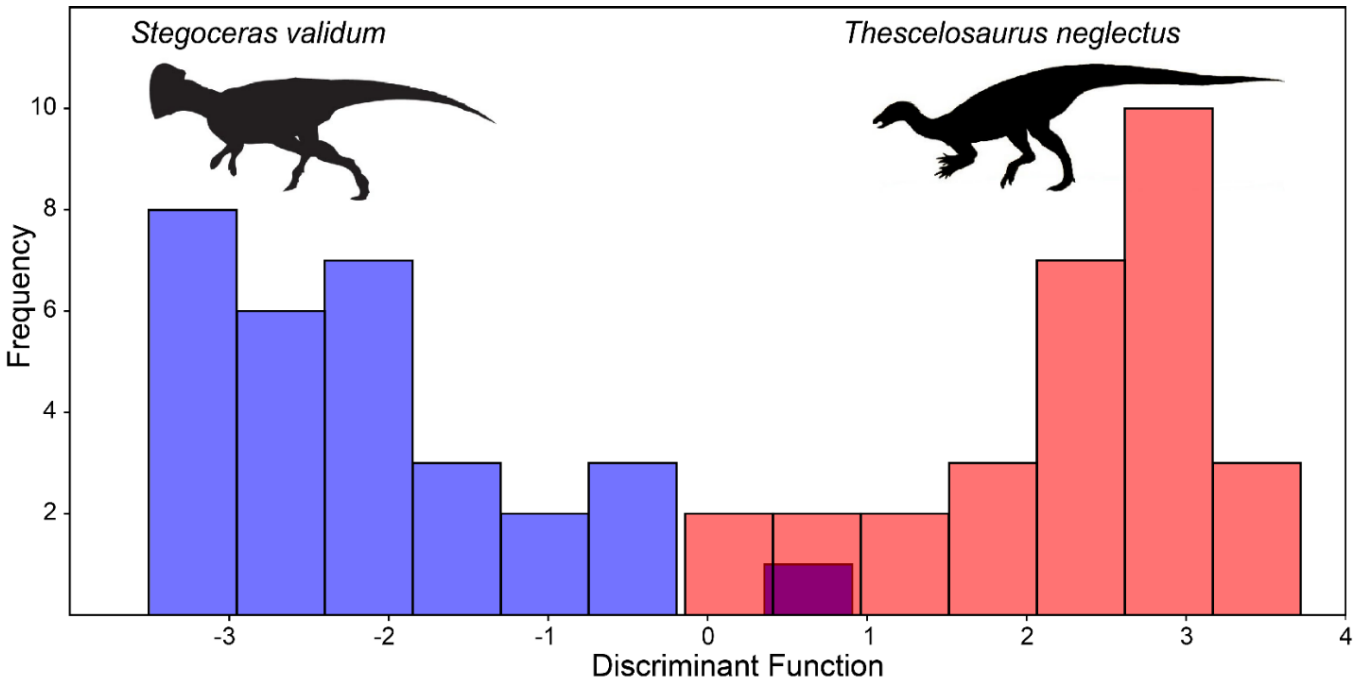

Figure 5.7. Results of LDA of premaxillary, maxillary, and dentary tooth series of *Stegoceras* (blue) and *Thescelosaurus* (red).

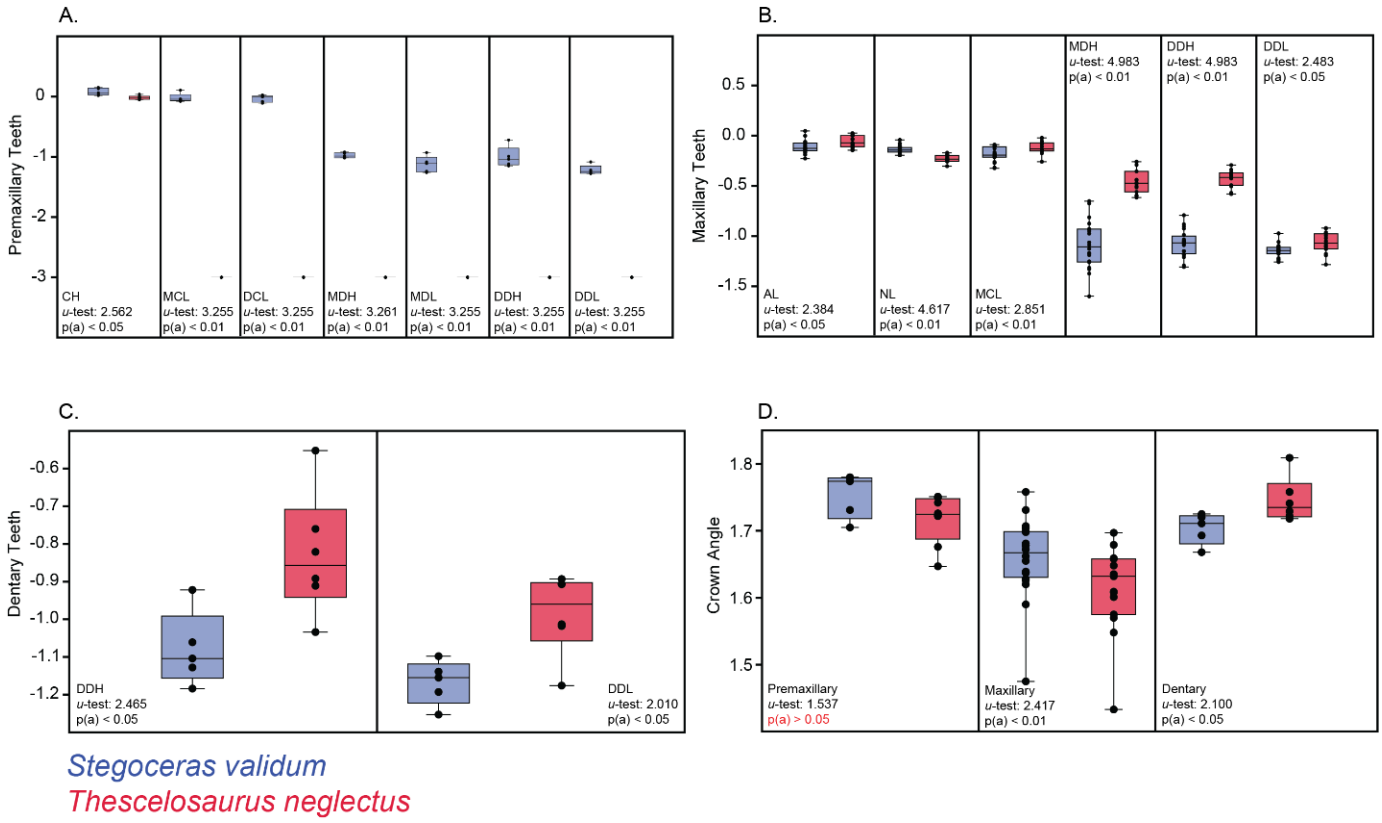

Figure 5.8. Boxplots and *U* test results of *Stegoceras* and *Thescelosaurus* teeth.

Boxplots of size-corrected, log-transformed linear measurements of premaxillary (A), maxillary (B), and dentary (C) teeth, and crown angle measurements for all three tooth types (D), for *Stegoceras* (blue) and *Thescelosaurus* (red), together with results of *U* tests comparing each measurement between the two species. Linear measurements that were not found to differ significantly between the two species for a particular tooth type are not shown. Red font indicates an insignificant *U* test result pertaining to crown angle.

Chapter 6. Conclusions

The research presented herein greatly expands upon preexisting knowledge of Thescelosauridae in Alberta, and these analyses have laid the groundwork for future research into thescelosaurid paleobiology, paleoecology, and evolution.

The partial skeleton (UALVP 56885) from the Horseshoe Canyon Formation described in this thesis is clearly assignable to *Parksosaurus warreni* (Chapter 3), based on comparisons with the holotype (ROM 804). This newly described *Parksosaurus* specimen represents the first specimen of this taxon to have been discovered within the last century and adds to the growing number of known diagnosable thescelosaurid body fossils. Five new pelvic autapomorphies were identified within *Parksosaurus* by considering ROM 804 and UALVP 56885 together. Recognition of new postcranial autapomorphies within *Parksosaurus* suggests that future research should concentrate on identifying diagnosable postcranial characters for other basal neornithischians.

The new thescelosaurid specimens from the Dinosaur Park and Wapiti Formations lack diagnostic features, and are best identified as Orodrominae and Thescelosaurinae indet., respectively (Chapter 4). The material from the Wapiti Formation represents the northernmost Canadian occurrence of a thescelosaurid and the oldest known occurrence of a thescelosaurine in North America. The geographic and stratigraphic provenance of the Wapiti thescelosaurine suggests that a thescelosaurine migration from Asia into North America took place during the Campanian. Moreover, the Wapiti thescelosaurine enhances our understanding of thescelosaurid paleobiology as the femur is robust compared to those of other thescelosaurids and possesses more prominent features related to the attachment of locomotor musculature, and the

osteohistology of the partial fibula expands our knowledge of bone tissue variation and diversity and growth strategies among thescelosaurids. Furthermore, the stratigraphic positions of orodromines occuring below the Bearpaw Formation and thescelosaurines occuring above the Bearpaw Formation (and, now, in Bearpaw-equivalent strata) suggest that the stratigraphic separation between these two clades is characteristic of the Alberta record. The stratigraphic position of the Wapiti thescelosaurine narrows the gap between the top of the orodromine range and the bottom of the thescelosaurine range in the Alberta record. This stratigraphic separation cannot be explained by changing climatic conditions, different habitat preferences, migration, or anagenetic transformation, but could potentially be explained by preservational biases. However, documenting the occurrence of a thescelosaurine during Bearpaw equivalent times, leaves unresolved the question of why orodromines disappeared just before, after, or during the onset of deposition of the Bearpaw Formation, with thescelosaurines dominant thereafter. This stratigraphic puzzle may be resolved with the recovery of additional thescelosaurid material from Cretaceous deposits in North America.

Identification of dental differences in the crown and denticle morphology, root and crown cross-sections, crown ornamentation, and wear facet patterns between *Stegoceras* and *Thescelosaurus* represents a step towards developing a clearer understanding of differences in dental morphology between pachycephalosaurids and thescelosaurids in general, and should act as a launching point for future research (Chapter 5). The analysis will help facilitate accurate identification of pachycephalosaurid and thescelosaurid teeth in field and museum settings. Qualitative morphological features, as opposed to morphometric measurements, proved most informative in differentiating between *Stegoceras* and *Thescelosaurus* teeth. The research

presented in Chapter 5 lays the groundwork for more accurately differentiating pachycephalosaurid and thescelosaurid teeth, which, in turn, should facilitate testing of hypotheses on the biogeography, macroevolution, paleoecology, species diversity, and temporal distribution of Pachycephalosauridae and Thescelosauridae using the microfossil record. However, further investigation is still required to determine the extent to which the differences documented in this chapter between *Stegoceras* and *Thescelosaurus* apply to other pachycephalosaurids and thescelosaurids.

This thesis has expanded our knowledge of thescelosaurid paleobiology, paleoecology, and evolution, and has opened pathways for comparative work on the postcrania of thescelosaurids and other basal neornithischians. Plenty of intriguing and fundamental paleobiological, paleoecological, and evolutionary questions regarding thescelosaurids still need addressing, in spite of low sample sizes and the fragmentary nature of much of the available record. Future paleobiological research on thescelosaurids should focus on growth curve and allometric analyses, respiratory biology, and myologic reconstructions; paleoecological research should test hypotheses on their diets, jaw mechanics, diversity, abundance, and ecological roles; and evolutionary studies should establish homologies, construct quality characters, identify cranial and postcranial autapomorphies, and establish robust phylogenies of Thescelosauridae. Any of these possibilities represents an encouraging avenue of research that will address unresolved questions about thescelosaurids.

References

Andrews, R. M. 1982. Patterns of growth in reptiles. In Gans, C. and F. H. Pough, Biology of the Reptilia. Vol. 13. Academic Press, London, pp. 273-320.

Arbour, V. M., and P. J. Currie. 2013. *Euoplocephalus tutus* and the Diversity of Ankylosaurid Dinosaurs in the Late Cretaceous of Alberta, Canada, and Montana, USA. PLOS ONE 8:e62421.

Averianov, A. O., A. V. Voronkevich, S. V. Leshchinskiy, and A. V. Fayngertz. 2006. A Ceratopsian dinosaur *Psittacosaurus sibiricus* from the Early Cretaceous of West Siberia, Russia and its phylogenetic relationships. Journal of Systematic Palaeontology 4:359–395.

Bamforth, E. L., C. L. Button, and H. C. E. Larsson. 2014. Paleoclimate estimates and fire ecology immediately prior to the end-Cretaceous mass extinction in the Frenchman Formation (66Ma), Saskatchewan, Canada. Palaeogeography, Palaeoclimatology, Palaeoecology 401:96–110.

Barbi, M., P. R. Bell, F. Fanti, J. J. Dynes, A. Kolaceke, J. Buttigieg, I. M. Coulson, and P. J. Currie. 2019. Integumentary structure and composition in an exceptionally well-preserved hadrosaur (Dinosauria: Ornithischia). PeerJ 7:e7875.

Baron, M. G., D. B. Norman, and P. M. Barrett. 2017. Postcranial anatomy of *Lesothosaurus diagnosticus* (Dinosauria: Ornithischia) from the Lower Jurassic of southern Africa: implications for basal ornithischian taxonomy and systematics. Zoological Journal of the Linnean Society 179: 125-168.

Barrett, P. M., R. J. Butler, and F. Knoll. 2005. Small-bodied ornithischian dinosaurs from the Middle Jurassic of Sichuan, China. Journal of Vertebrate Paleontology 25:4 823-834.

Barrett, P. M., and F.-L. Han. 2009. Cranial anatomy of *Jeholosaurus shangyuanensis* (Dinosauria: Ornithischia) from the Early Cretaceous of China. Zootaxa 2072:31–55.

Barrett, P. M. 2014. Paleobiology of Herbivorous Dinosaurs. Annual Review of Earth and Planetary Sciences 42:207–230.

Barta, D., and M. A. Norell. 2021. The Osteology of *Haya Griva* (Dinosauria: Ornithischia) from the Late Cretaceous of Mongolia. (Bulletin of the American Museum of Natural History, No. 445). American Museum of Natural History 1-103.

Behrensmeyer, A. K., D. Western, and D. E. D. Boaz. 1979. New perspectives in vertebrate paleoecology from a recent bone assemblage. Paleobiology 5:12–21.

Bell, P. R., F. Fanti, P. J. Currie, and V. M. Arbour. 2014. A Mummified Duck-Billed Dinosaur with a Soft-Tissue Cock's Comb. Current Biology 24:70–75.

Benson, R. B. J., R. J. Butler, M. T. Carrano, and P. M. O'Connor. 2012. Air-filled postcranial bones in theropod dinosaurs: physiological implications and the 'reptile'-bird transition. Biological Reviews of The Cambridge Philosophical Society 87:168–193.

Bertozzo, F., C. D. Sasso, M. Fabbri, F. Manucci, and S. Maganuco. Redescription of a remarkably large *Gryposaurus notabilis* (Dinosauria: Hadrosauridae) from Alberta, Canada. Memorie Della Società Italiana Di Scienze Naturali e Del Museo Civico Di Storia Naturale Di Milano 1-57.

Boaz, N. T., and A. K. Behrensmeyer. 1976. Hominid taphonomy: Transport of human skeletal parts in an artificial fluviatile environment. American Journal of Physical Anthropology 45:53–60.

Boyd, C. A., C. M. Brown, R. D. Scheetz, and J. A. Clarke. 2009. Taxonomic revision of the basal neornithischian taxa *Thescelosaurus* and *Bugenasaura*. Journal of Vertebrate Paleontology 29:758–770.

Boyd, C. A., T. P. Cleland, and F. Novas. 2011. Osteogenesis, homology, and function of the intercostal plates in ornithischian dinosaurs (Tetrapoda, Sauropsida). Zoomorphology 130:305–313.

Boyd, C. A. 2012. Taxonomic revision of latest Cretaceous North American basal neornithischian taxa and a phylogenetic analysis of basal ornithischian relationships. University of Texas at Austin, 1-453 pp.

Boyd, C. A. 2014. The cranial anatomy of the neornithischian dinosaur *Thescelosaurus neglectus*. PeerJ 2:e669.

Boyd, C. A. 2015. The systematic relationships and biogeographic history of ornithischian dinosaurs. PeerJ 3:e1523.

Bramble, K., A. R. H. LeBlanc, D. O. Lamoureux, M. Wosik, and P. J. Currie. 2017. Histological evidence for a dynamic dental battery in hadrosaurid dinosaurs. Scientific Reports 7:15787.

Britt, B. B. 1993. Pneumatic postcranial bones in dinosaurs and other archosaurs. Calgary, 1–317 pp.

Britt, B. B. 1997. Postcranial Pneumaticity, In Currie, P. J. and K. Padian: Encyclopedia of Dinosaurs. Elsevier. pp. 590–593.

Brocklehurst, R. J., E. R. Schachner, and W. I. Sellers. 2018. Vertebral morphometrics and lung structure in non-avian dinosaurs. Royal Society Open Science 5:180983.

Brocklehurst, R. J., E. R. Schachner, J. R. Codd, and W. I. Sellers. 2020. Respiratory evolution in archosaurs. Philosophical Transactions of the Royal Society B: Biological Sciences 375:20190140.

Brown, C. M. 2009. *Thescelosaurus* (Dinosauria: Ornithischia) and related taxa from the Late Cretaceous of Alberta and Saskatchewan. University of Calgary, 1–363 pp.

Brown, C. M., C. A. Boyd, and A. P. Russell. 2011. A new basal ornithopod dinosaur (Frenchman Formation, Saskatchewan, Canada), and implications for late Maastrichtian ornithischian diversity in North America: A new thescelosaur. Zoological Journal of the Linnean Society 163:1157–1198.

Brown, C. M., and P. Druckenmiller. 2011. Basal ornithopod (Dinosauria: Ornithischia) teeth from the Prince Creek Formation (early Maastrichtian) of Alaska. Canadian Journal of Earth Sciences 48:1342–1354.

Brown, C. M., J. H. Arbour, and D. A. Jackson. 2012. Testing of the Effect of Missing Data Estimation and Distribution in Morphometric Multivariate Data Analyses. Systematic Biology 61:941–954.

Brown, C. M., D. C. Evans, N. E. Campione, L. J. O'Brien, and D. A. Eberth. 2013a. Evidence for taphonomic size bias in the Dinosaur Park Formation (Campanian, Alberta), a model Mesozoic terrestrial alluvial-paralic system. Palaeogeography, Palaeoclimatology, Palaeoecology 372:108–122.

Brown, C. M., D. C. Evans, M. J. Ryan, and A. P. Russell. 2013b. New data on the diversity and abundance of small-bodied ornithopods (Dinosauria, Ornithischia) from the Belly River Group (Campanian) of Alberta. Journal of Vertebrate Paleontology 33:495–520.

Brusatte, S. L., M. A. Norell, T. D. Carr, G. M. Erickson, J. R. Hutchinson, A. M. Balanoff, G. S. Bever, J. N. Choiniere, P. J. Makovicky, and X. Xu. 2010. Tyrannosaur paleobiology: new research on ancient exemplar organisms. Science 329:1481–1485.

Buchholz P. W. 2002. Phylogeny and biogeography of basal Ornithischia. In: Brown D. E., ed. The Mesozoic in Wyoming. Casper: Tate Geological Museum, 18–34.

Buckley, L. G., D. W. Larson, M. Reichel, and T. Samman. 2010. Quantifying tooth variation within a single population of *Albertosaurus sarcophagus* (Theropoda: Tyrannosauridae) and implications for identifying isolated teeth of tyrannosaurids. This article is one of a series of papers published in this Special Issue on the theme Albertosaurus. Canadian Journal of Earth Sciences 47:1227–1251.

Butler, R. J., and P. M. Galton. 2008. The ‘dermal armour’ of the ornithopod dinosaur *Hypsilophodon* from the Wealden (Early Cretaceous: Barremian) of the Isle of Wight: a reappraisal. Cretaceous Research 29:636–642.

Butler, R. J., P. Upchurch, and D. B. Norman. 2008. The phylogeny of the ornithischian dinosaurs. Journal of Systematic Palaeontology 6:1–40.

Butler, R. J., and Q. Zhao. 2009. The small-bodied ornithischian dinosaurs *Micropachycephalosaurus hongtuyanensis* and *Wannanosaurus yansiensis* from the Late Cretaceous of China. Cretaceous Research 30:63–77.

Butler, R. J., J. Liyong, C. Jun, and P. Godefroit. 2011. The postcranial osteology and phylogenetic position of the small ornithischian dinosaur *Changchunsaurus parvus* from the Quantou Formation (Cretaceous: Aptian–Cenomanian) of Jilin Province, north-eastern China. Palaeontology 54:667–683.

Butler, R. J., P. M. Barrett, and D. J. Gower. 2012. Reassessment of the evidence for postcranial skeletal pneumaticity in Triassic archosaurs, and the early evolution of the avian respiratory system. PLoS ONE 7:1–23.

Button, D. J., and L. E. Zanno. 2020. Repeated Evolution of Divergent Modes of Herbivory in Non-avian Dinosaurs. Current Biology 30:158-168.e4.

Calvo, J. O., J. D. Porfiri, and F. E. Novas. 2007. Discovery of a new ornithopod dinosaur from the Portezuelo Formation (Upper Cretaceous), Neuquen, Patagonia, Argentina. Arquivos do Museu Nacional, Rio de Janeiro 65 (4): 471–483.

Campione, N. E., and D. C. Evans. 2012. A universal scaling relationship between body mass and proximal limb bone dimensions in quadrupedal terrestrial tetrapods. BMC Biology 10:60.

Campione, N. E. 2014. Postcranial Anatomy of *Edmontosaurus regalis* (Hadrosauridae) from the Horseshoe Canyon Formation, Alberta, Canada: In Eberth, D. A. and D. C. Evans, Hadrosaurs. 1st edition. Indiana University Press, 208-244.

Campione, N. E., D. C. Evans, C. M. Brown, and M. T. Carrano. 2014. Body mass estimation in non-avian bipeds using a theoretical conversion to quadruped stylopodial proportions. Methods in Ecology and Evolution 5:913–923.

Carpenter, K., and P. J. Currie. 1992. Dinosaur Systematics: Approaches and Perspectives. Cambridge University Press, 360 pp.

Carpenter, K., and D. B. Young. 2002. Late Cretaceous dinosaurs from the Denver Basin, Colorado. Rocky Mountain Geology 37:237–254.

Carpenter, K. 2004. Redescription of *Ankylosaurus magniventris* Brown 1908 () from the Upper Cretaceous of the Western Interior of North America. Canadian Journal of Earth Sciences 41:961–986.

Carpenter, K., J. Bartlett, J. Bird, and R. Barrick. 2008. Ankylosaurs from the Price River quarries, Cedar Mountain Formation (Lower Cretaceous), east-central Utah. Journal of Vertebrate Paleontology 28(4):1089-1101.

Carpenter, K., and M. C. Lamanna. 2015. The Braincase Assigned to the Ornithopod Dinosaur *Uteodon* McDonald, 2011, Reassigned to *Dryosaurus* Marsh, 1894: Implications for Iguanodontian Morphology and Taxonomy. Annals of Carnegie Museum 83:149–165.

Carr, T. D., D. J. Varricchio, J. C. Sedlmayr, E. M. Roberts, and J. R. Moore. 2017. A new tyrannosaur with evidence for anagenesis and crocodile-like facial sensory system. Scientific Reports 7:44942.

Carrano, M. T. 1999. What, if anything, is a cursor? Categories versus continua for determining locomotor habit in mammals and dinosaurs. Journal of Zoology 247:29–42.

Carrano, M. T., and J. R. Hutchinson. 2002. Pelvic and hindlimb musculature of *Tyrannosaurus rex* (Dinosauria: Theropoda). Journal of Morphology 253:207–228.

Carrier, D., and C. Farmer. 2000. The evolution of pelvic aspiration in archosaurs. Paleobiology 26:271-293.

Castanet, J. 1994. Age Estimation and Longevity in Reptiles. Gerontology 40:174–192.

Castanet, J., S. Croci, F. Aujard, M. Perret, J. Cubo, and E. de Margerie. 2004. Lines of arrested growth in bone and age estimation in a small primate: Microcebus murinus. Journal of Zoology 263:31–39.

Chapman, R. E., and M. K. Brett-Surman. 1990. Morphometric observations on hadrosaurid ornithopods; pp. 163–178 in K. Carpenter and P. J. Currie (eds.), Dinosaur Systematics, 1st ed. Cambridge University Press.

Chen, P., Z. Dong, and S. Zhen. 1998. An exceptionally well-preserved theropod dinosaur from the Yixian Formation of China. Nature 391:147–152.

Chen, J., A. R. H. LeBlanc, L. Jin, T. Huang, and R. R. Reisz. 2018. Tooth development, histology, and enamel microstructure in *Changchunsaurus parvus*: Implications for dental evolution in ornithopod dinosaurs. PLoS ONE 13.

Chinnery, B. J., and D. B. Weishampel. 1998. *Montanoceratops cerorhynchus* (Dinosauria: Ceratopsia) and relationships among basal neoceratopsians. Journal of Vertebrate Paleontology 18(3):569-585.

Chinsamy, A. 1995. Ontogenetic Changes in the Bone Histology of the Late Jurassic Ornithopod *Dryosaurus lettowvorbecki*. Journal of Vertebrate Paleontology 15:96–104.

Chinsamy, A., T. Rich, and P. Vickers-Rich. 1998. Polar dinosaur bone histology. Journal of Vertebrate Paleontology 18:385–390.

Chinsamy, A., I. Cerda, and J. Powell. 2016. Vascularised endosteal bone tissue in armoured sauropod dinosaurs. Scientific Reports 6:24858.

Clark, J. M., T. Maryańska, and R. Barsbold. 2004. Therizinosauroidea, in Weishampel, D. B., Dodson, P., Osmólska, H. (eds.), The Dinosauria (2nd Edition), Berkeley, University of California Press, 151-164.

Cleland, T. P., M. K. Stoskopf, and M. H. Schweitzer. 2011. Histological, chemical, and morphological reexamination of the "heart" of a small Late Cretaceous *Thescelosaurus*. Naturwissenschaften 98:203–211.

Codd, J. R., D. F. Boggs, S. F. Perry, and D. R. Carrier. 2005. Activity of three muscles associated with the uncinate processes of the giant Canada goose *Branta canadensis maximus*. The Journal of Experimental Biology 208:849–857.

Codd, J. R., P. L. Manning, M. A. Norell, and S. F. Perry. 2008. Avian-like breathing mechanics in maniraptoran dinosaurs. Proceedings of the Royal Society B: Biological Sciences 275:157–161.

Coombs, W. P. 1979. Osteology and Myology of the Hindlimb in the Ankylosauria (Reptillia, Ornithischia). Journal of Paleontology 53:666–684.

Coombs, W.P., Jr., and Maryańska, T. 1992. Ankylosauria. In the Dinosauria (paperback ed.). Edited by D.B. Weishampel, P. Dodson, and H. Osmólska. University of California Press, Berkeley, Calif. pp. 456–483.

Cooper, M. R. 1985. A revision of the ornithischian dinosaur *Kangnasaurus coetzeei* Haughton, with a classification of the Ornithischia. 95:281–317.

Cooper, L. N., A. H. Lee, M. L. Taper, and J. R. Horner. 2008. Relative growth rates of predator and prey dinosaurs reflect effects of predation. Proceedings of the Royal Society B: Biological Sciences 275:2609–2615.

Coria, R., and L. Salgado. 1996. A basal Iguanodontian (Ornithischia: Ornithopoda) from the Late Cretaceous of South America. Journal of Vertebrate Paleontology - J VERTEBRATE PALEONTOL 16:445–457.

Coria, R. A., and J. O. Calvo. 2002. A new iguanodontian ornithopod from Neuquen Basin, Patagonia, Argentina. Journal of Vertebrate Paleontology 22:503–509.

Corruccini, R. S. 1987. Shape in morphometrics: Comparative analyses. American Journal of Physical Anthropology 73:289–303.

Cullen, T. M., D. C. Evans, M. J. Ryan, P. J. Currie, Y. Kobayashi. 2014. Osteohistological variation in growth marks and osteocyte lacunar density in a theropod dinosaur (Coelurosauria: Ornithomimidae). BMC Evolutionary Biology. 14:231.

Currie, P. J., and E. Koppelhus. 2005. Dinosaur Provincial Park: A spectacular ancient ecosystem revealed. Life of the Past. Indiana, 54-82.

Currie, P. J., R. B. Holmes, M. J. Ryan, and C. Coy. 2016. A juvenile chasmosaurine ceratopsid (Dinosauria, Ornithischia) from the Dinosaur Park Formation, Alberta, Canada. Journal of Vertebrate Paleontology 36:e1048348.

Curry, K. A. 1999. Ontogenetic histology of *Apatosaurus* (Dinosauria: Sauropoda): New insights on growth rates and longevity. Journal of Vertebrate Paleontology 19:654–665.

de Buffrénil, V., and J. Castanet. 2000. Age Estimation by Skeletochronology in the Nile Monitor (*Varanus niloticus*), a Highly Exploited Species. Journal of Herpetology 34:414–424.

Dieudonné, P.-E., P. Cruzado-Caballero, P. Godefroit, and T. Tortosa. 2020. A new phylogeny of cerapodan dinosaurs. Historical Biology 0:1–21.

Dieudonné, P.-E., T. Tortosa, F. Torcida Fernández-Baldor, J. I. Canudo, and I. Díaz-Martínez. 2016. An Unexpected Early Rhabdodontid from Europe (Lower Cretaceous of Salas de los Infantes, Burgos Province, Spain) and a Re-Examination of Basal Iguanodontian Relationships. PLoS ONE 11:e0156251.

Dodson, P. 1975. Functional and ecological significance of relative growth in Alligator. Journal of Zoology 175:315–355.

Dodson, P., C. A. Forster, and S. D. Sampson. 2004. Ceratopsidae, in Weishampel, D.B., Dodson, P., Osmólska, H. (eds.), The Dinosauria (2nd Edition), Berkeley, University of California Press, 494-513.

Eberth, D. A. 1990. Stratigraphy and sedimentology of vertebrate microfossil sites in the uppermost Judith River Formation (Campanian), Dinosaur Provincial Park, Alberta, Canada. Palaeogeography, Palaeoclimatology, Palaeoecology 78:1–36.

Eberth, D. A., and A. P. Hamblin. 1993. Tectonic, stratigraphic, and sedimentologic significance of a regional discontinuity in the upper Judith River Group (Belly River wedge) of southern Alberta, Saskatchewan, and northern Montana. Canadian Journal of Earth Sciences 30:174–200.

Eberth, D. A., and D. R. Braman. 2012. A revised stratigraphy and depositional history for the Horseshoe Canyon Formation (Upper Cretaceous), southern Alberta plains. Canadian Journal of Earth Sciences 49:1053–1086.

Eberth, D. A., D. C. Evans, D. B. Brinkman, F. Therrien, D. H. Tanke, and L. S. Russell. 2013. Dinosaur biostratigraphy of the Edmonton Group (Upper Cretaceous), Alberta, Canada: evidence for climate influence. Canadian Journal of Earth Sciences 50:701–726.

Eberth, D. A., and S. L. Kamo. 2019. First high-precision U–Pb CA–ID–TIMS age for the Battle Formation (Upper Cretaceous), Red Deer River valley, Alberta, Canada: implications for ages, correlations, and dinosaur biostratigraphy of the Scollard, Frenchman, and Hell Creek formations. Canadian Journal of Earth Sciences 56:1041–1051.

Enlow, D., S. Brown, and H. C. Brown. 1957. A comparative histological study of fossil and recent bone tissues. Part III. Texas Journal of Science 187-230.

Erickson, G. M. 2005. Assessing dinosaur growth patterns: a microscopic revolution. Trends in Ecology & Evolution 20:677–684.

Erickson, G. M., K. Curry Rogers, D. J. Varricchio, M. A. Norell, and X. Xu. 2007. Growth patterns in brooding dinosaurs reveals the timing of sexual maturity in non-avian dinosaurs and genesis of the avian condition. Biology Letters 3:558–561.

Erickson, G. M., P. J. Makovicky, B. D. Inouye, C.-F. Zhou, and K.-Q. Gao. 2009. A Life Table for *Psittacosaurus lujiatunensis*: Initial Insights into Ornithischian Dinosaur Population Biology. The Anatomical Record 292:1514–1521.

Erickson, G. M., B. A. Krick, M. Hamilton, G. R. Bourne, M. A. Norell, E. Lilleodden, and W. G. Sawyer. 2012. Complex Dental Structure and Wear Biomechanics in Hadrosaurid Dinosaurs. Science 338:98–101.

Evans, D. C., and R. R. Reisz. 2007. Anatomy and Relationships of *Lambeosaurus magnicristatus*, a crested hadrosaurid dinosaur (Ornithischia) from the Dinosaur Park Formation, Alberta. Journal of Vertebrate Paleontology 27:373–393.

Evans, D. C. 2010. Cranial anatomy and systematics of *Hypacrosaurus altispinus*, and a comparative analysis of skull growth in lambeosaurine hadrosaurids (Dinosauria: Ornithischia). Zoological Journal of the Linnean Society 159:398–434.

Fabbri, M., J. Wiemann, F. Manucci, and D. E. G. Briggs. 2020. Three-dimensional soft tissue preservation revealed in the skin of a non-avian dinosaur. Palaeontology 63:185–193.

Fanti, F., and O. Catuneanu. 2009. Stratigraphy of the Upper Cretaceous Wapiti Formation, west-central Alberta, Canada. Canadian Journal of Earth Sciences 46:263–286.

Fanti, F., and T. Miyashita. 2009. A high latitude vertebrate fossil assemblage from the Late Cretaceous of west-central Alberta, Canada: evidence for dinosaur nesting and vertebrate latitudinal gradient. Palaeogeography, Palaeoclimatology, Palaeoecology 275:37–53.

Fanti, F., and O. Catuneanu. 2010. Fluvial Sequence Stratigraphy: The Wapiti Formation, West-Central Alberta, Canada. Journal of Sedimentary Research 80:320–338.

Fanti, F., P. J. Currie, M. E. Burns, and H.-D. Sues. 2015. Taphonomy, age, and paleoecological implication of a new *Pachyrhinosaurus* (Dinosauria: Ceratopsidae) bonebed from the Upper

Cretaceous (Campanian) Wapiti Formation of Alberta, Canada. Canadian Journal of Earth Sciences 52:250–260.

Farke, A., and E. Yip. 2019. A juvenile cf. *Edmontosaurus annectens* (Ornithischia, Hadrosauridae) femur documents a poorly represented growth stage for this taxon. Vertebrate Anatomy Morphology Palaeontology 7:59-67.

Fearon, J. L., and D. J. Varricchio. 2015. Morphometric analysis of the forelimb and pectoral girdle of the Cretaceous ornithopod dinosaur *Oryctodromeus cubicularis* and implications for digging. Journal of Vertebrate Paleontology 35:e936555.

Fearon, J. L., and D. J. Varricchio. 2016. Reconstruction of the forelimb musculature of the Cretaceous ornithopod dinosaur *Oryctodromeus cubicularis*: implications for digging. Journal of Vertebrate Paleontology 36:e1078341.

Fisher, P. E., D. A. Russell, M. K. Stoskopf, R. E. Barrick, M. Hammer, and A. A. Kuzmitz. 2000. Cardiovascular Evidence for an Intermediate or Higher Metabolic Rate in an Ornithischian Dinosaur. Science 288:503–505.

Fong, R. K. M., A. R. H. LeBlanc, D. S. Berman, and R. R. Reisz. 2016. Dental histology of Coelophysis bauri and the evolution of tooth attachment tissues in early dinosaurs. Journal of Morphology 277:916–924.

Fowler, D. W. 2016. Dinosaurs and time: chronostratigraphic frameworks and their utility in analysis of dinosaur paleobiology. 1–830.

Freimuth, W. J., and D. J. Varricchio. 2019. Insect trace fossils elucidate depositional environments and sedimentation at a dinosaur nesting site from the Cretaceous (Campanian) Two Medicine Formation of Montana. Palaeogeography, Palaeoclimatology, Palaeoecology 534:109262.

Galton, P. M. 1969. The pelvic musculature of the dinosaur *Hypsilophodon* (Reptila: Ornithischian). Postilla 131:1-64.

Galton, P. M. 1973. Redescription of the Skull and Mandible of *Parksosaurus* from the Late Cretaceous, with Comments on the Family Hypsilophodontidae (Ornithischia). Royal Ontario Museum, Toronto: Life Science Contributions Royal Ontario Museum 89:1-21.

Galton, P. M. 1974a. The ornithischian dinosaur *Hypsilophodon* from the Wealden of the Isle of Wight. Bulletin of the British Museum (Natural History), Geology 25:1–152.

Galton, P. M. 1974b. Notes on *Thescelosaurus*, a Conservative Ornithopod Dinosaur from the Upper Cretaceous of North America, with Comments on Ornithopod Classification. Journal of Paleontology 48:1048–1067.

Galton, P. M. 1978. Fabrosauridae, the basal family of ornithischian dinosaurs (Reptilia: Ornithopoda). Paläontologische Zeitschrift 52:138.

Galton, P. M., and H.-D. Sues. 1983. New data on pachycephalosaurid dinosaurs (Reptilia: Ornithischia) from North America. Canadian Journal of Earth Sciences 20:462–472.

Galton, P. M. 1995. The species of the basal hypsilophodontid dinosaur T*hescelosaurus* Gilmore (Ornithischia: Ornithopoda) from the Late Cretaceous of North America. Neues Jahrbuch Für Geologie Und Paläontologie - Abhandlungen 198:297–311.

Galton, P. M. 2014. Notes on the postcranial anatomy of the heterodontosaurid dinosaur *Heterodontosaurus tucki*, a basal ornithischian from the Lower Jurassic of South Africa. Revue de Paleobiologie, Geneve. 33:97-141.

Garland, T., and C. M. Janis. 1993. Does metatarsal/femur ratio predict maximal running speed in cursorial mammals? Journal of Zoology 229:133–151.

Gee, B. M., Y. Haridy, and R. R. Reisz. 2020. Histological skeletochronology indicates developmental plasticity in the early Permian stem lissamphibian *Doleserpeton annectens*. Ecology and Evolution 10:2153–2169.

Gilmore, C. W. 1913. A New Dinosaur from the Lance Formation of Wyoming. Smithsonian Miscellaneous Collections 61(5): 1-5.

Gilmore, C. W. 1915. Osteology of *Thescelosaurus*, an orthopodous dinosaur from the Lance formation of Wyoming. Proceedings of the United States National Museum 49(2127): 591-616.

Gittleman, J. L., and S. D. Thompson. 1988. Energy Allocation in Mammalian Reproduction. American Zoologist 28:863–875.

Godefroit, P., Y. L. Bolotsky, and J. V. Itterbeeck. 2004. The Lambeosaurine Dinosaur *Amurosaurus riabinini* from the Maastrichtian of Far Eastern Russia. Acta Palaeontologica Polonica 49(4): 585-618.

Godefroit, P., H. Demuynck, G. Dyke, D. Hu, F. Escuillié, and P. Claeys. 2013. Reduced plumage and flight ability of a new Jurassic paravian theropod from China. Nature Communications 4:1394.

Godefroit, P., S. M. Sinitsa, D. Dhouailly, Y. L. Bolotsky, A. V. Sizov, M. E. McNamara, M. J. Benton, and P. Spagna. 2014. A Jurassic ornithischian dinosaur from Siberia with both feathers and scales. Science 345:451–455.

Godefroit, P., S. M. Sinitsa, A. Cincotta, M. E. McNamara, S. A. Reshetova, and D. Dhouailly. 2020. Integumentary Structures in *Kulindadromeus zabaikalicus*, a Basal Neornithischian Dinosaur from the Jurassic of Siberia; pp. 47–65 in The Evolution of Feathers: From Their Origin to the Present. Fascinating Life Sciences Springer International Publishing, Cham.

Goloboff, P. A., J. S. Farris, and K. Nixon. 2008. TNT, a free program for phylogenetic analysis. Cladistics 24:774–786.

Gower, D. J. 2001. Possible postcranial pneumaticity in the last common ancestor of birds and crocodilians: evidence from *Erythrosuchus* and other Mesozoic archosaurs. Naturwissenschaften 88:119–122.

Griffin, C. 2018. Pathological bone tissue in a Late Triassic neotheropod fibula, with implications for the interpretation of medullary bone. New Jersey State Museum Investigation 5:1–10.

Griffin, C. T., M. R. Stocker, C. Colleary, C. M. Stefanic, E. J. Lessner, M. Riegler, K. Formoso, K. Koeller, and S. J. Nesbitt. 2021. Assessing ontogenetic maturity in extinct saurian reptiles. Biological Reviews. Biological Reviews 96: 470-525.

Hailu, Y., and P. Dodson. 2004. Basal Ceratopsia, in Weishampel, D.B., Dodson, P., Osmólska, H. (eds.), The Dinosauria (2nd Edition), Berkeley, University of California Press, 478-493.

Hammer, O., D. A. T. Harper, P. D. Ryan. 2001. PAST: paleontological statistics software package for education and data analysis. Palaeontologia Electronica 4(1): 1-9.

Hammer, O., D. A. T. Harper. 2006. Paleontological data analysis. Blackwell Publishing, Ltd., Malden, Mass.

Han, F.-L., P. M. Barrett, R. J. Butler, and X. Xu. 2012. Postcranial anatomy of *Jeholosaurus shangyuanensis* (Dinosauria, Ornithischia) from the Lower Cretaceous Yixian Formation of China. Journal of Vertebrate Paleontology 32:1370–1395.

Han, F., Q. Zhao, J. Stiegler, and X. Xu. 2020. Bone histology of the non-iguanodontian ornithopod *Jeholosaurus shangyuanensis* and its implications for dinosaur skeletochronology and development. Journal of Vertebrate Paleontology 40:e1768538.

He, X.-L., and K.-J. Cai. 1983. A new species of *Yandusaurus* (Hypsilophodont Dinosaur) from the Middle Jurassic of Dashanpu, Zigong, Sichuan. Journal of Chengdu College of Geology 5–14.

He, Y., P. J. Makovicky, K. Wang, S. Chen, C. Sullivan, F. Han, and X. Xu. 2015. A New Leptoceratopsid (Ornithischia, Ceratopsia) with a unique Ischium from the Upper Cretaceous of Shandong Province, China. PLoS ONE 10:e0144148.

Hedrick, B. P., C. Gao, A. R. Tumarkin-Deratzian, C. Shen, J. L. Holloway, F. Zhang, K. D. Hankenson, S. Liu, J. Anné, and P. Dodson. 2016. An Injured Psittacosaurus (Dinosauria: Ceratopsia) From the Yixian Formation (Liaoning, China): Implications for *Psittacosaurus* Biology. The Anatomical Record 299:897–906.

Heller, P. L., C. L. Angevine, N. S. Winslow, and C. Paola. 1988. Two-phase stratigraphic model of foreland-basin sequences. Geology 16:501–504.

Hendrickx, C., O. Mateus, and R. Araújo. 2015. A proposed terminology of theropod teeth (Dinosauria, Saurischia). Journal of Vertebrate Paleontology 35:e982797.

Herne, M. C., J. P. Nair, A. R. Evans, and A. M. Tait. 2019. New small-bodied ornithopods (Dinosauria, Neornithischia) from the Early Cretaceous Wonthaggi Formation (Strzelecki Group) of the Australian-Antarctic rift system, with revision of *Qantassaurus intrepidus* Rich and Vickers-Rich, 1999. Herne et al.—Barremian ornithopods from the Australian-Antarctic rift Journal of Paleontology. Journal of Paleontology 93:543–584.

Hofmann, R. R. 1973. The ruminant stomach. Stomach structure and feeding habits of East African game ruminants. East African monographs in biology. Volume 2. The Ruminant Stomach. Stomach Structure and Feeding Habits of East African Game Ruminants. East African Monographs in Biology. Volume 2.

Holmes, R. B., and M. J. Ryan. 2013. The postcranial skeleton of *Styracosaurus albertensis*. Kirtlandia 58:5-37.

Holmes, R. B. 2014. The postcranial skeleton of *Vagaceratops irvinensis* (Dinosauria, Ceratopsidae). Vertebrate Anatomy Morphology Palaeontology 1:1–21.

Holmes, R. B., W. S. Persons, B. S. Rupal, A. J. Qureshi, and P. J. Currie. 2020. Morphological variation and asymmetrical development in the skull of *Styracosaurus albertensis*. Cretaceous Research 107:104308.

Holtz, T. R. 2004. Tyrannosauroidea, in Weishampel, D. B., Dodson, P., Osmólska, H. (eds.), The Dinosauria (2nd Edition), Berkeley, University of California Press, 111-136.

Hone, D. W. E., and J. C. Mallon. 2017. Protracted growth impedes the detection of sexual dimorphism in non-avian dinosaurs. Palaeontology 60:535–545.

Horner, J. R., and R. Makela. 1979. Nest of juveniles provides evidence of family structure among dinosaurs. Nature 282:296–298.

Horner, J. R., and D. B. Weishampel. 1988. A comparative embryological study of two ornithischian dinosaurs. Nature 332:256–257.

Horner, J. R., A. de Ricqlès, and K. Padian. 1999. Variation in Dinosaur Skeletochronology Indicators: Implications for Age Assessment and Physiology. Paleobiology 25:295–304.

Horner, J. R., A. D. Ricqlès, and K. Padian. 2000. Long Bone Histology of the Hadrosaurid Dinosaur *Maiasaura peeblesorum*: Growth Dynamics and Physiology Based on an Ontogenetic Series of Skeletal Elements. Journal of Vertebrate Paleontology 20:115–129.

Horner, J. R., A. D. Ricqlès, K. Padian, and R. D. Scheetz. 2009. Comparative long bone histology and growth of the "hypsilophodontid" dinosaurs *Orodromeus makelai*, *Dryosaurus altus*, and *Tenontosaurus tillettii* (Ornithischia: Euornithopoda). Journal of Vertebrate Paleontology 29:734–747.

Horner, J. R., and E.-T. Lamm. 2011. Ontogeny of the parietal frill of *Triceratops*: A preliminary histological analysis. Comptes Rendus Palevol 10:439–452.

Hu, D., L. Hou, L. Zhang, and X. Xu. 2009. A pre-Archaeopteryx troodontid theropod from China with long feathers on the metatarsus. Nature 461:640–643.

Hudgins, M. N., P. R. Bell, N. E. Campione, F. Fanti, R. L. Sissons, M. J. Vavrek, D. W. Larson, and C. Sullivan. 2020a. New thescelosaurid (Dinosauria, Ornithischia) material from the Wapiti Formation (Campanian) of northern Alberta. Vertebrate Anatomy Morphology Palaeontology 8:42

Hudgins, M. N., M. D. Uhen, and L. A. Hinnov. 2020b. The evolution of respiratory systems in Theropoda and Paracrocodylomorpha, the end-Triassic extinction, and the role of Late Triassic atmospheric O2 and CO2. Palaeogeography, Palaeoclimatology, Palaeoecology 545:109638.

Huh, M., D.-G. Lee, J.-K. Kim, J.-D. Lim, and P. Godefroit. 2011. A new basal ornithopod dinosaur from the Upper Cretaceous of South Korea. Neues Jahrbuch Für Geologie Und Paläontologie - Abhandlungen 259:1–24.

Hulke, J. W. 1874. Supplemental Note on the Anatomy of *Hypsilophodon Foxii*. Quarterly Journal of the Geological Society 30:18–23.

Husson, F., and J. Josse. 2016. missMDA: A Package for Handling Missing Values in Multivariate Data Analysis. Journal of Statistical Software 70.

Hutton, J. M. 1986. Age Determination of Living Nile Crocodiles from the Cortical Stratification of Bone. Copeia 1986:332–341.

Huxley, T. J. 1869. On *Hypsilophodon*, a new genus of Dinosauria. Abstracts of the Proceedings of the Geological Society of London 204:3–4.

Huxley, T. H. 1870. On *Hypsilophodon Foxii*, a new Dinosaurian from the Wealden of the Isle of Wight. Quarterly Journal of the Geological Society 26:3–12.

Hwang, S. H. 2005. Phylogenetic patterns of enamel microstructure in dinosaur teeth. Journal of Morphology 266:208–240.

Hwang, S. H. 2011. The evolution of dinosaur tooth enamel microstructure. Biological Reviews 86:183–216.

Ibiricu, L. M., R. D. Martínez, A. Luna, and G. A. Casal. 2014. A reappraisal of *Notohypsilophodon comodorensis* (Ornithischia: Ornithopoda) from the Late Cretaceous of Patagonia, Argentina. Zootaxa 3786:401-422.

Irmis, R. B., W. G. Parker, S. J. Nesbitt, and J. Liu. 2007. Early ornithischian dinosaurs: the Triassic record. Historical Biology 19:3–22.

Jackson, D. A. 1993. Stopping Rules in Principal Components Analysis: A Comparison of Heuristical and Statistical Approaches. Ecology 74:2204–2214.

Ji, Q., and S. Ji. 1996. On the Discovery of the earliest fossil bird in China (*Sinosauropteryx* gen. nov.) and the origin of birds. Chinese Geology 233:30–33.

Jin, L.-Y., C. Jun, Z. Shuqin, R. J. Butler, and P. Godefroit. 2010. Cranial anatomy of the small ornithischian dinosaur *Changchunsaurus parvus* from the Quantou Formation (Cretaceous: Aptian–Cenomanian) of Jilin Province, northeastern China. Journal of Vertebrate Paleontology 30:196–214.

Josse, J., M. Chavent, B. Liquet, and F. Husson. 2012. Handling Missing Values with Regularized Iterative Multiple Correspondence Analysis. Journal of Classification 29:91–116.

Josse, J., and F. Husson. 2016. missMDA: A Package for Handling Missing Values in Multivariate Data Analysis. Journal of Statistical Software 70.

Köhler, M., N. Marín-Moratalla, X. Jordana, and R. Aanes. 2012. Seasonal bone growth and physiology in endotherms shed light on dinosaur physiology. Nature 487:358–361.

Koppelhus, E. B., and F. Fanti. 2019. Rare, non-marine deposits during the deposition of the Bearpaw Formation: Interpreting the palaeoenvironment of the DC bonebed (Wapiti Formation) using palynology and palaeobotany. Vertebrate Anatomy Morphology Palaeontology 7:25-26.

Krishtalka, L. 1993. Anagenetic Angst; pp. 331–344 in W. H. Kimbel and L. B. Martin (eds.), Species, Species Concepts and Primate Evolution. Springer US, Boston, MA.

Krumenacker, L. J. 2017. Osteology, phylogeny, taphonomy, and ontogenetic histology of *Oryctodromeus cubicularis*, from the middle Cretaceous (Albian-Cenomanian) of Montana and Idaho. 1–282.

Krumenacker, L. J., D. J. Varricchio, J. P. Wilson, A. Martin, and A. Ferguson. 2019. Taphonomy of and new burrows from *Oryctodromeus cubicularis*, a burrowing neornithischian dinosaur, from the mid-Cretaceous (Albian-Cenomanian) of Idaho and Montana, U.S.A. Palaeogeography, Palaeoclimatology, Palaeoecology 530:300–311.

Kubo, T., and M. O. Kubo. 2012. Associated evolution of bipedality and cursoriality among Triassic archosaurs: a phylogenetically controlled evaluation. Paleobiology 38:474–485.

Kuehn, A. L., A. H. Lee, R. P. Main, and E. L. R. Simons. 2019. The effects of growth rate and biomechanical loading on bone laminarity within the emu skeleton. PeerJ 7:e7616.

Kutter, M. M. 2003. New material of *Zephyrosaurus schaffi* (Dinosauria: Ornithischia) from the Cloverly Formation (Aptian-Albian) of Montana. Journal of Vertebrate Paleontology. 23 (3, Suppl.): 69A.

Lagarde, F., X. Bonnet, B. Henen, J. Corbin, K. Nagy, and G. Naulleau. 2001. Sexual size dimorphism in steppe tortoises (*Testudo horsfieldi*): Growth, maturity, and individual variation.

Canadian Journal of Zoology-Revue Canadienne De Zoologie - Canadian Journal of Zoology 79:1433–1441.

Lambe, L. M. 1902. New genera and species from the Belly River Series (mid-Cretaceous). Geological Survey of Canada, Contributions to Canadian Palaeontology 3:68.

Lambertz, M., F. Bertozzo, and P. M. Sander. 2018. Bone histological correlates for air sacs and their implications for understanding the origin of the dinosaurian respiratory system. Biology Letters 14:20170514.

Larson, D. W., D. B. Brinkman, and P. R. Bell. 2010. Faunal assemblages from the upper Horseshoe Canyon Formation, an early Maastrichtian cool-climate assemblage from Alberta, with special reference to the *Albertosaurus sarcophagus* bonebed. This article is one of a series of papers published in this Special Issue on the theme Albertosaurus. Canadian Journal of Earth Sciences 47:1159–1181.

LeBlanc, A. R. H., R. R. Reisz, D. C. Evans, and A. M. Bailleul. 2016. Ontogeny reveals function and evolution of the hadrosaurid dinosaur dental battery. BMC Evolutionary Biology 16:152.

LeBlanc, A. R. H., K. S. Brink, T. M. Cullen, and R. R. Reisz. 2017. Evolutionary implications of tooth attachment versus tooth implantation: A case study using dinosaur, crocodilian, and mammal teeth. Journal of Vertebrate Paleontology 37:e1354006.

Lee, A. H., and S. Werning. 2008. Sexual maturity in growing dinosaurs does not fit reptilian growth models. Proceedings of the National Academy of Sciences 105:582–587.

Lehman, T. M. 1987. Late Maastrichtian paleoenvironments and dinosaur biogeography in the western interior of North America. Palaeogeography, Palaeoclimatology, Palaeoecology 60:189–217.

Lull, R. S., and C. M. Le Vene. 1933. A Revision of the Ceratopsia or Horned Dinosaurs. Peabody Museum of Natural History New Haven, Conn., 1-173.

Lyson, T. R., and N. R. Longrich. 2011. Spatial niche partitioning in dinosaurs from the latest cretaceous (Maastrichtian) of North America. Proceedings of the Royal Society B: Biological Sciences 278:1158–1164.

Macaluso, L., and E. Tschopp. 2018. Evolutionary changes in pubic orientation in dinosaurs are more strongly correlated with the ventilation system than with herbivory. Palaeontology 61:703–719.

Maddison, W. P., and D. R. Maddison. 2009. Mesquite: a modular system for evolutionary analysis. 3.6.

Madzia, D., C. A. Boyd, and M. Mazuch. 2018. A basal ornithopod dinosaur from the Cenomanian of the Czech Republic. Journal of Systematic Palaeontology 16:967–979.

Maidment, S. C. R., and P. M. Barrett. 2011a. A new specimen of *Chasmosaurus belli* (Ornithischia: Ceratopsidae), a revision of the genus, and the utility of postcrania in the taxonomy and systematics of ceratopsid dinosaurs. Zootaxa 2963:1-47.

Maidment, S. C. R., and P. M. Barrett. 2011b. The locomotor musculature of basal ornithischian dinosaurs. Journal of Vertebrate Paleontology 31:1265–1291.

Maidment, S. C. R., and P. M. Barrett. 2012. Osteological Correlates for Quadrupedality in Ornithischian Dinosaurs. Acta Palaeontologica Polonica 59:53–70.

Maidment, S. C. R., K. T. Bates, and P. M. Barrett. 2014. Three-Dimensional Computational Modeling of Pelvic Locomotor Muscle Moment Arms in *Edmontosaurus* (Dinosauria, Hadrosauridae) and Comparisons with Other Archosaurs. In: Eberth, D. A., and Evans D. C. Hadrosaurs. 1st edition. Indiana University Press, 433-449.

Mahalanobis, P.C. 1936. On the generalised distance in statistics. Proceedings of the National Institute of Science India 2: 49–55.

Makovicky, P. J., Y., Kobayashi, and P. J. Currie. 2004, Ornithomimosauria, in Weishampel, D. B., Dodson, P., Osmólska, H. (eds.), The Dinosauria (2nd Edition), Berkeley, University of California Press, 137-150.

Makovicky, P. J., B. M. Kilbourne, R. W. Sadleir, and M. A. Norell. 2011. A new basal ornithopod (Dinosauria, Ornithischia) from the Late Cretaceous of Mongolia. Journal of Vertebrate Paleontology 31:626–640.

Mallon, J. C., D. C. Evans, M. J. Ryan, and J. S. Anderson. 2012. Megaherbivorous dinosaur turnover in the Dinosaur Park Formation (upper Campanian) of Alberta, Canada. Palaeogeography, Palaeoclimatology, Palaeoecology 350–352:124–138.

Mallon, J. C., and J. S. Anderson. 2013. Skull Ecomorphology of Megaherbivorous Dinosaurs from the Dinosaur Park Formation (Upper Campanian) of Alberta, Canada. PLoS ONE 8:e67182.

Mallon, J. C. 2017. Recognizing sexual dimorphism in the fossil record: lessons from nonavian dinosaurs. Paleobiology 43:495–507.

Marangoni, F., E. Schaefer, R. Cajade, and M. Tejedo. 2009. Growth-Mark Formation and Chronology of Two Neotropical Anuran Species. Journal of Herpetology 43:546–550.

Marsh, O. C. 1881. Principal characters of American Jurassic dinosaurs, Part V. American Journal of Science Series 3 Vol. 21:417–423.

Marsh, O. C. 1877. Notice of new dinosaurian reptiles from the Jurassic formations. American Journal of Science and Arts 14 (84): 514–516.

Marsh, O. C. 1878. Principal characters of American Jurassic dinosaurs. American Journal of Science, Series 316:411–416.

Martínez, R. D. F. 1998. *Notohypsilophodon comodorensis*, un Hypsilophodontidae (Ornithischia: Ornithopoda) del Cretácico Superior de Chubut, Patagonia Central, Argentina. Acta Geologica Leopoldensia 21:119–135.

Martínez, R., and F. Novas. 2006. *Aniksosaurus darwini* gen. et sp. nov., a new coelurosaurian theropod from the Early Late Cretaceous of Central Patagonia, Argentina. Revista Del Museo Argentino de Ciencias Naturales, Nueva Serie 8(2):243-259.

Marsh, O. C. 1881. Principal characters of American Jurassic dinosaurs, Part V. American Journal of Science Series 3 Vol. 21:417–423.

Maryańska, T., and H. Osmolska. 1974. Pachycephalosauria, a new suborder of ornithischian dinosaurs. 1-78.

Maryańska, T., R. E. Chapman, D. B. Weishampel. 2004. Pachycephalosauria, in Weishampel, D. B., Dodson, P., Osmólska, H. (eds.), The Dinosauria (2nd Edition), Berkeley, University of California Press, 464-477.

McDonald, A. T. 2012. The status of *Dollodon* and other basal Iguanodonts (Dinosauria: Ornithischia) from the Lower Cretaceous of Europe. Cretaceous Research 33:1–6.

McIver, E. E. 2001. The paleoenvironment of *Tyrannosaurus rex* from southwestern Saskatchewan, Canada. Canadian Journal of Earth Sciences 39:207–221.

Meng, Q., J. Liu, D. J. Varricchio, T. Huang, and C. Gao. 2004. Parental care in an ornithischian dinosaur. Nature 431:145–146.

Morris, W. J. 1976. Hypsilophodont dinosaurs: a new species and comments on their systematics, in: Churcher, C.S. (1st Ed.), Athlon. Toronto: Royal Ontario Museum. pp. 93-113.

Morschhauser, E. M., H. You, D. Li, and P. Dodson. 2018. Postcranial morphology of the basal neoceratopsian (Ornithischia: Ceratopsia) *Auroraceratops rugosus* from the Early Cretaceous (Aptian–Albian) of northwestern Gansu Province, China. Journal of Vertebrate Paleontology 38:75–116.

Norell, M. A., P. J. Makovicky. 2004. Dromaeosauridae, in Weishampel, D. B., Dodson, P., Osmólska, H. (eds.), The Dinosauria (2nd Edition), Berkeley, University of California Press, 196-209.

Norell, M. A., and D. E. Barta. 2016. A New Specimen of the Ornithischian Dinosaur *Haya griva*, Cross-Gobi Geologic Correlation, and the Age of The Zos Canyon Beds. American Museum Novitates 3851:1–20.

Norman D. B. 2004. Basal Iguanodontia. In: Weishampel D. B., Dodson P., Osmolska H. The Dinosauria. 2nd edition. Berkeley: University of California Press, 413–437.

Norman, D. B., Sues, H-D., Witmer, L. M., and Coria, R. A. 2004a. Basal Ornithopoda, in Weishampel, D. B., Dodson, P., Osmólska, H. (eds.), The Dinosauria (2nd Edition), Berkeley, University of California Press, 393–412.

Norman, D. B., L. M. Witmer, D. B. Weishampel. 2004b. Basal Ornithischia, in Weishampel, D. B., Dodson, P., Osmólska, H. (eds.), The Dinosauria (2nd Edition), Berkeley, University of California Press, 325-334.

Norman, D. B. 2012. Dinosaur Feeding; pp. In: eLS. John Wiley & Sons, Ltd: Chichester.

Novas, F. E., A. V. Cambiaso, and A. Ambrosio. 2004. A new basal iguanodontian (Dinosauria, Ornithischia) from the Upper Cretaceous of Patagonia 41(1): 75-82.

O'Connor, P. M. 2004. Pulmonary pneumaticity in the postcranial skeleton of extant Aves: A case study examining Anseriformes. Journal of Morphology 261:141–161.

O'Connor, P. M. 2006. Postcranial pneumaticity: An evaluation of soft-tissue influences on the postcranial skeleton and the reconstruction of pulmonary anatomy in archosaurs. Journal of Morphology 267:1199–1226.

Ogg, J. G., and L. A. Hinnov. 2012. The Cretaceous; pp. 793–853 in The Geologic Time Scale 2012, 2nd ed. Elsevier.

O'Gorman, E. J., and D. W. E. Hone. 2012. Body Size Distribution of the Dinosaurs. PLoS ONE 7:e51925.

Ősi, A., E. Prondvai, R. Butler, and D. B. Weishampel. 2012. Phylogeny, Histology and Inferred Body Size Evolution in a New Rhabdodontid Dinosaur from the Late Cretaceous of Hungary. PLoS ONE 7:e44318.

Osmolska, H., P. J. Currie, R. Barsbold. 2004, Oviraptorosauria, in Weishampel, D. B., Dodson, P., Osmólska, H. (eds.), The Dinosauria (2nd Edition), Berkeley, University of California Press, 165-183.

Owen, R. 1842. Report on British Fossil Reptiles. Part II. Report of the British Association for the Advancement of Science. Report of the British Association for the Advancement of Science 60–204.

Padian, K., A. J. De Ricqles, and J. R. Horner. 2001. Dinosaurian growth rates and bird origin dinosaurian growth rates and bird origins. Nature 412:405-408.

Padian, K., and E.-T. Lamm. 2013. Bone Histology of Fossil Tetrapods: Advancing Methods, Analysis, and Interpretation, 1st ed. University of California Press, pp. 1-285.

Parks, W. A. 1922. *Parasaurolophus walkeri*, a new genus and species of crested trachodont dinosaur. University of Toronto Studies, Geological Series 13:1–32.

Parks, W. A. 1926. *Thescelosaurus warreni*, a new species of orthopodous dinosaur from the Edmonton Formation of Alberta. University of Toronto Studies (Geological Series) 21:1–42.

Paul, G. S. 1994. Dinosaur reproduction in the fast lane: implications for size, success, and extinction. In Carpenter, K., Hirsch, K., and Horner, J. R. Dinosaur eggs and Babies, Cambridge University Press, 244-255.

Pearson, D. A., T. Schaefer, K. R. Johnson, D. J. Nichols, and J. P. Hunter. 2002. Vertebrate biostratigraphy of the Hell Creek Formation in southwestern North Dakota and northwestern South Dakota; pp. in The Hell Creek Formation and the Cretaceous-Tertiary boundary in the northern Great Plains: An Integrated continental record of the end of the Cretaceous. Geological Society of America.

Persons, W. S., and P. J. Currie. 2020. The Anatomical and Functional Evolution of the Femoral Fourth Trochanter in Ornithischian Dinosaurs. The Anatomical Record 303:1146–1157.

Prieto-Márquez, A. 2014. A juvenile *Edmontosaurus* from the late Maastrichtian (Cretaceous) of North America: Implications for ontogeny and phylogenetic inference in Saurolophine dinosaurs. Cretaceous Research 50:282–303.

Purwandana, D., A. Ariefiandy, M. J. Imansyah, A. Seno, C. Ciofi, M. Letnic, and T. S. Jessop. 2016. Ecological allometries and niche use dynamics across Komodo dragon ontogeny. The Science of Nature 103:27.

Qiang, J., P. J. Currie, M. A. Norell, and J. Shu-An. 1998. Two feathered dinosaurs from northeastern China. Nature 393:753–761.

R core team. 2013. R: A language and environment for statistical computing. R Foundation for Statistical Computing, Vienna, Austria. http://www.R-project.org.

Radermacher, V. J., V. Fernandez, E. R. Schachner, R. J. Butler, E. M. Bordy, M. N. Hudgins, W. J. de Klerk, K. E. Chapelle, and J. N. Choiniere. 2021. A new *Heterodontosaurus* specimen elucidates the unique ventilatory macroevolution of ornithischian dinosaurs. ELife 10:e66036.

Reid, R. E. H. 1984. The histology of dinosaurian bone, and its possible bearing on dinosaurian physiology. Structure, Development and Evolution of Reptiles Symposium of the Zoological Society of London No. 52. pp 629-663.

Reid, R. E. H. 1985. On Supposed Haversian Bone from the Hadrosaur *Anatosaurus*, and the Nature of Compact Bone in Dinosaurs. Journal of Paleontology 59:140–148.

Rhodes, M. M., G. F. Funston, and P. J. Currie. 2020. New material reveals the pelvic morphology of Caenagnathidae (Theropoda, Oviraptorosauria). Cretaceous Research 114:104521.

Rhodes, M. M., D. M. Henderson, and P. J. Currie. 2021. Maniraptoran pelvic musculature highlights evolutionary patterns in theropod locomotion on the line to birds. PeerJ 9:e10855.

Rogers, R. R., and M. E. Brady. 2010. Origins of Microfossil Bonebeds: Insights from the Upper Cretaceous Judith River Formation of North-Central Montana. Paleobiology 36:80–112.

Rose, K. D., and T. M. Bown. 1986. Gradual evolution and species discrimination in the fossil record; pp. 119–130 in K. M. Flanagan and J. A. Lillegraven (eds.), Vertebrates, Phylogeny, and Philosophy. University of Wyoming, Laramie, WY.

Rowe, T., E. F. McBride, and P. C. Sereno. 2001. Dinosaur with a Heart of Stone. Science 291:783–783.

Rozadilla, S., F. L. Agnolin, F. E. Novas, A. M. Aranciaga Rolando, M. J. Motta, J. M. Lirio, and M. P. Isasi. 2016. A new ornithopod (Dinosauria, Ornithischia) from the Upper Cretaceous of Antarctica and its palaeobiogeographical implications. Cretaceous Research 57:311–324.

Santa Luca, A. P., A. W. Crompton, A. J. Charig. 1976. A complete skeleton of the Late Triassic ornithischian *Heterodontosaurus tucki*. Nature 264 (5584): 324-328.

Santa Luca, A. P. 1980. The Postcranial Skeleton of *Heterodontosaurus tucki* (Reptilia, Ornithischia) from the Stormberg of South Africa. Annals of the South African Museum. Annale van die Suid-Afrikaanse Museum., Cape Town :, 1-416 pp.

Scannella, J. B., D. W. Fowler, M. B. Goodwin, and J. R. Horner. 2014. Evolutionary trends in *Triceratops* from the Hell Creek Formation, Montana. Proceedings of the National Academy of Sciences 111:10245–10250.

Schachner, E. R., T. R. Lyson, and P. Dodson. 2009. Evolution of the Respiratory System in Nonavian Theropods: Evidence from Rib and Vertebral Morphology. The Anatomical Record 292:1501–1513.

Schachner, E. R., J. R. Hutchinson, and C. G. Farmer. 2013. Pulmonary anatomy in the Nile crocodile and the evolution of unidirectional airflow in Archosauria. PeerJ 1:e60.

Schachner, E. R., R. L. Cieri, J. P. Butler, and C. G. Farmer. 2014. Unidirectional pulmonary airflow patterns in the savannah monitor lizard. Nature 506:367–370.

Scheetz, R. D. 1999. Osteology of *Orodromeus makelai* and the phylogeny of basal ornithopod dinosaurs. pp 1-204.

Schneider, C.A., W. S. Rasband, and K. W. Eliceiri. 2012. NIH Image to ImageJ: 25 years of image analysis. Nature Methods 9:671-675.

Seeley, H. G. 1888. On the classification of the fossil animals commonly named Dinosauria. Proceedings of the Royal Society of London 43:165–171.

Sereno, P.C. 1986. Phylogeny of the bird-hipped dinosaurs (order Ornithischia). National Geographic Research. 2 (2): 234–56.

Sereno, P. C., C. Shichin, C. Zhengwu, and R. Chenggang. 1988. *Psittacosaurus meileyingensis* (Ornithischia: Ceratopsia), a new psittacosaur from the Lower Cretaceous of northeastern China. Journal of Vertebrate Paleontology 8:366–377.

Sereno PC. 1991. *Lesothosaurus*, “fabrosaurids”, and the early evolution of Ornithischia. Journal of Vertebrate Paleontology 11:168–197.

Sereno, P. C. 1999. The Evolution of Dinosaurs. Science 284:2137–2147.

Simões, T. R., M. W. Caldwell, A. Palci, and R. L. Nydam. 2017. Giant taxon-character matrices: quality of character constructions remains critical regardless of size. Cladistics 33:198–219.

Słowiak, J., V. S. Tereshchenko, and Ł. Fostowicz-Frelik. 2019. Appendicular skeleton of *Protoceratops andrewsi* (Dinosauria, Ornithischia): comparative morphology, ontogenetic changes, and the implications for non-ceratopsid ceratopsian locomotion. PeerJ 7:e7324.

Smith, J. B., P. Dodson. 2003. A proposal for a standard terminology of anatomical notation and orientation in fossil vertebrate dentitions. Journal of Vertebrate Paleontology 23:1–14.

Smith, R. J. 2009. Use and misuse of the reduced major axis for line-fitting. American Journal of Physical Anthropology 140:476–486.

Snover, M., and A. Hohn. 2004. Validation and interpretation of the annual deposition of skeletal marks in loggerhead (*Caretta caretta*) and Kemp's ridley (*Lepidochelys kempii*) sea turtles. Fishery Bulletin- National Oceanic and Atmospheric Administration 102:682–692.

Solonias, N., M. Teaford, and A. Walker. 1988. Interpreting the Diet of Extinct Ruminants: The Case of a Non-Browsing Giraffid. Paleobiology 14:287–300.

Spencer M. R. 2007. A phylogenetic analysis of the basal Ornithischia (Reptilia, Dinosauria). Bowling Green: Department of Geology, Bowling Green State University, 1-140 pp.

Sternberg, C. M. 1937. A classification of *Thescelosaurus*, with a description of a new species. Proceedings of the Geological Society of America. 1936:375.

Sternberg, C. M. 1940. *Thescelosaurus edmontonensis*, n. sp., and Classification of the Hypsilophodontidae. Journal of Paleontology 14:481–494.

Strauss, R. E., M. N. Atanassov, and J. A. De Oliveira. 2003. Evaluation of the principal-component and expectation-maximization methods for estimating missing data in morphometric studies. Journal of Vertebrate Paleontology 23:284–296.

Strotz, L. C., and A. P. Allen. 2013. Assessing the role of cladogenesis in macroevolution by integrating fossil and molecular evidence. Proceedings of the National Academy of Sciences 110:2904–2909.

Sues, H. D. 1980. Anatomy and relationships of a new hypsilophodontid dinosaur from the Lower Cretaceous of North America. Palaeontographica Abteilung 169 (1–3):51–72.

Sullivan, R. M. 2003. Revision of the dinosaur *Stegoceras lambe* (Ornithischia, Pachycephalosauridae). Journal of Vertebrate Paleontology 23:181–207.

Sullivan, R. M. A Taxonomic review of the Pachycephalosauridae (Dinosauria: Ornithischia). Late Cretaceous Vertebrates from the Western Interior. New Mexico Museum of Natural History and Science Bulletin 35:347-365.

Teaford, M. F. 1994. Dental microwear and dental function. Evolutionary Anthropology: Issues, News, and Reviews 3:17–30.

Thulborn, R. A. 1971. Origins and Evolution of Ornithischian Dinosaurs. Nature 234:75-78.

Thulborn, R. A. 1972. The postcranial skeleton of the Triassic ornithischian dinosaur *Fabrosaurus australis*. Palaeontology 15:29–60.

Varricchio, D. J., A. J. Martin, and Y. Katsura. 2007. First trace and body fossil evidence of a burrowing, denning dinosaur. Proceedings. Biological Sciences 274:1361–1368.

Verdú, F. J., P. Godefroit, R. Royo-Torres, A. Cobos, and L. Alcalá. 2017. Individual variation in the postcranial skeleton of the Early Cretaceous *Iguanodon bernissartensis* (Dinosauria: Ornithopoda). Cretaceous Research 74:65–86.

Vickaryous, M. K., T. Maryańska, and D. B. Weishampel. 2004. Ankylosauria, in Weishampel, D.B., Dodson, P., Osmólska, H. (eds.), The Dinosauria (2nd Edition), Berkeley, University of California Press, 363-392.

Vinther, J., R. Nicholls, S. Lautenschlager, M. Pittman, T. G. Kaye, E. Rayfield, G. Mayr, and I. C. Cuthill. 2016. 3D Camouflage in an Ornithischian Dinosaur. Current Biology 26:2456–2462.

Virág, A., and A. Ősi. 2017. Morphometry, Microstructure, and Wear Pattern of Neornithischian Dinosaur Teeth from the Upper Cretaceous Iharkút Locality (Hungary). The Anatomical Record 300:1439–1463.

Vadstein, O., G. Øie, Y. Olsen, I. Salvesen, J. Skjermo, and G. Skjåk-Bræk. 1993. Fish Farming Technology; pp. 69–75 in A strategy to obtain microbial control during larval development of marine fish.

Wang, G., R. Cheng, P. Wang, Y. Gao, C. Wang, Y. Ren, and Q. Huang. 2009. Description of Cretaceous sedimentary sequence of the Quantou Formation recovered by CCSD-SK-Is borehole in Songliao Basin: lithostratigraphy, sedimentary facies and cyclic stratigraphy. Earth Science Frontiers 16:324–338.

Watabe, M., K. Tsogtbaatar, and R. M. Sullivan. 2011. A new pachycephalosaurid from the Baynshire Formation (Cenomanian-late Santonian), Gobi Desert, Mongolia. Fossil Record 3. New Mexico Museum of Natural History and Science, Bulletin 53:489-497.

Weishampel, D. B. 1984. Evolution of Jaw Mechanisms in Ornithopod Dinosaurs. Springer Berlin Heidelberg, Berlin, Heidelberg, pp 1-110.

Weishampel, D. B., R. E. Heinrich. 1992. Systematics of Hypsilophodontidae and basal Iguanodontia (Dinosauria: Ornithopoda). Historical Biology 6:159–184.

Weishampel, D.B., C-M. Juanu, Z. Csiki, D. B. Norman. 2003. Osteology and phylogeny of *Zalmoxes*, an unusual euornithopod dinosaur from the latest Cretaceous of Romania. Journal of Systematic Palaeontology 1:65–123.

Werning, S. 2012. The Ontogenetic Osteohistology of *Tenontosaurus tilletti*. PLoS ONE 7:e33539.

White, P. D., D. E. Fastovsky, and P. M. Sheehan. 1998. Taphonomy and Suggested Structure of the Dinosaurian Assemblage of the Hell Creek Formation (Maastrichtian), Eastern Montana and Western North Dakota. Palaios 13:41–51.

Wiens, J. J., R. M. Bonett, P. T. Chippindale, and F. (Andy) Anderson. 2005. Ontogeny discombobulates phylogeny: paedomorphosis and higher-level salamander relationships. Systematic Biology 54:91–110.

Williamson, T. E., and T. D. Carr. 2002. A new genus of highly derived pachycephalosaurian from western North America. Journal of Vertebrate Paleontology. 22(4):779–801.

Witmer, L. M. 1995. The Extant Phylogenetic bracket and the importance of reconstructing soft tissues in fossils; in Functional morphology in vertebrate paleontology. Cambridge University Press.

Witmer, L. M. 2009. Fuzzy origins for feathers. Nature 458:294–295.

Woodward, H. N., J. R. Horner, and J. O. Farlow. 2011. Osteohistological evidence for determinate growth in the American Alligator. Journal of Herpetology 45(3):339-342.

Woodward, H. N., E. A. Freedman Fowler, J. O. Farlow, and J. R. Horner. 2015. *Maiasaura*, a model organism for extinct vertebrate population biology: a large sample statistical assessment of growth dynamics and survivorship. Paleobiology 41:503–527.

Woodward, H. N., K. Tremaine, S. A. Williams, L. E. Zanno, J. R. Horner, and N. Myhrvold. 2020. Growing up *Tyrannosaurus rex*: Osteohistology refutes the pygmy "*Nanotyrannus*" and supports ontogenetic niche partitioning in juvenile *Tyrannosaurus*. Science Advances 6:eaax6250.

Wyenberg-Henzler, T. C. A. 2020. Ontogenetic Niche Shifts in Megaherbivorous Dinosaurs of Late Cretaceous North America and their Ecological Implications. Text, Carleton University pp 1-267.

Xiao-chun, W., D. B. Brinkman, D. A. Eberth, and D. R. Braman. 2007. A new ceratopsid dinosaur (Ornithischia) from the uppermost Horseshoe Canyon Formation (upper Maastrichtian), Alberta, Canada. Canadian Journal of Earth Sciences 44:1243-1265.

Xing, H., J. C. Mallon, and M. L. Currie. 2017. Supplementary cranial description of the types of *Edmontosaurus regalis* (Ornithischia: Hadrosauridae), with comments on the phylogenetics and biogeography of Hadrosaurinae. PLoS ONE 12(4):e0175253.

Xu, X., X. Wang, and H.-L. You. 2000. A primitive ornithopod from the Early Cretaceous Yixian Formation of Liaoning. Vertebrata PalAsiatica 38:318–325.

Xu, X., Z. Zhou, and R. O. Prum. 2001. Branched integumental structures in *Sinornithosaurus* and the origin of feathers. Nature 410:200–204.

Xu, X., K. Wang, X. Zhao, C. Sullivan, and S. Chen. 2010. A New Leptoceratopsid (Ornithischia: Ceratopsia) from the Upper Cretaceous of Shandong, China and Its Implications for Neoceratopsian Evolution. PLoS ONE 5:e13835.

Zan, S.-Q., C. Jun, L.-Y. Jin, and T. Li. 2005. A primitive ornithopod from the Early Cretaceous Quantou Formation of central Jilin, China. Vertebrata PalAsiatica 43:182–193.

Zan, S., C. B. Wood, G. W. Rougier, L. Jin, J. Chen, and C. R. Schaff. 2006. A new "Middle" Cretaceous Zalambdalestid mammal, from a new locality in Jilin Province, Northeastern China. Journal of Paleontology Society of Korea 22(1):153-172.

Zanno, L. E., R. T. Tucker, A. Canoville, H. M. Avrahami, T. A. Gates, and P. J. Makovicky. 2019. Diminutive fleet-footed tyrannosauroid narrows the 70-million-year gap in the North American fossil record. Communications Biology 2:6.

Zhao, Q., M. J. Benton, X. Xing, and P. M. Sander. 2013. Juvenile-only clusters and behaviour of the Early Cretaceous dinosaur *Psittacosaurus*. Acta Palaeontologica Polonica 59(4): 827-833.

Zheng, X.-T., H.-L. You, X. Xu, and Z.-M. Dong. 2009. An Early Cretaceous heterodontosaurid dinosaur with filamentous integumentary structures. Nature 458:333–336.

Zheng, W., X. Jin, M. Shibata, Y. Azuma, and F. Yu. 2012. A new ornithischian dinosaur from the Cretaceous Liangtoutang Formation of Tiantai, Zhejiang Province, China. Cretaceous Research 34:208–219.

Appendices

Appendix A. Raw femoral lengths used for the box and whisker plot of logarithmic femoral length (body size proxy) in different groups of late Cretaceous ornithischians.

Taxon	Specimen	Femur Length (mm)	Reference
Ankylosauria			
Ankylosaurus magniventris	AMNH 5214	660	Persons and Currie, 2020
Euoplocephalus tutus	AMNH 5404	548	Persons and Currie, 2020
Saichania chulsanensis	MPC 100/1305	380	Arbour, 2014
Pinacosaurus grangeri	PIN 614	400	Arbour, 2014
Sauropelta edwardsorum	AMNH 3035	770	Persons and Currie, 2020
Ceratopsidae			
Centrosaurus apertus	AMNH 5427	800	Persons and Currie, 2020
Chasmosaurus belli	ROM 839	825	Persons and Currie, 2020
Einiosaurus procurvicornis	MOR 456-8-18-6-1	567	Persons and Currie, 2020
Pachyrhinosaurus lakustai	TMP 89.55.384	620	Persons and Currie, 2020
Protoceratops andrewsi	AMNH 6424	250	Persons and Currie, 2020
Triceratops horridus	AMNH 5033	1030	Persons and Currie, 2020
Pentaceratops sternbergii	PMU.R268	880	Persons and Currie, 2020
Styracosaurus albertensis	CMN 344	810	Persons and Currie, 2020
Avaceratops lammersi	ANSP 15800	400	Wyenberg-Henzler, 2020
Anchiceratops ornatus	MOR 300	348	Wyenberg-Henzler, 2020
Hadrosauridae			
Edmontosaurus annectens	TMP1985.0019.0001	1250	Persons and Currie, 2020
Gryposaurus notabilis	ROM 764	1020	Persons and Currie, 2020
Lambeosaurus lambei	ROM 1218	1080	Persons and Currie, 2020
Probactrosaurus gobiensis	PIN AN SSR 2232/1	565	Persons and Currie, 2020
Shantungosaurus giganteus	GMV 1780-10	1650	Persons and Currie, 2020
Edmontosaurus regalis	CMN 2289	1280	Persons and Currie, 2020
Prosaurolophus maximus	ROM 787	1000	Persons and Currie, 2020
Saurolophus angustirostris	PIN 551-8	1200	Persons and Currie, 2020
Tsintaosaurus spinorhinus	IVPP v725	1193	Persons and Currie, 2020
Corythosaurus casuarius	AMNH 5338	987	Wyenberg-Henzler, 2020
Parasaurolophus walkeri	UAVLP 300	991	Wyenberg-Henzler, 2020
Hypacrosaurus altispinus	TMP1982.010.0001	890	Wyenberg-Henzler, 2020
Maiasaura peeblesorum	ROM 44770	940	Wyenberg-Henzler, 2020
Leptoceratopsidae			
Cerasinops hodgskissi	MOR 300	345	Persons and Currie, 2020
Ischioceratops zhuchengensis	ZCDM V0016	291	Persons and Currie, 2020
Montanoceratops cerorhynchus	AMNH 5464	346	Persons and Currie, 2020
Unescoceratops koppelhusae	TMP 1995.012.0006	265	Wyenberg-Henzler, 2020
Leptoceratops gracilis	CMN 8888	280	Wyenberg-Henzler, 2020
Prenoceratops pieganensis	MNHCM #	206	Wyenberg-Henzler, 2020
Pachycephalosauridae			
Homalocephale calathocercos	-	218	This Study

Prenocephale prenes	MgD-I/I04	222	This Study
Stegoceras validum	UALVP 2	225	This Study
Pachycephalosaurus wyomingensis	ROM 55378	430	Wyenberg-Henzler
Thescelosauridae			
Koreanosaurus boseongensis	KDRC-BB3	165	Huh et al., 2011
Orodromeus makelai	MOR 623	142	Persons and Currie, 2020
Oryctodromeus cubicularis	MOR 1642	240	Persons and Currie, 2020
Jeholosaurus shangyuanensis	IVPP V15939	128	This Study
Haya griva	IGM 100/2013	126	This Study
Parksosaurus warreni	ROM 804	270	Brown, 2009
Thescelosaurus assiniboiensis	RSM P 1225.1	301	Brown, 2009
Thescelosaurus neglectus	NCSM 15728	428	This Study
Thescelosaurus sp.	CMN 8537	335	Brown, 2009

Appendix B. Estimated raw data of *Stegoceras* (UALVP 2) and *Thescelosaurus* (NCSM 15728) dentition. Abbreviations: AL, apical length; CA, crown angle; CBL, crown base length; CH, crown height; DCL, distal carina length; DDH, distal denticle height; DDL, distal denticle length; M-CL, mid-crown length; MCL, mesial carina length; MDH, mesial denticle height; MDL, mesial denticle length; NL, neck length.

Tooth Type	CH	CBL	M-CL	AL	NL	MCL	DCL	MDH	MDL	DDH	DDL	CA
***Stegoceras* (UALVP 2)**												
Premaxilla	5.081	3.586	2.928	4.556	2.846	3.238	3.556	0.364	0.418	0.679	0.291	60.296
Premaxilla	5.945	4.400	3.583	5.735	3.580	5.607	4.670	0.498	0.237	0.443	0.230	53.824
Premaxilla	4.559	4.393	3.816	4.193	3.594	3.646	3.399	0.523	0.248	0.396	0.245	50.666
Premaxilla	4.984	4.588	3.787	4.612	3.164	4.024	3.791	0.435	0.351	0.320	0.238	59.978
Premaxilla	4.987	4.326	3.973	4.501	3.691	3.931	4.286	0.411	0.350	0.325	0.256	59.492
Maxilla	3.105	3.654	3.103	2.719	2.329	1.950	2.266	0.484	0.346	0.431	0.316	57.329
Maxilla	3.630	5.250	3.763	3.582	3.352	3.215	2.886	0.351	0.444	0.458	0.405	42.470
Maxilla	3.785	5.068	4.259	3.794	3.865	3.106	2.771	1.125	0.383	0.658	0.357	45.198
Maxilla	2.885	4.662	4.192	3.352	3.322	2.238	1.764	0.297	0.372	0.387	0.368	29.866
Maxilla	3.840	4.171	3.353	4.154	3.489	3.374	2.244	0.638	0.531	0.669	0.440	47.992
Maxilla	3.389	4.615	3.821	3.390	3.519	3.028	2.384	0.395	0.492	0.321	0.266	43.589
Maxilla	4.395	4.828	3.308	4.039	3.517	3.930	2.755	0.506	0.460	0.597	0.358	49.970
Maxilla	3.950	5.094	3.713	3.765	3.575	3.206	2.551	0.233	0.437	0.329	0.396	43.487
Maxilla	4.161	4.306	3.494	3.644	2.771	2.941	2.633	0.499	0.394	0.388	0.255	38.933
Maxilla	3.889	4.988	4.204	3.799	3.539	3.721	3.351	0.274	0.390	0.438	0.347	53.884
Maxilla	3.787	4.813	3.971	3.113	3.460	2.628	2.969	0.228	0.145	0.232	0.261	43.380
Maxilla	3.812	4.289	3.843	2.541	3.310	2.032	3.384	0.283	0.215	0.214	0.239	50.927
Maxilla	4.384	4.393	3.439	3.275	3.135	2.711	2.848	0.237	0.200	0.267	0.316	47.626
Maxilla	4.588	4.918	3.699	4.229	3.349	3.847	2.640	0.397	0.252	0.422	0.327	46.945
Maxilla	4.276	4.367	3.608	3.078	3.127	2.692	2.460	0.510	0.247	0.279	0.300	42.298
Maxilla	4.208	4.699	2.836	4.077	3.404	3.675	2.287	0.523	0.529	0.328	0.340	45.934
Maxilla	4.247	4.623	3.081	3.678	4.188	3.049	2.173	0.974	0.525	0.470	0.341	49.908
Maxilla	3.959	4.758	3.097	3.236	3.096	2.902	2.462	0.350	0.248	0.383	0.313	50.575
Maxilla	4.344	4.257	2.933	4.741	3.371	3.411	1.990	0.176	0.548	0.389	0.298	47.681
Maxilla	3.774	4.190	2.919	3.144	3.158	2.717	1.900	0.101	0.343	0.349	0.298	41.643
Dentary	5.590	4.943	3.257	4.909	3.809	4.361	5.598	0.487	0.283	0.319	0.354	52.485
Dentary	4.909	5.238	3.238	4.286	3.528	4.210	4.786	0.455	0.470	0.385	0.287	51.350
Dentary	4.443	5.160	3.331	4.257	3.462	4.073	4.454	0.505	0.447	0.443	0.356	49.338
Dentary	4.478	5.408	2.797	4.342	3.480	2.694	2.992	0.214	0.296	0.642	0.426	53.101
Dentary	3.653	5.185	3.414	4.107	2.733	3.385	2.788	0.377	0.344	0.403	0.327	46.574
***Thescelosaurus* (NCSM 15728)**												
Premaxilla	4.830	5.141	3.700	4.867	3.635	0.000	0.000	0.000	0.000	0.000	0.000	56.181
Premaxilla	4.650	5.250	4.388	4.562	4.036	0.000	0.000	0.000	0.000	0.000	0.000	55.171
Premaxilla	5.444	5.321	4.265	5.347	4.593	0.000	0.000	0.000	0.000	0.000	0.000	53.229

Premaxilla	4.922	5.054	4.311	5.516	3.889	0.000	0.000	0.000	0.000	0.000	0.000	52.823
Premaxilla	5.042	4.622	3.954	5.161	3.900	0.000	0.000	0.000	0.000	0.000	0.000	47.458
Premaxilla	5.071	5.437	3.911	5.594	4.074	0.000	0.000	0.000	0.000	0.000	0.000	56.357
Premaxilla	4.557	5.184	4.580	4.348	4.089	0.000	0.000	0.000	0.000	0.000	0.000	44.343
Premaxilla	5.509	5.752	4.381	5.643	4.848	0.000	0.000	0.000	0.000	0.000	0.000	52.727
Maxilla	4.313	5.497	4.367	4.647	3.129	3.868	3.565	2.424	0.751	2.265	0.551	49.764
Maxilla	4.226	5.405	4.695	4.357	3.242	3.858	2.899	1.644	0.597	1.413	0.476	40.679
Maxilla	4.304	5.478	4.305	4.564	3.193	4.027	2.667	1.846	0.445	2.243	0.591	40.591
Maxilla	3.722	5.055	3.332	5.346	3.200	4.782	2.139	1.676	0.325	1.578	0.602	35.302
Maxilla	3.600	5.858	3.932	4.187	2.902	3.911	3.110	1.479	0.752	2.197	0.692	37.147
Maxilla	4.355	5.136	3.648	4.738	2.919	3.987	3.219	1.864	0.549	2.205	0.417	43.111
Maxilla	5.340	5.391	3.850	5.392	3.030	5.130	3.718	2.760	0.502	2.742	0.455	47.802
Maxilla	4.357	5.620	3.395	4.215	3.322	3.910	3.063	1.356	0.393	1.510	0.432	42.806
Maxilla	4.481	5.992	5.050	4.642	3.306	4.381	3.325	2.159	0.442	2.408	0.393	45.467
Maxilla	4.050	5.296	3.259	4.165	3.249	3.777	2.111	1.332	0.284	1.695	0.335	39.868
Maxilla	4.348	5.301	2.743	5.364	3.435	4.681	2.917	1.660	0.356	1.994	0.271	44.432
Maxilla	5.376	5.433	4.040	5.525	3.002	4.471	2.910	1.819	0.492	2.305	0.513	37.589
Maxilla	2.970	5.645	4.357	4.048	3.685	3.104	1.707	1.552	0.356	2.146	0.414	27.131
Maxilla	5.746	5.506	4.640	5.530	3.052	4.657	2.848	3.029	0.511	2.517	0.576	45.613
Maxilla	5.168	4.965	4.042	4.590	3.352	4.123	2.688	2.723	0.421	1.902	0.389	43.167
Dentary	3.750	3.491	2.520	3.768	2.875	2.804	2.633	0.298	0.141	0.319	0.335	55.070
Dentary	3.920	4.258	3.042	4.300	3.305	3.227	3.147	0.212	0.395	0.639	0.404	52.727
Dentary	3.299	4.113	2.424	3.964	3.340	2.892	3.864	0.094	0.348	0.711	0.505	64.381
Dentary	4.007	4.415	3.537	4.233	3.171	2.691	3.163	0.935	0.323	0.538	0.290	53.586
Dentary	3.860	4.582	3.467	4.294	3.304	3.195	2.604	0.804	0.307	0.583	0.581	52.235
Dentary	4.008	4.494	3.439	4.189	2.781	3.654	3.501	0.612	0.146	1.257	0.554	57.233

Appendix C. Scores for PCA of *Stegoceras* and *Thescelosaurus* dentition for PC axes of size correct dataset.

	PC 1	PC 2	PC 3	PC 4	PC 5	PC 6	PC 7	PC 8	PC 9	PC 10
Premaxilla	0.29109	3.8044	0.12127	-0.43669	-0.18152	-0.16996	-0.12835	0.28343	0.081542	0.060637
Premaxilla	-0.07883	3.7046	0.080031	-0.35388	0.059293	-0.09533	0.16376	-0.24269	0.17022	-0.06373
Premaxilla	0.15753	1.652	1.169	0.28023	0.16354	0.13451	0.12045	-0.14591	0.11174	-0.01406
Premaxilla	0.3635	1.5255	0.45054	-0.57027	-0.32855	-0.35191	-0.1182	-0.25845	0.083527	-0.01906
Premaxilla	-0.01004	2.5433	1.4648	0.20473	0.16881	-0.08803	-0.04293	-0.12224	0.10633	0.025023
Maxilla	1.0759	-0.60055	1.1668	-0.3574	-0.41116	-0.13097	-0.12373	0.084818	-0.10376	0.088167
Maxilla	1.1514	-1.8655	0.19481	0.49636	-0.07642	-0.30217	-0.08121	-0.03677	-0.01596	0.000523
Maxilla	0.91797	-0.61107	1.3749	0.59357	0.57776	0.40839	-0.01231	-0.10675	-0.00119	0.046753
Maxilla	0.712	-1.6885	1.7803	0.35525	1.0234	-0.38176	-0.04871	-0.02213	-0.04217	-0.01421
Maxilla	0.70793	1.445	0.65335	0.57652	0.89978	0.12193	-0.18051	0.13729	-0.12836	-0.01642
Maxilla	0.66209	-0.80381	1.3158	0.84674	0.48182	-0.06262	-0.27155	-0.12586	0.077313	-0.02548
Maxilla	0.89486	0.24285	-0.32684	0.69843	-0.18426	0.10949	-0.13487	0.077899	0.007222	-0.05676
Maxilla	0.71265	-0.92806	0.28046	0.79375	-0.07144	-0.3493	-0.11106	0.027481	-0.0651	-0.05016
Maxilla	0.76552	0.29771	0.58853	-0.51089	-0.56459	-0.19644	-0.21746	-0.07592	0.013435	-0.00949
Maxilla	0.68591	-0.62382	1.2211	0.35387	0.18362	-0.38311	0.011811	-0.00366	0.11894	-0.0329
Maxilla	0.27169	-1.2739	1.3834	0.79182	-0.47289	-0.0711	0.39191	-0.13986	0.071959	-0.02222
Maxilla	0.30721	-0.80688	2.2592	1.1024	-0.98457	0.23042	0.13877	0.044344	0.065486	0.09871
Maxilla	0.33554	0.13527	0.7291	0.49792	-0.98029	-0.08834	0.2159	0.075307	-0.07272	-0.02934
Maxilla	0.55132	0.2528	0.11093	-0.00238	-0.31934	-0.15668	0.13871	-0.08198	-0.02	-0.11089
Maxilla	0.52767	-0.04324	1.2456	0.42015	-0.97078	0.24268	0.046443	-0.00748	-0.13627	-0.03548
Maxilla	0.87766	0.17521	-1.2491	0.98723	-0.16302	0.088579	-0.34702	-0.15354	-0.17178	-0.06134
Maxilla	0.69461	0.65325	-0.03688	1.9984	0.14536	0.88	-0.29381	0.054669	-0.13731	0.007175
Maxilla	0.90472	-1.2523	-0.4601	0.73462	-0.90041	0.074606	0.099354	0.00518	-0.03182	-0.04826
Maxilla	0.24512	1.8394	-0.7534	0.55666	0.47279	-0.45022	-0.3336	0.13789	0.023417	-0.10602
Maxilla	0.40283	-0.187	0.024393	1.2284	-0.4866	-0.2803	-0.05516	0.38752	0.083891	-0.12807
Dentary	0.41347	1.7561	-0.85492	0.69503	-0.49976	0.037293	0.12243	-0.25546	-0.07976	0.081979
Dentary	0.92869	-0.0342	-1.0842	0.66682	-0.74823	-0.06238	-0.19186	-0.20426	0.08964	0.055857
Dentary	1.0456	-0.27561	-0.80328	0.52001	-0.32682	-0.1278	-0.10702	-0.19998	0.008975	0.06376
Dentary	0.97589	-0.91582	-2.3872	0.98447	-0.55197	-0.18916	0.15121	0.17787	-0.00694	0.062536
Dentary	1.2711	-1.8647	-1.0046	-0.6745	-0.22944	-0.68069	-0.06283	-0.33688	-0.0215	-0.024
Premaxilla	-5.7653	-0.99762	-1.0227	-0.4923	-0.36262	-0.05105	-0.04427	-0.03004	-0.03114	0.003824
Premaxilla	-5.9051	-1.1833	0.30566	-0.23581	-0.08487	0.051672	0.001457	0.032216	0.025308	-0.00898
Premaxilla	-6.2532	0.13837	-0.11288	0.1228	0.079934	0.21819	-0.004	0.081157	-0.00223	0.004648
Premaxilla	-6.1552	-0.01139	-0.04034	-0.83401	0.32043	-0.18334	-0.01667	-0.05779	-0.01147	0.009517
Premaxilla	-6.3916	0.73782	0.082298	-0.45184	0.17314	0.033409	-0.01246	0.056112	-0.01848	0.003524
Premaxilla	-5.9083	-0.58588	-1.0971	-0.36529	0.081561	-0.05382	-0.03531	-0.07862	-0.02773	0.020175
Premaxilla	-5.9603	-1.2131	0.79438	-0.15871	-0.05447	0.096822	0.016081	0.068258	0.0431	-0.01609
Premaxilla	-6.1123	-0.30055	-0.43758	0.21349	0.14551	0.20016	-0.00641	0.030413	0.000475	0.012347
Maxilla	1.9623	-0.65895	0.31234	-1.2125	0.18237	0.066976	-0.20616	0.077439	-0.0162	0.10719

Maxilla	1.5583	-0.69173	1.0675	-1.0202	0.18143	0.009224	-0.1502	0.040527	-0.01868	0.010369
Maxilla	1.7347	-0.71465	0.26994	-1.0439	0.15692	0.12741	0.083289	0.15643	-0.06348	-0.01848
Maxilla	1.5414	-0.06571	-1.2567	-0.60399	1.2292	0.044338	0.19082	-0.18275	-0.20146	-0.08782
Maxilla	2.4402	-2.6993	-0.6969	-0.94339	0.091259	-0.23507	-0.15877	0.080834	-0.07094	0.060181
Maxilla	1.8022	-0.19592	-0.65579	-1.1525	0.026498	0.094253	-0.12018	0.053301	0.083078	0.052684
Maxilla	1.7801	0.68726	-0.81514	-1.5139	-0.31306	0.22499	-0.03268	0.054528	0.05264	0.01078
Maxilla	1.7328	-1.3595	-1.2803	0.043193	-0.41557	0.35678	0.048441	0.033946	0.031117	0.014116
Maxilla	1.7266	-1.2609	0.78622	-1.3768	0.03259	0.12845	0.053037	0.010408	0.20641	-0.0049
Maxilla	1.5146	-1.1758	-1.2147	0.031823	-0.07242	0.49672	0.15071	0.042169	0.12488	-0.08349
Maxilla	1.5128	0.015369	-2.7954	0.19457	0.46819	0.52081	0.015266	-0.17775	0.25719	-0.00753
Maxilla	1.5898	0.68535	-0.61537	-1.7255	-0.28207	-0.03371	-0.0333	0.14809	-0.042	-0.02929
Maxilla	1.6095	-2.5734	0.62492	0.070775	1.5161	0.35378	0.14512	0.002487	0.14483	-0.03708
Maxilla	1.6089	0.98049	0.26878	-2.0911	-0.38093	0.12176	-0.03615	0.15914	-0.13133	-0.04261
Maxilla	1.2726	1.1347	0.51496	-0.75687	-0.23526	0.64553	-0.02403	0.1563	0.009762	-0.03012
Dentary	0.15941	2.0676	-0.32473	0.57792	0.2948	-0.00258	0.3972	-0.07704	-0.16855	0.004284
Dentary	0.59236	1.1485	-0.32165	0.5866	0.57743	-0.3707	0.032852	0.21313	0.056559	0.035942
Dentary	0.75374	0.40759	-1.4536	1.6289	0.87243	-0.50222	0.22558	0.35305	0.098117	0.12667
Dentary	0.72954	0.79131	0.43551	-0.21977	0.4098	0.11029	-0.03293	-0.2282	-0.01576	0.12777
Dentary	0.9362	0.41683	0.11671	0.097907	0.61145	0.001561	0.14723	-0.0886	-0.32372	0.03161
Dentary	1.1307	0.22418	-0.09203	-0.84696	0.02617	-0.18027	0.66791	0.096935	-0.0693	0.007547

Appendix D. Loadings for PCA of *Stegoceras* and *Thescelosaurus* dentition for PC axes of size correct dataset. Abbreviations: AL, apical length; CA, crown angle; CH, crown height; DCL, distal carina length; DDH, distal denticle height; DDL, distal denticle length; M-CL, mid-crown length; MCL, mesial carina length; MDH, mesial denticle height; MDL, mesial denticle length; NL, neck length.

	PC 1	**PC 2**	**PC 3**	**PC 4**	**PC 5**	**PC 6**	**PC 7**	**PC 8**	**PC 9**	**PC 10**
CH	-0.29765	0.8778	-0.01786	-0.0668	-0.36657	0.034351	-0.00382	0.022697	-0.00344	-0.00127
M-CL	-0.2621	0.14362	0.89985	-0.30963	0.064007	-0.03097	0.002937	0.002012	0.002058	-0.00065
AL	-0.30683	0.77353	-0.34255	-0.31745	0.2922	-0.06029	-0.00122	-0.01919	-0.00165	0.001321
NL	-0.5257	0.48116	0.22895	0.63447	0.17774	0.073993	0.00499	0.00759	0.002515	0.0005
MCL	0.97206	0.18215	0.051888	0.10473	-0.02102	-0.05082	0.026672	-0.04696	0.021185	-0.04325
DCL	0.95852	0.19636	0.077243	0.13595	-0.06252	-0.08138	0.048592	-0.05529	0.033684	0.034014
MDH	0.95378	0.099549	0.04862	-0.16532	0.041561	0.21051	-0.01849	-0.06069	-0.02467	0.004535
MDL	0.96918	0.13784	0.063574	0.097906	0.019466	-0.06173	-0.15253	0.024277	0.002547	0.003431
DDH	0.97368	0.080835	-0.03757	-0.12563	0.090016	0.078911	0.042482	0.099768	0.046238	0.000192
DDL	0.97918	0.11917	0.050963	0.089973	0.025498	-0.06932	0.05462	0.042129	-0.07813	0.001757